INFORMATION TO USERS

This manuscript has been reproduced from the microfilm master. UMI films the text directly from the original or copy submitted. Thus, some thesis and dissertation copies are in typewriter face, while others may be from any type of computer printer.

The quality of this reproduction is dependent upon the quality of the copy submitted. Broken or indistinct print, colored or poor quality illustrations and photographs, print bleedthrough, substandard margins, and improper alignment can adversely affect reproduction.

In the unlikely event that the author did not send UMI a complete manuscript and there are missing pages, these will be noted. Also, if unauthorized copyright material had to be removed, a note will indicate the deletion.

Oversize materials (e.g., maps, drawings, charts) are reproduced by sectioning the original, beginning at the upper left-hand corner and continuing from left to right in equal sections with small overlaps.

ProQuest Information and Learning
300 North Zeeb Road, Ann Arbor, MI 48106-1346 USA
800-521-0600

Université d'Ottawa · University of Ottawa

To my parents, for everything.

A mis padres, por todo.

Abstract

This thesis focuses on different aspects of photobiology. The first chapters address the photophysical and photochemical characterization of two pharmaceutical products, fenofibric acid and ketoprofen, both containing the benzophenone chromophore. These studies have been performed with the aim of better understanding the photostability of these drugs. These compounds are shown to undergo efficient photodecarboxylation in basic solutions, with concomitant formation of carbanions. Time-resolved studies lead us to propose a singlet mediated reaction in the case of ketoprofen, whereas the photoreactivity of fenofibric acid results from the triplet state of this compound; further, dramatic solvent dependence is encountered in the photochemical reactions of the latter drug and its photoproducts.

In the case of ketoprofen photodegradation, the photogenerated benzylic carbanion can be monitored, and lifetime measurements at different temperatures and in different solvents have been performed to determine its dynamic parameters. The decay of this carbanion, resulting from protonation by water, is found to occur within a few hundred nanoseconds; and the protonation rate is shown to be dependent on the solvent and the degree of substitution of the carbanion center.

The case of α-diketones as potential photosensitizers is also addressed with the example study of a di-thienyl α-diketone; *i.e.*, 2,2'-thenil. Direct spectroscopic evidence is given for the formation of a molecular oxygen-triplet adduct (Bartlett-Schenck intermediate), a previously described, though never isolated, reactive oxygen species about which little is known. The formation and yield of this intermediate are discussed in terms of the energy of its triplet precursors.

The subsequent chapters in this thesis deal with two other biologically relevant problems where photochemistry and photophysics are employed as a tool in order to better

understand the systems under study. Thus the properties of the adrenaline derived radical are evaluated, as a case study for the catecholamine group in general. Absolute rate constants for *tert*-butoxyl radical scavenging and triplet benzophenone quenching are reported, and a reactivity comparison is established with other intermediates involved in the reaction of melanin formation *via* catecholamines.

A second aspect involves the development of a novel technique to assess DNA-damage, based on fluorescence of dye-DNA complexes. The rigidity imposed by the DNA base pairs on intercalating chromophores is exploited. Its retardation effect on the relaxation of a photoexcited DNA-stain probe is employed to determine the amounts of DNA existing as double and single stranded form; which is ultimately an expression of the damage the DNA has suffered.

Acknowledgements

I am very grateful to Tito (Professor Scaiano) for his help over all these years. He has always been there when I needed him, regardless of the nature of the problem. He has also given me a lot of room to try new things, allowing me to grow scientifically under his guidance. His qualities as an excellent person and scientist will always be treasured in my mind, together with the many good moments spent in his lab.

I also want to thank Professors Miguel A. Miranda, and Hermenegildo García, for their help and direction while on a short stay at the Instituto de Tecnología Química, Universidad Politécnica de Valencia. The evening discussions in their labs were always very fruitful. Dr. Jack R. N. McLean, at Health Canada, helped us a lot when we embarked in the DNA project. I am very grateful for his emails and phone calls, intended to clarify one other doubt.

I have had the opportunity to meet many great people while at the Scaiano group. I have learnt from them all. In particular I would like to acknowledge Sonia and Will, who received me in the group full of joy, and from whom I still get good advice. Their friendship was extremely important in my first months here. Lydia and Salvo, for their supervision and friendship. Nadereh, the first member of the group I met, and who taught me so much on the picosecond system "picoman". Chris, my lab mate for more than four years; together we have built our friendship based on so many good, and a very few less good times, friendship of which I am very happy. Anne, Michelle, and Enrique, I am glad to have worked with you guys, you added diversity to the sometimes dull days in the lab. Luca and Marius, with whom I have shared the office in the last moments of writing, who patiently overlooked the crowding and mess in our little office. Andre and Gerry, as well as Betty, Anita, and Cheryl, who have been extremely helpful repairing whatever was broken, and assisting me with whatever I needed.

I also want to acknowledge Kathy-Sarah, and Setu, whom I supervised on summer terms, learning from them while at the same time getting their everyday help, making it a great experience for me.

Many people in the Chemistry Department has also helped me over these years, to all them goes my gratitude.

I want to thank Paco, Marisa, Chelo and Angel, who helped me so much while at the Instituto de Tecnología Química, Universidad Politécnica de Valencia. The many "charlas de bodeguita" with Chelo and Angel are a great memory.

The funding provided by the Ontario Graduate Scholarship Program during part of my thesis is greatly appreciated. I am also grateful to Canada as a country, for receiving me as a graduate student.

Marcelo, Elena, Gonzalo, Mabel, Dago, and Irina have been great friends, who at their time, have managed to pull me out into the light. I am very glad to have crossed paths with you.

Irina, I am thankful to you for too many reasons, your love sums them up.

Finalmente, les agradezco a mis padres, que con mucho sacrificio de su parte me ayudaron a venir a Ottawa, en la parte inicial de esta empresa. Su amor durante toda mi vida es el pilar sobre el que me he sustentado, y que me permitirá seguir adelante. Gracias viejos, por todo.

Table of Contents

List of Figures

List of Schemes

List of Tables

List of Abbreviations

1,4-CHD	1,4-cyclohexadiene
1-NM	1-naphthalenemethanol
4Cl-4'I-BP	4-chloro-4'-isopropoxybenzophenone
4-MBP	4-methoxybenzophenone
ALS	alkaline labile sites
CD	circular dichroism
CT DNA	calf thymus DNA
DAPI	4'-6-diamidino-2-phenylindole
ddH_2O	distilled deionized water
di-*t*-butyl peroxide	di-*tert*-butyl peroxide
DSB	double strand break
dsDNA	double strand DNA
ethidium bromide	2,7-diamino-10-ethyl-9-phenylphenanthridium
FA	fenofibric acid
FADU	fluorometric analysis of DNA unwinding.
FB	fenofibrate
GS	ground state
HBSS	Hank's balanced salt solution
IC	internal conversion
ICD	induced circular dichroism
IR	infrared
ISC	intersystem crossing
KP	ketoprofen
KSE	kinetic solvent effect
LED	diode
LFP	laser flash photolysis
M	molar
mM	millimolar
mmol	millimol
ms	millisecond
N-LFP	nanosecond laser flash photolysis
nmol	nanomol
ns	nanosecond
NSAID	non-steroidal anti-inflammatory drug
PBS	phosphate buffer solution
PIH	propidium iodide hydrate
P-LFP	picosecond laser flash photolysis

ps	picosecond
ROS	reactive oxygen species
S_1	lowest energy singlet excited state
SB	strand break
SSB	single strand break
ssDNA	single strand DNA
ST DNA	salmon testes DNA
T_1	lowest energy triplet excited state
***t*-butoxyl**	*tert*-butoxyl
TL	2,2'-thenil
TMAOH	tetramethylammonium hydroxide
TMPD	tetramethyl-*p*-phenylendiamine
TN	2,2'-thenoin
TOT	2-(then-2-oyl)thiophene
T-T	triplet-triplet
UV-A	ultraviolet radiation ranging from 320-400 nm.
UV-B	ultraviolet radiation ranging from 280-320 nm.
UV-Vis	ultraviolet-visible
VR	vibrational relaxation
YAG	ytterium-argon-garnate
$^1\Delta_g$ O_2	singlet oxygen
ΔOD	Changes in transmitted light from the probe beam, before and after laser excitation.
γ radiation	gamma radiation
μM	micromolar
μs	microsecond

1. Photosensitization: Understanding, Preventing and Quantifying the Damage

1.1 Introduction: Solar Radiation and Human Skin

An analysis of the solar radiation spectrum reaching the surface of the earth, shown in Figure 1-1, reveals that ultraviolet light, characterized for its short wavelength and high energy, is able to pass trough the different layers of the atmosphere. Thus, wavelengths of the UV-B (290-320 nm) and UV-A (320-400 nm) region of the spectrum, imperceptible to the human eye, are an inherent part of our everyday life. In the case of UV-B, however, the protecting effect of the ozone layer results in a decreased flux of photons impinging on the earth, as compared to the outer layers of the atmosphere.

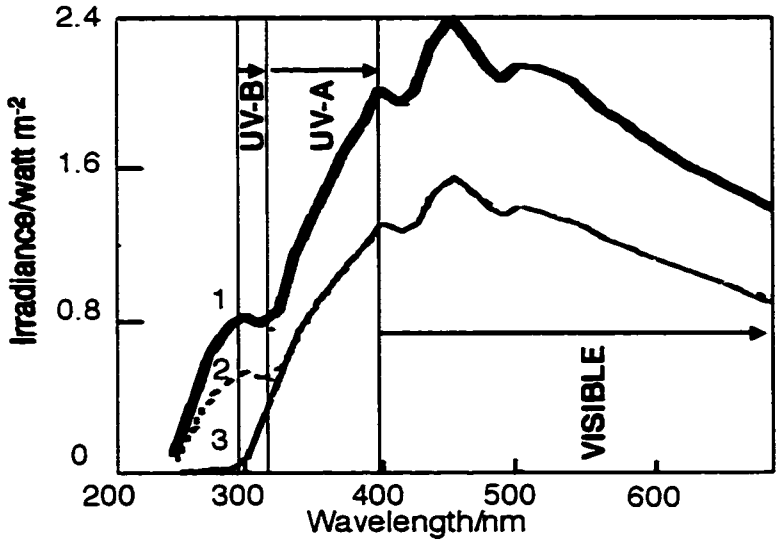

Figure 1-1: Variation of the intensity of solar radiation with wavelength. (1) Solar radiation outside the atmosphere. (2) Intensity of light absorbed by ozone. (3) Solar radiation at the sea level.[1,2]

Pigmentation, as well as hair and limited exposure time to sun are strategies that living organisms have developed to protect themselves from this incident radiation.[2] As a result of pigmentation, the penetration through the skin by the different wavelengths of solar radiation is a function of their frequency; the lower it is (*i.e.*, red light), the larger its transmittance through the body tissue. In the case of UV-B frequencies, they are absorbed in the first

layers of the skin, composed by the dead cells of the stratum corneum; however wavelengths in the UV-A region are able to reach the blood irrigation system, as can be seen in Figure 1-2.

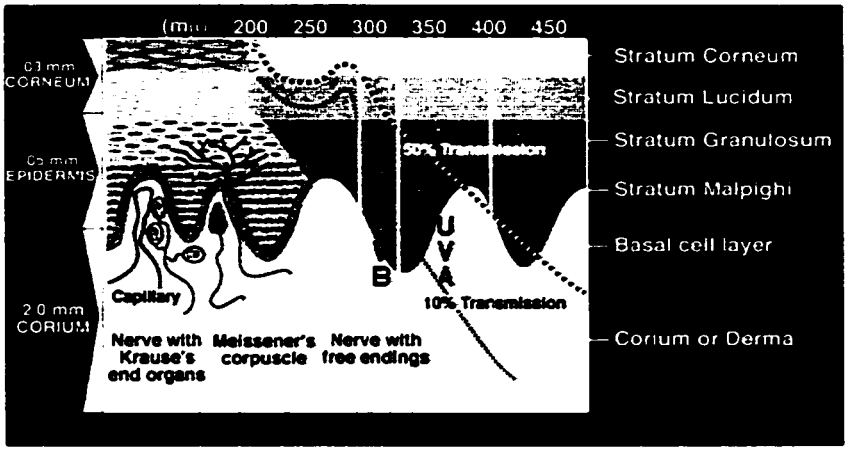

Figure 1-2: Penetration of human skin by ultraviolet light.[3]

Whereas most of the natural components of our organism are transparent to UV-A and longer wavelengths, precluding any interaction between light and chemical substances, a different situation arises upon consumption of food with preservatives or dyes, or upon ingestion of pharmaceutical products.[4] These xenobiotic species transported through the blood system will eventually reach superficial areas in the body, where they will readily absorb the incident radiation.[4] An ample range of possibilities, involving photophysical and photochemical reactions will then be open for these molecules, reactions for which the organism has not evolved to protect itself. It is this type of interactions, xenobiotic-incident sunlight, that can be very detrimental for the different tissues (*vide infra*).

Phototoxic and photoallergic responses will be the result of the interactions mentioned above. Phototoxicity will be determined by direct damage to the tissue induced by a photo-generated chemical agent.[5] Photoallergies are the response to a chemical modification of a substrate into an allergen (which as its name indicates, will promote the formation of a specific antibody to its new structure). Upon subsequent sun exposure, an inflammatory antibody-antigen reaction will be elicited.[1,5,6]

1.2 State Energy Diagrams: An Ample Range of Possibilities for a Chromophore

Two elements are necessary for a photoprocess to occur; one is light and the other is a chemical substrate capable of absorbing it. Following the interaction of the electromagnetic radiation and the substrate, resulting in its photoexcitation, the substrate will dissipate the excess energy and repopulate the ground state. Many different chemical and physical events are prone to take place at this instance. Figure 1-3 shows all the different physical transitions that may occur between the different electronic states of a substrate, in what is called a Jablonski diagram.[7] Radiative transitions are represented as straight arrows, whereas nonradiative transitions are shown as wiggly ones.

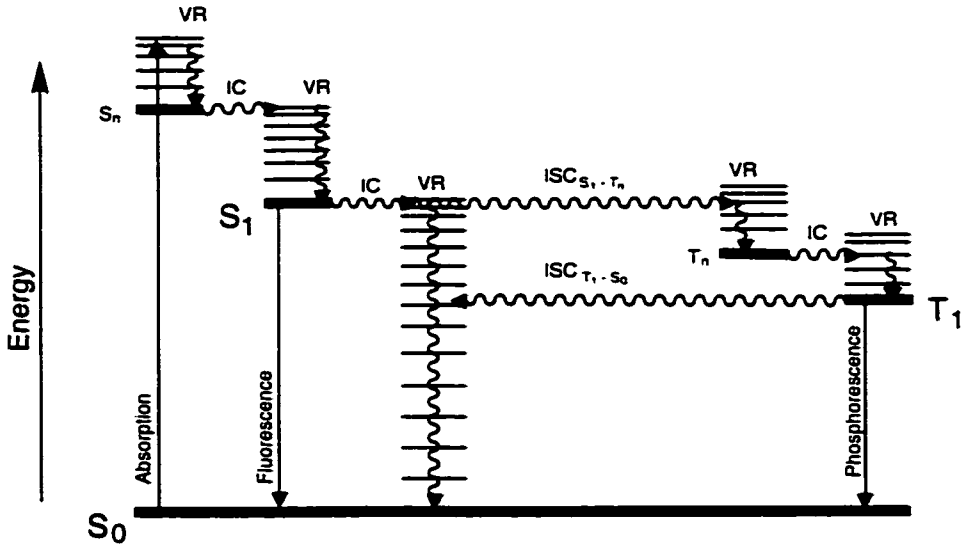

Figure 1-3: Jablonski energy diagram. Following absorption to an excited singlet state (S_n), the excess energy will be dissipated in the form of heat by vibrational relaxations (VR), and the lowest singlet excited state (S_1) will be populated. These processes of interconversion among states of same multiplicity by VR are commonly known as internal conversion (IC). S_1 will either decay by fluorescence or by internal conversion to the ground state. Alternatively, it will undergo intersystem crossing (ISC) and populate an excited triplet state (commonly T_1, although higher energy triplet states (T_n) may also be populated). Note that intersystem crossing involves an interconversion between states of different multiplicity, *i.e.*, singlet to triplet or

triplet to singlet. If the triplet state is higher in energy than T_1, it will undergo fast IC to populate the lowest triplet state, where from decay to the ground state following phosphorescence or ISC will occur.[7]

Interconversion among different electronic states is very fast. The observed chemical reactivity of an excited state is usually the result of competition between a relatively slow decay to a state of lower energy, compared to a relatively fast rate constant for chemical reactions. It is the competition between photophysical and photochemical events, which determine if a given excited state will undergo chemical reactions, or deactivate either radiatively, or by heat dissipation. The lowest excited singlet and triplet states are bottlenecks in the downward way towards ground state. In particular, the lower triplet state, having a forbidden transition back to the ground state,[8] can be a very long-lived species. Photoinduced chemical reactions, with a few exceptions, will therefore occur from S_1 or T_1 as schematically illustrated in Figure 1-4.

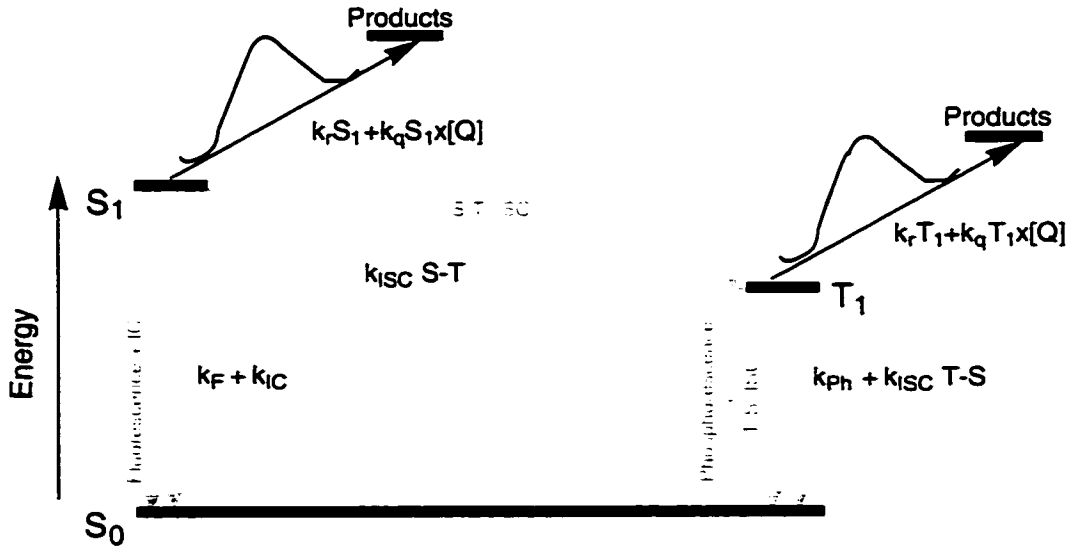

Figure 1-4: Modified Jablonski diagram, showing the many possibilities of deactivation for an excited state. Photophysical (gray arrows) and photochemical (black arrows) processes are illustrated. Rate constants for each process are also shown, thus k_r and k_q are rearrangement and quenching rate constants respectively; k_F and k_{Ph} are fluorescence and phosphorescence rate constants respectively; and k_{IC} and k_{ISC} are

the rate constants for internal conversion and intersystem crossing. The probability of a chemical reaction from S_1 will be given by the ratio of chemical rate constants ($k_r S_1+k_q S_1 x[Q]$) over chemical and physical ($k_F+k_{IC}+k_{ISC}ST$) rate constants. In the same way, the probability of chemical reaction from T_1 is given by the relative values of ($k_r T_1+k_q T_1 x[Q]$) over $[(k_{Ph}+k_{ISC}TS)+(k_r T_1+k_q T_1 x[Q])]$.

In order to predict the chemical reactivity of a newly populated electronic level, it is desirable not only to know its relative energy with respect to the ground state, but also it is important to establish its electronic configuration (*i.e.*, which set of molecular orbitals is most probably involved in the transition). A good example is given by formaldehyde, as shown in Figure 1-5.

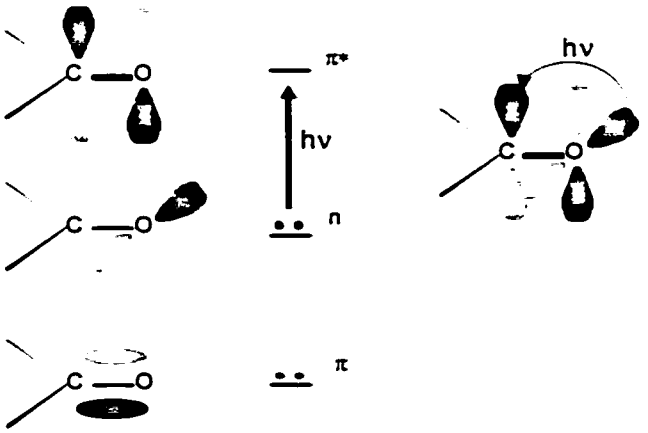

Figure 1-5: Ground state electronic configuration of formaldehyde (n^2). Also shown is the change in configuration to an n,π* excited state following light absorption.[8]

Thus, upon irradiation, the lowest energy transition involves the promotion of an electron from the n nonbonding orbital of oxygen, to the π* antibonding orbital. The configurataion of S_1 and that of T_1 is therefore denoted as n,π*.[8] We note that this configuration results in a very electrophilic oxygen atom for both S_1 and T_1, with an alkoxyl radical character (*vide infra*). This type of configuration is very common in the lowest triplet and singlet excited states of carbonyl containing compounds, like benzophenone.

1.3 Photosensitization, Type I and Type II Reactions

The previous sections are intended to explain that sunlight will be able to promote any of the xenobiotic agents into one of its many electronic levels while in a biologically relevant system. Following this excitation the potential danger of transporting exogenous chromophores in the blood stream will suddenly (*i.e.*, in few picoseconds) be transformed in a real toxic problem.

Once formed, an excited state, commonly named sensitizer in the field of photobiology, can transfer its energy to an acceptor, promoting the latter to a new excited state which otherwise may not be formed, given the low molar absorptivity of the acceptor molecule along the frequencies of solar radiation. The sensitizer can also react directly with other substrates,[9] and in the specific case that excitation occurs in the presence of oxygen the previous reaction is defined as a Type I. Under oxygen atmosphere the sensitizer will also interact directly with oxygen, either by energy transfer to form singlet oxygen, or by electron transfer; these are commonly known as Type II reactions.[10] These different reaction pathways are illustrated in Scheme 1-1.

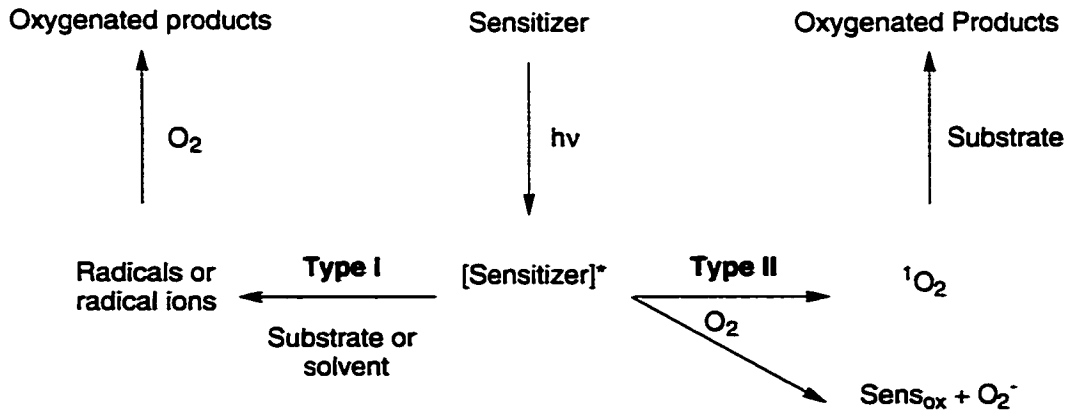

Scheme 1-1: Type I and type II photosensitized reactions.[10]

Photosensitized reactions are detrimental for important components of the cell. One such reaction is hydrogen abstraction by an excited chromophore (type I process). Schemes

1-2 and 1-3 show the consequences of hydrogen atom abstraction from a lipid and from deoxyribose sugar (which constitutes the DNA backbone), respectively. These types of photoprocesses are commonly encountered in studies of pharmaceutical products under short wavelength (*i.e.*, UV-A) irradiation conditions, and constitute a diagnostic for the phototoxicity of the former.[11-13]

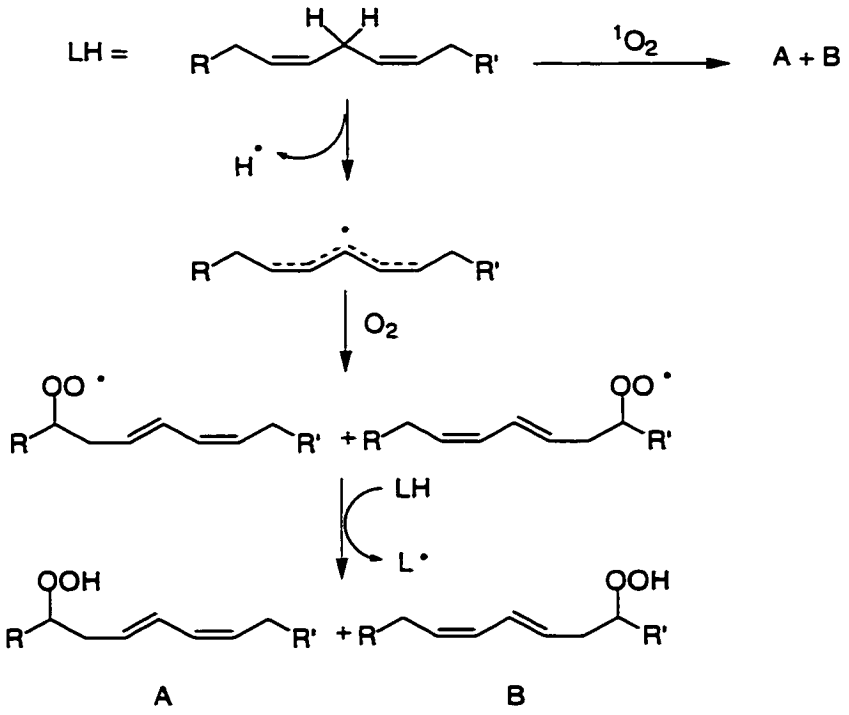

Scheme 1-2: Photooxidation of a β unsaturated phospholipid.[14]

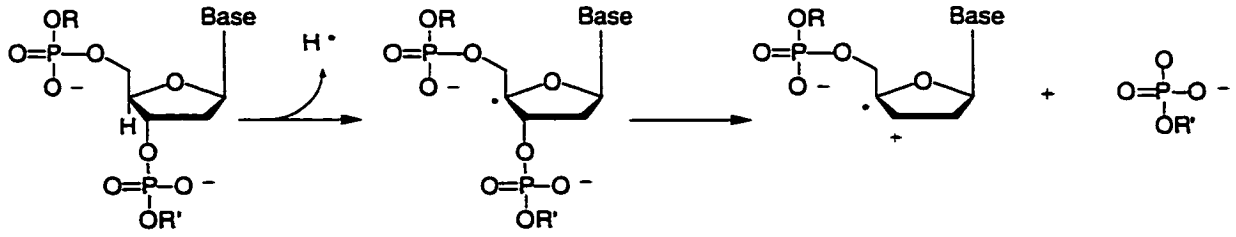

Scheme 1-3: Sequence of reactions following hydrogen abstraction from 2-deoxyribose.[15]

In the first case the result is the hydroperoxidation of a fatty acid, independently of the attacking reagent *i.e.*, singlet oxygen (type II) or excited chromophore and/or radical (type I). This type of reaction will most probably change the properties of the biological structure of which the lipid forms part; usually a cellular membrane. In the case of Scheme 1-3 the damage results in DNA cleavage, with potential mutagenic implications.[16]

Many species are responsible for the previously shown types of damage, they all belong to the category of reactive oxygen species (ROS) (*vide infra*).[17] Although their formation is sensitized by the action of a chromophore, it is the former species (*i.e.*, the ROS) that is mostly responsible for the biological damage. Note however that in the case of carbonyl compounds, their triplet state configuration has an alkoxyl-like radical structure, which reflects in their chemical behavior (see Scheme 1-4). Thus excited ketones do not only sensitize the formation of ROS; but also it is common to observe hydrogen abstraction reactivity, as well as carbon-carbon bond cleavage in position α to the carbonyl group for this type of chromophores.[7,8] Note that in the case of hydrogen abstraction, the ketone has to be located in the close proximity of the target.

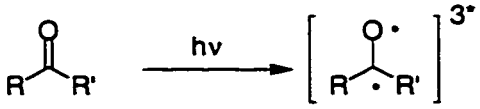

Scheme 1-4: Representation of the biradical character of a triplet ketone.

The previous observations acquire an even more dramatic perspective when it is realized that many of the pharmaceutical products employed as non-steroidal anti-inflammatory agents (NSAIDs), as well as other drugs intended for different treatments, are related to benzophenone, a diaryl ketone that has received ample attention in the literature as the "prototype" of an alkoxyl-like triplet state.[7,8] Thus, we can mention ketoprofen, fenofibric acid, tolmetin, tiaprofenic acid and suprofen as a few examples of a large list of compounds where a similar structure to that of benzophenone is found.

1.4 Reactive Oxygen Species

As it was previously mentioned many of the reactive oxygen species commonly encountered in oxidative stress can actually arise as a result of a sensitized reaction by a chromophore like benzophenone or a similar compound. Table 1-1 presents a list of these species.[17]

Table 1-1: Reactive oxygen species.[17]

Species	Name	Remarks
$O_2^{\bullet-}$	superoxide radical anion	One electron reduction state formed on quenching of radical anions.
$HO_2^{\bullet}$	hydroperoxyl radical	Protonated form of superoxide.
H_2O_2	hydrogen peroxide	Formed following hydroperoxide dismutation, or hydroxyl radical encounter.
$HO^{\bullet}$	hydroxyl radical	Formed by Fenton reaction, upon consumption of hydrogen peroxide.
$RO^{\bullet}$	alkoxyl radical	Formed by Fenton reaction, upon consumption of alkylhydroperoxide.
$ROO^{\bullet}$	alkylperoxyl radical	Formed following oxygen addition to a carbon centered radical.
ROOH	alkylhydroperoxide	Formed following hydrogen abstraction by the alkylperoxyl radical, or after singlet oxygen attack.
$^1\Delta_g\ O_2$	singlet oxygen	Formed following energy transfer by a sensitizer.
$[RR'CO]^3$	triplet carbonyl	Formed by direct excitation with light, or after energy transfer from a suitable donor.

Our organism is prepared to cope with the action of most of the species mentioned in Table 1-1, ever since they are natural intermediates of the metabolism. Thus enzymatic mechanisms exist for superoxide consumption (by means of superoxide dismutase), hydrogen peroxide elimination (by catalase), or alkylhydroperoxide dismutation (Cytochrome P-450).[17] These enzymatic mechanisms are also assisted in their preventive action by antioxidants and scavengers (*vide infra*), as a whole their role is to consume the ROS.

We can not anticipate to which extent if any, the photosensitized production of ROS outgrows that resulting from normal metabolism. However, local accumulation of sensitizers might result in a specific action as observed from the number of reports existing on adverse effects following ingestion of pharmaceutical products and sun exposure.[11,12]

1.5 Sunscreens and Antioxidants, Towards Prevention

Evolution has provided complex living organisms with solutions to confront environmental risks, thus the pigmentation existing in mammals and plants prevents their deterioration by direct excitation of their genetic material, *i.e.*, DNA, by UV-B light.[18] This pigmentation is absent in viruses or bacterias which render them vulnerable to high frequency radiation. One of those pigments protecting mammals is melanin, a polymer constituted by dihydroxyindole units, as shown in Figure 1-6. The brown color of this pigment is mainly due to the quinoid chromophores resulting from the oxidation of the dihydroxy groups.

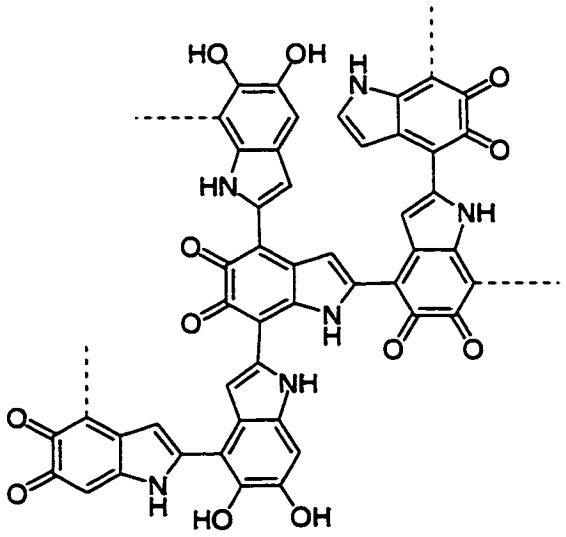

Figure 1-6: Structure of eumelanine.[19]

Melanin structure has a radical scavenger potential due to its phenol groups. Many studies have therefore been addressed to determine its capability as an antioxidant.[19-21]

An antioxidant is a molecule capable of scavenging ROS, while simultaneously rendering an innocuous radical which will not react with other biological substrates. Phenols have proved to be an excellent source of natural defense against ROS. Their mechanism of action is given by a series of consecutive steps represented in Scheme 1-5.

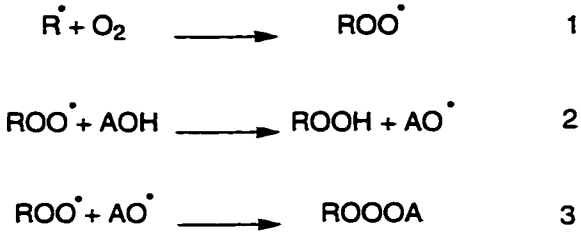

Scheme 1-5: Phenol inhibited peroxidation of unsaturated fatty acids.[22,23]

The first step and the chain event that results from this oxidation have already been exemplified in Scheme 1-2 with a generic β-unsaturated fatty acid. Step 2 involves the hydrogen abstraction by the alkylperoxyl radical from the phenol. Energetic considerations, as well as availability of the hydrogen from the phenoxy group will determine the feasibility of this reaction.[24,25] The final step involves the formation of nonradical products, a reaction that has been proven to be extremely fast for vitamin E.[22]

The combination of steps 2 and 3 thus eliminates two reactive oxygen species, rendering an innocuous compound.

The combined passive (as a sunscreen) and active (as a ROS scavenger) role of melanin shows that it is a very protective substrate. It is interesting in this sense to evaluate its role against excited carbonyl compounds.

1.6 Assessing the Damage

Photosensitization reactions have been studied *in vitro* with various biomolecules. Thus results on lipid peroxidation, protein crosslinking and DNA strand cleavage are frequently encountered in drug studies, as revealed in two recent reviews on the topic.[11,12]

Lipid peroxidation is monitored with UV spectrometry, which evidences the appearance of conjugated dienic hydroperoxides at 233 nm, upon oxidation of β unsaturated fatty acids (see also Scheme 1-2).[5,26]

Drug-protein adduct formation is usually determined by the retention of the photosensitizer absorption properties in the protein eluent following gel permeation chromatography (GPC) of an irradiated mixture containing a given drug and the protein.[27] Alternatively, a radiolabelled pharmaceutical product may be employed, and the radioactivity is measured in the different eluents following GPC.[28]

In the case of DNA photosensitization studies, a simple assay relies in the use of supercoiled DNA from bacteria, which upon strand scission results in a relaxed structure with a different migration pattern following gel electrophoresis.[29-31]

Studies of photosensitized cell lysis are commonly performed with erythrocytes and they are followed with absorption spectroscopy at 650 nm. The optical density at this wavelength (due to scattering by the erythrocytes) is proportional to the number of intact cells. Upon hemolysis the solution turns microscopically homogeneous and the scattering reduces in a linear manner with the amount of cells destroyed.[32,33]

The study of the nuclear DNA-damage in a cell is, on the other hand, much more involved than the previous experimental procedures. The methodology most commonly employed is the Comet Assay technique.[34] The complication of this technique relies in part on the necessity of isolating the nuclear material from the rest of the cell components; however the major factor lies in the measurement of the actual experimental parameter, given by the ratio in distance migration, following gel electrophoresis, for damaged *vs.* intact DNA.[35-38]

Care should be taken when analyzing DNA-damage that both no RNA is left as a contaminant in the solution to be analyzed, and that all damaged sites in DNA have resulted in a strand scission. Thus, whereas hydrogen abstraction from the sugar backbone of DNA ultimately results in a strand cleavage,[16] as shown in Scheme 1-4, oxidation resulting in nucleotide chemical modification will most certainly leave intact the polymer structure of DNA.[39]

In order to express this damage in terms of a strand scission, a second chemical step has to be employed. This step relies in the nature of the glycosidic bond between the base and the sugar. Following oxidation, electron density is removed from the nucleotide rendering it a better leaving group. Upon alkali treatment (usually performed with piperidine), the weakened glycosidic bonds connecting oxidized bases to deoxyribose are readily hydrolyzed, whereas the non-modified bases are left intact. The hydrolysis of the base is followed immediately by phosphate elimination at the resulting abasic site, as observed in Scheme 1-6.[39] It should be noted however, that not all oxidized bases are actually hydrolized, in which case repair enzymes can also be employed to produce strand scissions at the damaged sites.[39]

The alkaline conditions necessary to convert all the oxidized sites into strand scissions in DNA, also result in a complete hydrolysis of RNA phosphodiester linkages due to the participation of the 2-hydroxyl group in ribose (and which is absent in 2-deoxyribose) as shown in Scheme 1-7.[39]

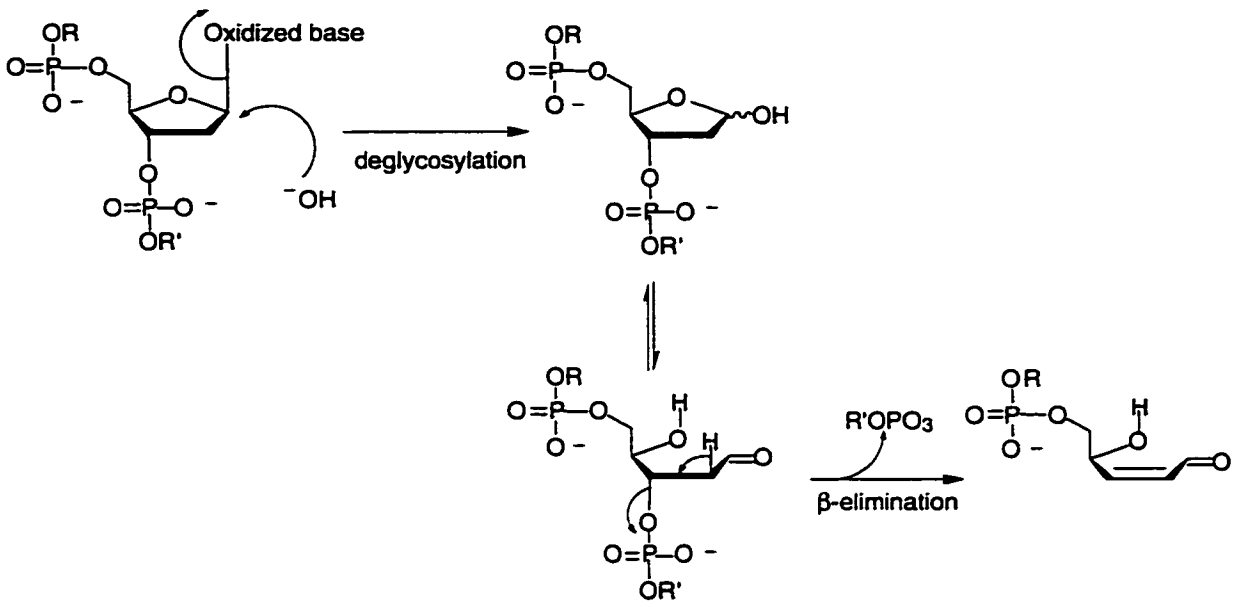

Scheme 1-6: Deglycosylation and strand scission under alkaline conditions following oxidation of a DNA base.[39]

The previous discussion is intended to show how delicate and sensitive the DNA-damage assessment is for an *in vivo* oxidized sample. This oxidation might be in particular the result of a photosensitized damage. While the other techniques provide us with a picture of the phototoxic potential of a given pharmaceutical product, the result on DNA-damage will be by far the most valuable one, given the implications on the long range that DNA-damage has on living organisms. These lesions, if unrepaired, will ultimately determine mutagenesis, cancer, aging and cell death.

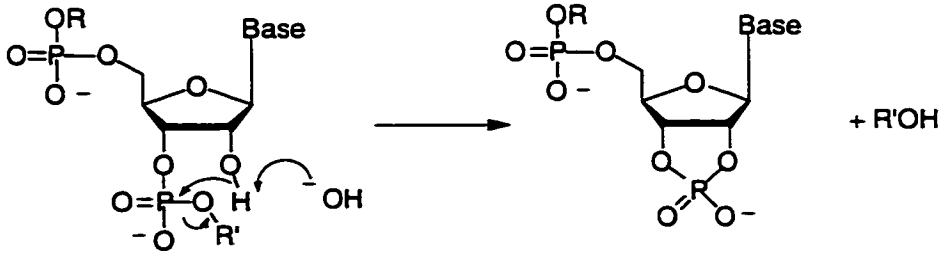

Scheme 1-7: Hydrolysis of RNA under alkaline conditions.[39]

1.7 Summary

This section has been intended to acquaint the reader with one of the problematic areas of photobiology, that of photosensitization. All the parameters that converge towards the end result of photosensitization have been analyzed; thus the sun as the source of radiation, the live tissue components as a source of sun-screening and as a media of reaction, and the active role that a xenobiotic chromophore might play, have been presented. Defense mechanisms that evolution has provided were briefly discussed.

A final part has also introduced the biological markers employed in estimating the potential photosensitizing behavior a given product has. This section has also briefly discussed the currently available methodologies employed in establishing the damage this markers suffer.

The following chapters in this thesis will address the photophysical and photochemical characterization of two pharmaceutical products, fenofibric acid and ketoprofen, both related to benzophenone. This analysis will also be performed with an α-diketone, precursor of a triplet state-oxygen adduct, a reactive oxygen species which has never before been monitored.

An analysis of antioxidants will also be performed keeping a close view on melanin precursors, and employing benzophenone triplet state as a reactive oxygen species.

The development of a novel technique to assess DNA-damage (a project performed with the collaboration of A. L. Vinette) will be presented, intended not only to be employed in quantitative evaluations of the photosensitizing potential on DNA-damage by certain pharmaceutical products, but also in the more general field of diagnostic of human exposure to radiation.

1.8 References

(1) Porter, G. Solar Energy; In *Light, Chemical Change and Life: A Source Book in Photochemistry*; J. D. Coyle, R. R. Hill and D. R. Roberts, Eds.; The Open University Press: Milton Keynes, 1982; 2-9.

(2) Robberecht, R. Environmental Photobiology; In *The Science of Photobiology*; Second Edition ed.; K. C. Smith, Ed.; Plenum Press: New York, 1989; 135-144.

(3) Bezzant, J. L., Penetration of Human Skin by Ultraviolet Light, *www-medlib.med.utah.edu/kw/derm/pages/meet_2.htm*,

(4) Condorelli, G.; Constanzo, L. L.; De Guidi, G.; Giuffrida, S.; Miano, P.; Sortino, S.; Velardita, A., Photosensitization Induced by Non Steriodal Anti Inflammatory Drugs: An Overview of Molecular Mechanisms in Biological Systems, *EPA Newsletter*, **1996**, *58*, 60-77.

(5) Miranda, M. A. Phototoxicity of Drugs; In *In Vitro Methods in Pharmaceutical Research*; Academic Press Limited: London, 1997; 290-315.

(6) Epstein, J. H. Photomedicine; In *The Science of Photobiology*; Second Edition ed.; K. C. Smith, Ed.; Plenum Press: New York, 1989; 155-192.

(7) Gilbert, A.; Baggott, J., *Essentials of Molecular Photochemistry*; Blackwell Scientific Publications: Oxford, 1991.

(8) Turro, N. J., *Modern Molecular Photochemistry*; University Science Books: Sausalito, 1991.

(9) Peak, M. J.; Peak, J. G. Photosensitized Reactions of DNA; In *CRC Handbook of Organic Photochemistry and Photobiology*; W. M. Horspool and P.-S. Song, Eds.; CRC Press, Inc.: Boca Raton, 1995; 1318-1325.

(10) Foote, C., Definition of Type I and Type II Photosensitized Oxidation, *Photochem. Photobiol.*, **1987**, *54*, 659.

(11) Boscá, F.; Miranda, M. A., Photosensitizing Drugs Containing the Benzophenone Chromophore, *J. Photochem. Photobiol. B: Biology*, **1998**, *43*, 1-26.

(12) Boscá, F.; Marín, M. L.; Miranda, M. A., Photoreactivity of the Nonsteroidal Anti-inflammatory 2-Arylpropionic Acids with Photosensitizing Side Effects, *Photochem. Photobiol.*, **2001**, *74*, 637-655.

(13) Mohtat, N.; Cozens, F. L.; Hancock-Chen, T.; Scaiano, J. C.; McLean, J.; Kim, J., Magnetic Field Effects on the Behavior of Radicals in Protein and DNA Environments, *Photochem. Photobiol.*, **1998**, *67*, 111-118.

(14) Girotti, A. W., Photodynamic Lipid Peroxidation in Biological Systems, *Photochem. Photobiol.*, **1990**, *51*, 497-509.

(15) Dizdaroglu, M.; von Sonntag, C.; Schulte-Frohlinde, D., Strand Breaks and Sugar Release by γ-Irradiation of DNA in Aqueous Solution, *J. Am. Chem. Soc.*, **1975**, *97*, 2277-2278.

(16) Pogozelski, W. K.; Tullius, T. D., Oxidative Strand Scission of Nucleic Acids: Routes Initiated by Hydrogen Abstraction from the Sugar Moiety, *Chem. Rev.*, **1998**, *98*, 1089-1107.

(17) Sies, H., Biochemistry of Oxidative Stress, *Angew. Chem. Int. Ed. Engl.*, **1986**, *25*, 1058-1071.

(18) Beddard, G. Biological ffects of Ultraviolet Radiation; In *Light, Chemical Change and Life: A Source Book in Photochemistry*; J. D. Coyle, R. R. Hill and D. R. Roberts, Eds.; The Open University Press: Milton Keynes, 1982; 178-197.

(19) Zhang, X.; Erb, C.; Flammer, J.; Nau, W. M., Absolute Rate Constants for the Quenching of Reactive Excited States by Melanin and Related 5,6-Dihydroxyindole Metabolites: Implications for Their Antioxidant Activity, *Photochem. Photobiol.*, **2000**, *71*, 524-533.

(20) Reszka, K. J.; Matuszak, Z.; Chignell, C. F., Lactoperoxidase-catalyzed Oxidation of Melanin by Reactive Nitrogen Species Derived from Nitrite (NO_2^-): an EPR Study, *Free Rad. Biol. Med.*, **1998**, *25*, 208-216.

(21) Stepién, K.; Porebska-Budny, M.; Hollek, A. M.; Wilczok, T., The Inhibiting Effect of Catecholamine-melanins on UV-induced Lecithin Peroxidation, *J. Photochem. Photobiol. B: Biol.*, **1992**, *15*, 223-231.

(22) Bowry, V. W.; Ingold, K. U., The Unexpected Role of Vitamin E (α-Tocopherol) in the Peroxidation of Human Low-density Lipoprotein, *Acc. Chem. Res.*, **1999**, *32*, 27-34.

(23) Ahrens, B.; Davidson, M. G.; Forsyth, V. T.; Mahon, M. F.; Johnson, A. L.; Mason, S. A.; Price, R. D.; Raithby, P. R., Neutron Diffraction Study of a Phenol·Nitroxide Radical Adduct: A Structural Model for Hydrogen Atom Abstraction by Peroxyl Radicals from Vitamin E and Related Phenolic Antioxidants, *J. Am. Chem. Soc.*, **2001**, *123*, 9164-9165.

(24) Paul, T.; Young, M. J.; Hill, I. E.; Ingold, K. U., Strand Cleavage of Supercoiled DNA by Water-soluble Peroxyl Radicals. The Overlooked Importance of Peroxyl Radical Charge, *Biochemistry*, **2000**, *39*, 4129-4135.

(25) Snelgrove, D. W.; Lusztyk, J.; Banks, J. T.; Mulder, P.; Ingold, K. U., Kinetic Solvent Effects on Hydrogen-atom Abstractions: Reliable, Quantitative Predictions Via a Single Empirical Equation, *J. Am. Chem. Soc.*, **2001**, *123*, 469-477.

(26) Vargas, F.; Canudas, N.; Miranda, M. A.; Boscá, F., Photodegradation and *in vitro* Phototoxicity of Fenofibrate, a Photosensitizing Anti-hyperlipoproteinemic Drug, *Photochem. Photobiol.*, **1993**, *58*, 471-476.

(27) Boscá, F.; Cuquerella, M. C.; Marín, M. L.; Miranda, M. A., Photochemistry of 2-Hydroxy-4-trifluoromethylbenzoic Acid, Major Metabolite of the Photosensitizing Platelet Antiaggregant Drug Triflusal, *Photochem. Photobiol.*, **2001**, *73*, 463-468.

(28) Miranda, M. A.; Castell, J. V.; Hernandez, D.; Gomez-Lechon, M. J.; Boscá, F.; Morera, I. M.; Sarabia, Z., Drug-photosensitized Protein Modification: Identification of the Reactive Sites and Elucidation of the Reaction Mechanisms with Tiaprofenic Acid/Albumin as Model System, *Chem. Res. Toxicol.*, **1998**, *11*, 172-177.

(29) Artuso, T.; Bernadou, J.; Meunier, B.; Piette, J.; Paillous, N., Mechanism of DNA Cleavage Mediated by Photoexcited Non-steroidal Antiinflammatory Drugs, *Photochem. Photobiol.*, **1991**, *54*, 205-213.

(30) Chouini-Lalanne, N.; Defais, M.; Paillous, N., Non-steroidal Antiinflammatory Drug-photosensitized Formation of Pyrimidine Dimer in DNA, *Biochem. Pharmacol.*, **1998**, *55*, 441-446.

(31) Maguery, M. C.; Chouini-Lalanne, N.; Ader, J. C.; Paillous, N., Comparison of the DNA Damage Photoinduced by Fenofibrate and Ketoprofen, Two Phototoxic Drugs of Parent Structure, *Photochem. Photobiol.*, **1998**, *68*, 679-684.

(32) Constanzo, L. L.; De Guidi, G.; Condorelli, G.; Cambria, A.; Fama, M., Molecular Mechanism of Drug Photosensitization-II. Photohemolysis Sensitized by Ketoprofen, *Photochem. Photobiol.*, **1989**, *50*, 359-365.

(33) Valenzeno, D. P.; Trank, J. W., Measurement of Cell Lysis by Light Scattering, *Photochem. Photobiol.*, **1985**, *42*, 335-339.

(34) Agapakis-Caussé, C.; Boscá, F.; Castell, J. V.; Hernández, D.; Marín, M. L.; Marrot, L.; Miranda, M. A., Tiaprofenic Acid-photosensitized Damage to Nucleic Acids: A Mechanistic Study Using Complementary *in vitro* Approaches, *Photochem. Photobiol.*, **2000**, *71*, 499-505.

(35) Olive, P. L., DNA Damage and Repair in Individual Cells: Applications of the Comet Assay in Radiobiology, *Int. J. Radiat. Biol.*, **1999**, *75*, 395-405.

(36) Ostling, O.; Johanson, K. J., Microelectrophoretic Studies of Radiation-induced DNA Damages in Individual Mammalian Cells, *Biochem. Biophys. Res. Commun.*, **1984**, *123*, 291-298.

(37) Rojas, E.; Lopez, M. C.; Valverde, M., Single Cell Gel Electrophoresis Assay: Methodology and Applications, *J. Chromatogr., B:*, **1999**, *722*, 225-254.

(38) Collins, A. R.; Dobson, V. L.; Dusinská, M.; Kennedy, G.; Stetina, R., The Comet Assay: What Can it Really Tell Us?, *Mutat. Res.*, **1997**, *375*, 183-193.

(39) Burrows, C. J.; Muller, J. G., Oxidative Nucleobase Modifications Leading to Strand Scission, *Chem. Rev.*, **1998**, *98*, 1109-1151.

2. Time-resolved Laser Techniques

2.1 Introduction

This chapter deals with photophysical time-resolved techniques applied to the mechanistic study of drug photodegradation. Most of the techniques here (phosphorescence being the exception) rely on the excitation of the sample by means of lasers emitting wavelengths from the UV-A to UV-B regions. The availability of short pulses (up to femtosecond time duration) makes lasers an excellent tool to study the mechanism of photodegradation of compounds. The scope of this chapter is to show which techniques are available in our group, and the information that can be extracted from them. Examples related to the problem of drug photochemistry will be shown whenever possible.

A section is also presented, intended to keep any researcher, new in the laser techniques field, from falling into common, though nontrivial, mistakes. Thus, in "Notes from the Bench" some hints are given as to what to do to get the best out of the measurements.

This chapter thus intends to summarize Prof. Scaiano's as well as previous group members' teachings. It also intends to keep the spirit that techniques are a necessary tool to learn more about the particular systems of interest under study.

2.2 Time-resolved Absorption Techniques

In this section different time-resolved absorption techniques are discussed, where the transient species are monitored over time by registering their electronic transitions. These techniques allow us studying both the disappearance of the originally formed transients, as well as the formation of new species.

Following a short light pulse, the excited state formed is interrogated by light beams from the UV-visible. The experimental magnitude measured is a change in absorbance (ΔOD) reflecting changes in transmitted light from the probe beam, before ($I_{t=0}$), and after ($I_{t=t}$) laser excitation (see Equation 2-1 and Figure 2-1).

Equation 2-1

$$\Delta OD_{t=t} = -\log\left(\frac{I_{t=t}}{I_{t=0}}\right)$$

2.2.1 Nanosecond Laser Flash Photolysis

Most of the time-resolved data currently available on the photodegradation of drugs have been obtained with nanosecond laser flash photolysis (N-LFP). First developed in the late 1960s,[1] this technique allows the observation of the absorption (or emission) of transients generated following excitation by short laser pulses (*ca.* 5 ns).

2.2.1.1 Experimental Setup

Figure 2-1 shows the main components of the nanosecond laser flash photolysis setup.

The concept of the instrument is the same as the original one, first employed by Lindqvist,[1] *i.e.*, it is a spectrophotometer capable of acquiring data at a high sampling rate. Significant changes have been made however in terms of size, price and operation capability of the instrument over three decades.

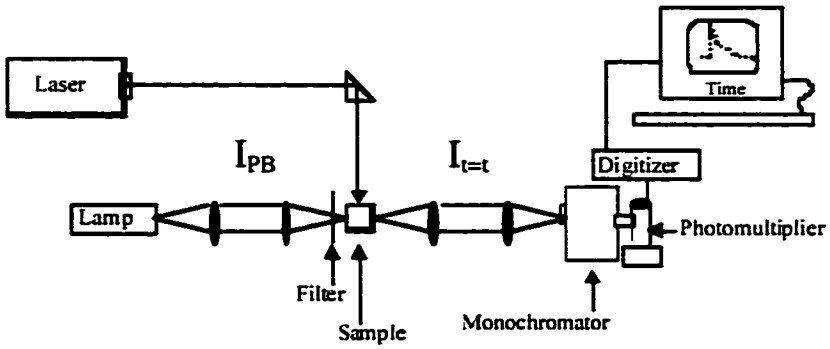

Figure 2-1: Schematic diagram of a nanosecond laser system.[2]

We have recently developed a "minisystem" where in addition to an improvement in time resolution and manipulation of the software, we have extensively reduced the space requirements.

2.2.1.2 Types of Measurement

2.2.1.2.1 Transient Spectroscopy

The use of Xenon lamps as monitoring beams permits the acquisition of transient spectra from *ca.* 250 nm, and throughout the visible spectrum, and up to 800 nm. The spectra are usually recorded on a point by point basis, where the time of data capture is preset before the acquisition, and the wavelength is changed over the course of the experiment. The resultant spectrum obtained is called a difference spectrum (ΔOD), and results from the difference in the molar absorptivity (at the probed wavelength) of the ground state (ε_{gs}) and the transient (ε_T) formed following excitation. This is best described by Equations 2-1 to 2-6.

Equation 2-2: $$OD_{t=0} = \varepsilon_{gs} \times l \times C_{gs}$$ Abs. at t = 0

Equation 2-3: $$OD_{t=t} = \varepsilon_{gs} \times l \times (C_{gs} - C_T) + \varepsilon_T \times l \times C_T$$ Abs. at t = t

where $OD_{t=0}$ and $OD_{t=t}$ are the absorbances before and after excitation respectively; C_{gs} is the ground state concentration before excitation, C_T is the transient concentration produced following excitation, and l is the cell optical path. Combining Equations 2-2 and 2-3 we obtain the change in absorbance after laser excitation (see Equation 2-4).

Equation 2-4: $$\Delta OD_{t=t} = (\varepsilon_T - \varepsilon_{gs}) \times l \times C_T$$

from Lambert and Beer's law we know that the transmitted intensity of the probe beam before and after the laser excitation is given by Equations 2-5 and 2-6.

Equation 2-5: $$I_{t=0} = I_{PB} \times 10^{(-\varepsilon_{gs} \times l \times C_{gs})}$$

Equation 2-6: $$I_{t=t} = I_{PB} \times 10^{(-\varepsilon_{gs} \times l \times C_{gs} + (\varepsilon_T - \varepsilon_{gs}) \times l \times C_T)}$$

from Equation 2-4, 2-5 and 2-6: $$\Delta OD_{t=t} = -\log\left(\frac{I_{t=t}}{I_{t=0}}\right)$$

which is the same expression as Equation 2-1, where I_{PB} is the probe beam intensity incident in the sample (see Figure 2-1), $I_{t=0}$ is the transmitted light (from the probe beam and into the detector) before excitation, and $I_{t=t}$ is that following laser excitation.

Experimentally, the magnitudes employed are those observed in Figure 2-2 and Equation 2-7.

Equation 2-7: $$\Delta OD_{t=t} = -\log\left(1 - \frac{signal_{t=t}}{I_{t=0}}\right)$$

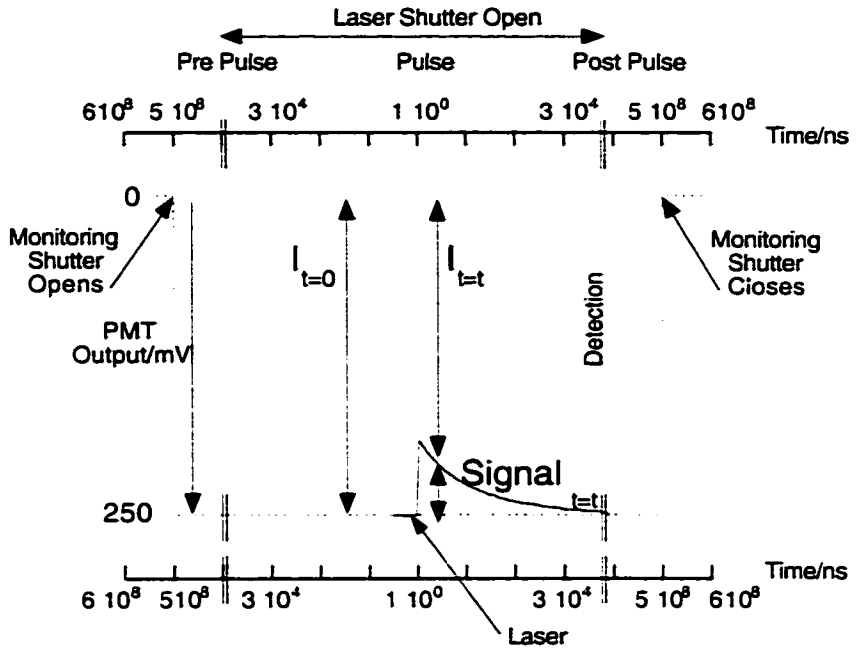

Figure 2-2: Plot of the PMT output versus time for a period starting 0.6 seconds before and ending 0.6 seconds after the laser pulse.

The difference spectrum obtained is characteristic of the transient in those wavelengths where the ground state is transparent (*i.e.*, $\varepsilon_{gs} = 0$), however, this is not the case at those wavelengths where the ground state absorbs, where the observed spectrum is precursor-dependant. Further, if $\varepsilon_{gs} > \varepsilon_T$, a negative signal is obtained; if $\varepsilon_{gs} < \varepsilon_T$, the observed signal is positive, and if both molar absorptivities are equal, no signal is observed, *i.e.*, $\Delta OD = 0$.

As an example, in Figure 2-3 we observe the triplet-triplet (T-T) absorption band of fenofibric acid measured in water and acetonitrile, together with the ground state absorption spectra for the molecule in the same solvents. Note that the T-T absorption shows a negative band where the ground state absorbs (*i.e.*, $\varepsilon_{gs} > \varepsilon_T$ at these wavelengths). Further, the 40 nm red shift in the maximum of the T-T absorption band is a reflection of the bathochromic shift observed in the ground state absorption (*ca.* 15 nm), upon an increase in solvent polarity.

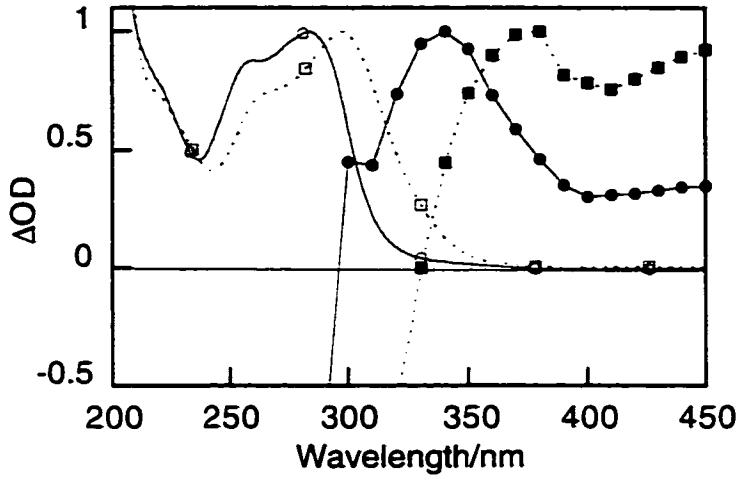

Figure 2-3: Normalized ground state absorption spectra of fenofibric acid in (O) acetonitrile and (□) water (a few points are shown to assist in the visualization). Also shown is the normalized T-T absorption band in (●) acetonitrile 640 ns after the laser pulse, N_2; and (■) water, 160 ns after the laser pulse, N_2O, pH 7.4.[3]

Transients can be assigned based on their spectra following N-LFP. When a given species is suspected upon direct excitation of the substrate under study, the nature of the species can further be confirmed by observing the absorption spectrum of an *in situ* "synthesized" homologue; that is, by finding an alternate source of the same intermediate. Two approaches can be employed; one relies in choosing an appropriate precursor which, following excitation by the laser, will react with the ground state of the substrate of interest, to give the suspected transient. Alternatively, the excited state of the substrate can be chemically quenched by ground state species to produce the suspected transient in high yields. Table 2-1 presents some common precursors, and the transients they produce following reaction with the ground state substrate. Also shown are common quenchers of excited substrates. In the case of energy transfer systems, the precursor is referred to as a sensitizer.

Table 2-1: Precursors most commonly employed in the study of pharmaceutical products, as well as the product of their reaction.[a]

Chromophore	Ground state quencher	Reaction	Product observed	Ref.
$SO_4^{\cdot-}$	substrate	electron transfer	1 e^- oxidized	4-6
chloranil triplet				7
substrate	chloranil	electron transfer	1 e^- oxidized	8
	$MeV^{2+\cdot}$			9
substrate	triethylamine, aniline	electron transfer	1 e^- reduced	10,11
tert-butoxyl radical	substrate	hydrogen abstraction	radicals	12-14
triplet sensitizers	substrate	energy transfer	triplet state	15-18

[a] **"Substrate" can be a ground or excited state.**

2.2.1.2.2 Kinetics

The ability to monitor a transient over time makes laser flash photolysis (LFP) an excellent technique for the study of the mechanism of reactions by following the kinetics of the transients formed following laser excitation. With N-LFP we are limited to transients whose lifetimes are at least two times longer than the duration of the laser pulse, *i.e.*, 15 ns. The digitizer determines the limit for the longest measurable lifetime, and values up to 100 ms are currently observable with our mini LFP system.

We can approach the discussion of a given problem with examples, now that we have established the time window where the technique can be employed,

Figure 2-4 shows common situations encountered in mechanistic studies. These traces are analyzed with the kinetic equations described in Table 2-2, or an appropriate combination of them. A detailed description of the derivation of these equations can be found in any kinetics textbook (see for example the work by F. Wilkinson[19]) only the method to follow the transient species, i.e., registering its absorption over time, is particular to N-LFP.

Table 2-2: Mathematical expressions for the observed evolution of the transient absorption with time.

Kinetic equation	Mathematical expression
first order decay	$\Delta OD_{t=t} = \Delta OD_{t=0} \times e^{(-k_{exp} \times t)}$
first order growth	$\Delta OD_{t=t} = \Delta OD_{t\to\infty} - \Delta OD_{t\to\infty} \times e^{(-k_{exp} \times t)}$
second order decay	$\Delta OD_{t=t} = \left[\frac{1}{\Delta OD_{t=0}} + \frac{k_{exp}}{\varepsilon_T \times l} \times t \right]^{-1}$
second order growth	$\Delta OD_{t=t} = \left[\frac{1}{\Delta OD_{t\to\infty}} \right]^{-1} - \left[\frac{1}{\Delta OD_{t\to\infty}} + \frac{k_{exp}}{\varepsilon_T \times l} \times t \right]^{-1}$

where l represents the cell optical path length, ε_T the transient molar absorptivity, k_{exp} is the experimental rate constant and $t\to\infty$ is the time for a growth to reach its plateau.

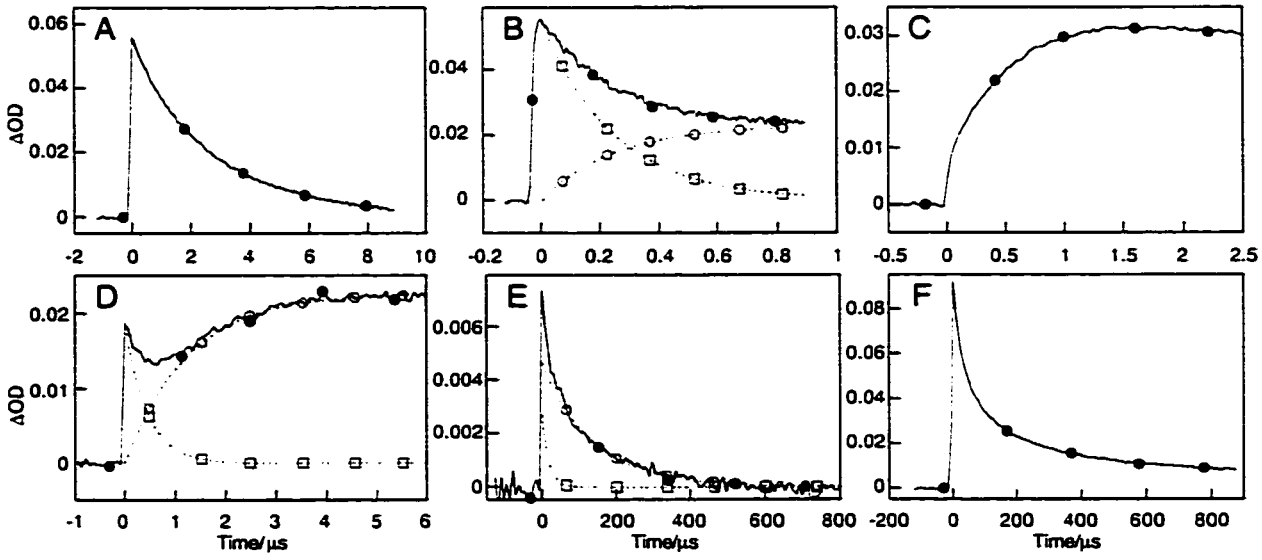

Figure 2-4: Representative N-LFP traces recorded under a variety of conditions (a few points are shown to assist in the visualization). The reader is referred to the original publication for mechanistic details. Only a few representative points are shown with labels in each trace. (A) (●) First order transient decay of ketoprofen in water-acetonitrile solution; X_{water} 0.7, recorded at 520 nm.[20] (B) (●) Transient decay of ketoprofen in methanol solution recorded at 520 nm. Also shown are the calculated traces for the first order decay of the triplet state (□), and for the first order growth of the ketyl radical (○).[20] (C) (●) First order transient growth of a sample

containing melatonin in 2:3 di-*tert*-butyl peroxide:acetonitrile recorded at 490 nm.[21] (D) (●) Transient absorption evolution with time for fenofibric acid in phosphate buffer solution recorded at 340 nm. Also shown are the calculated traces for the first order decay of the triplet state (□), and for the first order growth of the ketyl radical (○).[3] (E) (●) Transient decay of naphazoline in phosphate buffer solution recorded at 640 nm. Also shown are the modeled traces for the first order decay of the triplet state of naphazoline (□), and for the first order decay of the naphazoline radical cation (○).[4] (F) (●) Second order transient decay of diflunisal in phosphate buffer solution recorded at 350 nm.[14]

The examples shown correspond to relatively simple cases, but more complex situations might arise. The information obtained from these traces can further be increased by a selection of quenchers, which upon altering the observed kinetics, provide further information regarding the nature of the transient.

The simple first order decay observed in Figure 2-4-A is characteristic of a transient that generates a product with the same molar absorptivity than that of the starting material (*ca.* 0 in the present case) at the probed wavelength, or simply does not undergo any net chemistry. The triplet state of ketoprofen in acetonitrile is a good example of the latter situation (see also Chapter 4).[22]

Most commonly encountered is the case exemplified in Figure 2-4-B in which the transient decays to form a new species, which also absorbs at the monitoring wavelength. The second transient can further be studied by monitoring over longer times, to determine its fate. The example shown is that of ketoprofen in methanol, where the triplet state of ketoprofen abstracts hydrogen from the solvent to form a ketyl radical also absorbing at the probed wavelength (see also Chapter 4).[20] A close view of Figure 2-4-B shows that the resultant profile is due to the first order decay of the triplet (open squares), and the first order growth of the ketyl radical (open circles), both with the same rate constant given their precursor-product relationship.

In both the situations observed in Figures 5.A and 5.B it is common to add a quencher that will introduce a new mechanism for the deactivation of the transient (T) produced following excitation of the ground state (GS). Energy acceptors, radical traps, hydrogen donors, O_2, electron donors or acceptors, etc. (see Tables 2-1 and 2-3), are the most common. We observe how (if any) the experimental rate constant (k_{exp}) increases in the presence of these quenchers (Q). The situation is exemplified in Scheme 2-1.

$GS \xrightarrow{h\nu} T \longrightarrow P_T$	without quencher	$k_{exp} = k_0$
$GS \xrightarrow{h\nu} T \xrightarrow{Q} P_T + P_Q$	with quencher	$k_{exp} = k_0 + k_Q \times [Q]$

Scheme 2-1: Change in the decay rate constant with the addition of a quencher.

The linear dependence of k_{exp} with quencher concentration yields the value for k_q (see Figure 2-5-A for a quenching plot example). The nature of the observed transient can be assigned based on a comparison of the obtained k_q with literature values.

The selection of a given quencher aims to rule out or confirm the identity of a given type of transient. Many different types of quenchers can be used, and naming only some of them may appear arbitrary. We have chosen to mention only those most commonly employed in the study of drug photostability, which are presented in Table 2-3.

The situation observed in Figure 2-4-C is quite different to those previously discussed. Here a "transparent" transient (T) is decaying following quenching by Q to form a product (P), which readily absorbs at the monitoring wavelength. In this example T is *tert*-butoxyl (*t*-butoxyl) radical, Q is melatonin and P the radical of melatonin (see Scheme 2-2).[21]

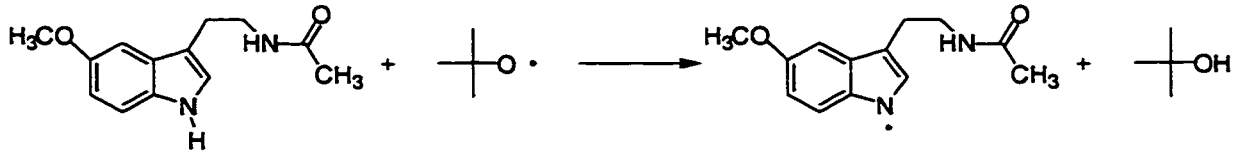

melatonin *t*-butoxyl radical

Scheme 2-2: Hydrogen abstraction from melatonin.

Table 2-3: Most commonly encountered transients and the quenchers employed in their study.

Transient	Quencher	Ref.
solvated electron	2-chloroethanol	23
	O_2	3
	N_2O	24
triplet state ($E_T \geq 240$ kj/mol)	naphthalene, 1-naphthalenemethanol	3,25
	1,3-cyclohexadiene	8,20
	sorbic acid	4,22
triplet state ($E_T < 240$ kj/mol)	β-carotene	15
	O_2	16
	4-OH-TEMPO	26
[a] carbon centered radical	O_2	27
	TEMPO	28,29
carbanion	O_2	20,22
	Cu^{2+}	26,30
	MeV^{2+}	26
radical anion	electrophile	31
carbocation	sodium azide, H_2O	6,32
	Cl^-, ethanol	33
radical cation	cysteine, sodium azide, HO^-,	5,8
	N,N,N',N'-tetramethyl-*p*-phenylendiamine,	4,34
	MeOH, Br^-, $CH_3CO_2^-$, Cl^-	7
[b] singlet oxygen	sodium azide, DABCO, β-carotene	35

[a] Other type of radicals are described by Fossey *et al.*[36] [b] This quenchers react with singlet oxygen without net chemical change,[35] contrary to many other species (*vide infra*).

In the case that the product (P) does not lead to a signal producing species, an appropriate probe (S) can be added to the system. The condition for S is that following reaction with the transient of interest, it produces an absorbing species (P'); solutions are then prepared containing a fixed amount of S, and where the amount of quencher (Q) is varied, to determine k_q in a similar way as observed in Scheme 2-1. This situation is exemplified in Scheme 2-3. Interestingly, this "probe" methodology provides a way of determining rate constants for a reaction between T and Q where all the reagents and all the products are transparent to the technique employed. The price of course is that the medium of reaction must be established independently, since this methodology provides kinetic, not mechanistic information.

$GS \xrightarrow{h\nu} T \xrightarrow{Q} P_T + P_Q$	No signal observed	$k_{exp} = k_0 + k_Q \times [Q]$
$GS \xrightarrow{h\nu} T \xrightarrow{S} P_T + P_S$	Observed growth	$k_{exp} = k_0 + k_S \times [S]$
$GS \xrightarrow{h\nu} T \xrightarrow{S+Q} P_T + P_S + P_Q$	k_q determined	$k_{exp} = k_0 + k_S \times [S] + k_Q \times [Q]$

Scheme 2-3: Quenching kinetics with transparent transients.

The case of Figure 2-4-D is interesting to mention, given that the valley observed in the kinetic trace indicates that parallel reactions originating from two different transients are occurring. The decay and the growth have different rate constants, contrary to the case shown in Figure 2-4-B. In the example (see Scheme 2-4) we observe that the fenofibric acid excited triplet state is decaying following decarboxylation, while simultaneously photogenerated solvated electrons are reacting with ground state fenofibric acid to produce an absorbing transient at the monitoring wavelength (a ketyl radical in this case).[3] Whenever such a situation is found (*i.e.*, a "valley" in the transient absorption time evolution), the researcher should be aware that two transients with similar decay kinetics are reacting. Furthermore, a window where only one of the transients is observed must be found to analyze the mechanism of deactivation pertaining to this transient.

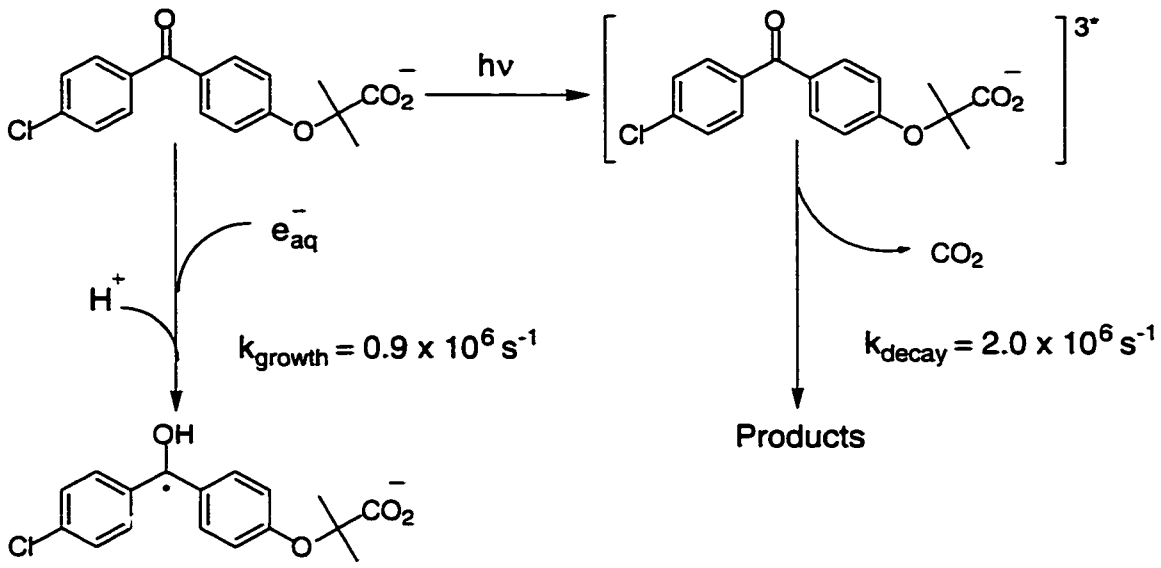

Scheme 2-4: Decay mechanism for transients formed following fenofibric acid excitation at pH 7.4 (see also Chapter 3).[3]

The parallel evolution of two different transients is also observed in Figure 2-4-E, however in this case, contrary to that of Figure 2-4-D, both transients are decaying, and the trace follows a biexponential rate law. In the example shown the observed traces are due to the triplet state and the radical cation of naphazoline, both generated in separate, independent ways.[4] However care should be taken since this type of time profile may also be obtained when the faster decaying transient is a precursor to the slower decaying species.[26]

The example shown in Figure 2-4-F is commonly encountered with very long lived transients, such as radicals under an inert atmosphere, and is due to the reaction involving two of these species. The second order decay shown reveals the time dependence of the phenoxyl radical of diflunisal, which reacts with the aryl radical of diflunisal formed after defluorination (see Scheme 2-5).[14]

Experimentally, biexponential and second order decays may occasionally be difficult to distinguish from one another; yet, the latter result from phenomena arising at very long times after the excitation. In fact, the shortest estimate for the half-life ($t_{1/2}$) value of a

transient decaying by reaction with another transient is *ca.* 1.7 x 10^{-6} s. Processes that are characterized by shorter lifetimes can be safely described by biexponential rate laws.

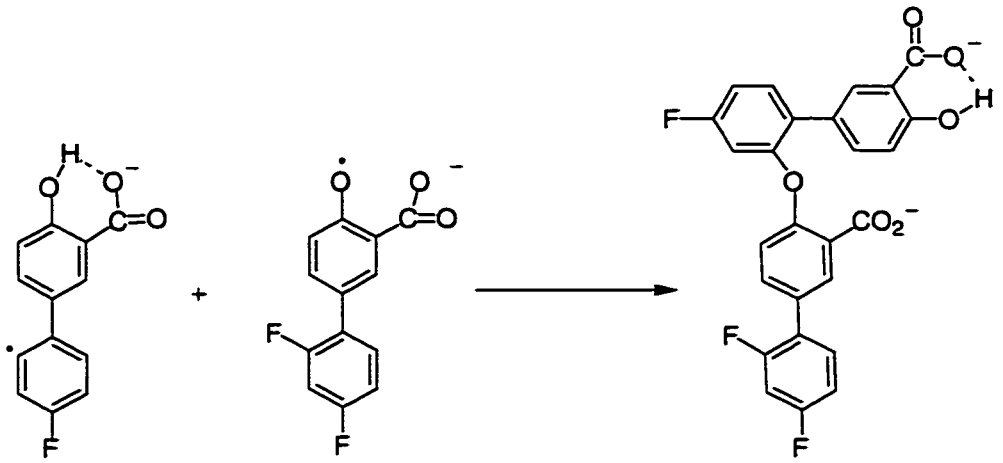

Scheme 2-5: Mechanism of reaction of diflunisal transients.[14]

The lowest estimate for the half life of a second order proces is obtained assuming that the concentration of transients ([*T*]) produced by a laser is *ca.* 6 x 10^{-5} M, (*vide infra*); and that they further react with a diffusion controlled rate constant (k_{diff}), *i.e.*, k_{exp} = 1 x 10^{10} M^{-1} s^{-1} (see Equation 2-8).

Equation 2-8:
$$t_{1/2} = \frac{1}{k_{exp} \times [T]}$$

2.2.1.2.3 Arrhenius Parameters

The capability of determining kinetics also allows the evaluation of the Arrhenius parameters for a given mechanism. This has proven very useful in those circumstances where it is difficult to determine if a reaction proceeds *via* a unimolecular or bimolecular step. The three order of magnitude differences in preexponential factors characterizing both processes is then employed as a diagnostic test. Measurement of rate constants (k_{exp}) in a temperature (T) range of *ca.* 50 K allows to establish both activation energies (E_a) and preexponential factors (A) for a given process according to Equation 2-9.

Equation 2-9: $$k_{exp} = A \times e^{\left(\frac{E_a}{R \times T}\right)}$$

The preexponential factor is a measurement of the probability of the reaction. Those chemical events which are unimolecular in nature are characterized by preexponential factors in the order of 10^{12} s^{-1} to 10^{14} s^{-1}. Reactions which require the encounter of two species are characterized by preexponential values in the range of 10^6 $M^{-1}s^{-1}$ to 10^8 $M^{-1}s^{-1}$.[37]

Arrhenius parameters have been of the utmost help in assigning decarboxylation processes. In this manner the preexponential values obtained for the decay of the transient formed after excitation of fenofibric acid (*ca.* 2 x 10^{12} s^{-1}),[3] or that obtained for tiaprofenic acid (*ca.* 1 x 10^{14} s^{-1}),[38] are a clear indication that a unimolecular process (decarboxylation) is involved in their deactivation. Similar temperature studies imply that ketoprofen decarboxylates within the duration (*ca.* 10 ns or less) of the laser pulse (see also Chapter 4).[20,39]

2.2.1.2.4 Transient Quantum Yield and Transient Molar Absorptivity

Two methods (closely related to each other) are employed to determine the quantum yield of transient formation in LFP.

1. Techniques that rely on the knowledge of the molar absorptivity of the transient.
2. Methods where an internal standard or actinometer is employed.

The value for the transient molar absorptivity (ε_u) is a prerequisite in the first approach. To determine this value we first search for a sensitizer of the transient of interest (benzophenone triplet state in our example). This sensitizer is the standard, and its molar absorptivity (ε_s) has to be known at a wavelength where the unknown transient (nabumetone triplet state) does not absorb.

The triplet state of benzophenone, with a molar absorptivity at 520 nm of 6500 $M^{-1}cm^{-1}$,[40] and a quantum yield for triplet generation of 1,[41] is well suited. We then establish the conditions for 95% quenching efficiency (or a similarly high percentage) of our standard (and therefore sensitization of our unknown). This is exemplified in Figure 2-5-A. Once the

conditions for efficient sensitization are established, we determine under these conditions the value for the molar absorptivity of the unknown transient (ε_u) based on Equation 2-10 (see also Figure 2-5-B).

Equation 2-10: $$\varepsilon_u = \frac{\Delta OD_u}{\Delta OD_s} \times 0.95 \times \varepsilon_s$$

On a third and final step, a power dependence of the transient absorption signals is performed both for the standard (ΔOD_s), and our unknown (ΔOD_u), at the wavelengths where the ratio of their molar absorptivities have been determined (see Figure 2-5-C). To that effect optically matched solutions at the excitation wavelength are employed.

At a given laser power, the ratio of concentrations of standard ($[T_s]$) and unknown transients ($[T_u]$) is given by the Lambert and Beer's Law, see Equation 2-11.

Equation 2-11: $$\frac{[T_u]}{[T_s]} = \frac{\dfrac{\Delta OD_u}{\varepsilon_u \times l}}{\dfrac{\Delta OD_s}{\varepsilon_s \times l}}$$

The ratio of concentration is proportional to that of the quantum yield of generation for the standard (Φ_s) and unknown (Φ_u); and replacing ΔOD values by the slopes obtained from power dependence, we obtain:

Equation 2-12: $$\Phi_u = \frac{\dfrac{slope_u}{\varepsilon_u}}{\dfrac{slope_s}{\varepsilon_s}} \times \Phi_s$$

where l is the optical path length, and $slope_s$ and $slope_u$ are the slopes of the curves of standard and unknown transient absorbance *vs.* power, respectively.

A value of quantum yield for triplet state generation of 0.24 ± 0.03 is obtained in this manner for nabumetone.[8]

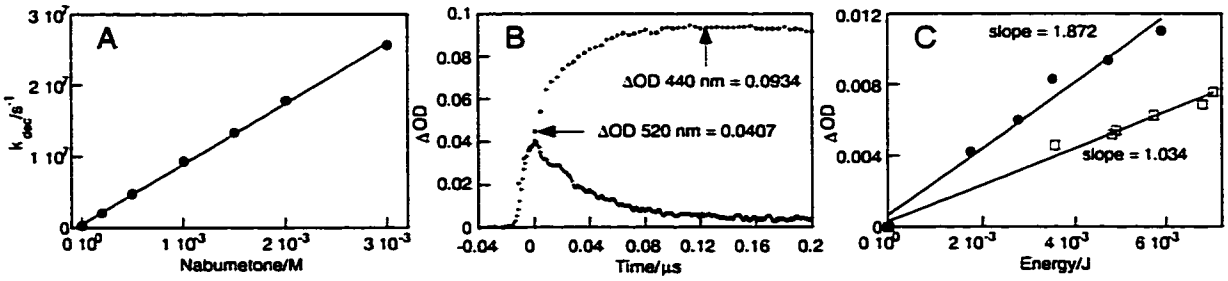

Figure 2-5: (A) Decay rate constant for benzophenone triplet state in acetonitrile at different nabumetone concentrations. (B) Kinetic profiles (●) for the decay of benzophenone triplet state monitored at 520 nm in the presence of 3 mM nabumetone and (□) for the sensitized growth of the triplet state of nabumetone monitored at 440 nm. (C) (●) Power dependence of the absorption of benzophenone triplet state and of (□) nabumetone triplet state.[22]

The second method for transient quantum yield determination employs two samples (an unknown and the standard) that following excitation produce the same type of transient. The two samples are optically matched at the excitation wavelength. We then make use of a reaction of this transient (common to both standard and unknown) with a suitable quencher that gives an observable absorption signal in LFP. Care should be taken at this point that the quenching efficiency is the same for both standard and unknown transient. The comparison of the value of the signal obtained for the quencher following reaction with the unknown transient (ΔOD_{Q-u}) and standard samples (ΔOD_{Q-s}), gives us the quantum yield for transient generation for the unknown, by knowing that of the standard (see Equation 2-13).

Equation 2-13:
$$\Phi_u = \frac{\Delta OD_{Q-u}}{\Delta OD_{Q-s}} \times \Phi_s$$

As an example we can quote the determination of the quantum yield for triplet generation of arylpropionic acids related to the benzophenone chromophore. In this case we use as an actinometer benzophenone, which is known to have a quantum yield for triplet formation of 1;[41] and we use the energy transfer to 1-methylnaphthalene as the monitoring reaction (following energy transfer, the growth of 1-methylnaphthalene triplet absorption is

monitored near its *ca.* 420 nm maximum). If the arylpropionic acid generates its triplet state with the same quantum yield as that of benzophenone, same signal intensity for the triplet state of 1-methylnaphthalene will be observed when both samples are analyzed in the laser system, provided the fraction of triplet quenching is the same. The ratio of the 420 nm signals is equal to that of the quantum yield of formation for the triplet states.

The mechanistic importance of determining transient quantum yields relies in that it enables us to compare the transient quantum yield with the product quantum yield, and in this way we can determine if a transient leads exclusively to products, or some of it regenerates starting material. An interesting example is the case of nabumetone previously discussed; the fluorescence of this molecule accounts for *ca.* 22% of its excited state deactivation. The triplet quantum yield is *ca.* 29%. Thus, we have a 49% of deactivation of the singlet excited state unaccounted for. The latter is assumed to proceed through intramolecular β-aryl quenching.[8]

2.2.2 Picosecond Laser Flash Photolysis

Picosecond Laser Flash Photolysis (P-LFP) has seldom been employed in the study of drug photochemistry. Due to the higher cost of the necessary equipment, and the time necessary for the maintenance of the instrument and sample measurement, it is a less frequent choice unless time resolution in the subnanosecond time regime is essential.

The principle is the same behind N-LFP, however, the experimental methodology is quite different.

2.2.2.1 Experimental Setup

The basic components are the same as those necessary in N-LFP. The main difference reflects the detection system employed. The fast evolution of events prevents the use of a normal digitizer, whose sampling rate is at best 2.0 GHz.[42] Two approaches are then used to obtain a time and wavelength profile, one implies the use of a streak camera (*vide infra*), the other, the use of a two-pulse, or pump-probe, technique.[42,43]

The two-pulse approach uses the same laser pulse for both excitation of the sample, and as a source of the probing light. In this way both the excitation and probing beams are locked in time with respect to each other. By choosing an appropriate delay between the arrival time of the excitation beam (always kept constant) and the probing beam (whose optical path is changed by reflecting it through a mobile reflector) the optical transmittance is recorded at different times following excitation. In this way, the detector simply acts as an intensity-measuring device, without the need to have a fast time response. A time profile is obtained at the wavelength of the probing beam by measuring the transmittance at different preset delays. Alternatively, the probe beam can be transformed in a continuous distribution of wavelengths,[44] and by employing a spectrograph, we can detect the transmittance of the excited sample over a spectral range, at a given time following excitation. The higher time limit is set in this type of setup by the optical path twice the physical displacement of the reflector. Note that this makes a fundamental difference between nanosecond and picosecond techniques. In the former, time delays are introduced by electronic devices. In contrast, in picosecond techniques time delays are based on changes in the optical path. In this sense picosecond techniques use the speed of light as the "calibration" for optical timing. Figure 2-6 illustrates this latter setup, which is the one currently employed in our lab.

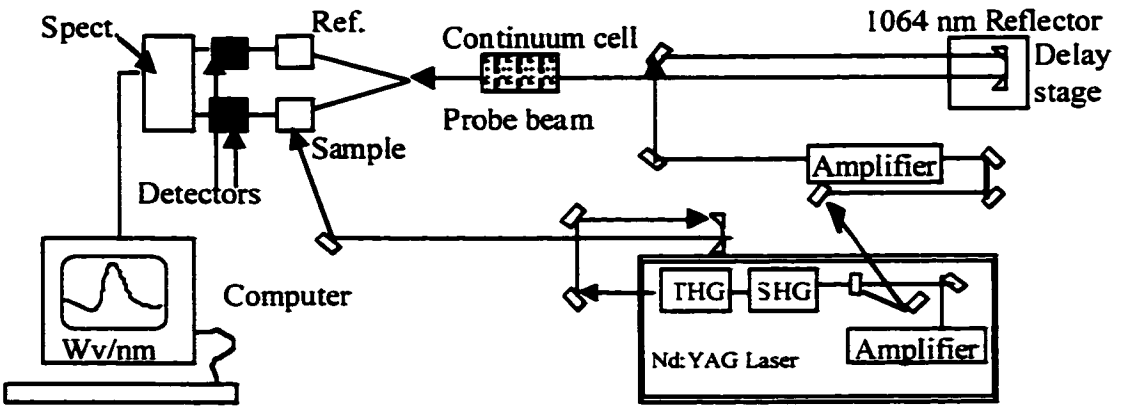

Figure 2-6: Schematic diagram of the picosecond laser system operated in the absorption mode. SHG and THG stand for second- and third- harmonic generating crystals, respectively.

2.2.2.2 Types of Measurement

Transient spectroscopy and kinetic measurements are available with the picosecond laser flash photolysis technique. However, in what regards to bimolecular kinetics, it is important to mention that very few quenching experiments are possible. This is a result of the short lifetime of transients explored, *i.e.*, up to 5 ns in P-LFP (k_{dec} = 2 x 10^8 s^{-1}). The quenching rate constants should be on the order of diffusional rates (*i.e.*, 1 x 10^{10} $M^{-1}s^{-1}$) for the quencher to be able to compete with such a fast decay, if its concentration is to be kept ≤ 0.1 M (see Scheme 2-6).

$k_{exp} = k_{dec} + k_Q \times [Q]$ $\qquad$ $k_Q \times [Q] \geq 10 \times k_{dec}$ $\qquad$ if 90% efficiency quenching is to occur.

Scheme 2-6: Considerations on quencher concentration.

Smaller quenching rate constants imply higher concentrations of quencher needed, which in turn may affect the polarity, viscosity and other solvent characteristics of the system.

The impossibility to perform reliable quenching experiments also pose difficulties for P-LFP techniques to be employed in determining transient quantum yields by means of internal or external actinometers.

The results most commonly reported with this technique involve intersystem crossings, intramolecular rearrangements, electron ejection, and other first order processes.

2.3 Time-resolved Luminescence Techniques

Time-resolved luminescence techniques are used to monitor the evolution of the excited state concentration of the particular compound under study. The amount of information attainable is reduced when compared to that available with absorption techniques, since we can only follow the fate of emissive states; yet, there is no information on species formed following its deactivation. The technique is extremely sensitive, since only emitted photons are counted on a background of zero emission, as compared with time-resolved absorption spectroscopy where the experimental magnitude is a difference in transmitted light.

We will discuss three different techniques of time-resolved luminescence (fluorescence, phosphorescence and near IR luminescence) each characteristic to a different type of excited states. Important time-resolved information on the photochemical behavior of drugs has been obtained with these techniques.

2.3.1 Fluorescence

The events observed in fluorescence are decays from the excited singlet state (S_1) back to the ground state of a molecule. These processes are very fast (with rate constants ranging from 1×10^6 s^{-1} and up to 1×10^{12} s^{-1}) and require the use of short laser, lamp or diode (LED) pulses to excite the sample. Two types of detection are commonly employed in time-resolved fluorescence studies; based on single photon counting or on streak camera detection.

2.3.1.1 Experimental Setup

2.3.1.1.1 Streak Camera

A streak camera is a device where the key component consists of a streak tube where the incident light is converted to electrons upon hitting a photocathode (see Figure 2-7). An accelerating electrode further accelerates the electrons. These are deflected with a sweep

voltage applied across their path, where the applied voltage changes with time, resulting in a time profile of the incident electrons.[45]

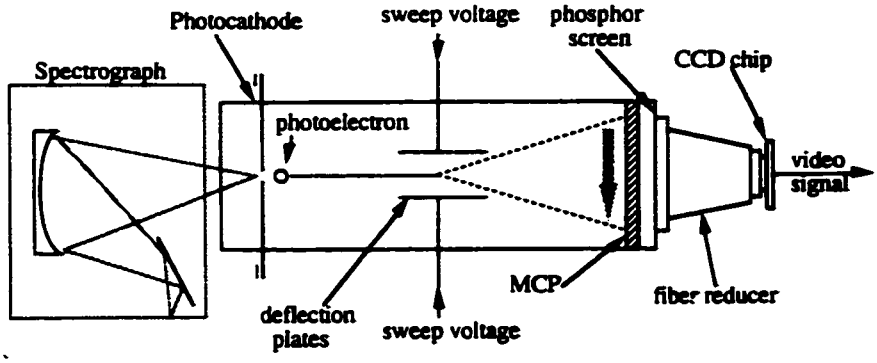

Figure 2-7: The various components in an electronic streak camera.[45]

After the electrons are deflected they are amplified in a multichanel plate (MCP), and then they hit a phosphor screen which is further read by a CCD camera, thus the electrical signal is reconverted to an optical one. If a polychromator is attached such that the light incident in the streak tube is already resolved in its component wavelengths, a three dimensional image is obtained where wavelength, time and intensity are obtained simultaneously.[45] This represents a great advantage in comparison with the single photon counting device method, where either the variation of intensity with time or with wavelength are acquired at a given time.

The time spent in data acquisition is much shorter in a streak camera than in a single photon counting since the former can be operated with a high light throughput. However, we find the intensity-time profile is not reliable after two intensity decades, and multiexponential analyses beyond three-exponential, are not recommended.

2.3.1.2 Types of Measurement

Time-resolved fluorescence should only be employed for those drugs where excited state deactivation is mediated by a radiative mechanism. Steady-state fluorescence is a very sensitive and simple technique, and can save a lot of time when used as a diagnostic prior to

time-resolved work. Pharmaceutical products where the chromophore is given by an arylketone structure are poor candidates for fluorescence time-resolved studies, given the fast intersystem crossing (ISC) that characterizes them.[37] Fluoroquinolones on the other hand are good candidates for this technique. The same applies to those compounds where their main structure can be associated with a fluorescent chromophore, such as nabumetone and naphazoline, both containing a naphthalene moiety.[4,8,46-48]

2.3.1.2.1 Kinetics

Time-resolved and steady-state fluorescence are interdependent as seen from Equation 2-14 which expresses the radiative lifetime (τ_{rad}) for a given compound in terms of the fluorescence quantum yield (Φ_F) and the lifetime of the excited state (τ_{dec}).

Equation 2-14: $$\tau_{rad} = \frac{\tau_{dec}}{\Phi_F}$$

Changes in fluorescence quantum yields (Φ_F) are normally correlated with fluorescence lifetimes. Thus, a modification in singlet state lifetime by intra and/or intermolecular quenchers can be studied. As an example of the former, we note the reduced Φ_F for naphazoline and nabumetone in comparison to that of their parent compound naphthalene. These reductions are accompanied by shorter singlet state lifetimes as compared to that of naphthalene, and are explained in terms of assisted intersystem crossing,[47] and β-aryl quenching respectively.[8] The basic concept behind this analysis is that radiative lifetimes are more or less constant for the basic chromophore.

Intermolecular quenching is often more difficult to monitor given the fast decay of excited singlet states. The problem is similar to that encountered in P-LFP, and described in Scheme 2-6 (*vide supra*), and relates to rate constants for quenching and practical quencher concentration limits.

The effect the environment exerts on the chromophore can also be probed by monitoring the fluorescence decay kinetics; in this regard, pH effects are commonly observed

in fluorescence lifetimes and Φ_F.[46] Environmental effects on singlet lifetimes can prove very informative in studies of the complexation of a pharmaceutical products with biopolymers. In this case modifications to the nonradiative deactivation pathway of the fluorophore can occur, resulting in a change in the fluorescence lifetime. Furthermore, the possibility of more than one type of complexation of a pharmaceutical product with a biomolecule will result in multiexponential decay traces, where the weight of each decay will indicate the relative abundance of a given type of drug-biomolecule complex. This type of phenomena is commonly encountered in fluorescent probes for DNA. In this case, dyes that intercalate at low dye/DNA ratio, will present a second type of binding upon further increase in their concentration. This situation will result in a biexponential decay, (see Equation 2-15)

Equation 2-15: $$I = a \times e^{(-k_{int} \times t)} + b \times e^{(-k_{groove} \times t)}$$

where *a* represents the weight of the fluorescence component arising from those DNA-intercalated dye molecules, *b* is the weight corresponding to the second type of complex (groove binding in most cases) and k_{int} and k_{groove} are the corresponding rate constants for decay of each type of complex.

2.3.1.2.2 Time-resolved Fluorescence Spectra

This type of information is less frequently reported. Changes in spectra with time are most commonly the result of solvent relaxation or intramolecular relaxation of the chromophore. They mostly relate to the interaction of the chromophore with its immediate environment.

2.3.2 Phosphorescence

Phosphorescence reflects the radiative decay of the triplet state to the ground state involving intersystem crossing. These processes are very slow (with rate constants ranging from 1 s^{-1} to ~ 1 x 10^6 s^{-1}) and therefore do not require the use of fast laser excitation. The study of this type of phenomena is greately facilitated in glass matrixes formed with solvent

mixtures at 77 K. Modern fluorimeters equipped with a flash lamp can be conveniently employed for this type of measurement.

Phosphorescence can be employed in the assignment of the symmetry of a given excited state. Transitions involving a change in the angular dipole moment (*i.e.*, $n,\pi^* - n^2$) result in a much faster decay from the triplet back to the singlet ground state than those where the angular momentum is conserved (*i.e.*, $\pi,\pi^* - \pi^2$). This is stated in El Sayed's rules (see scheme 2-7).

S_1-T_n transition	T_1-S_0 transition
$n,\pi^* - n,\pi^*$ forbidden	$n,\pi^* - n^2$ allowed
$n,\pi^* - \pi,\pi^*$ allowed	$\pi,\pi^* - \pi^2$ forbidden
$\pi,\pi^* - \pi,\pi^*$ forbidden	

Scheme 2-7: El Sayed's rules. The terms "allowed" and "forbidden" relate to symmetry. They are all spin forbidden.[16]

For example fenofibric acid presents an inversion in the first triplet excited state from n,π^* to π,π^* in going from low to high polarity solvents. The measured ten-fold increase in phosphorescence decay lifetime in a high polarity glass of ethylene glycol:water 2:1 as compared to a methylcyclohexane glass (see following chapter) can be rationalized within El Sayed's rules. This value and those for the reactivity of the triplet state of fenofibric acid are confirmatory of the occurrence of n,π^* to π,π^* triplet state inversion.

The use of glasses at 77 K prevents dynamic quenching since there is no diffusion in such systems. Phosphorescence lifetimes are therefore not employed in the study of dynamic quenching processes in glasses.

2.3.3 Near Infrared Emission

The great importance of near infrared emission is that singlet oxygen ($^1\Delta_g$ O_2) emits in this wavelength range, with a maximum at 1270 nm. This type of emission is

phosphorescence, given that singlet oxygen regenerates the ground state triplet oxygen following a radiative intersystem crossing.

Singlet oxygen is a common product arising from the interaction of excited states, most commonly triplet state, with molecular oxygen. After its sensitized formation, $^1\Delta_g$ O_2 can further react with biological substrates as well as the ground state of its sensitizer, producing a new chemistry not observed in anaerobic media.

Singlet oxygen is a better oxidating agent than molecular oxygen; its reactions include addition to double bonds, of particular importance in lipid peroxidation (see Scheme 1-2). We also include the ene reaction, as well as 2+4 and 2+2 additions in this category.[49] Because of this high reactivity, it is common practice to determine singlet oxygen quantum yield ($\Phi^1\Delta_g$) in oxygen or air equilibrated solutions when in the process of studying the photosensitizing properties of a drug. The quantum yield is determined by comparing the signal given by a previously selected standard with that resulting from an optically matched solution of the drug under study, immediately after the laser pulse, and in the same solvent and under the same oxygen pressure. Common sensitizers are those presented in Table 2-4.

Table 2-4: Common singlet oxygen sensitizers.

Sensitizer	Solvent	Φ_Δ	Ref.
$Ru^{2+}(bpy)_3$	water	0.41	50
rose bengal	acetonitrile	0.54	51
benzophenone	acetonitrile	0.37	51
hematoporphyrin	D_2O/buffer pH 7.4	0.65	52
phenalenone	CD_3OD	0.97	51
phenalenone	acetonitrile	0.98	53
phenalenone	H_2O	0.98	53

For a more extensive list including values in solvents of lower polarity see Carmichael *et al.*[15] and Wilkinson *et al.*[51]

Although it is common to report $\Phi^1\Delta_g$ in drug studies, the reactivity of singlet oxygen with its sensitizer is seldom mentioned. This should be considered, since upon $^1\Delta_g$ induced oxidation of ground state, the sensitizer might result in an even more photoactive species. On the other hand, if the sensitizer depletes $^1\Delta_g$ O_2, the latter will not be available to react with biologically relevant substrates.[4,54]

An important aspect in studying singlet oxygen generation is the choice of solvent. The following simple rules let us anticipate changes in lifetimes of singlet oxygen as a function of the solvent:[55-57]

1. The longest lifetimes are observed in perhalogenated solvents, although they are frequently poor solvents for most molecules of interest, particularly in the case of perfluorinated solvents.
2. The singlet oxygen lifetime (τ_{dec}^{Δ}) decreases upon increasing the number of hydrogen atoms in the solvent molecule.
3. The shortest τ_{dec}^{Δ} are observed with solvents having O-H groups, in particular, water.
4. The presence of heavy atoms reduces τ_{dec}^{Δ}.
5. Solvent deuteration invariably increases τ_{dec}^{Δ}.

Given the long radiative lifetime for singlet oxygen (τ_{rad}^{Δ}) in solution (it varies from *ca.* 5 s in H_2O to 0.33 s in CH_2I_2),[58] compared to a very fast deactivation rate constant (*e.g.* in water $\tau_{dec}^{\Delta} = 4 \times 10^{-6}$ s,[59]) it is difficult to observe its emission. Thus from Equation 2-14, we have that $\Phi_{emission}$ for $^1\Delta_g$ O_2 is *ca.* 1.25×10^{-6} in water. In order to do studies in this solvent it is therefore recommended to employ D_2O, or avoid it whenever possible, although this frequently proves difficult when biologically-relevant conditions need to be maintained.

2.3.3.1 Experimental Setup

Given the weak nature of its emission, the most important aspect in singlet oxygen measurements lies in the detector choice. Commercially available germanium diodes are most commonly employed. Figure 2-8 presents a scheme of our singlet oxygen setup.

A fast source of excited sensitizers (*i.e.*, a laser) is also necessary given the short lifetime of singlet oxygen (4 μs in water, 140 μs in acetonitrile, and 11μs in methanol).[59]

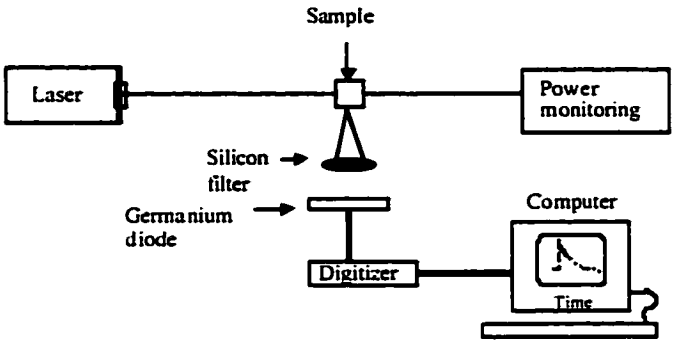

Figure 2-8: Singlet oxygen detection system.

2.4 Getting Reliable Data; Notes from the Bench

There are many "tricks" that contribute to make laser techniques a reliable source of mechanistic information, yet, as obvious as they might seem for researchers in the field, they might easily be overlooked by newcomers. In this section we introduce some of these ideas that help in the analysis and interpretation of data. They involve instrumental, mathematical and practical issues. Originally introduced in a review on polymer studies,[2] we further adapt this information to mechanistic studies of pharmaceutical products in solution.

2.4.1 Sample Absorbance

The ground state absorption of the sample (OD), should be in the order of 0.3 to 0.5 at the excitation wavelength and in the sample cuvette for LFP experiments, in order to maximize transient production. This results from the compromise between:

1. The exponential growth on the number of transients formed ($T_{(Cgs)}$) with ground state concentration for a given optical path (l), and quantum yield for the transient generation (Φ_T), see Equation 2-16.
2. The exponential decay on incident light ($I_{(l)}$) with distance along the optical path for a given sample concentration (C_{gs}), see Equation 2-17.

Equation 2-16 $$T_{(C_{gs})} = \left[1 - 10^{(-\varepsilon_{gs} \times C_{gs} \times l)}\right] \times I_0 \times \Phi_T$$

Equation 2-17: $$I_{(l)} = 10^{(-\varepsilon_{gs} \times C_{gs} \times l)} \times I_0$$

where the ground state absorption is given by the product (_gs x Cgs x l), and I0 is the incident light on the sample. This situation is better exemplified in Figure 2-9.

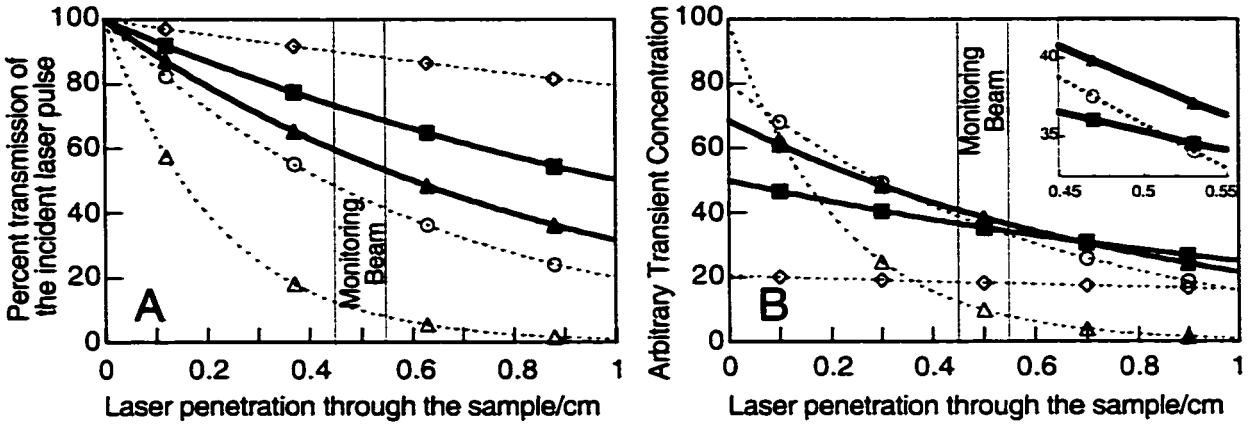

Figure 2-9: (A) Transmission of the laser pulse along the cell, and (B) percent absorbed photons along the path of the exciting laser beam for a ground state absorbance of: (△) 2.0; (○) 0.7; (▲) 0.5; (■) 0.3; (◇) 0.1. The inset in (B) shows the region explored by the monitoring beam.

The previous analysis holds true for a perpendicular configuration between probe beam and laser in LFP, however the situation is quite different in the case where both beams are parallel or nearly parallel, i.e., front-face configuration. In this case, there is no limit in the absorbance imposed by the previous restrictions; however, other factors make it important to keep the absorbance moderate. One of these factors is the potential generation of acoustic waves, which result from the deposition of the pulse energy in a thin layer of solution due to its high absorbance. The resultant acoustic wave is observed as a superposition (its pattern depending on the cell geometry and speed of sound of the solvent) on the decay trace. It should be avoided employing solutions with lower ground state absorbance.

When monitoring fluorescence with right angle emission detection, similar considerations as those presented for LFP apply. Further, if the Stokes shifts of the samples measured are small, self-absorption will be present at ground state absorption values of 0.3 at the excitation wavelength, this in turn will result in distorted fluorescence spectra. The absorbance should be kept below 0.1 in order to avoid this problem.

2.4.2 Transient Concentration

This is a very important consideration to be analyzed when contemplating transient-transient reactions or precursor-product relationships (vide infra). To establish the transient concentration, we assume what we find are our "best conditions" in terms of laser power, e.g., a 308 nm laser with energy delivery at the sample of 10 mJ/pulse. We also assume a volume irradiated by the laser (V) equal to 0.2 cm3 (i.e., 0.4 x 0.5 x 1 cm).

The number of moles of photons (I0) reaching the sample is given by equation 2-18.

Equation 2-18:
$$I_0 = \left(N_A \times \frac{h \times c}{\lambda} \right)^{-1} \times P$$

where h is Planck's constant, c is the speed of light, λ is the excitation wavelength, N_A is Avogadro's constant and P is the laser power per pulse.

The number of transient molecules formed (proportional to the number of photons absorbed, where Φ_T is the proportionality factor) is given by combining Equations 2-16 and 2-18 (see Equation 2-19).

Equation 2-19:
$$T_{(C)} = \left[1 - 10^{(-\varepsilon_B \times C_B \times l)} \right] \times \left(N_A \times \frac{h \times c}{\lambda} \right)^{-1} \times P \times \Phi_T$$

Assuming a ground state absorbance of 0.3 at the excitation wavelength, and a quantum yield for transient generation of 1, and upon dividing by the irradiated volume, we obtain that the excited state concentration is *ca.* 64 μM. It should be kept in mind that this value is a higher limit to the situation commonly encountered when employing laser techniques. In particular, picosecond lasers are characterized by a pulse energy which is at least an order of magnitude smaller.

2.4.3 Laser Power

In order to have good signal-to-noise ratios in any type of experiment, intense signals are always preferred, however, in the case of LFP care should be taken that in the setup

employed the overlap between the probe beam and the excitation beam should be optimum. If this is not the case, systematic errors will arise; further, these errors will be larger the higher the transient absorbance. These errors will affect both the measured ΔOD as well as the lifetime of the transient (the measured magnitude being smaller than the actual one for both cases).[2]

In the case of fluorescence studies, high intensities (and therefore big signals) are not desirable, this is particularly true in the case of Single Photon Counting (*vide supra*), but it is also a problem when employing a Streak Camera, due to saturation of the detector.

A big signal is the result of a high transient concentration, which in turn is directly proportional to the laser power (see Equation 2-19). We will mention two more reasons, common to all laser techniques, that suggest it is best not to work under high laser power conditions:

1. The number of transient-transient reactions will increase under these conditions, introducing new mechanisms for transient decay, see Lamp vs. Laser section (vide infra).
2. There exists the possibility that under these conditions, a transient formed following absorption of a photon by the ground state, will further absorb a second photon, which can result in a completely new type of chemistry: the photochemistry of transients. This effect is commonly encountered in our lab when employing high output lasers. We frequently find that an electron and a radical cation are formed following absorption of the second photon by a pharmaceutical product in aqueous solution.[4,14,20,22,26,47,60] Clearly, many of these molecules are prone to photoionization.

The dependence of the transient absorbance signal (*ΔOD*) with the laser power is a good diagnostic to establish if the observed photochemistry results from the absorption of only one photon (monophotonic) or two photons (biphotonic). The former presents a linear

dependence of ΔOD with power, contrary to the quadratic one encountered usually (but not always) in biphotonic processes (see Figure 2-10 and Equation 2-20).

Equation 2-20: $\Delta OD = a \times E + b \times E^2$

where ΔOD is the differential absorption following the laser pulse, E is the laser pulse energy, and a and b are coefficients depending on the yield of monophotonic and biphotonic processes respectively.[61]

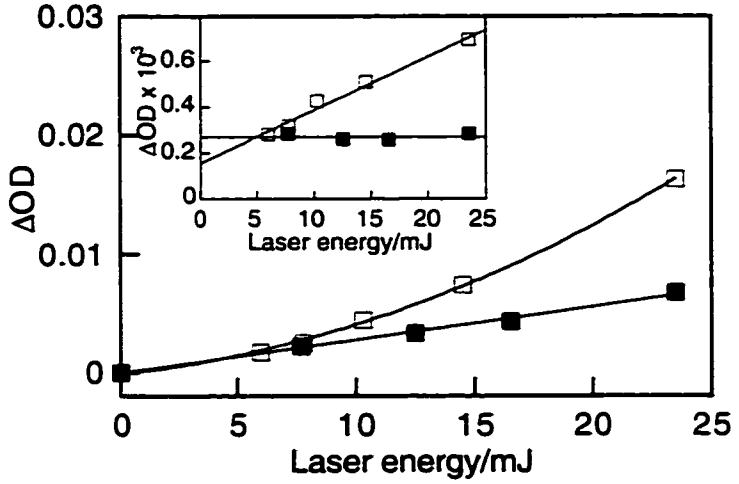

Figure 2-10: Laser power dependence for the transient absorption signal, taken 0.05 μs after the 308 nm laser pulse, observed in a tolmetin solution in phosphate buffer 10^{-2} M, pH 7.4. (□) 720 nm in N_2 equilibrated solution; (■) 640 nm in N_2O equilibrated solution. Inset: laser power dependence of the ratio between the transient absorption signal and the pulse energy.[26]

To avoid the problems arising from large transient concentrations we recommend employing a moderate laser power. This is very important when absorption of a second photon by a transient is to be avoided. Given the high molar absorptivity at the excitation wavelength for many of the compounds studied, it is not unusual to employ chromophore concentrations in the micromolar range in order to have a ground state absorbance of *ca.* 0.3. Under these conditions, complete depletion of the ground state can occur (as observed from the result of Equation 2-19), and will most probably result in the absoprtion of a second

photon by the excited state or by other reaction intermediates formed during the laser pulse. Depletion of the ground state is easily diagnosed by a power dependence measurement of the ΔOD. The observed trace will turn to a plateau at high laser powers, rather than presenting a linear or quadratic dependence (*vide supra*). An alternative to employing low laser powers is to irradiate with a longer wavelength laser, where higher ground state concentrations are frequently employed in order to have an appropriate absorbance at the excitation wavelength.

2.4.4 Lamp *vs.* Laser

To understand the importance of this section, we note that following lamp irradiation, steady-state transient concentrations of *ca.* 1×10^{-8} - 1×10^{-9} M are produced. From this value and that previously derived for laser experiments it is clear that there is at least a three order of magnitude difference between the transient concentration produced with lasers *vs.* lamps. This means that transient-transient reactions are more prone to occur in laser experiments, processes which would not be competitive when employing lamp excitation.

A clear example is that of the reaction of a carbon-centered radical with a scavenger, in competition with its own dimerization. Assuming a quenching rate constant of 1×10^{6} $M^{-1}s^{-1}$ and a quencher (scavenger) concentration of *ca.* 0.01 M, the initial pseudo first order rate constant for this process will be of *ca.* 1×10^{4} s^{-1}. In the case of the radical-radical dimerization, the initial rate constant, following laser excitation, will be 6×10^{4} s^{-1} (assuming a dimerization rate constant of 1×10^{9} $M^{-1}s^{-1}$, and a radical concentration of 60 μM). Thus, dimerization will be favored. When a lamp is employed, radical-radical dimerization events will be negligible, given that the initial pseudo rate constant for dimerization will be of only 1×10^{1} s^{-1}, *i.e.*, 1×10^{4} fold lower than radical trapping.

Care should be taken in the interpretation of results obtained with laser techniques, and their extrapolation to real case scenarios of drug photosensitization following sun light exposure. Transient-transient chemistry will not occur under the latter conditions in live tissue.[62]

2.4.5 Product Studies *vs.* Transient Studies

A good knowledge of the products formed is always desirable before undertaking a mechanistic study. Quantum yields of formation of transients, as well as products, are also useful before assigning a transient as the precursor of a given product.

We need to keep in mind that a transient molar absorptivity and the detection threshold set a limit in LFP for the quantum yield of generation of an observable species.

The lower limit for detectable ΔOD in N-LFP is *ca.* 0.005 at the maximum. Assuming it results from a strongly absorbing transient that has a high molar absorptivity (*ca.* 1 x 10^4 $M^{-1}cm^{-1}$), we obtain from Equation 2-21 that its concentration will be *ca.* 0.5 μM for a 1 cm optical path. Considering that 60 μM is the highest estimate for any given transient concentration to be produced (*vide supra*) we obtain that the lowest limit of quantum yield for transient formation resulting in an observable signal in N-LFP is *ca.* 0.5:60.

Equation 2-21: $$C_T = \frac{\Delta OD \times l}{\varepsilon_T}$$

Low quantum yields in product formation will then be the result of transients formed inefficiently following excitation (and which will therefore lead to a weak signal), or transients that although are formed in high yields (strong signal), decay without undergoing any net chemistry. This is the case of the triplet state of protonated ketoprofen in acetonitrile.[20]
We can also establish from the previous analysis that transients which molar absorptivity is smaller than ca 100 $M^{-1}cm^{-1}$ will not be normally detected even if produced with a quantum yield of 1.

2.4.6 Fittings and Chemistry

In the first part of this chapter we have shown complex kinetic traces observed due to the occurrence of more than one transient absorbing at a given wavelength (cases of Figures 2-4-B, 2-4-D, and 2-4-E). This type of situation is the rule rather than the exception in everyday work. The researcher is then faced with the option of either applying complex

mathematical equations, or simplifying the chemistry observed to whatever extent it is possible.

Two reasons determine that whereas mathematical techniques can safely be applied in fluorescence time-resolved studies,[63] they should be avoided in LFP whenever possible.

1. First, in luminescence techniques, such as single photon counting, the signal can be monitored over several intensity decades. In LFP the decay can be monitored over one or two intensity decades.
2. Second, in luminescence techniques it is usually a valid assumption that after infinite time the intensity of the light emitted will decay to zero. This is not the case in absorption spectroscopy, where residual absorption by stable, or transient but long-lived products, determines the signal level after "infinite time" (for example, see Figure 2-4-B).

Laser flash photolysis is a technique where chemical simplification is preferred to complex mathematical analysis. We illustrate this with the case of the photochemistry of fenofibric acid in aqueous buffer solution.

Following excitation of this compound with a 308 nm laser, solvated electrons, ketyl radicals and the triplet state of fenofibric acid can be simultaneously observed. When the same experiment is done with a 355 nm laser, only the decay of the triplet state of fenofibric acid is observed (see also Chapter 3).[3] Although the number of photons injected per unit volume of sample is approximately the same in both cases under our experimental conditions, ground state depletion in the 355 nm case is highly unlikely, since concentrations are 10 fold higher than those employed at 308 nm excitation. The photons are absorbed only by ground state molecules of fenofibric acid when employing 355 nm, rather than by excited triplet states of this molecule (in competition with the ground state), as is the case when the 308 nm laser is employed.

A complex situation with two transients decaying (fenofibric acid triplet state and solvated electron) and one being formed (ketyl radical), is simplified to that of only one transient decaying when employing the 355 nm laser.[3]

2.4.7 Same Kinetics, Same Transient?

No; same kinetics in two different absorption bands will not necessarily imply that the two bands are from the same transient. When an intermediate decays to form two new species, they will be formed with equal rate constants; that for the decay of their precursor. This is the principle applied in Scheme 2-3 to obtain quenching rate constants for a quencher that gives a transparent product from a transparent transient.

2.4.8 Flow System

As a general rule flow systems should be used when the sample will receive more than 2 laser shots per milliliter of solution. Three different effects in the observed kinetics might be encountered otherwise.

1. Substrate depletion. The signal will have a lower intensity after each laser shot; we can mention the photolysis of fenofibric acid sodium salt in low polarity media, which produces 4-chloro-4'-(1-hydroxy-1-methylethyl) benzophenone with a quantum yield of 0.35 (see the following chapter).[3]
2. Accumulation of a product capable of either leading to strong signals and/or a reduction of substrate excitation by absorbing part of the laser dose (internal screening). This is the case of the photodecarboxylation of ketoprofen, which results in the formation of ethylbenzophenone with a quantum yield of 0.75.[64,65] The new photoproduct retains the chromophore structure of ketoprofen intact, competing with the latter for the photons.
3. Generation of a substance which will participate in the transient photochemistry, *i.e.*, a quencher. This will be a problem with very long-lived transients.

Two more points are worth of consideration before finishing this section.

When recording an absorption spectrum without a flow system, *i.e.*, with a static cell, it is always convenient to start the acquisition from the red edge of the spectrum, and move towards shorter wavelengths. The probe beam may photodegrade the sample at short wavelengths, however the filters employed when probing longer wavelengths will preclude this from happening, until it becomes absolutely essential to use wavelengths causing sample damage.

It is always better to acquire transient kinetics with a static setup, given that air leakage might occur more easily in a flow system, thus altering the real transient behavior.

2.5 Conditions Employed in Time-resolved Experiments in this Thesis

The laser flash photolysis system has been previously described.[66,67] Samples were excited either with a Lumonics EX-530 laser with a Xe/HCl/Ne mixture generating pulses at 308 nm of 6 ns and ≤ 100 mJ output at the source, with the third or fourth harmonic of a Surelite Nd:YAG laser generating pulses at 355 or 266 nm respectively of 8 ns duration and 25 mJ output, or with a Molectron UV-24 nitrogen laser generating pulses at 337 nm of 6 ns duration and ≤ 6 mJ output at the source. The signals from the monochromator/photomultiplier system were initially captured by a Tektronix 2440 digitizer and transferred to a PowerMacintosh computer that controlled the experiment with a software developed in the LabVIEW 4.1 environment from National Instruments (Austin, TX, U.S.A.).

Fluorescence time-resolved studies for short-lived singlet states were carried out using the second or third harmonic (532 and 355 nm respectively) pulse from a Continuum PY-61 Nd:YAG laser (35 ps, ≤4 mJ/pulse) as the excitation source. A Hamamatsu C4334 streak camera was used for time resolved fluorescence detection and data acquisition.[68] The instrument response is *ca.* 80 ps.

All transient spectra and kinetics were recorded employing a flow system with a 7 x 7 mm, 2 ml capacity, fused silica cuvettes from Luzchem Research (Morin Heights, QC, Canada), unless otherwise stated. Samples were purged in a storage tank for 30 min either with N_2, O_2, or N_2O. The quenching rate constants were obtained with static samples contained in 7 x 7 mm fused silica cuvettes unless otherwise specified. A fresh solution was employed to obtain each decay rate; two to four laser shots were delivered to the sample and the solution was shaken between shots to avoid any interference due to the accumulation of photoproducts. Each solution was purged for 15 min with N_2, O_2, or N_2O, before data acquisition.

2.6 References

(1) Lindqvist, L., Utilisation d'un Laser à Émission Ultraviolette Pulse en Photolyse-éclairs: Étude de l'Etat Triplet de l'Acridine, *C. R. Hebd. Séances Acad. Sci., Ser. C*, **1966**, *263*, 852-854.

(2) Scaiano, J. C. Laser Photolysis in Polymer Chemistry; In *Degradation and Stabilization of Polymers*; H. H. G. Jellinek and H. Kachi, Eds.; Elsevier: Amsterdam, 1989; Vol. 2; 1-39.

(3) Cosa, G.; Boscá, F.; Miranda, M. A.; Scaiano, J. C., A Laser Flash Photolysis Study of Fenofibric Acid in Aqueous Buffered Media. Unexpected Triplet State Inversion in a 4-Methoxybenzophenone Derived Compound, *Photochem. Photobiol.*, **2002**, *75*, 193-200.

(4) Sortino, S.; Scaiano, J. C., Photogeneration of Hydrated Electrons, Nitrogen-centered Radicals and Singlet Oxygen from Naphazoline: A Laser Flash Photolysis Study., *Photochem. Photobiol.*, **1999**, *70*, 590-595.

(5) Steenken, S. C.; Warren, J.; Gilbert, B. C., Generation of Radical Cations from Naphthalene and Some Derivatives, both by Photoionization and Reaction with $SO_4^{\cdot-}$: Formation and Reactions Studied by Laser Flash Photolysis, *J. Chem. Soc. Perkin Trans. 2*, **1990**, 335-342.

(6) McClelland, R. A.; Mathivanan, N.; Steenken, S., Laser Flash Photolysis of 9-Fluorenol. Production and Reactivities of 9-Fluorenol Radical Cation and the 9-Fluorenyl Cation, *J. Am. Chem. Soc.*, **1990**, *112*, 4857-4861.

(7) Lew, C. S. Q.; Brisson, J. R.; Johnston, L. J., Reactivity of Radical Cations: Generation, Characterization, and Reactivity of 1,3-Diene Radical Cations, *J. Org. Chem.*, **1997**, *62*, 4047-4056.

(8) Martínez, L. J.; Scaiano, J. C., Characterization of the Transient Intermediates Generated from the Photoexcitation of Nabumetone: A Comparison with Naproxen., *Photochem. Photobiol.*, **1998**, *68*, 646-651.

(9) Das, P. K., Electron Transfer Reactions from Aromatic Carbonyl Triplets to Paraquat Dication, *Tetrahedron Lett.*, **1981**, *22*, 1307-1310.

(10) Cosa, G.; Chesta, C. A., Estimation of Bimolecular Rate Constant for Exciplex Formation from the Analysis of its Emission Spectrum, *J. Phys. Chem. A*, **1997**, *101*, 4922-4928.

(11) Bhattacharyya, K.; Das, P. K., Nanosecond Transient Processes in the Triethylamine Quenching of Benzophenone Triplets in Aqueous Alkaline Media. Substituent Effect, Ketyl Radical Deprotonation, and Secondary Photoreduction Kinetics, *J. Phys. Chem.*, **1986**, *90*, 3987-3993.

(12) Das, P. K.; Encinas, M. V.; Steenken, S.; Scaiano, J. C., Reaction of *tert*-Butoxy Radicals with Phenols. Comparison with the Reactions of Carbonyl Triplets, *J. Am. Chem. Soc.*, **1981**, *103*, 4162-4166.

(13) Evans, C.; Scaiano, J. C.; Ingold, K. U., Absolute Kinetics of Hydrogen Abstraction from α-tocopherol by Several Reactive Species Including an Alkyl Radical, *J. Am. Chem. Soc.*, **1992**, *114*, 4589-4593.

(14) Sortino, S.; Scaiano, J. C.; Condorelli, G., Transient Photochemistry of Diflunisal: Photoejection and Trapping of Hydrated Electrons Leading to the Formation of Phenoxy Radicals, Photostimulated Defluorination, and Cross Combination Reaction., *J. Phys. Chem. B*, **1999**, *103*, 9279-9284.

(15) Carmichael, I.; Hug, G. L. Spectroscopy and Intramolecular Photophysics of Triplet States; In *Handbook of Organic Photochemistry*; J. C. Scaiano, Ed.; CRC Press: Boca Raton, Florida, 1989; Vol. I; 369-403.

(16) Gilbert, A.; Baggott, J., *Essentials of Molecular Photochemistry*; Blackwell Scientific Publications: Oxford, 1991.

(17) Wood, P. D.; Redmond, R. W., Triplet State Interactions Between Nucleic Acid Bases in Solution at Room Temperature: Intermolecular Energy and Electron Transfer, *J. Am. Chem. Soc.*, **1996**, *118*, 4256-4263.

(18) Gut, I. G.; Wood, P. D.; Redmond, R. W., Interaction of Triplet Photosensitizers with Nucleotides and DNA in Aqueous Solution at Room Temperature, *J. Am. Chem. Soc.*, **1996**, *118*, 2366-2377.

(19) Wilkinson, F., *Chemical Kinetics and Reaction Mechanisms*; Van Nostrand Reinhold Company: New York, 1980.

(20) Cosa, G.; Martínez, L. J.; Scaiano, J. C., Influence of Solvent Polarity and Base Concentration on the Photochemistry of Ketoprofen: Independent Singlet and Triplet Pathways, *PCCP*, **1999**, *1*, 3533-3537.

(21) Scaiano, J. C., Exploratory Laser Flash Photolysis Study of Free Radical Reactions and Magnetic Field Effects in Melatonin Chemistry, *J. Pineal Res.*, **1995**, *19*, 189-195.

(22) Martínez, L. J.; Scaiano, J. C., Transient Intermediates in the Laser Flash Photolysis of Ketoprofen in Aqueous Solutions: Unusual Photochemistry for the Benzophenone Chromophore, *J. Am. Chem. Soc.*, **1997**, *119*, 11066-11070.

(23) Sortino, S.; Scaiano, J. C.; De Guidi, G.; Monti, S., Effect of β-Cyclodextrin Complexation on the Photochemical and Photosensitizing Properties of Tolmetin: A Steady-state and Time-resolved Study., *Photochem. Photobiol.*, **1999**, *70*, 549-556.

(24) Buxton, G. V.; Greenstock, C. L.; Helman, W. P.; Ross, A. B., Critical Review on Rate Constants for Reactions of Hydrated Electrons, Hydrogen Atoms and Hydroxyl Radicals ($\cdot OH/\cdot O^-$) in Aqueous Solution, *J. Phys. Chem. Ref. Data*, **1988**, *17*, 516-886.

(25) Boscá, F.; Miranda, M. A., A Laser Flash Photolyisis Study on Fenofibric Acid, *Photochem. Photobiol.*, **1999**, *70*, 853-857.

(26) Sortino, S.; Scaiano, J. C., Laser Flash Photolysis of Tolmetin: A Photoadiabatic Decarboxylation with a Triplet Carbanion as the Key Intermediate in the Photodecomposition, *Photochem. Photobiol.*, **1999**, *69*, 167-172.

(27) Maillard, B.; Ingold, K. U.; Scaiano, J. C., Rate Constants for the Reactions of Free Radicals with Oxygen in Solution, *J. Am. Chem. Soc.*, **1983**, *105*, 5095-5099.

(28) Lusztyk, J.; Kanabus-Kaminska, J. M. Representative Kinetic Behavior of Selected Reaction Intermediates: Free Radicals; In *Handbook of Organic Photochemistry*; J. C. Scaiano, Ed.; CRC Press: Boca Raton, Florida, 1989; Vol. II; 369-403.

(29) Chateauneuf, J.; Lusztyk, J.; Ingold, K. U., Absolute Rate Constants for the Reactions of some Carbon Centered Radicals with 2,2,6,6-tetramethylpiperidine-*N*-oxyl, *J. Org. Chem.*, **1988**, *53*, 1629-1632.

(30) Sortino, S.; Scaiano, J. C.; De Guidi, G.; Costanzo, L. L., Copper (II), in the Parts Per Million Range, Modulates Photochemical and Photosensitizing Properties of Tolmetin Via Electron Transfer with a Triplet Carbanion., *Chem. Commun.*, **1999**, 2003-2004.

(31) Albini, A.; Fasani, E.; Mella, M., PEt-reactions of Aromatic Compounds, *Top. Curr. Chem.*, **1993**, *168*, 143-173.

(32) McClelland, R. A.; Kanagasabapathy, V. M.; Steenken, S., Nanosecond Laser Flash Photolytic Generation and Lifetimes in Solvolytic Media of Diarylmethyl and *p*-Methoxyphenethyl Cations, *J. Am. Chem. Soc.*, **1988**, *110*, 6913-6914.

(33) Barcellona, M. L.; Cardiel, G.; Gratton, E., Time-resolved Fluorescence of DAPI in Solution and Bound to Polydeoxynucleotides, *Biochem. Biophys. Res. Commun.*, **1990**, *170*, 270-280.

(34) Fujita, S.; Steenken, S., Pattern of OH addition to Uracil and Methyl- and Carboxyl-substituted Uracils. Electron transfer of OH Adduct with *N,N,N',N'*-tetramethyl-*p*-phenylendiamine and tetranitromethane., *J. Am. Chem. Soc.*, **1981**, *103*, 2540-2545.

(35) Foote, C. Type I and Type II Mechanisms of Photodynamic Action; In *Light Activated Pesticides*; K. R. Downum, Ed.; American Chemical Society: 1987; Vol. Ser. 339; 22-38.

(36) Fossey, J.; Lefort, D.; Sorba, J., *Free Radicals in Organic Chemistry*; John Wiley & Sons: Paris, 1995, 83-100.

(37) Turro, N. J., *Modern Molecular Photochemistry*; University Science Books: Sausalito, 1991.

(38) Encinas, S.; Miranda, M. A.; Marconi, G.; Monti, S., Transient Species in the Photochemistry of Tiaprofenic Acid and its Decarboxylated Photoproduct, *Photochem. Photobiol.*, **1998**, *68*, 633-639.

(39) Borsarelli, C. D.; Braslavsky, S. E.; Sortino, S.; Marconi, G.; Monti, S., Photodecarboxylation of Ketoprofen in Aqueous Solution. A Time-resolved Laser-induced Optoacustic Study, *Photochem. Photobiol.*, **2000**, *72*, 163-171.

(40) Carmichael, I.; Hug, G. L., Triplet-Triplet Absorption Spectra of Organic Molecules in Condensed Phases, *J. Phys. Chem. Ref. Data*, **1986**, *15*, 1-250.

(41) Lamola, A. A.; Hammond, G. S., Mechanisms of Photochemical Reactions in Solution. XXXIII. Intersystem Crossing Efficiencies., *J. Chem. Phys.*, **1965**, *43*, 2129-2135.

(42) Hubig, S. M.; Rodgers, M. A. J. Picosecond Absorption Spectroscopy; In *Handbook of Organic Photochemistry*; J. C. Scaiano, Ed.; CRC Press, Inc: Boca Raton, 1989; Vol. 2; 231-238.

(43) Schmidt, J. A.; Hilinski, E. F., Concurrent Pump-probe and Streak Camera Measurements with a Single Mode-locked Nd:YAG Laser: A Picosecond Absorption/Emission Spectrometer, *Rev. Sci. Instrum.*, **1989**, *60*, 2902-2914.

(44) Hilinski, E. F.; Rentzepis, P. M., Picosecond Spectroscopy: Methods and Recent Applications, *Anal. Chem.*, **1983**, *55*, 1121 A-1140 A.

(45) Watanabe, M.; Koishi, M.; Roehrenbeck, P. W. In *The International Society for Optical Engineering*; SPIE: Los Angeles, California, 1993; pp 155.

(46) Sortino, S.; Cosa, G.; Scaiano, J. C., pH Effects on the Efficiency of the Deactivation Pathways of Naphazoline: A Combined Steady State and Time Resolved Study, *New J. Chem.*, **2000**, *24*, 159-163.

(47) Sortino, S.; Giuffrida, S.; Scaiano, J. C., Phototoxicity of Naphazoline. Evidence that Hydrated Electrons, Nitrogen-Centered Radicals, and OH Radicals Trigger DNA Damage: A Combined Photocleavage and Laser Flash Photolysis Study, *Chem. Res. Toxicol.*, **1999**, *12*, 971-978.

(48) de la Peña, D.; Martí, C.; Nonell, S.; Martínez, L. A.; Miranda, M. A., Time-resolved Near Infrared Studies on Singlet Oxygen Production by the Photosensitizing 2-Arylpropionic Acids, *Photochem. Photobiol.*, **1997**, *65*, 828-832.

(49) Gorman, A. A., The Bimolecular Reactivity of Singlet Molecular Oxygen, *Adv. Photochem.*, **1992**, *17*, 217-274.

(50) Tanielian, C.; Wolff, C.; Esch, M., Singlet Oxygen Production in Water: Aggregation and Charge-Transfer Effects, *J. Phys. Chem.*, **1996**, *100*, 6555-6560.

(51) Wilkinson, F.; Helman, W. P.; Ross, A. B., Quantum Yields for the Photosensitized Formation of the Lowest Electronically Excited Singlet State of Molecular Oxygen in Solution, *J. Phys. Chem. Ref. Data*, **1993**, *22*, 113-262.

(52) Reddi, E.; Jori, G.; Rodgers, M. A. J.; Spikes, J. D., Flash Photolysis Studies of Hemato- and Copro-porphyrins in Homogeneous and Microheterogeneous Aqueous Dispersions, *Photochem. Photobiol.*, **1983**, *38*, 639-645.

(53) Schmidt, R.; Tanielian, C.; Dunsbach, R.; Wolff, C., Phenalenone, a Universal Reference Compound for the Determination of Quantum Yields of Singlet Oxygen $O_2(^1\Delta_g)$ Sensitization, *J. Photochem. Photobiol. A: Chem.*, **1994**, *79*, 11-17.

(54) Motten, A. G.; Martínez, L. J.; Holt, N.; Sik, R. H.; Reszka, K.; Chignell, C. F.; Tonnesen, H. H.; Roberts, J., Photophysical Studies on Antimalarial Drugs, *Photochem. Photobiol.*, **1999**, *69*, 282-287.

(55) Hurst, J. R.; Schuster, G. B., Nonradiative Relaxation of Singlet Oxygen in Solution, *J. Am. Chem. Soc.*, **1983**, *105*, 5756-5760.

(56) Rodgers, M. A. J., Solvent-induced Deactivation of Singlet Oxygen: Additivity Relationships in Nonaromatic Solvents, *J. Am. Chem. Soc.*, **1983**, *105*, 6201-6205.

(57) Schmidt, R., Influence of Heavy Atoms on the Deactivation of Singlet Oxygen ($^1\Delta_g$) in Solution, *J. Am. Chem. Soc.*, **1989**, *111*, 6983-6987.

(58) Hild, M.; Schmidt, R., The Mechanism of the Collision-induced Enhancement of the $a^1\Delta_g \rightarrow X^3\Sigma_g^-$ and $b^1\Sigma_g \rightarrow a^1\Delta_g$ Radiative Transitions of O_2, *J. Phys. Chem. A*, **1999**, *103*, 6091-6096.

(59) Wilkinson, F.; Helman, W. P.; Ross, A. B., Rate Constants for the Decay and Reactions of the Lowest Electronically Excited Singlet State of Molecular Oxygen in Solution. An Expanded and Revised Compilation, *J. Phys. Chem. Ref. Data*, **1995**, *24*, 663-1021.

(60) Monti, S.; Sortino, S.; De Guidi, G.; Marconi, G., Photochemistry of 2-(3-Benzoylmethyl)propionic Acid (Ketoprofen). 1. A Picosecond and Nanosecond Time Resolved Study in Aqueous Solution, *J. Chem. Soc., Faraday Trans.*, **1997**, *93*, 2269-2275.

(61) Lachish, U.; Shafferman, A.; Stein, G., Intensity Dependence in Laser Flash Photolysis Experiments: Hydrated Electron Formation from Ferrocyanide, Tyrosine, and Tryptophan, *J. Chem. Phys.*, **1976**, *64*, 4205-4211.

(62) Porter, G. Criteria for Solar Energy Conversion; In *Light, Chemical Change and Life: A Source Book in Photochemistry*; J. D. Coyle, R. R. Hill and D. R. Roberts, Eds.; The Open University Press: Milton Keynes, 1982; 339-345.

(63) Phillips, D.; Rumbles, G. Time-resolved Laser Spectroscopy Nanosecond and Picosecond Techniques: Principles, Devices, and Applications; In *Lasers in Polymer Science and Technology : Applications*; J. P. Fouassier and J. F. Rabek, Eds.; CRC Press: Boca Raton, 1990; Vol. 1; 91-145.

(64) Boscá, F.; Miranda, M. A.; Carganico, G.; Mauleón, D., Photochemical and Photobiological Properties of Ketoprofen Associated with the Benzophenone Chromophore, *Photochem. Photobiol.*, **1994**, *60*, 96-101.

(65) Constanzo, L. L.; De Guidi, G.; Condorelli, G.; Cambria, A.; Fama, M., Molecular Mechanism of Drug Photosensitization-II. Photohemolysis Sensitized by Ketoprofen, *Photochem. Photobiol.*, **1989**, *50*, 359-365.

(66) Scaiano, J. C., Solvent Effects in the Photochemistry of Xanthone, *J. Am. Chem. Soc.*, **1980**, *102*, 7747-7753.

(67) Scaiano, J. C.; Tanner, M.; Weir, D., Exploratory Study of the Intermolecular Reactivity of Excited Diphenylmethyl Radicals, *J. Am. Chem. Soc.*, **1985**, *107*, 4396-4403.

(68) Mohtat, N.; Cozens, F. L.; Scaiano, J. C., Multistage Exit of Excited Xanthone from Micelles, *J. Phys. Chem.: B*, **1998**, *102*, 7557-7562.

3. A Photophysical and Photochemical Study on Fenofibric Acid

3.1 Introduction

The photochemistry of pharmaceutical products has received much attention in the last decade, prompted by reports on photosensitization reactions produced by certain active ingredients in drugs. Those related to the benzophenone chromophore have been studied in great detail, and a recent review has been published on the topic.[1] These issues were discussed in great detail in the first chapter, and in what follows we want to analyze in particular the photochemical behavior of fenofibric acid, a benzophenone related compound.

Fenofibric acid (FA) is an hypolipidaemic drug circulating in the blood stream following the metabolism of the commercial prodrug, fenofibrate (FB) (see Scheme 3-1).[2,3] Its peak plasma concentration after administration of a single dose of 300 mg is *ca.* 24 μg/ml, equivalent to a 7.5 x 10^{-5} M concentration.[4]

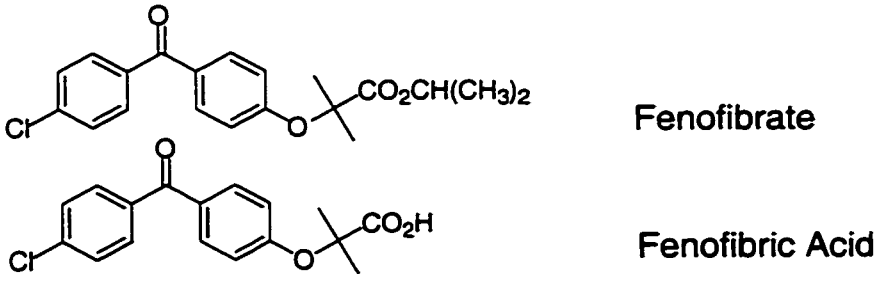

Scheme 3-1: Fenofibrate and fenofibric acid structure.

This molecule consists of a substituted benzophenone, its ground state absorption extending over the UV-A part of the solar spectrum,[5] as can be seen from Figure 3-1. The combined effects of UV-A and FA can result in photosensitized DNA damage,[6] peroxidation of fatty acids,[7] and red blood cell hemolysis.[1] However, its phototoxic effect is reportedly lower compared to another benzophenone-derived drug, *i.e.*, ketoprofen.[6] The reactivity of FA and FB in ethanol suggest an n,π* lowest triplet state, in agreement with calculations.[8] At the time we started working with this compound, no such reactivity had been measured in water. This prompted our interest to study this molecule under conditions closer to physiological ones, *i.e.* pH 7.4, to understand its photochemical behavior in more biologically

relevant situations. We undertook our studies in collaboration with Professors M. A. Miranda and F. Boscá , at the Instituto de Tecnología Química, Universidad Politécnica de Valencia.

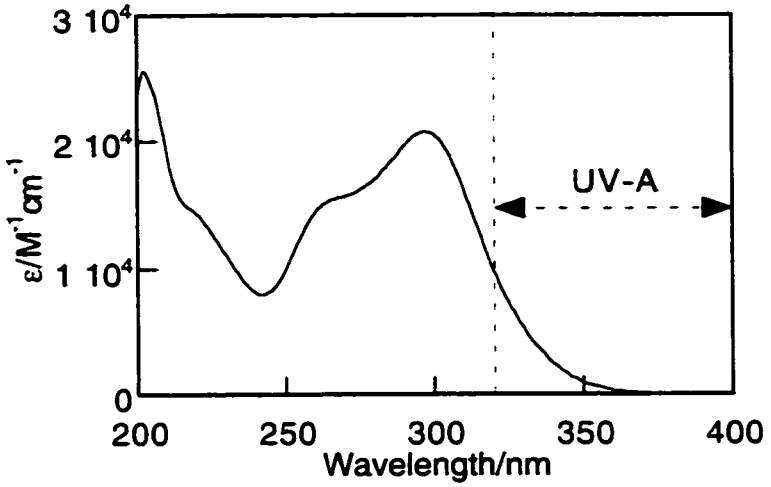

Figure 3-1: Molar absorptivity of fenofibric acid in phosphate buffer 0.1 M, pH 7.4. Also shown is the UV-A region of the solar spectrum.

Our work, presented in this chapter, consists of steady-state absorption and phosphorescence, as well as time-resolved phosphorescence studies, that allow a clear assessment on the nature of the excited species involved in FA photochemical degradation. These results as well as those obtained from photoproduct studies following FA irradiation are included in this chapter.

We also report laser flash photolysis (LFP) studies performed on FA and its ester, FB, as well as on 4-methoxybenzophenone (4-MBP), the simplest structure of which fenofibric acid is a derivative. These studies are aimed at characterizing the spectroscopy and understanding the reactivity of FA triplet excited state, the species that according to our results is involved in FA photodegradation.

All the parameters measured indicate that an inversion of the lower triplet state of fenofibric acid (n,π^* to π,π^*) occurs in going from acetonitrile to water; this would account for the lower reactivity of FA and its photoproducts as compared to those of ketoprofen in

aqueous media. Our results also show that biphotonic processes occur under pulsed laser excitation, where solvated electrons, together with ketyl and cyclohexadienyl radicals, are readily observable.

Some of the measurements presented here were obtained by S. Purohit while working as part of the Undergraduate Research Scholarship Program at the University of Ottawa. His help is greatly appreciated.

3.2 Results

3.2.1 Absorption and Phosphorescence

The absorption spectra for FA and 4-MBP in different polarity solvents are shown in Figure 3-2. From the analysis of these data we can establish a low energy n,π* singlet state band with absorbption at *ca.* 340 nm, and a higher energy π,π* singlet state band at *ca.* 290 nm (see also Table 3-1). Upon increase in solvent polarity, the n,π* band observed in methylcyclohexane is masked by the bathochromic shift exhibited by the π,π* band.[8]

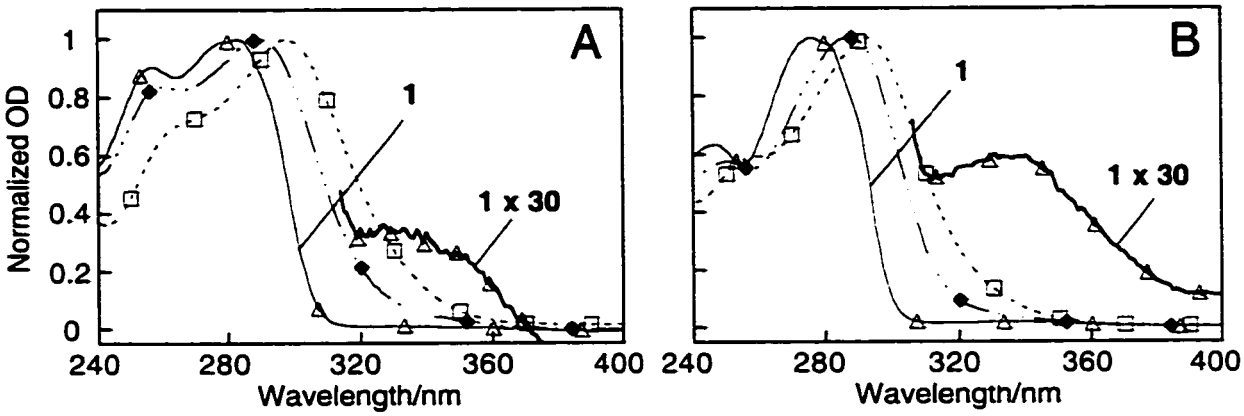

Figure 3-2: Normalized ground state absorption spectra for (A) FA in (□) water, (◆) 4:1 ethanol:methanol, (△) methylcyclohexane. (B) 4-MBP in (□) water, (◆) 4:1 ethanol:methanol, (△) methylcyclohexane. A few points are shown to assist in the visualization

The triplet energies for FA and 4-MBP were determined in a glass at 77 K from the maximum of the lowest energy band of the phosphorescence spectra (*i.e.*, the 0-0 band) shown in Figures 3-3-A and 3-3-C respectively. The data is summarized in Table 3-1, and it shows that a decrease in triplet energy accompanies an increase in water content, for a total triplet energy change of 13 kJ/mol. These changes in triplet energy were also accompanied by changes in the phosphorescence lifetime (longer in higher polarity glasses, as shown in Figure 3-3), consistent with a switch towards π,π* character.[9] We note this evolution may

be more complete in solution at room temperature, where solvation may be more extensive, and where the species is the carboxylate anion, as opposed to the acid at 77 K in the experiments of Table 3-1.

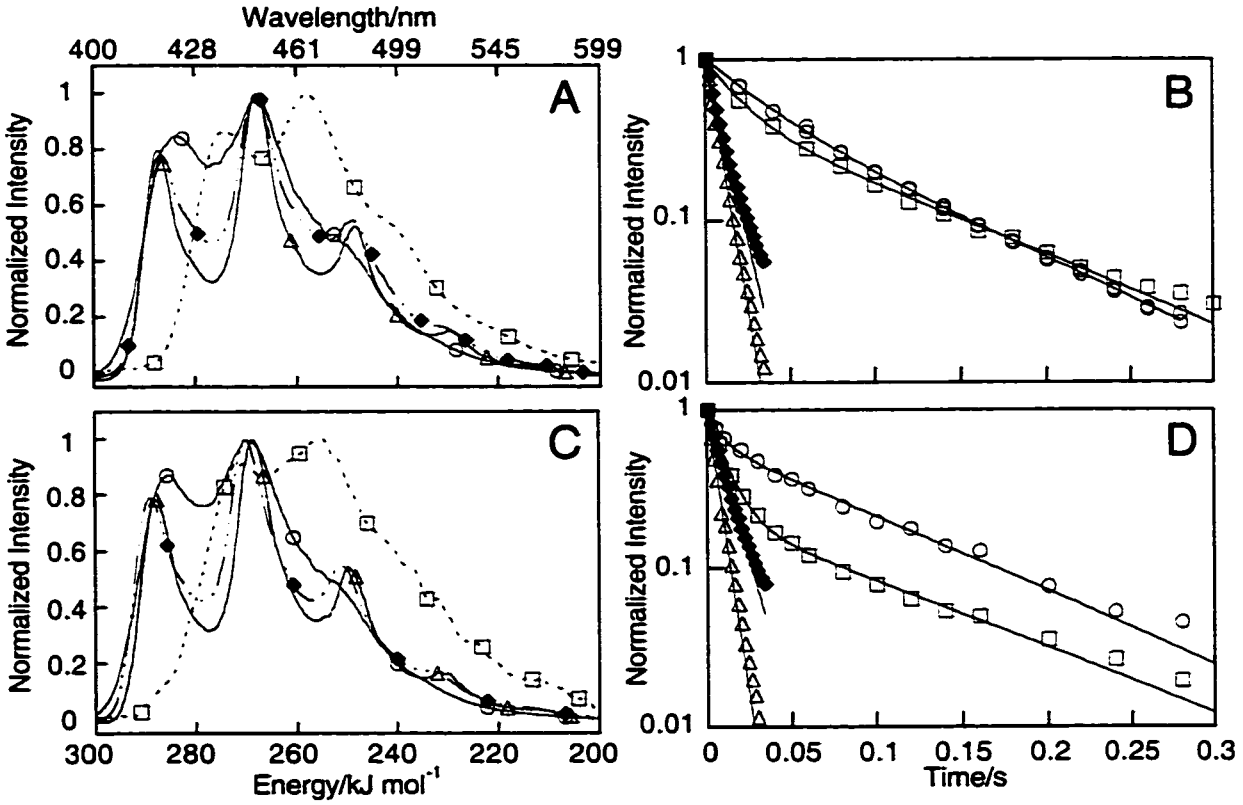

Figure 3-3: Normalized phosphorescence spectra of (A): FA in (□) water, saturated solution, λ_{exc} 310 nm. (○) 2:1 ethylene glycol:water, λ_{exc} 314 nm. (◆) 4:1 methanol:ethanol, λ_{exc} 305 nm. Also shown is the spectrum of FB in methylcyclohexane (△) λ_{exc} 288 nm. (C): 4-MBP in (□) water, saturated solution, λ_{exc} 300 nm. (○) 2:1 ethylene glycol:water, λ_{exc} 320 nm. (◆) 4:1 methanol:ethanol, λ_{exc} 303 nm. (△) methylcyclohexane, λ_{exc} 294 nm. In all cases the ground state absorption was ca 0.8 ± 0.1 at the excitation wavelength, except saturated FA solution in water (OD = 0.23 at λ_{exc}). A few points are shown to assist in the visualization. Plots (B) and (D) show the decay traces for the triplet state phosphorescence of FA and 4-MBP respectively, in the previous glasses. The excitation wavelength was the same as that employed in registering the phosphorescence spectra, and the intensity was recorded at 450 nm in all cases.

Table 3-1: Solvent effects on the singlet and triplet energy of fenofibric acid and 4-methoxybenzophenone at 77 K. Also shown are the phosphorescence decay rate constants and their respective weights.

Solvent	Compound	Max. OD nm	0,0 band nm	T Energy kJ/mol	k_1/s^{-1}	A_1	k_2/s^{-1}	A_2
[a] methylcyclohexane	FB	283	418	286	144	1	-	-
4:1 methanol:ethanol	FA	290	417	286	103	1	-	-
2:1 ethylene glycol:water	FA	-	423	283	29	0.47	11	0.53
water	FA	298	437	274	51	0.54	10	0.46
methylcyclohexane	4-MBP	276	415	288	169	1	-	-
4:1 methanol:ethanol	4-MBP	287	414	288	87	1	-	-
2:1 ethylene glycol:water	4-MBP	-	419	285	128	0.37	11	0.62
water	4-MBP	293	442	271	95	0.79	10	0.21

[a] A solution containing fenofibrate was employed. A1 and A2 represent the weight corresponding to each component in the phosphorescence decay.

3.2.2 Laser Flash Photolysis Studies, Biphotonic Chemistry

Laser excitation of FA at pH 7.4 under nitrogen leads to the spectrum of Figure 3-4. The early spectrum corresponds to a mixture of two species, as revealed by a number of confirmatory experiments (vide infra). The bands at 360 and 460 nm are assigned to the triplet state of FA, which at this pH is present as the anion, while the absorption at _> 700 nm is probably dominated by the hydrated electron, with contributions from triplet absorption.

At 340 nm we also observe the formation of another species following triplet decay, Figures 3-4 and 3-5. The fact that the time profile for the change in absorbance (_OD) shows a valley at 340 nm implies that the triplet state can not be the immediate precursor of this species (see the inset of Figure 3-4).

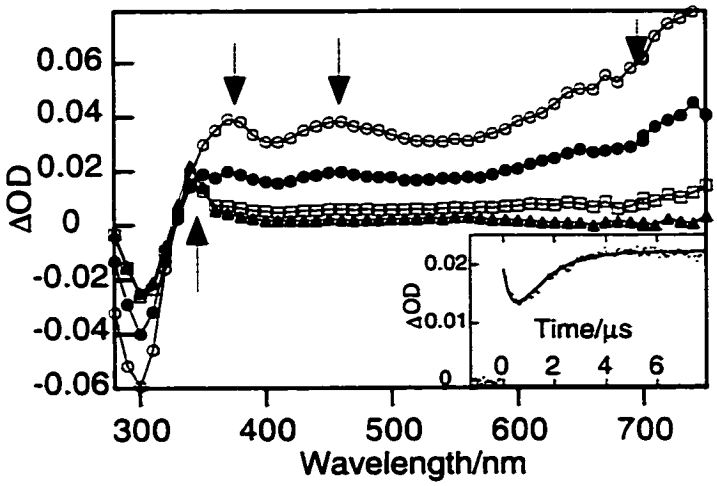

Figure 3-4: Transient absorption spectra of 3.5 x 10^{-5} M FA in 0.01 M pH 7.4 phosphate buffer solution. Laser 308 nm, N_2 bubbled. Time windows: (○) 0.04 μs; (●) 0.40 μs; (□) 1.28 μs; (▲) 4.04 μs after the laser pulse. Inset: kinetic profile at 340 nm.

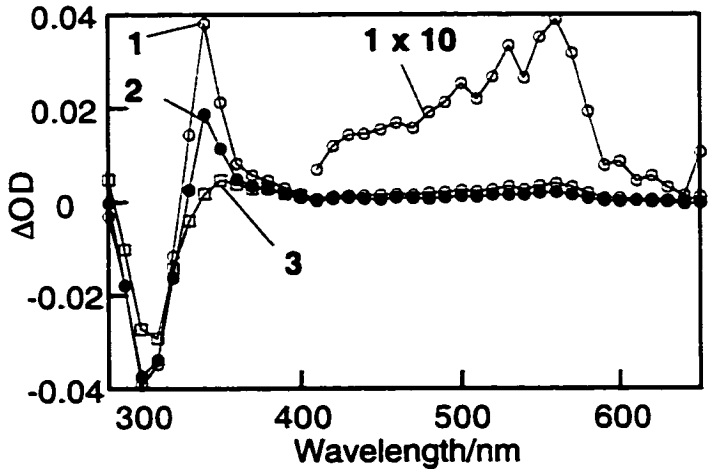

Figure 3-5: Transient absorption spectra of 3.5 x 10^{-5} M FA in 0.01 M pH 7.4 phosphate buffer solution. Laser 308 nm, N_2 bubbled. Time windows: (○) 8 μs; (●) 139 μs; (□) 1740 μs after the laser pulse. Also shown is an enlarged section of the 8 μs time window (○).

In order to verify the assignment of the long wavelength signals to the solvated electron we carried out experiments in N_2O saturated solutions. This is a common diagnostic test for hydrated electrons, which are efficiently scavenged by N_2O (see Scheme 3-2).[10] The result is shown in Figure 3-6, which includes a difference spectrum obtained by subtracting the spectra under N_2O from that recorded under N_2. This difference spectrum is in full agreement with that expected for the hydrated electron,[11] while the signal at short times and under N_2O corresponds to that of the FA triplet state (*vide infra*).

$$N_2O + e^-_{(aq)} + H_2O \longrightarrow N_2 + HO^{\bullet} + HO^-$$

Scheme 3-2: Reaction of solvated electrons with N_2O.[12]

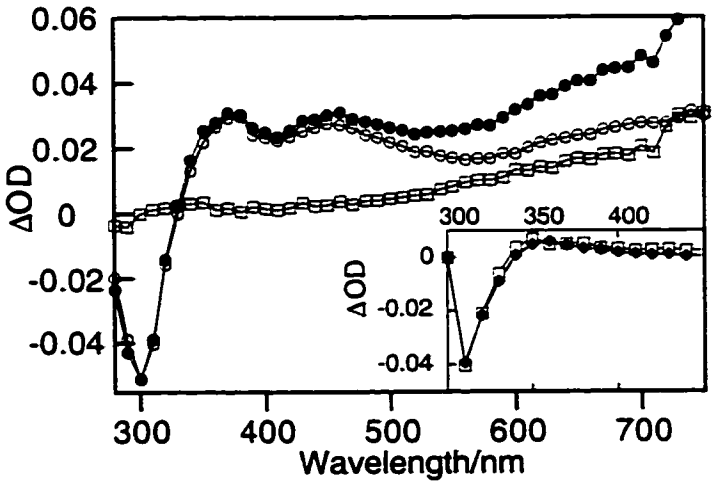

Figure 3-6: (□) Solvated electron absorption spectrum obtained from the difference between: (●) the spectrum of 3.5 x 10^{-5} M FA in 0.01 M pH 7.4 phosphate buffer, laser 308 nm, N_2 bubbled; and (○) the spectrum of a solution under the same conditions, but equilibrated with N_2O. The observed time windows are those registered 0.16 μs after the laser pulse. The spectra were normalized to the same value at 380 nm prior to subtraction. Inset: transient absorption spectra of 3.5 x 10^{-5} M FA in 0.01 M pH 7.4 phosphate buffer solution. Laser 308 nm, N_2O bubbled. Time windows: (□) 8 μs; (◆) 344 μs after the laser pulse.

We now turn our attention to the growth observed at 340 nm under N_2 atmosphere. As already indicated, the presence of a valley in the time profile requires that the growth either has a different precursor (*i.e.*, other than the triplet state), or that one or more intermediates be involved in the reaction path. Further, these intermediates need to be transparent, or at least less absorbing than both the triplet state, and the species responsible for the signal growth. In our case the simplest hypothesis is that the 340 nm signal is derived from the hydrated electron. This is confirmed by the fact that electron scavenging with N_2O eliminates the growth at 340 nm. The 340 nm transient, which also shows a signal at 540 nm (see Figure 3-5), is assigned to the ketyl radical formed by reduction of FA. Its absorption agrees well with the spectrum of the acid form of FA reported in methanol, where efficient hydrogen abstraction to generate FA ketyl radical occurs.[13] The ketyl radicals have a lifetime of *ca.* 140 μs under our conditions, and decay by mixed first-second order kinetics.

Fitting the trace in the inset of Figure 3-4 with the sum of two exponentials gives rate constants of 2.05×10^6 s^{-1} (triplet decay) and 8.9×10^5 s^{-1} (ketyl growth). From the latter number, and concentration of FA (3.5×10^{-5} M), we estimate that the hydrated electron reacts with FA with a rate constant of 2.6×10^{10} $M^{-1}s^{-1}$, a value in line with others for aromatic ketones.[14-18] Interestingly, the presence of a negative charge (*i.e.*, the carboxylate) does not cause any significant slow down in the electron capture reaction. We note that the actual value may be slightly lower than our estimate if the electron decays by other pathways in addition to trapping by FA. We also observe that in addition to the transients discussed above, there is a considerable bleaching at 300 nm (see inset Figure 3-6). This indicates that the processes taking place (including triplet decay), lead to irreversible chemical changes.

In order to determine the origin of the various transients, we also carried out power dependence studies. These measurements are normally used to differentiate monophotonic and multiphotonic processes. In a qualitative experiment we used 355 nm excitation; the laser available for these experiments has considerably lower peak power than the excimer laser used for 308 nm excitation. Under these conditions the experiments under nitrogen give

a spectrum virtually identical to that obtained with 308 nm under N_2O, showing that hydrated electrons are not produced under the former conditions (data not shown).

In a separate experiment we determined the power dependence at 308 nm for three different transients. For the electron (720 nm) and the triplet state (460 nm) immediately after the laser pulse, and for the ketyl radical (340 nm) after its growth was complete (see inset Figure 3-4). The plot shown in Figure 3-7 shows a quadratic dependence for the electron and the ketyl radical signals (fitted with a parabola) and linear, as expected, for the triplet state absorption. This shows that electron ejection (and as a consequence ketyl radical formation) is dominantly (and probably exclusively) the result of two-photon ionization.

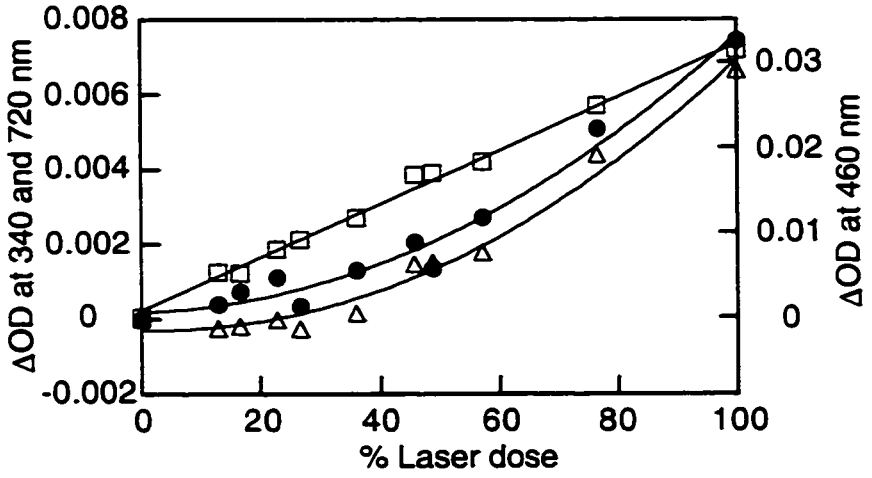

Figure 3-7: Power dependence of 3.5 x 10^{-5} M FA in 0.01 M pH 7.4 phosphate buffer solution. Laser 308 nm, N_2 bubbled. The full dose corresponds to *ca.* 20 mJ/pulse. Taken at: (●) 340 nm, 3.5 μs after the laser pulse; (□) 460 nm, immediately after the laser pulse; (△) 720 nm, immediately after the laser pulse, and corrected for triplet contribution.

3.2.3 Laser Flash Photolysis Studies, Triplet State Spectroscopy

The triplet state assignment is not as straightforward as that for the hydrated electron, *i.e.*, 360 and 460 nm are not in the region for the typical absorption of substituted

benzophenones.[19] In fact, for FA triplet state in methanol it has been reported λ_{max} values of 340 and 520 nm.[13] To test the hypothesis that the 360 and 460 nm signals are due to the triplet state, we carried out quenching experiments with two selective triplet quenchers, sorbic acid and 1-naphthalenemethanol (1-NM), and obtained quenching rate constants of 1.9 x 10^9 and 2.9 x 10^9 $M^{-1}s^{-1}$, respectively. Further, in the case of 1-NM the decay of the FA triplet (monitored at 480 nm) occurs concurrently with the growth of the 420 nm signal characteristic of the triplet state of 1-NM (see Figure 3-8).

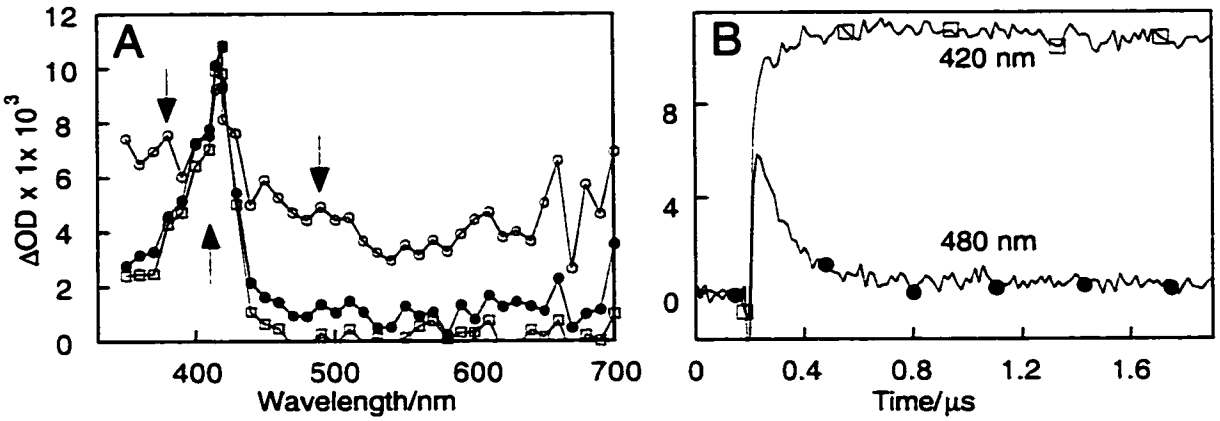

Figure 3-8: (A) Transient absorption spectra of 8.9 x 10^{-4} M FA in 0.1 M pH 7.4 phosphate buffer solution. 1-Naphthalenemethanol 2 x 10^{-3} M was used as quencher. Laser 355 nm, N_2 bubbled. Time windows: (○) 29 ns; (●) 200 ns; (□) 680 ns after the laser pulse. (B) Kinetic traces obtained at (●) 480 nm and (□) 420 nm (a few points are shown to assist in the visualization).

Consistently with our triplet state assignment, the 340 and 460 nm signals are also quenched by oxygen. The triplet decays with a rate constant of 5.9 x 10^6 s^{-1} under O_2 saturated solution, compared with *ca.* 2.0 x 10^6 s^{-1} under nitrogen or N_2O. From the difference we estimate the quenching rate constant for oxygen at 4 x 10^9 $M^{-1}s^{-1}$, a value in the expected range for these reactions.

We have attributed the triplet signals to triplet FA. However, two questions remain. Conceivably, the triplet state observed could be that of the carbanion produced following FA photodecarboxylation; further, the lifetime of the triplet (0.5 μs) is rather short for a

substituted benzophenone in water,[19] suggesting that reactive pathways play a key role in determining the triplet lifetime.

The ester fenofibrate (FB) is a good control compound, since it does not undergo the decarboxylation/rearrangement that characterizes the photolysis of the FA anion in methanol.[7,20] In order to ensure solvent compatibility it was necessary to carry out these experiments in acetonitrile:water mixtures. Figure 3-9 shows the spectra for FA, FB; as well as that obtained for 4-chloro-4'isopropoxybenzophenone (4Cl-4'I-BP) and 4-MBP in various solvent mixtures. Base has been added to the FB solution to match the conditions used with FA in organic solvents (*vide infra*). Clearly all three compounds undergo the same shifts as FA in water thus supporting the assignment of the early transient of Figure 3-4 to triplet FA. However the triplet lifetime of FB is much longer than that of FA (see also Table 3-2). For example in 8:2 acetonitrile:water the FB triplet decay rate constant is $2.64 \times 10^5\ s^{-1}$, thus supporting a reactive decay pathway for FA. The FB triplet lifetime does not change significantly in different acetonitrile:water mixtures; similar results are obtained with 4Cl-4'I-BP and 4-MBP. In the case of FA in the presence of base (tetramethyl ammonium hydroxide), the decay rate constant increases as the fraction of organic solvent in the mixture increases and is $3.9 \times 10^7\ s^{-1}$ in 93:7 acetonitrile:water, about 20 times faster than in water at pH 7.4. Product studies (*vide infra*) show that the excited state decarboxylation is responsible for the fast triplet decay in the case of FA anion.

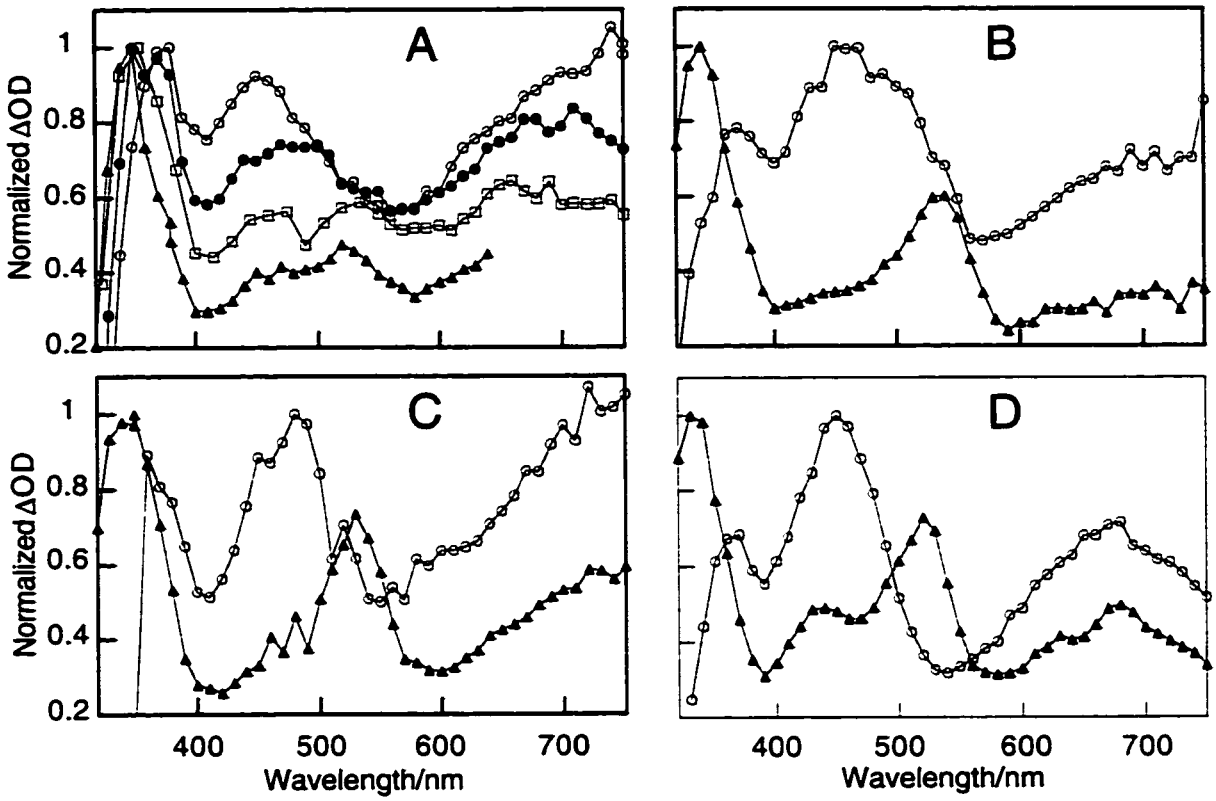

Figure 3-9: Normalized transient absorption spectra of (A) FA 0.035 mM under N_2 atmosphere in different acetonitrile:water mixtures with TMAOH 8 mM; (○) water, 160 ns after the laser pulse, N_2O, pH 7.4, (●) 4:6 acetonitrile:water, 32 ns after the laser pulse, N_2, (□) 8:2 acetonitrile:water, 32 ns after the laser pulse, N_2, (▲) 93:7 acetonitrile:water 32 ns after the laser pulse, N_2. (B) FB 0.035 mM under N_2 atmosphere in different acetonitrile:water mixtures with NaOH 10 mM; (○) 2:8 acetonitrile:water, 320 ns after the laser pulse, (▲) pure acetonitrile 640 ns after the laser pulse, (no NaOH). (C) 4-Chloro-4'isopropoxybenzophenone 0.042 mM under N_2 atmosphere in different acetonitrile:water mixtures (○) 2:8 acetonitrile:water, 240 ns after the laser pulse, (▲) pure acetonitrile 240 ns after the laser pulse. (D) 4-MBP (○) water, saturated solution, 640 ns after the laser pulse, N_2O atmosphere, (▲) 0.123 mM, pure acetonitrile 640 ns after the laser pulse, N_2. Laser wavelength 308 nm.

3.2.4 Laser Flash Photolysis Studies, Triplet State Reactivity

Given the large difference in FA triplet lifetime in aqueous systems at pH 7.4 and in basic 93:7 acetonitrile:water, we decided to explore the reactivity of the triplet with 1,4-cyclohexadiene (1,4-CHD), a good hydrogen donor. In order to ensure solvent compatibility, water was replaced by a 2:8 acetonitrile:water mixture, and the longer lived FB triplet was used as a model. The results were compared to those obtained under similar conditions for 4-MBP (see also Table 3-2).

Table 3-2: Decay parameters obtained for FA, FB, 4Cl-4'I-BP and 4-MBP in different acetonitrile:water mixtures.

Reaction	Compound	Ratio acetonitrile:water				
		93:7	8:2	4:6	2:8	0:1
[a] k_{dec}/s^{-1}	FA	3.9×10^7	2.4×10^7	5.3×10^6	-	1.6×10^6
[b] k_{dec}/s^{-1}	FB	2.71×10^5	2.64×10^5	3.10×10^5	2.54×10^5	-
[b] k_{dec}/s^{-1}	4Cl-4'I-BP	2.03×10^5	2.15×10^5	2.57×10^5	3.26×10^5	-
[c] k_{dec}/s^{-1}	4-MBP	1.5×10^5	-	-	1.15×10^5	1.45×10^5
[c] k_q 1,4-CHD/$M^{-1}s^{-1}$	FB	3.0×10^8	-	-	$\leq 1 \times 10^7$	-
[c] k_q 1,4-CHD/$M^{-1}s^{-1}$	4-MBP	1.3×10^8	-	-	$\leq 1 \times 10^7$	-
[c] k_q isopropanol/$M^{-1}s^{-1}$	4-MBP	4.8×10^5	-	-	-	$\leq 1 \times 10^4$
[d] Φ photodegradation	FA	0.70	-	-	-	0.06
[e] Φ triplet generation	4-MBP	0.86			0.29	

[a] The solution was prepared with TMAOH 8 mM; the rate constants were measured at 650 nm. [b] The rate constants were measured at 450 nm. [c] The rate constants were measured at 700 nm. [d] Values obtained with TMAOH 80 mM. [e] Measured at 420 nm, following 1-methylnaphthalene sensitization, and comparing with an optically matched solution of benzophenone (Φ triplet generation = 1; see also Equation 2-13).

Figure 3-10 shows quenching plots in both solvents for FB triplet state. The second order rate constant (anticipated to be due to hydrogen abstraction), corresponds to the slope of these plots. The rate constant is 3.0 x 10^8 $M^{-1}s^{-1}$ in the acetonitrile rich solvent, which compares well with the value of 2.9 x 10^8 $M^{-1}s^{-1}$ for benzophenone itself in acetonitrile (for 4-MBP we obtained a value of 1.3 x 10^8 $M^{-1}s^{-1}$).[21] In contrast, in the water-rich solvent we see no quenching, leading to a conservative upper limit of *ca.* 1 x 10^7 $M^{-1}s^{-1}$ for the quenching rate constant. The observation is consistent with a change in the nature of the excited triplet from n,π* (acetonitrile) to π,π* (water). This change is characteristic of the 4-alkoxybenzophenone structure, as can be inferred from the results with 4-MBP (see table 3-2).

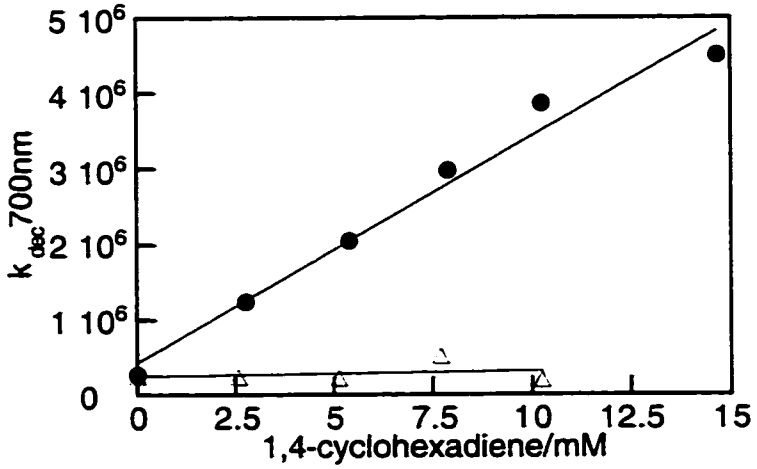

Figure 3-10: Observed rate constant of decay of the triplet state of fenofibrate measured at 700 nm in the presence of different amounts of 1,4-cyclohexadiene. (●) FB 0.06 mM, 93:7 acetonitrile:water, N_2 bubbled. (△) Saturated solution of FB in 2:8 acetonitrile:water, N_2 bubbled, laser 308 nm.

The temperature dependence of the decay of triplet FA was also examined in 93:7 acetonitrile:water in the presence of tetramethylammonium hydroxide and in water at pH 7.4. These plots are shown in Figure 3-11, and yield preexponential values of 5.0 x 10^{12} and 7.9 x 10^{11} for the aqueous and acetonitrile rich solutions; the corresponding activation energies are

36.9 and 23.4 kJ/mol, respectively, as determined from the Arrhenius equation (see Equation 2-9).

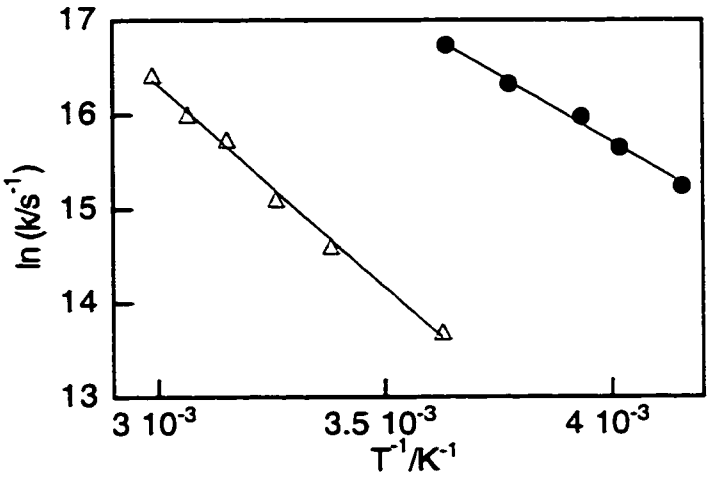

Figure 3-11: Arrhenius plot for the decay of the triplet state of FA anion. (●) Determined in 93:7 acetonitrile:water, under N_2 atmosphere; FA 0.08 mM, TMAOH 3.4 mM. (△) Determined in buffer pH 7.4 0.1 M, under N_2O atmosphere; FA 0.07 mM. Laser 308 nm.

3.2.5 Product Studies

Product studies were performed using as the excitation source a 355 and a 308 nm laser. A total of 100 shots were delivered on each of 2 ml samples and ten samples were collected. These samples exposed at a given wavelength were then combined, and extracted with dichloromethane. Following concentration under reduced pressure the samples were injected on a GC/MS instrument. The same procedure was followed with a non-irradiated sample for comparison. From the analysis of the mass spectra corresponding to each of the peaks in the chromatogram, we were able to identify 4Cl-4'I-BP (**1**) and 4-chloro-4'-(1-hydroxy-1-methylethyl) benzophenone (**2**), in agreement with the results previously obtained in methanol solutions (see Scheme 3-3).[13] No difference in product distribution was found in using different lasers as the excitation source.

The analysis of photoproducts was also done in an HPLC provided with a reverse phase column. The same product ratio was obtained for compounds **1** and **2** when FA was irradiated either at 355 or 308 nm in buffer solution. Minor amounts of FA dimers originating from the FA ketyl radical were also detected in the 308 nm irradiated sample.

The quantum yield (Φ) for FA photodegradation was determined following steady-state irradiation of FA in 93:7 acetonitrile:water and water, under basic conditions and using ketoprofen as a standard (Φ of ketoprofen photodecarboxylation is 0.75[22]); the values are presented in Table 3-2. In both cases, photoproducts **1** and **2** where the only species formed. The ratio of compound **1** to **2** in aqueous solutions is 69:31, that in 93:7 acetonitrile:water is 1:1. The product **2** is rationalized by a Wittig rearrangement of the carbanion, which is disfavored in more polar solvents; this results in the observed change in product ratio with solvent composition, in agreement with previous results in phosphate buffer solution, acetone and methanol.[23]

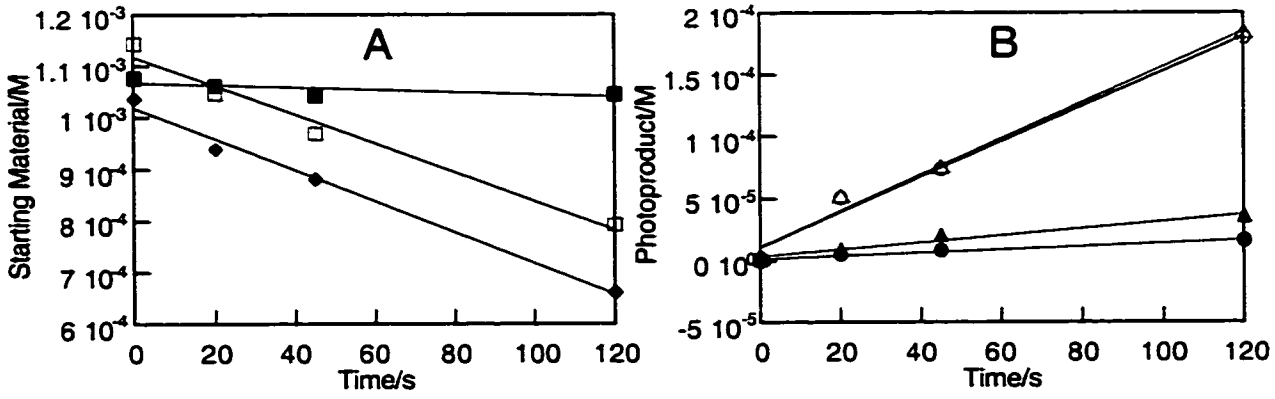

Figure 3-12: (A) Concentration of FA following different irradiation times with a 254 nm 8 W Hg lamp under N_2 atmosphere, TMAOH 0.08 M, in: (■) water, (□) acetonitrile:water 93:7, (◆) also shown is the evolution of ketoprofen concentration (employed as standard) in water. (B) Product formation over time, following FA irradiation: (▲) photoproduct 1, water, (●) photoproduct 2, water, (△) photoproduct 1, acetonitrile:water 93:7, (○) photoproduct 2, acetonitrile:water 93:7. The concentrations were measured by HPLC.

The preceding results lead us to propose a reaction scheme for FA similar to that encountered in methanol solutions. The general mechanism shown in Scheme 3-3 seems to apply to the FA anion photochemistry in all conditions employed.

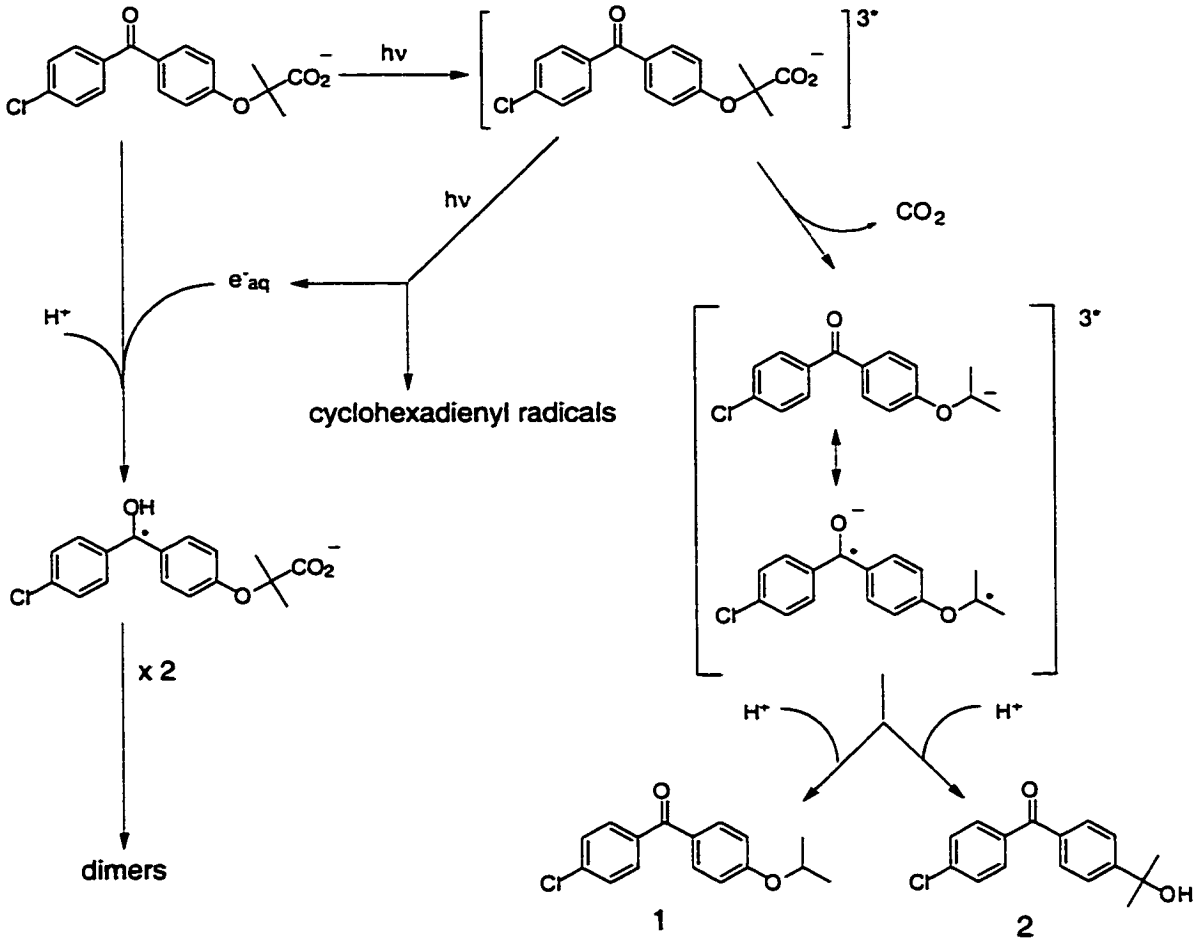

Scheme 3-3: Photodegradation mechanism for FA.

3.3 Discussion

3.3.1 Biphotonic Processes

There are several differences between the photobehavior of FA in aqueous solutions and in organic polar solvents, such as methanol, where its photochemistry is already well understood.[13] One of these differences relates to the occurrence of photoionization processes; it is not unusual for these processes to be enhanced in aqueous media. Further in the case of FA at pH 7.4, where it is present as the carboxylate, photoionization does not need to overcome electrostatic attractions in order to eject the electron (as is the case for neutral species). Similar processes have been reported for benzophenone and ketoprofen.[12,15,24,25]

Hydrated electrons decay predominantly by addition to the ground state of FA with a rate constant of *ca.* 2.6 x 10^{10} $M^{-1}s^{-1}$. Interestingly, the rate constant is just as fast as if no negative charge was present in the substrate. Similar observations were made in the case of 3,3',4,4'-benzophenonetetracarboxylate ion.[16]

We note that the spectrum observed following electron trapping by FA is clearly that of the ketyl radical, rather than the benzophenone radical anion. This is not unexpected, since the pKa of the ketyl radical from benzophenone is 9.25,[19] and thus, rapid protonation should occur at pH 7.4.

Power dependence studies show that electron photoejection and the resulting ketyl radical formation are predominantly (and presumably exclusively) two photon processes. The implication of this is that from a biological point of view these processes are not important, since they will not occur under conditions of ambient (solar or artificial) illumination.[5]

Small transient absorption extending from 330 to 420 nm is observed at very long time scales. These may be due to either a cyclohexadienyl radical proposed as product from the benzophenone cation following photoionization,[26] or to the LATs (light absorbing

transients) that participate in the rearrangement of FA to product **2** in Scheme 3-3.[13] Detailed interpretation of these minor signals is not essential to understand the details of the mechanism.

3.3.2 Monophotonic Processes

The other key transient observed in this work is the triplet state of FA, which not surprisingly results from a monophotonic process. This transient will be important under conditions of both laser or ambient illumination. Product studies show that the fast triplet decay reflects decarboxylation, ultimately leading to products **1** and **2**.

Several aspects of triplet state spectroscopy and lifetimes need to be considered together:

1. The triplet lifetime of the FA anion is much shorter than for FB, or 4Cl-4'I-BP.
2. The triplet lifetime of the anion form of FA is 10 and 20 times shorter in methanol and acetonitrile-rich solvents respectively, than in water.
3. The quantum yield of FA photodegradation is *ca.* 12 times larger in acetonitrile-rich solutions than in water.
4. The quantum yield of 4-MBP triplet formation is *ca.* 3 times larger in acetonitrile-rich solutions than in 2:8 acetonitrile:water.
5. The triplet-triplet absorption of FA in water no longer resembles the typical benzophenone triplet structure observed in methanol,[13] *i.e.*, the visible maximum is at 460 nm rather than 525 nm.
6. The triplet state of FB (a model for FA triplet state) reacts readily with hydrogen donors in organic solvents, but is at least 20 times less reactive in water, similar results are observed for 4-MBP.
7. The phosphorescence spectra and lifetimes at 77 K suggest a change in the lower triplet excited state from n,π^* in organic solvents to π,π^* in water.

The seven items raised above can be easily rationalized by invoking a π,π^* triplet in water for FA. Such state inversion is common for acetophenone and xanthone derivatives,

but less so for benzophenones, which are usually the archetypes for n,π* behavior, although singlet photochemistry has been recently reported for ketoprofen, another substituted benzophenone (see following chapter).[12,24]

The spectral shifts observed for triplet FA, FB, 4Cl-4'I-BP, or 4-MBP are in line with those observed for xanthone and azaxanthone.[27,28] The band in the T-T absorption spectrum of FA is 34 kJ/mol higher in energy in water (460 nm) than in acetonitrile (525 nm).

An interesting observation from this work is that decarboxylation, which in the case of FA involves the triplet state, is much faster for the n,π* than for the π,π* triplet, and thus, triplet lifetimes for the anionic form of FA are longer in water than in organic solvents; (similar results have been obtained for tiaprofenic acid).[29] At least part of this slow down is reflected in the activation energy. See for example in Figure 3-11 that the lower line clearly has the steeper slope, even if differences in preexponential factors are probably within experimental error, given the limited temperature range available.

If decarboxylation occurs from the triplet state of FA anion, then it is reasonable to assume that at least the nascent carbanion must be in the triplet state. In Scheme 3-3 we have written the carbanion and the biradical as resonant structures. While singlet and triplet states should be essentially isoenergetic in the biradical case, large differences in energy are anticipated for the carbanion. Thus the carbanion should be the preferred resonance structure for the singlet, while in the triplet manifold the biradical will be dominant. In order for the biradical to be the nascent species, an electron transfer (carboxylate to carbonyl) may precede decarboxylation.

Phosphorescent studies support the analysis presented above, *i.e.*, increase of aqueous content leads to a decrease in triplet energy and an increase in triplet lifetime. However the switch to a π,π* state with aqueous content is probably more complete at room temperature than in a glass at 77 K, since in the latter the phosphorescence spectrum shows some vibrational resolution in water, as well as a short lifetime component; while at room

temperature the lack of reactivity of the triplet towards hydrogen transfer (see Figure 3-10) suggests a complete inversion of states.

3.4 Conclusions

We have presented in this work results on the photochemistry of FA both at high and low laser power (*i.e.*, 308 and 355 nm excitation wavelengths respectively) in aqueous buffer solutions. In its dissociated form FA decarboxylates from the triplet manifold following excitation, in a similar way to that previously reported in alcohol mixtures in the presence of base.[13] This deactivation mode is inactive when FA is in its ester form (FB). In the latter case, the triplet state decays with a similar rate independently of the solvent media, however in the presence of good hydrogen donors hydrogen abstraction is faster in lower polarity acetonitrile:water mixtures, compared to pure water. This is paralleled with a higher reactivity towards decarboxylation for FA anion in acetonitrile-rich mixtures as compared to water. This in turn correlates with a higher triplet energy in ethanol *vs.* water and is also accompanied with hypsochromic shift in the visible T-T absorption band in water compared to that in acetonitrile, similarly to the behavior of xanthone,[28] or azaxanthone.[27] These results are explained in terms of FA presenting a π,π^* nature lowest triplet state in water; whereas in lower polarity acetonitrile:water mixtures the lowest triplet is higher in energy and has n,π^* character (see Figure 3-13). Both decarboxylation and hydrogen abstraction are processes arising from the latter state.

The data corresponding to experiments performed with 4Cl-4'I-BP and 4-MBP further reveal that the switch in the lower triplet state is inherent to the structure of a 4-alkoxybenzophenone, the chlorine atom present in FA having little or no effect.

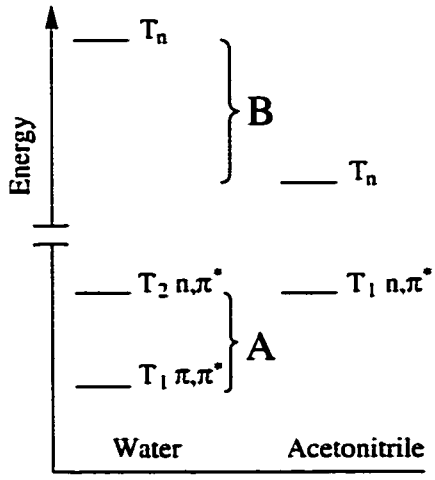

Figure 3-13: Energy level diagram for the lowest triplet state (T_1) of FA in water and acetonitrile, the second lowest triplet state (T_2) of FA in water, and the higher triplet state level giving rise to the T_1-T_n absorption band; where A is probably in the 5-15 kJ/mol range and B (based on the spectral shift for T-T absorption) is likely to be somewhat higher.

From a biological point of view, these results are of significance. We can now explain the lower reactivity exhibited by FA and its photoproducts when compared to ketoprofen and its respective photoproducts. In the latter case it has been established that the deleterious effects to cell membranes arise from lipid peroxidation. This is a radical mediated mechanism involving the action of an n,π* triplet ketone acting as an initiator.[30-32] Photoproduct **1**, whose structure and excited state spectroscopic behavior following LFP is similar to that of FB (see Figure 3-9) should present a π,π* lower triplet state in water, like FB, therefore being less reactive towards lipid peroxidation at physiological pH. A similar conclusion can be used to explain the lower reactivity of FA as compared to ketoprofen towards DNA cleavage. As it has been shown, this is a process inhibited by radical quenchers, and is therefore most probably initiated following hydrogen abstraction by the arylketones,[6] those having n,π* lowest triplet states being more reactive than π,π* ones.

3.5 Materials and Methods

Materials. Fenofibrate (2-[4-(4-chlorobenzoyl)phenoxy]-2-methylpropanoic acid isopropyl ester), tetramethylammonium hydroxide (TMAOH), sodium phosphate (monobasic), sodium hydroxide semiconductor grade, sorbic acid (2,4-hexadienoic acid), 1-naphthalenemethanol (1-NM) and ethanol were purchased from Sigma-Aldrich Canada (Oakville, ON, Canada). All solvents were HPLC-grade and purchased from OmniSolv (Gibsstown, NJ, USA), and were used without further purification. Water was purified through a Millipore MilliQ system. The 0.1 M, pH 7.4 phosphate buffer was prepared with monobasic sodium phosphate in water, and the solution was brought to pH with NaOH.

3.5.1 Synthesis

2-[4-(4-Chlorobenzoyl)phenoxy]-2-methylpropanoic acid (Fenofibric acid). It was obtained following hydrolysis of fenofibrate with NaOH (2.7 M) in 50:50 H_2O:methanol under reflux for 5 hours. Following solvent concentration under reduced pressure the aqueous mixture was subsequently extracted with ether to remove any non-reacted FB. The resulting aqueous mixture was brought to pH 5 with aqueous HCl 3.5% w:v. The suspension obtained was extracted with ethyl acetate, the organic phase was dried with $NaHSO_4$, filtered, and the solvent was removed under reduced pressure. A white powder was obtained. It was confirmed to be FA by comparing the ^{1}H-NMR ($CDCl_3$) spectra taken before and after the saponification, showing the disappearance of the peaks corresponding to the isopropyl group [δ 1.2 (d, J1 = 6Hz, 6H), 5.1 (m, 1H)].[7]

3.5.2 Steady-state and Time-resolved Studies

Nanosecond Laser Flash Photolysis. Fenofibric acid (FA) concentration was *ca.* 0.035 mM for irradiation at 308 nm. When the excitation was carried out at 355 nm the sample concentration was *ca.* 1 mM. These values ensured an absorbance of 0.3-0.5 in the laser cell at the excitation wavelength.

Aqueous solutions of FA were prepared in pH 7.4 buffers, 10 mM and 100 mM in phosphate, for irradiation at 308 and 355 nm respectively. The solutions prepared in methanol or acetonitrile:water had 10 mM TMAOH to ensure that FA was present in its dissociated form.

The 355 nm pulses from a Nd:YAG laser were used to determine quenching rate constants with 1-naphthalenemethanol (1-NM), in order to avoid absorption by the quencher.

Other details have been described in Section 2.5 of this thesis.

Steady-state Measurements. Phosphorescence spectroscopy was performed using a Perkin Elmer LST 50 luminescence spectrometer. The spectra were recorded at 77 K in different glasses. Absorption spectra were recorded using a Varian CARY 1E spectrophotometer.

3.5.3 Product Studies

Photolysis of FA in phosphate buffer aqueous solution were done with 308 and 355 nm lasers as the excitation sources. The samples received 100 laser shots and were then extracted with dichloromethane. The solvent was removed under vacuum, and the resulting mixture was analyzed with a Fisons GC/MS 8060/8000 Series equipped with a J&W DB5 30 m x 0.32 mm column.

HPLC studies of the irradiated solutions were carried out on a Varian instrument using a reverse phase 4.6 x 250 mm analytical Zorbax SB-C18 column, the mobile phase used was 15:85 water:methanol, the flow rate employed was 1 ml/min. The detection used a Varian 9065 Polychrom diode array detector. The absorption spectra of the products were compared to those previously reported.[7]

Quantum Yield Determination. Steady-state photolysis were carried out in a photoreactor, with only one 254 nm 8 W mercury lamp, and for the periods described in Figure 3-12. Ketoprofen was employed as a standard (the quantum yield of photodecarboxylation is 0.75 at pH 7.4[22]) The solutions were 1 mM in the substrate, and 80

mM in TMAOH, to ensure that all the photons would be absorbed under these conditions, and that FA, as well as ketoprofen, would be in their anionic form. To quantitate the starting material, as well as the photoproducts produced, a calibration curve was made with FA at 254 nm, and employed equally for FA and for photoproduct **1**, which has the same chromophore structure. In the case of photoproduct **2**, the concentration was corrected for the difference in molar absorptivities existing between FA and this compound at 254, as reported in the literature.[7] A separate curve was prepared for ketoprofen.

3.6 References

(1) Boscá, F.; Miranda, M. A., Photosensitizing Drugs Containing the Benzophenone Chromophore, *J. Photochem. Photobiol. B: Biology*, **1998**, *43*, 1-26.

(2) Kloer, H. U., Structure and Biochemical Effects of Fenofibrate, *Am. J. Med.*, **1987**, *83*, 3-8.

(3) Elsom, L. F.; Hawkins, D. R.; Chasseaud, L. F., Identification of a Major Metabolite of the New Hypolipidaemic Agent, isopropyl 2-[4'(*p*-chlorobenzoyl)phenoxy]-2-methylpropionate (procetofene) in Humans by Gas Chromatography-Mass Spectrometry, *J. Chromatogr.*, **1976**, *123*, 463-467.

(4) Chapman, M. J., Pharmacology of Fenofibrate, *Am. J. Med.*, **1987**, *83*, 21-25.

(5) Porter, G. Solar Energy; In *Light, Chemical Change and Life: A Source Book in Photochemistry*; J. D. Coyle, R. R. Hill and D. R. Roberts, Eds.; The Open University Press: Milton Keynes, 1982; 2-9.

(6) Maguery, M. C.; Chouini-Lalanne, N.; Ader, J. C.; Paillous, N., Comparison of the DNA Damage Photoinduced by Fenofibrate and Ketoprofen, Two Phototoxic Drugs of Parent Structure, *Photochem. Photobiol.*, **1998**, *68*, 679-684.

(7) Miranda, M. A.; Boscá, F.; Vargas, F.; Canudas, N., Photosensitization by Fenofibrate. II. *In vitro* Phototoxicity of the Major Metabolites., *Photochem. Photobiol.*, **1994**, *59*, 171-174.

(8) Lhiaubet, V.; Gutierrez, F.; Penaud-Berruyer, F.; Amouyal, E.; Daudey, J.-P.; Poteau, R.; Chouini-Lalanne, N.; Paillous, N., Spectroscopic and Theoretical Studies of the Excited States of Fenofibric Acid and Ketoprofen in Relation with Their Photosensitizing Properties, *New J. Chem.*, **2000**, *24*, 403-410.

(9) Klessinger, M.; Michl, J., *Excited States and Photochemistry of Organic Molecules*; VCH Publishers, Inc.: New York, 1995, pp 255-260.

(10) Buxton, G. V.; Greenstock, C. L.; Helman, W. P.; Ross, A. B., Critical Review on Rate Constants for Reactions of Hydrated Electrons, Hydrogen Atoms and Hydroxyl Radicals (·OH/·O⁻) in Aqueous Solution, *J. Phys. Chem. Ref. Data*, **1988**, *17*, 516-886.

(11) Hug, G. L., *Optical Spectra of Nonmetallic Inorganic Transient Species in Aqueous Solution*; National Bureau of Standards: Washington, 1981; Vol. NSRDS-NBS 69, 160.

(12) Martínez, L. J.; Scaiano, J. C., Transient Intermediates in the Laser Flash Photolysis of Ketoprofen in Aqueous Solutions: Unusual Photochemistry for the Benzophenone Chromophore, *J. Am. Chem. Soc.*, **1997**, *119*, 11066-11070.

(13) Boscá, F.; Miranda, M. A., A Laser Flash Photolyisis Study on Fenofibric Acid, *Photochem. Photobiol.*, **1999**, *70*, 853-857.

(14) Hayon, E.; Ibata, T.; Lichtin, N. N.; Simic, M., Electron and Hydrogen Atom Attachment to Aromatic Carbonyl Compounds in Aqueous Solution. Absorption Spectra and Dissociation Constants of Ketyl Radicals, *J. Phys. Chem.*, **1972**, *76*, 2072-2078.

(15) Elisei, F.; Favaro, G.; Görner, H., Ion Forming Processes on 248 nm Laser Excitation of Benzophenone in Aqueous Solution: a Time Resolved Absorption and Conductivity Study, *J. Photochem. Photobiol. A: Chem.*, **1991**, *59*, 243-253.

(16) Säuberlich, J.; Beckert, D., Photoionization of Benzophenocarboxylic Acids in a Two-photon Process. A Fourier Transform EPR Study, *J. Phys. Chem.*, **1995**, *99*, 12520-12524.

(17) Brede, O.; Helmstreit, W.; Mehnert, R., Pulse Radiolysis of Benzophenone in Aqueous Solution, *Z. Phys. Chem.*, **1975**, *256*, 513-521.

(18) Lerat-Parizot, O.; Potier, J.; Hickel, B., Electron Transfer of Cadmium (I), *J. Chim. Phys. Phys.-Chim. Biol.*, **1993**, *90*, 789-800.

(19) Bensasson, R. V.; Gramain, J.-C., Benzophenone Triplet Properties in Acetonitrile and Water, *J.C.S. Faraday I*, **1980**, *76*, 1801-1810.

(20) Vargas, F.; Canudas, N.; Miranda, M. A.; Boscá, F., Photodegradation and *in vitro* Phototoxicity of Fenofibrate, a Photosensitizing Anti-hyperlipoproteinemic Drug, *Photochem. Photobiol.*, **1993**, *58*, 471-476.

(21) Encinas, M. V.; Scaiano, J. C., Reaction of Benzophenone Triplets with Allylic Hydrogens. A Laser Flash Photolysis Study, *J. Am. Chem. Soc.*, **1981**, *103*, 6393-6397.

(22) Constanzo, L. L.; De Guidi, G.; Condorelli, G.; Cambria, A.; Fama, M., Molecular Mechanism of Drug Photosensitization-II. Photohemolysis Sensitized by Ketoprofen, *Photochem. Photobiol.*, **1989**, *50*, 359-365.

(23) Miranda, M. A.; Boscá, F.; Vargas, F.; Canudas, N., Unusual (1,2) Wittig Rearrangement of a Carbanion Generated in Neutral Aqueous Medium by Photodecarboxylation of a Phenoxyacetic Acid Analogue, *J. Photochem. Photobiol. A: Chem.*, **1994**, *78*, 149-151.

(24) Cosa, G.; Martínez, L. J.; Scaiano, J. C., Influence of Solvent Polarity and Base Concentration on the Photochemistry of Ketoprofen: Independent Singlet and Triplet Pathways, *PCCP*, **1999**, *1*, 3533-3537.

(25) Monti, S.; Sortino, S.; De Guidi, G.; Marconi, G., Photochemistry of 2-(3-Benzoylmethyl)propionic Acid (Ketoprofen). 1. A Picosecond and Nanosecond Time Resolved Study in Aqueous Solution, *J. Chem. Soc., Faraday Trans.*, **1997**, *93*, 2269-2275.

(26) Säuberlich, J.; Brede, O.; Beckert, D., Photoionization of Benzophenone Carboxylic Acids in Aqueous Solution. A FT EPR and Optical Spectroscopy Study of Radical Cation Decay, *J. Phys. Chem.*, **1996**, *100*, 18101-18107.

(27) Martínez, L. J.; Scaiano, J. C., The Photochemistry of 1-Azaxanthone in Aqueous Solutions and in Micellar Environments, *J. Phys. Chem.*, **1999**, *103*, 203-208.

(28) Scaiano, J. C., Solvent Effects in the Photochemistry of Xanthone, *J. Am. Chem. Soc.*, **1980**, *102*, 7747-7753.

(29) Encinas, S.; Miranda, M. A.; Marconi, G.; Monti, S., Transient Species in the Photochemistry of Tiaprofenic Acid and its Decarboxylated Photoproduct, *Photochem. Photobiol.*, **1998**, *68*, 633-639.

(30) Chignell, C. F.; Sik, R. H., The Effect of Static Magnetic Fields on the Photohemolysis of Human Erythrocytes by Ketoprofen, *Photochem. Photobiol.*, **1998**, *67*, 591-595.

(31) Boscá, F.; Miranda, M. A.; Carganico, G.; Mauleón, D., Photochemical and Photobiological Properties of Ketoprofen Associated with the Benzophenone Chromophore, *Photochem. Photobiol.*, **1994**, *60*, 96-101.

(32) Chignell, C. F.; Sik, R. H., Magnetic Field Effects on the Photohemolysis of Human Erythrocites by Ketoprofen and Protoporphyrin IX, *Photochem. Photobiol.*, **1995**, *62*, 205-207.

4. Photochemistry of Ketoprofen: Role of a Carbanion Intermediate

4.1 Introduction

A rather simple substituted benzophenone currently commercialized as a non-steroidal anti-inflammatory drug (NSAID) under the name ketoprofen (KP), has been involved in adverse photosensitization reactions (see Scheme 4-1 for KP structure).[1,2] A number of studies have been performed to understand the photobiological effects of ketoprofen. Thus there exist reports in the literature where photohemolysis,[2-4] lipid peroxidation,[5] DNA damage,[6,7] and other assays,[8] evidence its *in vitro* phototoxicity. Photodegradation studies also exist that report a photodecarboxylation with a quantum yield of *ca.* 0.75 as the main reaction pathway.[2,5]

This drug has an absorption spectra with a weak transition extending over the UV-A region of the solar spectrum, as is shown in Figure 4-1. Under normal ingestion conditions (*ca.* 100 mg dose), it reaches a peak concentration of 3 μg/ml (equivalent to 1.18×10^{-5} M) in the blood stream.[9]

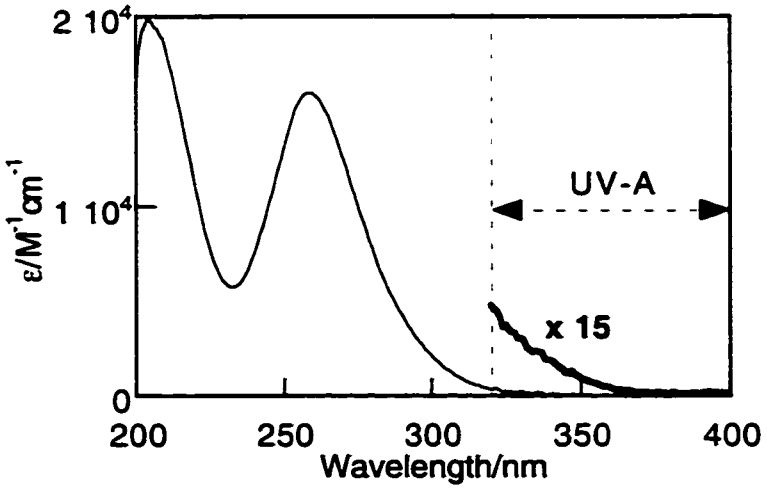

Figure 4-1: Molar absorptivity of ketoprofen in phosphate buffer 0.1 M pH 7.4. The absorption in the UV-A region of the solar spectrum has been enlarged by a factor of 15.

Ketoprofen presents unusual pH-dependent photochemistry.[4,5,10-13] In particular, the acid form of ketoprofen behaves as a conventional benzophenone, with high intersystem

crossing yields and triplet radical-like behavior.[11,12] In contrast, the carboxylate form (which is present at physiological pH) undergoes rapid decarboxylation to yield a carbanion, which is responsible for the formation of 3-ethylbenzophenone, as illustrated in Scheme 4-1.

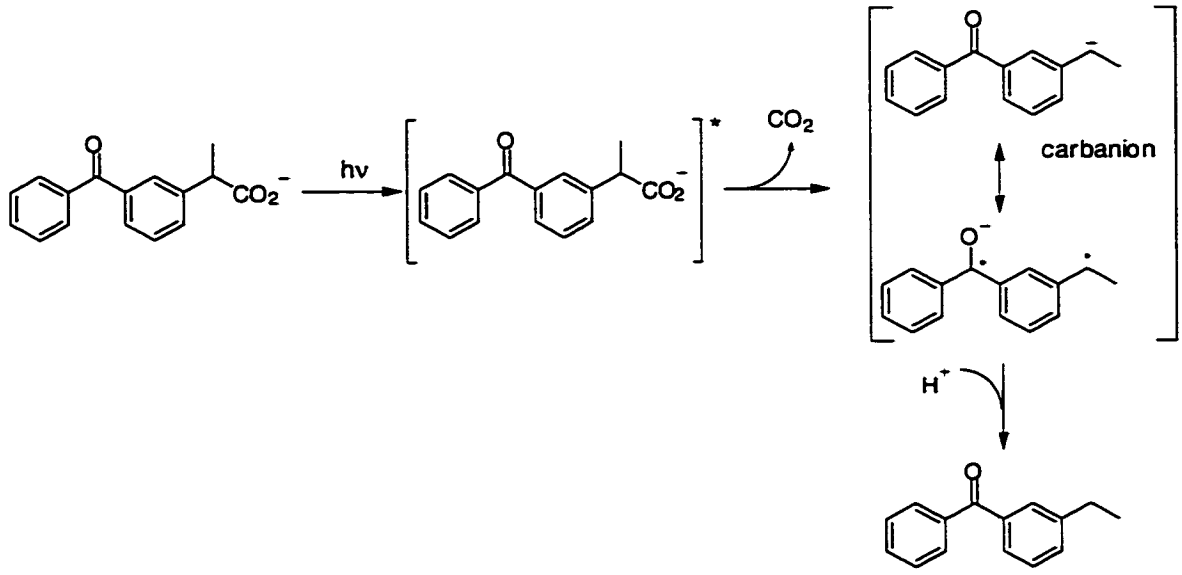

Scheme 4-1: Mechanism of decarboxylation of ketoprofen.[11]

The proposed carbanion shows a strong absorption at around 580 nm and a lifetime of *ca.* 210 ns in water and is believed to originate from the singlet manifold.[11] There is some uncertainty on the assignment of this transient (which absorbs in the visible region) and on its precursor. Some results suggest a triplet precursor in the photochemistry of the deprotonated form of ketoprofen, which following intramolecular electron transfer in the triplet manifold forms the visible absorbing transient characterized by a lifetime of *ca.* 200 ns. This transient is assumed to decay later on *via* decarboxylation to yield a triplet carbanion.[12]

A number of studies in the first part of this report have been designed to establish the nature of the carbanion precursor and the detailed mechanism of its formation. In particular, we have attempted, and succeeded, in finding experimental conditions under which, both the benzophenone-like triplet and the carbanion can be detected simultaneously. By monitoring both species in a single experiment, it is possible to establish if they are mechanistically

linked or if they form through independent pathways. Our research was planned in order to address this question.

A second part in this chapter is dedicated to exploring the properties and reactivity of the carbanion formed following KP photodecarboxylation. In this regard we have designed and synthesized molecules that enable the study of the nucleophilic attack to haloalkanes by the carbanion, as well as give an insight into the factors affecting the protonation rate of this reactive intermediate in water. This second part is the result of a fruitful collaboration with Professor M. A. Miranda at the Instituto de Tecnología Química, Universidad Politécnica de Valencia.

4.2 Formation of 3-Ethylbenzophenone, a Mechanistic Study

4.2.1 Laser Flash Photolysis Results in Methanol

When 0.4 mM KP in methanol is irradiated in the presence of 8 mM base (NaOH or TMAOH) the species detected is a short lived transient (τ 204 ns) with a spectrum characterized by maxima at 330 nm and 580 nm (Figure 4-2), very similar to that observed in aqueous solutions at pH 7.4.[11,12] A similar behavior was observed in basic ethanol where the lifetime was 208 ns.

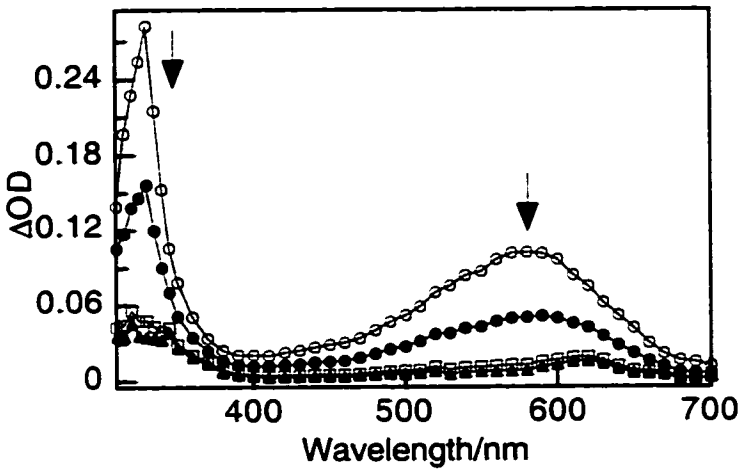

Figure 4-2: Transient absorption spectra of KP 4.1 x 10^{-4} M in methanol solution, NaOH 8.2 x 10^{-3} M. Laser 308 nm. N_2 bubbled. Time windows: (○) 56 ns; (●) 230 ns; (□) 800 ns; (▲) 1500 ns after the laser pulse.

We examined the temperature dependence of the decay kinetics for the 580 nm transient under basic conditions in both, methanol and water. These experiments were largely carried out in an attempt to establish if the pre-exponential factor for its decay was consistent with a unimolecular cleavage process involving loss of CO_2, as suggested in earlier reports (*vide supra*).[12] As it turned out (*vide infra*), the pre-exponential factors obtained are too low for such a mechanism. The corresponding data for water and methanol are shown in an Arrhenius-type plot in Figure 4-3. The plot leads to an activation energy of 13.2 kJ/mol

and a pre-exponential factor of 1.07 x 10^9 s^{-1} in methanol under nitrogen. The values are very similar to those obtained in water (see Figure 4-3) saturated with N_2O; under these conditions any solvated electrons would be rapidly scavenged by N_2O. Clearly, in this situation solvated electrons do not play any role in determining the Arrhenius parameters obtained.

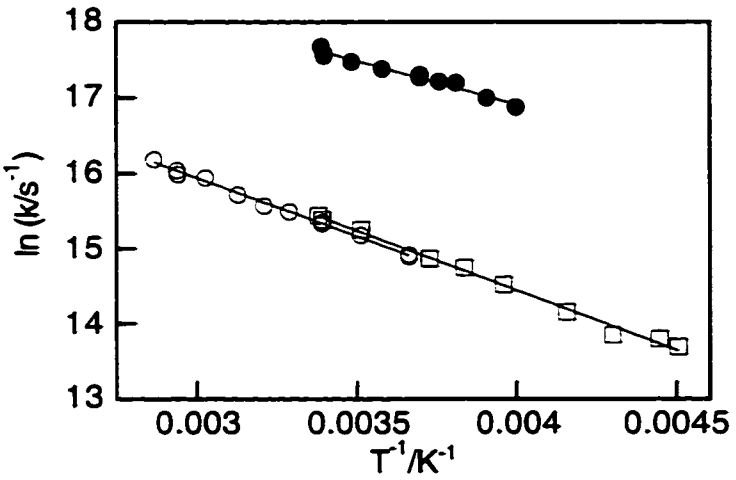

Figure 4-3: Arrhenius plot for the decay of the KP transient. (□) Determined in MeOH at 600 nm, N_2 bubbled. (○) Determined in H_2O at 600 nm, N_2O bubbled. (●) Determined in water:acetonitrile (measured at 635 nm), N_2 bubbled. X_{water} 0.13, KP 4.9 x 10^{-4} M, TMAOH 2.5 x 10^{-3} M. Laser 308 nm.

In the absence of base, the transient behavior of KP in methanol is dramatically different from that mentioned above. The transient spectrum immediately after laser excitation shows maxima at 330 and 530 nm (see Figure 4-4-A). With time, the visible band shifts towards 550 nm, with the overall process being complete in less than 1 μs. The rate constant for decay monitored at 520 nm was 4.1 x 10^6 s^{-1}; within experimental error, the same value was obtained at 330 nm for the signal growth (see Figure 4-4-B). Note also that at $\lambda >$ 600 nm (where ketyl radicals do not absorb[14]) the decay is essentially complete after 750 ns. This behavior is characteristic for a typical benzophenone triplet chromophore, essentially the same as for benzophenone itself.

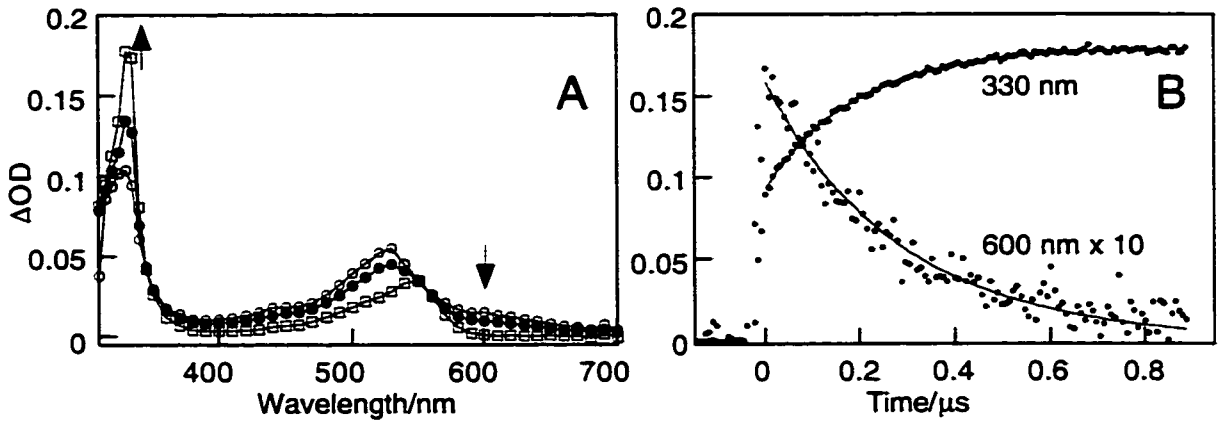

Figure 4-4: (A) Transient absorption spectra of KP 3.0 x 10^{-4} M in methanol solution, no NaOH. Laser 308 nm, N_2 bubbled. Time windows: (○) 28 ns; (●) 130 ns; (□) 750 ns after the laser pulse. (B) Transient absorption time evolution monitored at 330 nm and 600 nm.

4.2.2 Laser Flash Photolysis Results in Acetonitrile:Water Mixtures

In another series of experiments KP solutions were irradiated in water:acetonitrile mixtures with the molar fraction of water (X_{water}) ranging from 1.0 to 0.13; the latter corresponds to 5% water (v:v). Again, a marked difference was observed in the presence and absence of base. A spectrum recorded with a mole fraction of water of 0.7 in the absence of base was identical (see Figure 4-5) to that in methanol (no base) immediately following laser excitation. The decay rate constant in this case (3.5 x 10^5 s^{-1}) was much smaller than that obtained in methanol (*vide supra*) suggesting that the rapid decay in the latter involved reaction with methanol, a moderately efficient hydrogen donor. Essentially the same rate constant for decay and spectral characteristics were obtained in various water:acetonitrile mixtures in the absence of base, with mole fractions of acetonitrile ranging from 0.3 to 1.0.

In order to verify that the transient species observed in the experiments described above was the benzophenone-like triplet state of KP, we carried out a series of quenching experiments.

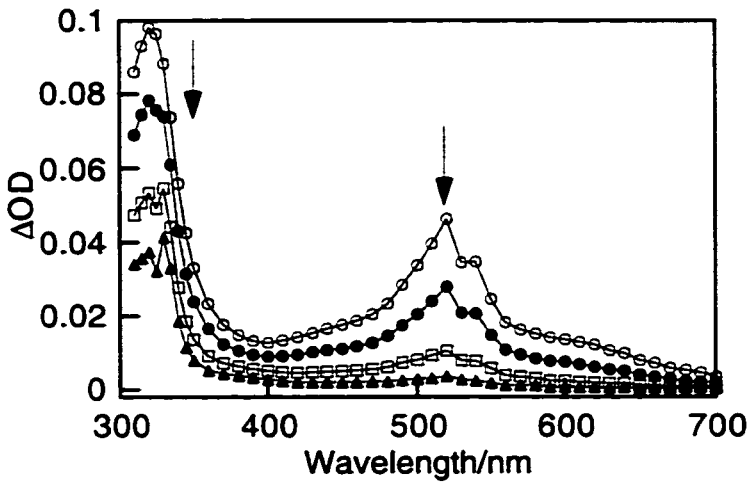

Figure 4-5: Transient absorption spectra of KP 3.2 x 10^{-4} M in water:acetonitrile solution, X_{water} 0.7, no NaOH. Laser 308 nm. N_2 bubbled. Time windows: (○) 0.96 μs; (●) 3.90 μs; (□) 9.44 μs; (▲) 15.6 μs after the laser pulse.

Sorbic acid (a conjugated diene) and 1-methylnaphthalene quench the 530 nm transient with rate constants of 7.3 x 10^9 and 1.1 x 10^{10} $M^{-1}s^{-1}$, respectively in water:acetonitrile (X_{water} 0.7). Both are well known triplet quenchers, with triplet energies significantly below that of benzophenone.[15] In the case of 1-methylnaphthalene quenching is accompanied by the formation of its readily detectable triplet state, characterized from its T-T absorption maximum at *ca.* 420 nm,[16] see Figure 4-6.

Beyond its diagnostic value, the formation of triplet 1-methylnaphthalene can be employed as a 'triplet counter' in order to determine the efficiency of intersystem crossing (see also Section 2.2.1.2.4). In these experiments samples of benzophenone and of KP (in water:acetonitrile, X_{water} 0.7) of matched absorbance at the laser wavelength (337 nm) were irradiated in the presence of enough 1-methylnaphthalene to quench at least 99% of the carbonyl triplets. Considering that the intersystem crossing efficiency of benzophenone is 1.0, [17] one can determine that for KP by comparison of the signal intensities at 420 nm. These experiments led to an intersystem crossing quantum yield of 1.0 ± 0.1 for KP in this solvent mixture.

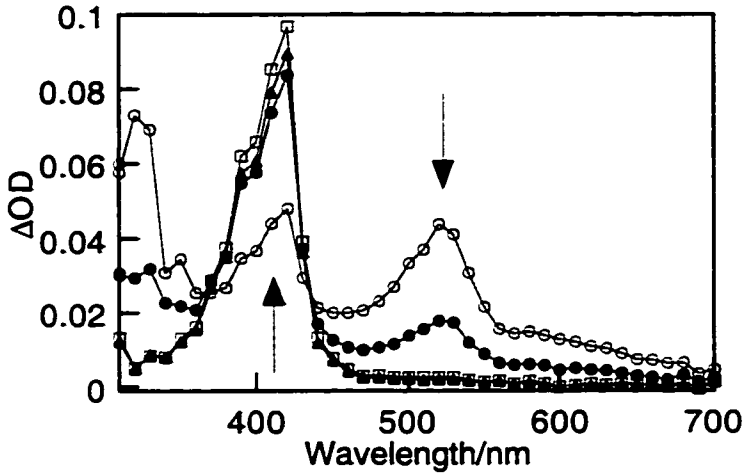

Figure 4-6: Transient absorption spectra of KP 6.4 x 10^{-4} M in water:acetonitrile solution, X_{water} 0.7, no NaOH, 1-methylnaphthalene 1.41 x 10^{-3} M was used as quencher. Laser 337 nm, N_2 bubbled. Time windows: (○) 20 ns; (●) 92 ns; (□) 316 ns; (▲) 704 ns after the laser pulse.

In contrast with the results in the absence of base, irradiation of KP in the presence of 8 mM base in water:acetonitrile (X_{water} 0.7) led to the carbanion with maxima at 330 and *ca.* 600 nm and a lifetime of 100 ns, about half the value observed in pure water. In fact, the carbanion decay rate constant showed an interesting dependence with the mole fraction of water, as illustrated in Figure 4-7. A spectral change was also observed in the visible region, with the maxima at 580, 600 and 620 nm for water mole fractions of 1.0, 0.7 and 0.13, respectively.

A study of the transients detected as a function of the solvent composition led us to select a mixture with a water mole fraction of 0.13 (5% v:v) for many of our mechanistic studies. These samples contained 8 mM base and 0.4 mM KP, and revealed two components in the transient absorption spectra, as shown in Figure 4-8-A. The fast component has a lifetime of 25-30 ns and is spectroscopically similar to that obtained in aqueous buffered solutions, while the longer-lived component resembles that observed in the absence of base in acetonitrile-rich solutions (*vide supra*). Addition of 10 mM 1,3-cyclohexadiene, an efficient triplet quencher, completely quenched the slow decaying

component (see Figure 4-8-B) with a bimolecular rate constant of 9.9 x 10^9 $M^{-1}s^{-1}$ (see Figure 4-9). We also determined the rate constant for quenching by biphenyl, which led to k_q 1.1 x 10^9 $M^{-1}s^{-1}$. Neither the rate of decay nor the signal intensity of the fast 620 nm component were affected by these typical triplet quenchers.

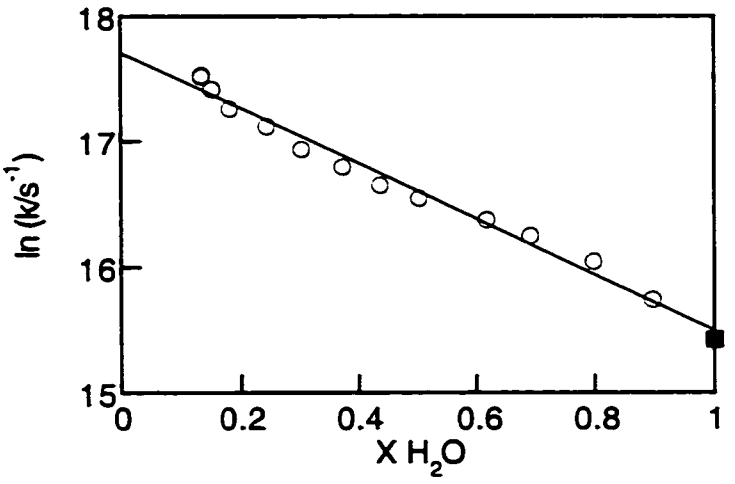

Figure 4-7: Dependence of the natural logarithm of the rate constant of decay of the KP transient (measured at 600 nm) with the molar fraction of water in water:acetonitrile mixtures. KP 2.85 x 10^{-4} M, TMAOH 8.02 x 10^{-3} M, (O) N_2 bubbled, (■) N_2O bubbled to scavenge the electron. Laser 308 nm.

The Arrhenius parameters characterizing the decay of the 620 nm transient were also determined for the 5% v:v water:acetonitrile mixture used above under basic conditions. The activation energy was 9.6 kJ/mol and the pre-exponential factor 2.3 x 10^9 s^{-1}. The corresponding fit has also been included in Figure 4-3. We note that in these experiments the base concentration was reduced to 2.5 mM to avoid its precipitation at the lower temperatures.

Finally, experiments were carried in fresh water:acetone mixtures as solvent in the presence of base irradiating with a 355 nm laser. Once more, the absorption of the transient produced after irradiation of KP resembles those observed in base-rich solutions in water, methanol and water:acetonitrile mixtures. As already observed in water:acetonitrile, the

transient decays faster as the water content decreases showing a lifetime of 180 ns and 20 ns for X_{water} 0.5 and 0.18 in acetone, respectively. A red shift of the maximum on the visible part of the spectrum is also evident (λ_{max} 620-630 nm for X_{water} 0.18), thus qualitatively supporting the results found in water:acetonitrile mixtures.

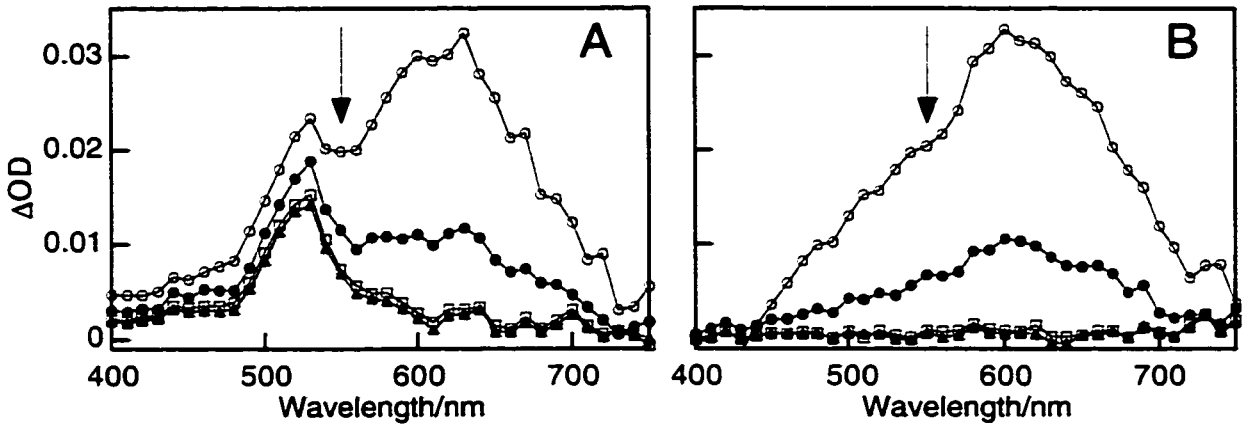

Figure 4-8: Transient absorption spectra of KP 2.5 x 10^{-4} M in water:acetonitrile solution, X_{water} 0.13, TMAOH 7.0 x 10^{-3} M, Laser 308 nm, N_2 bubbled. (A) In the absence of 1,3-cyclohexadiene. (B) 1,3-Cyclohexadiene 1.04 x 10^{-2} M used as quencher. Time windows: (○) 12 ns; (●) 45 ns; (□) 153 ns; (▲) 390 ns after the laser pulse.

4.2.3 Product Studies

Product analysis following laser irradiation of KP in 5% water:acetonitrile in the presence of base (8 mM) showed 3-ethylbenzophenone as the only product. In order to accumulate sufficient amounts of products, ten separate 2 ml samples were exposed to 200 laser shots and then combined.

Steady-state photolysis experiments were also performed. The quantum yield (Φ) for KP photodegradation was determined in 7% v:v water:acetonitrile under basic conditions and using ketoprofen in buffer pH 7.4 as a standard;[2] a value of 0.85 was determined in this solvent mixture. In both cases, ethylbenzophenone was the only species formed.

The product studies in the system of water:acetone as solvent reveal once more that only 3-ethylbenzophenone is formed upon irradiation.

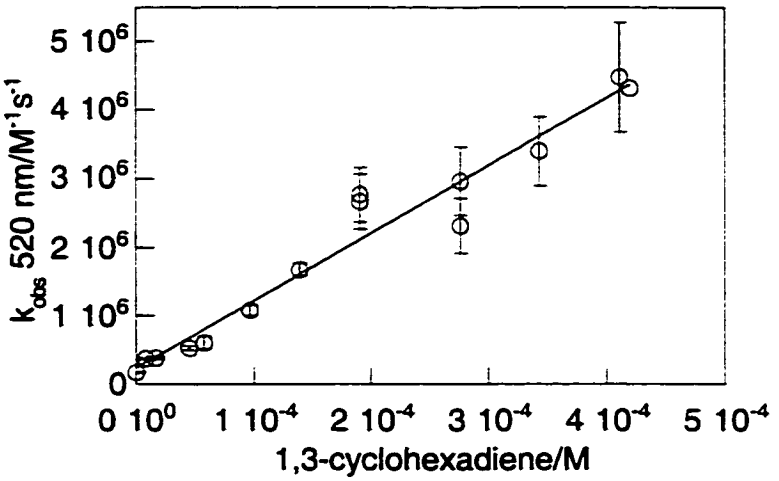

Figure 4-9: Dependence of the observed decay rate constant for KP 2.5 x 10^{-4} M, monitored at 520 nm with different 1,3-cyclohexadiene concentrations. X_{water} 0.13, TMAOH 7.0 x 10^{-3} M, Laser 308 nm. N_2 bubbled.

4.2.4 Discussion

The results obtained in the absence of base indicate that KP behaves as a conventional substituted benzophenone; *i.e.*, intersystem crossing yields are high and lead to a triplet state with virtually identical spectroscopic properties to those of benzophenone itself.[18,19] Energy acceptors, such as 1-methylnaphthalene, 1,3-cyclohexadiene and sorbic acid can readily quench this triplet. Further, while the KP triplet is moderately long lived in water:acetonitrile mixtures; in methanol it decays by hydrogen abstraction to yield the corresponding ketyl radical, according to Scheme 4-2.

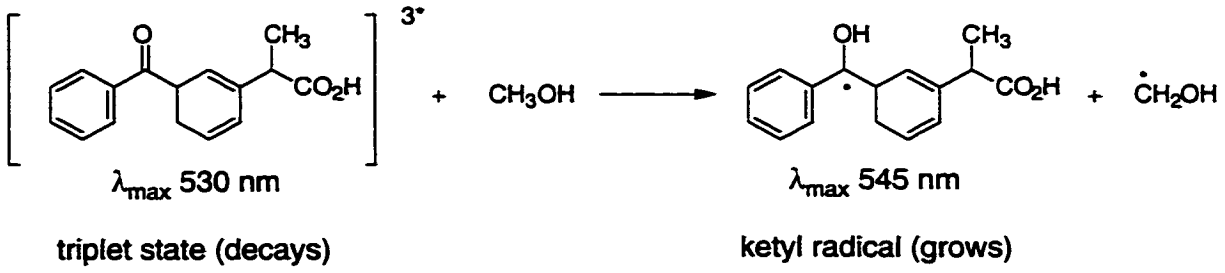

Scheme 4-2: Hydrogen abstraction from methanol by ketoprofen.

In contrast with the behavior outlined above, experiments in the presence of base in either methanol or water-rich acetonitrile (with water content > 5% v:v) lead to the characteristic carbanion absorbance in the 600 nm region. This transient signal shifts with the polarity of the solvent from 580 nm in water to 620 nm in 5% v:v water:acetonitrile. This suggests that the ground state carbanion is considerably more stabilized than its excited state in hydrogen bonding media. Similar shifts have been observed in other studies involving nitrocarbanions.[20,21] In the latter case laser flash photolysis studies reveal that 2,4-dinitrobenzyl carbanion has a band centered at 500 nm in water; the same species is observed in acetonitrile with a maximum at 640 nm.[21] These shifts are reasoned by a carbanion which exists in two different solvated forms; in one it is tightly hydrogen bonded to water molecules, whereas in the second form it is unspecifically solvated by the acetonitrile molecules.[20,21]

We can apply the same reasoning to the carbanion formed following ketoprofen decarboxylation (see Scheme 4-3). Thus unspecific solvation exists in highly enriched acetonitrile (λ_{max} 620 nm in X_{water} 0.13) or acetone mixtures (λ_{max} 630 nm in X_{water} 0.18), whereas in water, methanol or ethanol, the carbanion maximum is at 580 nm in all cases, due to a hydrogen bonded 1-(3-Benzoyl-phenyl)-ethyl carbanion.

In solvent mixtures with higher water contents both forms of solvation are present, as can be inferred from maximum values ranging between 580 and 620 nm.

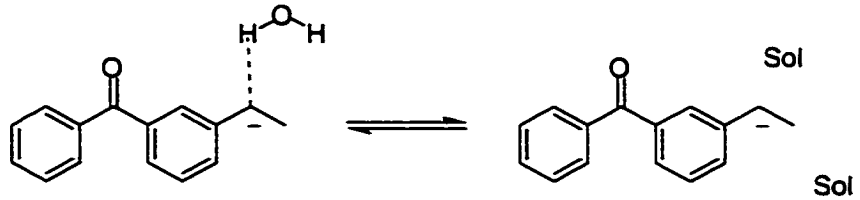

Scheme 4-3: Solvation of KP carbanion.

The hydrogen bonding accounting for the hypsochromic shift of the carbanion absorption would also explain its lower reactivity towards protonation in water or methanol

compared to 5% v:v water:acetonitrile mixtures. An analysis of Arrhenius parameters for the carbanion decay in water, methanol, and 95:5 acetonitrile:water shows that the different rate constant values at room temperature are due to different activation energies, higher in water or methanol (where the values are the same within experimental error) than in water enriched acetonitrile. Thus the *ca.* 13 kJ/mol stabilization observed in the absorption spectra of the carbanion in hydrogen bonding solvents compared to 95:5 v:v acetonitrile:water, is paralleled by a *ca.* 4.7 kJ/mol higher activation barrier for the protonation of the carbanion in the former solvent compared to acetonitrile:water mixtures, as obtained from the linear fit in Figure 4-7.

The question arises concerning the origin of the 600 nm transient. Specifically, is its precursor the excited singlet or triplet state of KP? The former would be an unusual behavior for a benzophenone chromophore. Benzophenones rarely show any excited singlet chemistry; normally singlet events are dominated by intersystem crossing to the triplet state, although some processes, such as delayed fluorescence have been characterized.[22] Whatever the precursor state it must be very short lived, given that the 600 nm signal grows-in within the duration (*ca.* 6 ns) of the short laser pulse. Figure 4-8 shows that the 600 nm and a long-lived triplet (λ_{max} 530 nm) can be detected simultaneously. The long lived triplet KP may initially be the undissociated carboxylic acid form of KP, which we already know (from the base-free experiments) does not yield any significant amounts of carbanion. However, acid-base equilibria are usually quite fast, and in the presence of 8 mM base, one would expect the deprotonation to be established in the excited triplet state of KP within 10 ns if the process was near diffusion-controlled. Even if this were two orders of magnitude slower, it should take less than 1 μs to establish acid-base equilibration; this would be expected to shorten the triplet lifetime. Clearly, added base does not lead to accelerated decay of the triplet signal (see Figure 4-10); in fact there is no indication that this equilibrium plays any significant role in the formation of the carbanion, or in controlling the KP triplet lifetime. Thus, we conclude that when the triplet KP is produced it does not lead to the formation of the 600 nm

carbanion, even when the conditions are controlled (with base) in such a way as to promote the formation of the carboxylate form of the KP triplet.

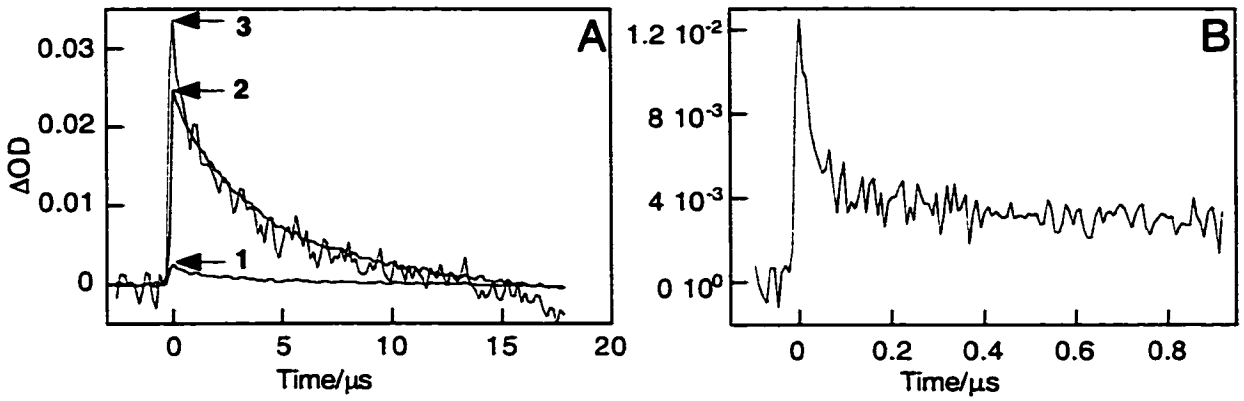

Figure 4-10: (A) Decay trace for KP 2.7 x 10^{-4} M, monitored at 510 nm, in water:acetonitrile solution (X_{water} 0.13). 308 nm laser, N_2 bubbled. (1) [TMAOH] 7.1 x 10^{-3} M; (2) no base; (3) Same as trace 1 multiplied by 12 to facilitate visual comparison. (B) Same conditions as curve 1 but monitored in a shorter time scale; note that the rapid decay of the carbanion is now detectable, even at 510 nm.

If the triplet state of KP, in either its acid or dissociated carboxylate form, cannot yield the carbanion, then one must conclude that the process of decarboxylation must be singlet-mediated. While this may be counter-intuitive in the context of benzophenone photochemistry, it does have the appeal of being able to produce a ground state carbanion in a spin-allowed process. A few examples of triplet mediated carbanion formation have been reported in the literature (see also Chapter 3). They generally involve adiabatic processes leading to the formation of triplet carbanions,[23-25] thus also meeting spin conservation requirements. This does not appear to be the case for KP, given that neither the lifetime nor the yield of the 600 nm species are influenced by the addition of triplet quenchers (see Figure 4-8).[11]

In view of the analysis presented above, we conclude that the mechanism of Scheme 4-4 accommodates all the experimental data available. In particular, we note that in this mechanism the triplet state (in either prototropic form) and the carbanion are not connected.

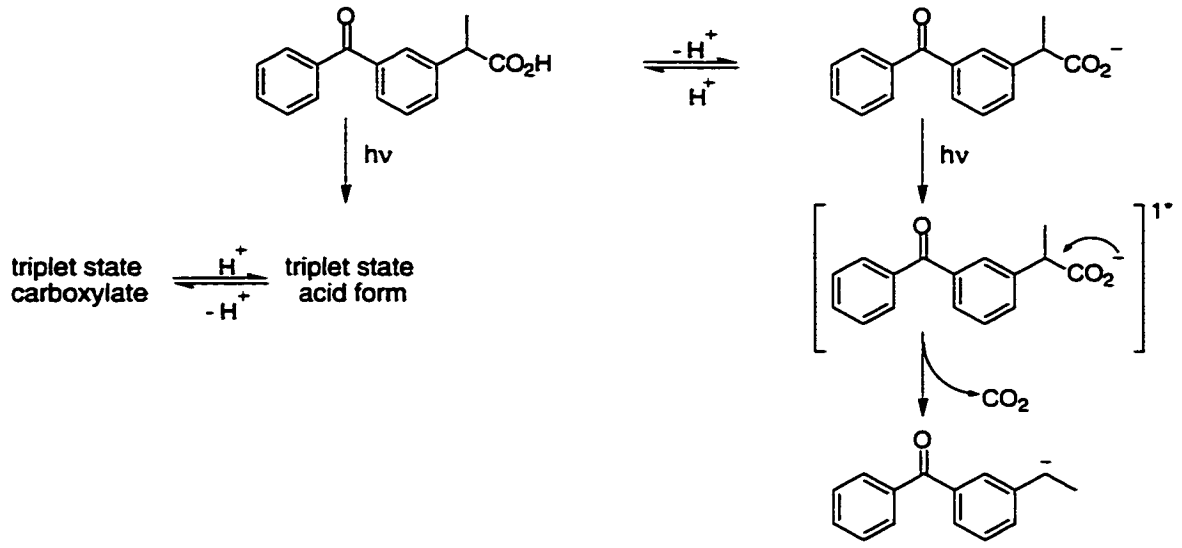

Scheme 4-4: Prototropic equilibrium and KP decarboxylation following excitation.

Another important piece of evidence consistent with this mechanism, is that the preexponential factors obtained for the decay at 600 nm are ~ 10^9 s^{-1}, further supporting the idea that the observed decay cannot reflect a bond fragmentation (*e.g.*, decarboxylation) process. The preexponential factors for such a process would be expected to be around 10^{12} s^{-1} or higher, reflecting the entropic gains associated with bond fragmentation.[22,25,26] The observed values may reflect a pseudo-first order reaction, such as the protonation of the carbanion.

Finally, results in water:acetonitrile with X_{water} 0.7 and containing equimolar KP and base (0.3 mM) show a biexponential decay that can be readily explained by incomplete dissociation of KP leading to laser excitation of both KP and its conjugate base, each undergoing its intrinsic photochemistry (data not shown). This is in line with results found by Wan and coworkers on the photodecarboxylation of diarylacetic acids in aqueous solutions.[27]

4.2.5 Conclusions to this Section

Our results demonstrate that the decarboxylation of KP occurs, not just in aqueous solution, but also in a range of less polar solvents and solvent mixtures, if the carboxylate

form of KP is present. The reaction path favored under a given set of conditions (solvent, presence of base) is determined exclusively by the ground state degree of dissociation of the substrate, given that the two pathways are not interconnected in the excited state manifold. In order to find the appropriate conditions for the simultaneous detection of the triplet and carbanion pathways it was necessary to study the system in solvent mixtures, including solvents such as acetonitrile and methanol.

Three general mechanisms have been proposed for a photodecarboxylation; homolytic, mesolytic, and heterolytic.[28] Our results, in combination with a recent study by Wan and coworkers with different analogs of ketoprofen, show that the mechanism of decarboxylation is heterolytic in nature,[29] contrary to the mesolytic type (*i.e.*, involving intramolecular electron transfer) previously proposed.[12] The heterolytic mechanism (shown in Scheme 4-4 for ketoprofen) has also proved operative in the photo-retro-aldol type reactions of nitrobenzyl derivatives.[30] Thus nitrobenzyls and aroylphenylmethyl groups may be thought of as photolabile carbanion leaving groups, as suggested by Wan *et al.*[29]

New results in the literature, obtained with time-resolved laser-induced optoacoustic studies of KP, have further shown that KP decarboxylates within the laser pulse duration to produce the carbanion with an enthalpy of formation relative to the ground state anionic form of KP of *ca.* 256 kJ/mol. The heat released following prompt protonation of this species in *ca.* 200 ns indicates that ethylbenzophenone enthalpy of formation is *ca.* 45 kJ/mol higher than that of ground state KP anion.[31] These results further corroborate our herein proposed mechanism for the photodegradation of KP anion.

While our results have been obtained under a considerable deviation from physiological conditions, we note that in living systems organized assemblies such as lipid bilayers and proteins are also expected to provide environments of reduced polarity. The fast and efficient deactivation of excited ketoprofen anion precludes its interaction with any cell component. Similar ideas can be applied to the short lived KP carbanion. This lifetime for the carbanion would even be shorter in the reduced polarity environments of lipoproteins

or lipid bilayers. We therefore anticipate that the phototoxic effect of KP relies in its photoproduct, 3-ethylbenzophenone. The photobehavior of the later would be similar to that of benzophenone, given their structural resemblance.

4.3 Properties and Reactivity of 1-(3-Benzoyl-phenyl)-alkyl Carbanions

4.3.1 Laser Flash Photolysis Studies of Alkyl Derivatives of KP

The possibility of generating a carbanion within the duration of a laser pulse provides a very interesting intermediate on which to perform mechanistic studies. Thus, beyond the importance of the KP photogenerated carbanion as an intermediate involved in the photodegradation of a pharmaceutical product, it is an attractive substrate to study in order to understand the chemistry of this reactive species in different systems, in particular, water.

Our efforts were directed towards gaining an insight in the carbanion reactivity; to that effect we synthesized molecules **3** and **4**, shown in Scheme 4-5. These molecules in combination with commercially available **1** and **2** render a complete set where primary, secondary and tertiary 1-(3-benzoyl-phenyl)-alkyl carbanions are attainable for kinetic and spectroscopic investigation following light induced photodecarboxylation of **1**, **2**, and **3** and **4**, respectively.

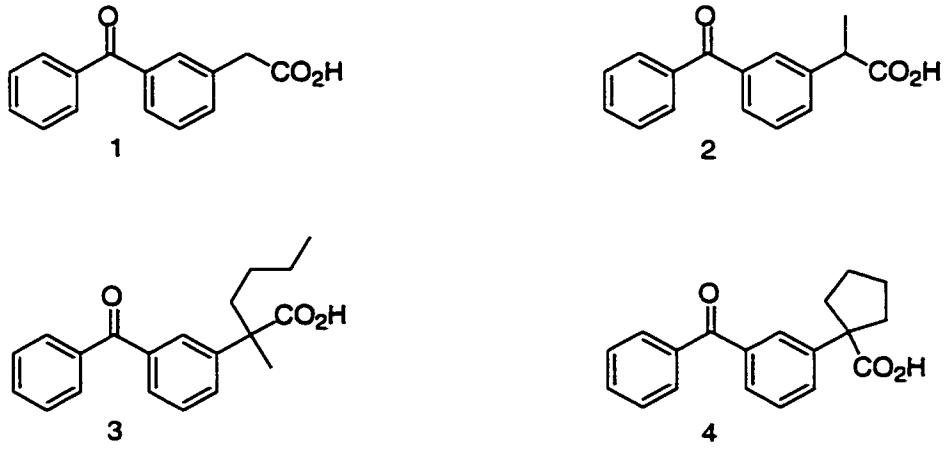

Scheme 4-5: Structure of alkyl derivatives of ketoprofen.

Following 308 nm laser excitation in 0.1 M KOH aqueous solutions, compounds **1**, **3** and **4** give rise to transient absorption spectra similar to that observed following LFP studies of KP (species **2** in Scheme 4-5). These spectra, including that of KP carbanion for

comparison, are shown in Figure 4-11. Note that they have been normalized in the visible region.

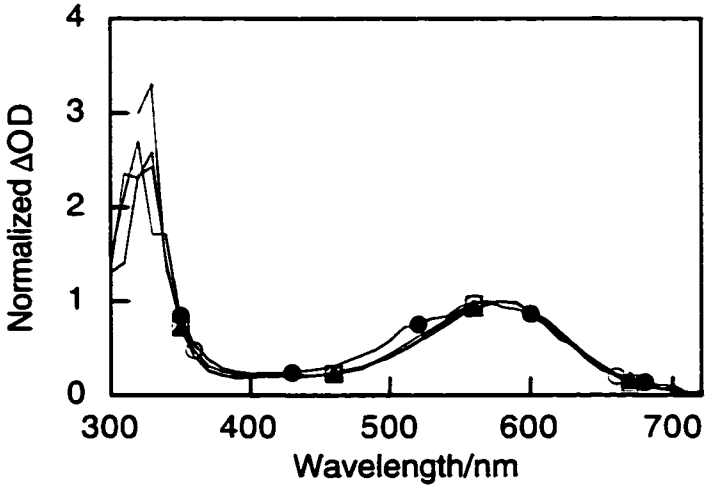

Figure 4-11: Normalized transient absorption spectra obtained following 308 nm laser excitation of a KOH 0.1 M, 1% v:v MeOH aqueous solution (a few points are shown to assist in the visualization). (●) species 1, 16 ns after the laser pulse; (□) species 2, 48 ns after the laser pulse; (▲) species 3, 48 ns after the laser pulse; (○) species 4, 64 ns after the laser pulse. Solutions were equilibrated under N_2O. Experimental points were acquired at a 10 nm interval.

The visible part of the spectrum is the same for all species, with a broad maximum located at *ca.* 580 nm (see also Table 4-1). In the case of species **1**, a shoulder is noticeable at *ca.* 520 nm. This is due to a contribution by absorption from the triplet state of species **1**, as determined from time windows monitored at longer times following excitation (data not shown). This is similar to the situation encountered for ketoprofen in acetonitrile:water mixtures with X_{water} 0.13 (see Figure 4-8-A).

The time evolution of the transient absorption for species **1** to **4**, recorded at 600 nm, is shown in Figure 4-12. These traces are best fit by a first order decay. The values for the observed rate constants are presented in Table 4-1.

Table 4-1: Decay rate constant and absorption maxima for various carbanions photogenerated from KP and KP alkyl-derivatives.

Compound	λ max/nm	Decay rate constant/s^{-1}	Relative rate constant
1	570	$26.8 \pm 0.3 \times 10^6$	(1:2) 5.79 ± 0.1
2	570	$4.63 \pm 0.04 \times 10^6$	(2:2) 1.00 ± 0.02
3	580	$2.17 \pm 0.01 \times 10^6$	(3:2) 0.469 ± 0.006
4	580	$2.04 \pm 0.01 \times 10^6$	(4:2) 0.440 ± 0.006

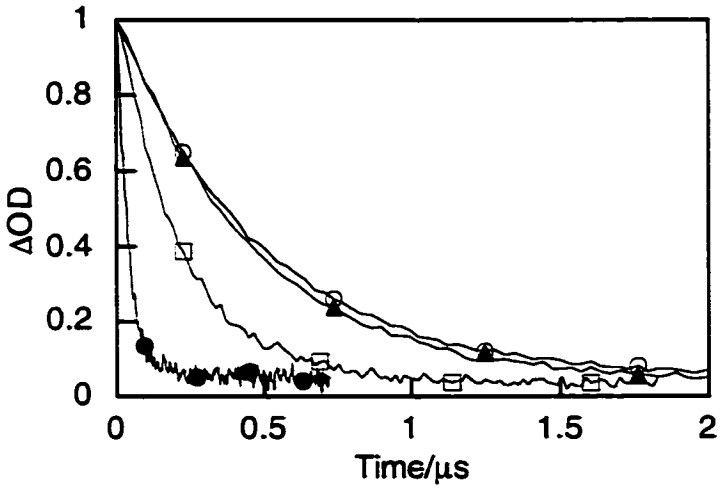

Figure 4-12: Normalized transient absorption time evolution traces obtained following 308 nm laser excitation of a KOH 0.1 M aqueous solution (a few points are shown to assist in the visualization). (●) species 1; (□) species 2; (▲) species 3; (○) species 4. Solutions were equilibrated under N_2O.

An analysis of Figure 4-12 and of the data of Table 4-1 shows that there is a large effect attributable to alkyl substitution on the decay rate constant of the carbanion. Introduction of a first alkyl group in **1** structure increases the lifetime of the resulting secondary carbanion by a factor of five in comparison to the value registered for the carbanion formed following **1** photoexcitation.

Inclusion of a second alkyl group (structure **3** and **4**) increases the lifetime of the resulting tertiary carbanion by a factor of *ca.* ten with respect to the primary one. The change is not so marked with respect to the secondary carbanion, and the lifetime is only two times longer for tertiary as compared to secondary carbanions. There is also a slight difference in the lifetime of carbanions photogenerated from **3** and **4**; the latter being longer lived.

4.3.2 Laser Flash Photolysis Studies of Halo-alkyl Derivatives of KP

In order to study the nucleophilic behavior of the photogenerated carbanion, and given the fast protonation of this species in water (*vide supra*), we synthesized derivatives of structures **2** and **3** where an electrophilic center was tethered to the KP molecule (see Scheme 4-6). Thus this center would effectively compete with water for the carbanion. Upon their excitation, structures **3 a** to **3 c**, as well as **2 a**, are expected to render their respective 1-(3-benzoyl-phenyl)-alkyl carbanions. The nucleophile thus formed will either react with the solvent molecules (*i.e.*, water), or undergo an intramolecular reaction where the different leaving groups (I, Br, and Cl) attached at the end of a 4-carbon alkyl chain are expected to play a key role.

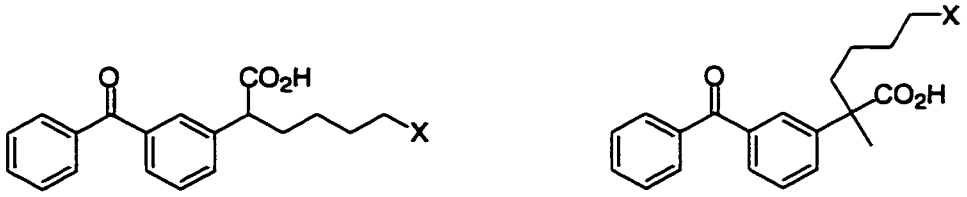

2 a X = I

3 a X = I
3 b X = Br
3 c X = Cl

Scheme 4-6: Structure of alkyl-substituted derivatives of ketoprofen.

The transient absorption spectra corresponding to each of the carbanions generated following excitation of structures **2 a** to **3 c** are shown in Figure 4-13. Note that all the spectra are similar, and similar to those obtained with structures **1** to **4**.

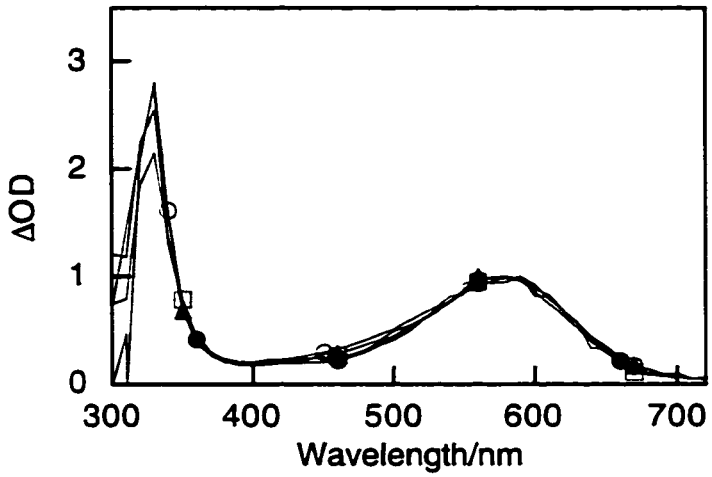

Figure 4-13: Normalized transient absorption spectra obtained following 308 nm laser excitation of a KOH 0.1 M, 1% v:v MeOH, aqueous solution (a few points are shown to assist in the visualization). (●) species 2 a, 16 ns after the laser pulse; (□) species 3 a, 48 ns after the laser pulse; (▲) species 3 b, 48 ns after the laser pulse; (○) species 3 c, 48 ns after the laser pulse. Solutions were equilibrated under N_2O. Experimental points were acquired at a 10 nm interval.

The time evolution of the carbanion signal is shown in Figure 4-14. Included in Figure 4-14-A is the decay corresponding to the carbanion from **3**, to facilitate visual comparison with the different carbanions resulting from excitation of **3 a** to **3 c**. Figure 4-14-B shows the decay traces for the carbanions photogenerated from **2** and **2 a**. From the inspection of Figure 4-14, and the analysis of the first order decay rate constants for the different carbanions listed in Table 4-2, we observe that the better the leaving group in the alkyl chain, the faster the decay of the carbanion.

The observed trend is within the same range of values for structures **2** and **3** and their 6-iodo-pentyl derivatives **2 a** and **3 a** respectively.

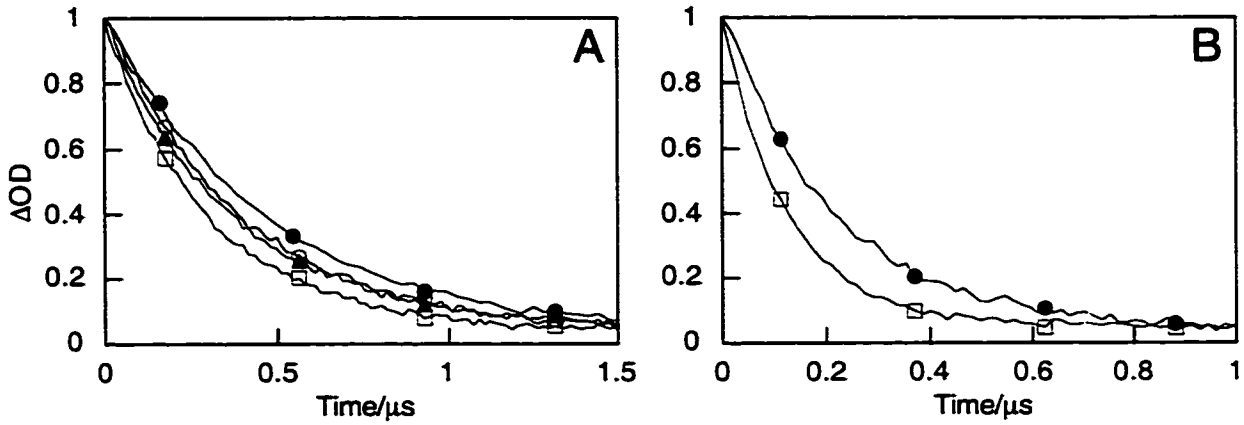

Figure 4-14: Normalized transient absorption time evolution traces obtained following 308 nm laser excitation of a KOH 0.1 M aqueous solution (a few points are shown to assist in the visualization). (A): (●) species 3; (□) species 3 a; (▲) species 3 b; (○) species 3 c. (B) (●) species 2; (□) species 2 a. Solutions were equilibrated under N_2O.

Table 4-2: Decay rate constant and absorption maximum for various carbanions photogenerated from KP and halo-alkyl substituted KP derivatives.

Compound	λ max/nm	Decay rate constant/s^{-1}	Relative rate constant
2 a	580	$7.94 \pm 0.06 \times 10^6$	**(2:2 a)** 0.58 ± 0.01
3 a	580	$3.20 \pm 0.04 \times 10^6$	**(3:3 a)** 0.68 ± 0.01
3 b	560	$2.77 \pm 0.02 \times 10^6$	**(3:3 b)** 0.78 ± 0.01
3 c	580	$2.57 \pm 0.02 \times 10^6$	**(3:3 c)** 0.84 ± 0.01

4.3.3 Discussion

Product studies performed with species **1** and other ketoprofen derivatives have demonstrated that the photodecarboxylation pattern characteristic of KP is in fact a common denominator in (aroyl-phenyl)-alkyl carboxylic acids.[29] Our results obtained with a series of 2-(3-benzoyl-phenyl)-alkyl carboxylic acids further confirm these results. Thus, the transient absorption spectra obtained are independent of the acid employed, and in all cases are equal to that of KP carbanion.

Two sets of molecules were studied. In the first one, involving substrates **1** to **4**, different alkyl substituents have been attached to the parent structure of compound **1** ((3-benzoyl-phenyl)-ethanoic acid). In this first series all the carbanions generated upon photoexcitation can only decay *via* protonation by the water (considering that KOH 0.1 M was employed in these experiments, the protonation by free H^+ can be ruled out). In this regard, it is interesting the observed trend in decay rate constants presented in Table 4-1, where a primary carbanion reacts faster than a secondary one, which in turn is more reactive than a tertiary carbanion. We can preclude a lower stabilization of the carbanion resulting from **1**, in comparison to that obtained from **2**, **3**, or **4**, as a viable explanation for the observed tendency. Such lower stabilization would be accompanied by a bathochromic shift of the carbanion spectra (*vide supra*); no such shift is observed when comparing carbanions from **3** or **4** with that from **1**. Further the carbanion stability order is tertiary < secondary < primary <methyl, given that substitution by electron-donating alkyl groups result in a greater negative charge density at the carbanion central carbon atom.[32] Thus, the trend in protonation is contrary to previous expectations.

A possible explanation is that protonation is determined by entropic rather than enthalpic factors. In fact, the resonance with the benzoyl-phenyl group, common to all these carbanions, would account for most of the stabilization effects, turning negligible the role of alkyl substitution and thus resulting in all these carbanions being isoenergetic. The reactivity is then determined by the size of the alkyl groups attached to the carbanion center, where steric impedance to protonation occurs with bulkier groups. This would also account for the slight difference observed in the protonation rates of carbanions photogenerated from **3** and **4**, where the cyclopentyl ring existing in the tertiary carbanion generated from **4** would add an extra constrain compared to the tertiary carbanion from **3**.

The second set of synthesized molecules was intended to explore the feasibility of intramolecular S_N2 and/or E2 reactions, as shown in Scheme 4-7.

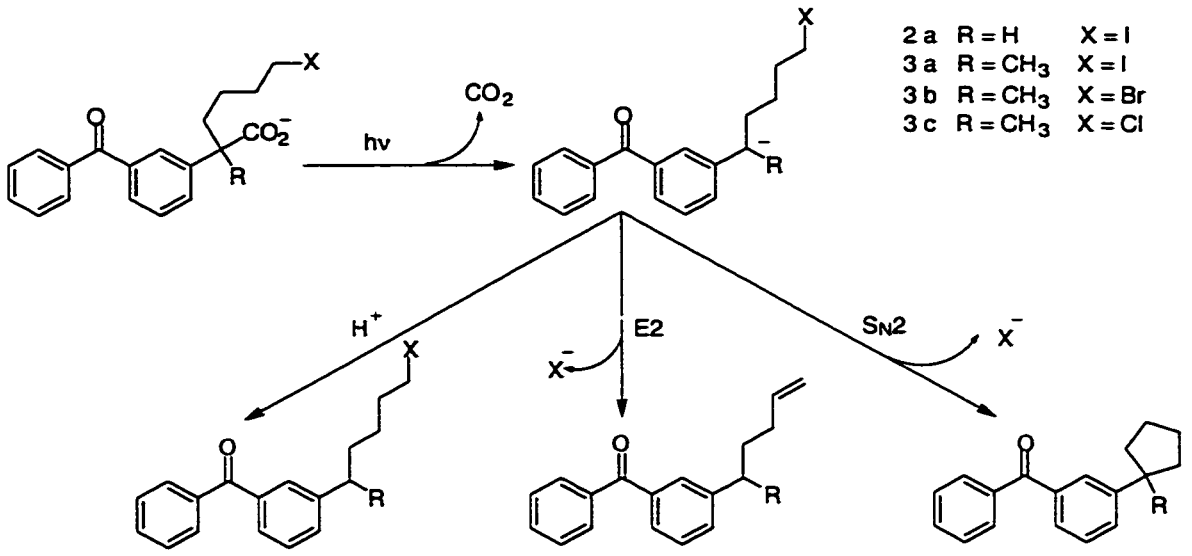

Scheme 4-7: Reactions of 1-(3-benzoyl-phenyl)-alkyl carbanions.

Carbanions generated upon photolysis of **2 a** and **3 a** to **3 c** are expected to have an additional decay pathway, in comparison to the carbanions from parent structures **2** and **3**, given by intramolecular reaction. This would result from the existence of electrophilic centers tethered at the end of the alkyl chain; centers that are absent in structures **2** and **3**. In all cases the measured decay rate constants for carbanions from substituted **2** and **3** and a comparison to those of the parent structures indicate that these intramolecular deactivation channels are operational. This is best shown by Equations 4-1 and 4-2.

Equation 4-1: $k_{exp}\,parent = k_{H^+}$

Equation 4-2: $k_{exp}\,subst. = k_{H^+} + k_{intra}$

where $k_{exp}parent$ is the observed decay rate constant of the parent carbanions generated from **2** and **3**, due only to protonation (k_{H+}) by the solvent, and $k_{exp}subst.$ is the observed decay rate constant measured for substituted structures **2 a** to **3 c** due both to protonation and intramolecular reactions (k_{intra}). We expect no difference in k_{H+} for a given set of molecules

(*i.e.*, **3** and its derivatives, as well as **2** and its derivatives), and therefore the different decay rate constants measured are due to intramolecular decay reactions.

The fraction of halogen-substituted carbanions undergoing protonation reactions (Φ_{H^+}) is determined by the relative rate constants listed in Table 4-2, as shown in Equation 4-3.

Equation 4-3: $$\Phi_{H^+} = \frac{k_{exp}\, parent}{k_{exp}\, subst.}$$

An analysis of the relative yield of intramolecular reactions ($1-\Phi_{H^+}$) shows that the reactivity of the carbanion towards the different electrophilic centers (given by different substitution patterns) follows the expected trend where iodo-alkyl carbanions react faster than bromo-alkyl ones, which in turn are faster than the chloro-alkyl. This is the same order for the leaving group ability for halides, *i.e.*, I > Br > Cl.[33]

The relative yield of intramolecular reaction for carbanions from **2 a** and **3 a** reports on the steric effect a methyl group has in the nucleophilic attack by the carbanion to the iodo-alkyl chain. Thus intramolecular nucleophilic attack is *ca.* 1.3 fold faster for the secondary carbanion, in comparison to the tertiary one. It is interesting that this steric effect is smaller compared to that for protonation of the parent carbanions photogenerated from **2** and **3** (*vide supra*).

At the present stage of development, product studies are necessary in order to determine to which extent intramolecular E2 reactions are taking place, as compared to S_N2 ones. Although the primary electrophilic centers would give rise to S_N2, the presence of strong base might also favor elimination over substitution. These topics will be solved with the previously mentioned product studies, currently under way with the assistance of Dr. L. Llauger, who has become actively involved in this research project.

4.3.4 Conclusions to this Section

The possibility of attaining "instant" generation of carbanions has allowed obtaining preliminary results on their reactivity in water, where steric factors have been determined in their reaction of protonation by the solvent. A second series of results have also shown the carbanion reactivity towards different halo-alkyl derivatives. This approach gives the possibility of obtaining absolute rate constants for the reactions of these species in different solvent media. Thus we foresee studies in dimethylsulfoxide, dimethylformamide or tetrahydrofuran solutions in the presence of NaH, under argon atmosphere, that will report more information on different mechanistic aspects of these type of carbanions. These will support the existing data published by Bocrath *et al.*,[34,35] which to our knowledge is the only other group that has reported such type of results.

Note:

During the reviewing period of this thesis, product studies have been performed on substrates **2a**, and **3a** to **3c**, following irradiation in water with KOH 0.1M. This study has also been done in DMSO solutions containing NaH and 2-(3-benzoyl-phenyl)-6-iodo-heptanoic acid. The results indicate that whereas in water the only product observed is that arising from carbanion protonation, following irradiation in DMSO of 2-(3-benzoyl-phenyl)-6-iodo-heptanoic acid solutions,[39] the cyclization is observed.

4.4 Conclusions

The pharmaceutical product ketoprofen has been shown to decarboxylate from the excited singlet state to render a very short lived carbanion. Temperature, solvent as well as substitution effects have been analyzed for the protonation of this intermediate. We have been able to elucidate the ketoprofen mechanism of photodegradation. We further believe the carbanion generated as an intermediate poses an interesting system as a probe to learn more about the reactivity of this species. In this sense, results not included in this chapter and involving a project currently under way with the assistance of M. N. Chrétien, have given promising results, where the deactivation of the carbanion is extremely prolonged in the anhydrous zeolite environment, as determined by diffuse reflectance time-resolved studies. These results are further supported by deuterium incorporation in ethylbenzophenone, following irradiation of ketoprofen included within a zeolite, under D_2O atmosphere. These results will further be explored in the near future, to establish the possibility of performing intermolecular alkylation reactions within the zeolite framework.

4.5 Materials and Methods

Materials. Ketoprofen (2-(3-benzoyl-phenyl)-propionic acid), sodium hydroxide, potassium hydroxide, tetramethylammonium hydroxide (TMAOH) sorbic acid (2,4-hexadienoic acid), 1-methylnaphthalene, and biphenyl were used as received; 1,3-cyclohexadiene was distilled before use. They were all purchased from Sigma-Aldrich Canada (Oakville, ON, Canada). The compound (3-benzoyl-phenyl)-ethanoic acid was purchased from Karl Industries Inc. (Aurora, OH, U.S.A.). All the reagents employed in the synthesis were obtained from Sigma-Aldrich Canada.

All solvents were HPLC-grade and purchased from OmniSolv (Gibsstown, NJ, USA), and were used without further purification. Water was purified through a Millipore MilliQ system.

4.5.1 Synthesis

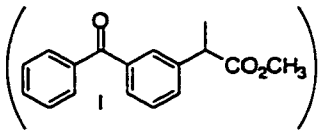

I **2-(3-Benzoyl-phenyl)-propionic acid methyl ester (I).** To a solution of KP (1.00 g, 3.93 mmol) in methanol (10.0 ml) was added 0.5 ml of H_2SO_4 98% under stirring. The solution was heated under reflux for 3 h. The reaction mixture was concentrated under reduced pressure, and the oily residue was neutralized with a 10% w:v aqueous solution of Na_2CO_3. The resulting mixture was extracted with ethyl acetate, the solvent was removed under reduced pressure and the final product was purified by flash chromatography with a 1:1 ethyl acetate:hexane mixture to afford 1.00 g (3.73 mmol, 94.6% yield) of the ester.

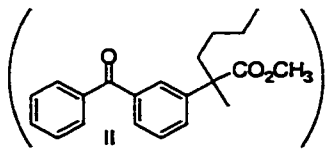

II **2-(3-Benzoyl-phenyl)-2-methyl hexanoic acid methyl ester (II).** This step follows the basic procedure described by Arnó *et al.*[36] A solution of KP methyl ester I (2.00 g, 7.46 mmol) in anhydrous THF (100 ml) was cooled down under stirring in a

dry ice-acetone bath (-78 °C). LDA (4.10 ml, 8.20 mmol) was added dropwise through a syringe, under constant stirring. The solution turned red wine-colored after the first 3 to 4 drops. HMPA (1.30 ml, 7.40 mmol) and 1-bromobutane (2.40 ml, 22.40 mmol) were successively added *via* a syringe, and the solution was left stirring for another 15 min, after which the dry ice-acetone bath was replaced by an ice bath. The ice bath was removed, and upon warming up to room temperature, the solution decolored into a pale yellow. The solution was quenched with aqueous saturated NH_4Cl. It was later on extracted with ether, the solvent was removed under reduced pressure and the final product was purified by flash chromatography with a 1:4 ethyl acetate:hexane mixture to afford 1.82 g (5.62 mmol, 75.3% yield) of the product.

2-(3-Benzoyl-phenyl)-2-methyl hexanoic acid (3). To a suspension of compound **II** (0.9 g, 2.78 mmol) in 100 ml of 10% w:v NaOH, were added 105 ml of methanol under stirring. The solution turned clear upon warming up, and it was heated under reflux for 3 h. The reaction mixture was concentrated under reduced pressure, and the oily residue was acidified to pH 3 with aqueous HCl. It was extracted with ethyl acetate, to yield 0.79 g of pure acid (2.56 mmol, 92% yield). ^{1}H-NMR (300 MHz, $CDCl_3$) δ 7.83-7.82 (m, 1H), 7.79-7.76 (m, 2H), 7.67-7.53 (m, 3H), 7.47-7.41 (m, 3H), 2.08-1.89 (m, 2H), 1.59 (s, 3H), 1.35-1.07 (m, 4H), 0.85 (t, J=7.0, 3H); ^{13}C-NMR (300 MHz, $CDCl_3$) δ 197.03 (C_4), 182.43 (C_4), 143.74 (C_4), 137.92 (C_4), 137.83 (C_4), 132.9 (CH), 130.93 (CH), 130.51 (CH) x 2, 129.21 (CH), 128.69 (CH), 128.66 (CH) x 2, 128.33 (CH), 50.44 (C_4), 39.08 (CH_2), 27.14 (CH_2), 23.49 (CH_2), 22.78 (CH_3), 14.33 (CH_3). HRMS calculated: 310.1570; obtained: 310.1594.

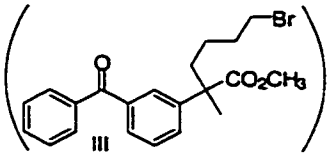

III

2-(3-Benzoyl-phenyl)-6-bromo-2-methyl-hexanoic acid methyl ester (III). The procedure was the same as that employed for the synthesis of **II**. 1,4-dibromobutane was employed, in a 4/1 mol ratio to KP methyl ester (rather than 3/1 as with compound **II**). The solution decolored at 0 ° C. The yield obtained was 82%. ^{1}H-

NMR (300 MHz, $CDCl_3$) δ 7.79-7.72 (m, 3H), 7.66-7.39 (m, 6H), 3.65 (S, 3H), 3.36 (t, J=6.8, 2H), 2.09-1.78 (m, 4H), 1.58 (s, 3H), 1.37-1.26 (m, 2H); ^{13}C-NMR (300 MHz, $CDCl_3$) δ 196.98 (C_4), 176.53 (C_4), 144.29 (C_4), 138.04 (C_4), 137.85 (C_4), 132.94 (CH), 130.58 (CH), 130.47 (CH) x 2, 129.12 (CH), 128.75 (CH), 128.68 (CH) x 2, 127.93 (CH), 52.71 (CH_3), 50.62 (C_4), 38.67 (CH_2), 33.77 (CH_2), 33.31 (CH_2), 23.71 (CH_2), 23.05 (CH_3). HRMS calculated: 402.0831; obtained: 402.0807.

2-(3-Benzoyl-phenyl)-6-iodo-2-methyl-hexanoic acid (3 a). This hydrolysis follows the procedure described by Olah *et al.*[37] Compound **III** (1.28 g, 3.18 mmol) and NaI (1.91 g, 12.73 mmol) were dissolved in a 50 ml round bottom flask, with 25 ml of dry acetonitrile. Chlorotrimethylsilane (1.62 ml, 12.73 mmol) was added with continuous stirring and the solution was heated under reflux for 50 h. Note that there was no change after 24 h of reflux, as determined by TLC. The solution was cooled down to room temperature and the reaction was quenched by addition of water. The resulting solution was extracted with ether, and the ether solution, brown in color and containing the desired product, was washed with sodium thiosulfate, rendering a clear solution. The solvent was removed under reduced pressure and the obtained mixture, consisting on the desired iodo-acid, as well as its methyl ester, in a 1/3 ratio, was purified by flash chromatography with a 1:1 ethyl acetate:hexane mixture to afford 0.2070 g (0.475 mmol, 15% yield) of the product. ^{1}H-NMR (300 MHz, $CDCl_3$) 7.83 (broad S, 1H), 7.78 (broad S, 1H), 7.76 (broad S, 1H), 7.67-7.54 (m, 3H), 7.47-7.42 (m, 3H) 3.12 (t, J=6.9, 2H), 2.09-1.90 (m, 2H), 1.84-1.72 (m, 2H), 1.62 (s, 3H), 1.41-1.23 (m, 2H); ^{13}C-NMR (300 MHz, $CDCl_3$) δ 197.06 (C_4), 182.45 (C_4), 143.35 (C_4), 138.01 (C_4), 137.74 (C_4), 133.01 (CH), 130.88 (CH), 130.54 (CH) x 2, 129.43 (CH), 128.83 (CH) x 2, 128.72 (CH), 128.20 (CH), 50.36 (C_4), 38.17 (CH_2), 34.01 (CH_2), 25.97 (CH_2), 22.63 (CH_2), 6.84 (CH_3). HRMS calculated: 436.0536; obtained: n/a.

2-(3-Benzoyl-phenyl)-6-bromo-2-methyl-hexanoic acid (3 b). This hydrolysis follows the procedure described by Abad *et al.*[38] To 3 g of compound **III** (9.9 mmol) were added 250 ml of methanol. A solution prepared with 200 ml of methanol, 40 ml of water and

10 g of KOH was added to the previous solution. The resulting reaction mixture turned yellow. The solution was left stirring at room temperature for 60 h, after which it was quenched by adding aqueous HCl 3.5% w:v, to bring the pH to a final value of 6. The resulting solution was concentrated under reduced pressure to eliminate the methanol. The obtained suspension was washed with ethyl acetate. The solvent was removed under reduced pressure and the crude, consisting on a mixture of 4 products (product 3 b, the starting material, as well as the acid and ester where Br was substituted by OMe) was purified by flash chromatography with a 1:1 ethyl acetate:hexane mixture to afford 0.3084 g (1.07 mmol, 10% yield) of the product. ^{1}H-NMR (300 MHz, $CDCl_3$) δ 10.7 (broad S, 1H) 7.83 (broad S, 1H), 7.78-7.75 (m, 2H), 7.67-7.41 (m, 6H), 3.34 (t, J=6.7, 2H), 2.10-1.91 (m, 2H), 1.88-1.75 (m, 2H), 1.62 (s, 3H), 1.49-1.24 (m, 2H); ^{13}C-NMR (300 MHz, $CDCl_3$) δ 197.09 (C_4), 182.38 (C_4), 143.38 (C_4), 137.99 (C_4), 137.74 (C_4), 133.03 (CH), 130.89 (CH), 130.54 (CH) x 2, 129.42 (CH), 128.83 (CH), 128.72 (CH) x 2, 128.21 (CH), 50.40 (C_4), 38.43 (CH_2), 33.76 (CH_2), 33.31 (CH_2), 23.68 (CH_2), 22.64 (CH_3). HRMS calculated: 388.0674; obtained: 388.0665.

2-(3-Benzoyl-phenyl)-6-chloro-2-methyl-hexanoic acid (3 c). A solution of compound **III** (1.8 g, 5.9 mmol) was prepared with 160 ml of isopropanol and 320 ml of HCl 3.5% w:v. The solution was heated under reflux for 24 h, under constant stirring. The solution was concentrated under reduced pressure and the organic substrates were extracted with ethyl acetate. The solvent was removed under reduced pressure and the final product was purified by flash chromatography with a 1:1 ethyl acetate:hexane mixture to afford the final product with 45% yield. ^{1}H-NMR (300 MHz, $CDCl_3$) δ 10.37 (broad S, 1H) 7.84-7.82 (m, 1H), 7.79-7.75 (m, 2H), 7.67-7.53 (m, 3H), 7.47-7.25 (m, 3H), 3.48 (t, J=6.7, 2H), 2.11-1.91 (m, 2H), 1.85-1.67 (m, 2H), 1.62 (s, 3H), 1.49-1.21 (m, 2H); ^{13}C-NMR (300 MHz, $CDCl_3$) δ 197.07 (C_4), 182.42 (C_4), 143.35 (C_4), 138.01 (C_4), 137.75 (C_4), 133.00 (CH), 130.93 (CH), 130.86 (CH), 130.52 (CH) x 2, 129.41 (CH), 128.82 (CH), 128.71 (CH) x 2,

128.19 (CH), 50.40 (C_4), 45.02 (CH_2), 38.58 (CH_2), 33.16 (CH_2), 22.62 (CH_3), 22.40 (CH_2). HRMS calculated: 344.1180; obtained: 344.1178.

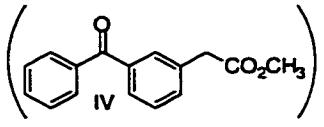

(3-Benzoyl-phenyl)-acetic acid methyl ester (IV).[39] Prepared in the same way as **I**, but employing (3-benzoyl-phenyl)-acetic acid (*i.e.*, **1**) rather than KP. The obtained yield was 80%.

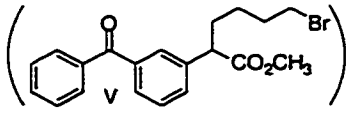

2-(3-Benzoyl-phenyl)-6-bromo-hexanoic acid methyl ester (V).[39] Prepared in the same way as **III**, but employing **IV** ((3-benzoyl-phenyl)-acetic acid methyl ester). The obtained yield was 37%. ^{1}H-NMR (500 MHz, $CDCl_3$) δ 7.76-7.71 (m, 3H), 7.66-7.39 (m, 6H), 3.61 (S, 3H), 3.60 (t, J=7.7, 1H), 3.32 (t, J=6.6, 2H), 2.11-2.06 (m, 1H), 1.86-1.77 (m, 3H), 1.43-1.34 (m, 2H); ^{13}C-NMR (300 MHz, $CDCl_3$) δ 196.18 (C_4), 173.66 (C_4), 144.29 (C_4), 138.04 (C_4), 137.85 (C_4), 132.94 (CH), 130.58 (CH), 130.47 (CH) x 2, 129.12 (CH), 128.75 (CH), 128.68 (CH) x 2, 127.93 (CH), 52.00 (CH_3), 51.12 (CH_3), 33.10 (CH_2), 32.38 (CH_2), 32.22 (CH_2), 25.96 (CH_2). HRMS calculated: 388.0674; obtained: 388.0685.

2-(3-Benzoyl-phenyl)-6-iodo-hexanoic acid (2 a).[39] Prepared in the same way as **3 a**, but employing **V** (2-(3-benzoyl-phenyl)-6-bromo-hexanoic acid methyl ester). The obtained yield was 41.2%. ^{1}H-NMR (300 MHz, $CDCl_3$) 7.79 (broad S, 1H), 7.75 (broad S, 2H), 7.67-7.54 (m, 3H), 7.48-7.43 (m, 3H) 3.62 (t, J=7.6, 1H), 3.12 (t, J=7, 2H), 2.13-2.09 (m, 1H), 1.86-1.76 (m, 3H), 1.40-1.33 (m, 1H); ^{13}C-NMR (300 MHz, $CDCl_3$) δ 196.84 (C_4), 179.79 (C_4), 51.53 (CH), 33.37 (CH_2), 32.23 (CH_2), 28.69 (CH_2), 6.59 (CH_2). HRMS calculated: 422.0378; obtained: 422.0380.

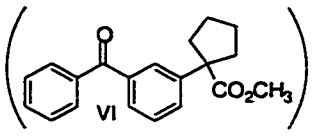

1-(3-Benzoyl-phenyl)-cyclopentanecarboxylic acid methyl ester (VI).[39] Obtained as a byproduct from the synthesis of **V** (2-(3-benzoyl-phenyl)-6-bromo-hexanoic acid methyl ester).

1-(3-Benzoyl-phenyl)-cyclopentanecarboxylic acid (4).[39] Prepared in the same way as **3**, but employing **VI** as the substrate. ^{1}H-NMR (300 MHz, $CDCl_3$) δ 7.83-7.83 (m, 1H), 7.78-7.75 (m, 2H), 7.66-7.54 (m, 3H), 7.47-7.41 (m, 3H), 2.70-2.64 (m, 2H), 2.02-1.89 (m, 2H), 1.79-1.75 (m, 4H), ^{13}C-NMR (300 MHz, $CDCl_3$) δ 196.98 (C_4), 182.21 (C_4), 59.17 (C_4), 36.46 (CH_2) x 2, 23.93 (CH_2) x 2. HRMS calculated: 308.1413; obtained: 308.1423.

4.5.2 Time-resolved Studies.

Samples at concentrations ranging from 0.2 to 0.4 mM were prepared in methanol, ethanol and water:acetonitrile mixtures either in the presence or in the absence of base and were irradiated with an excimer laser at 308 nm.

The 337 nm or 355 nm laser sources were employed for the experiments involving the use of 1-methylnaphthalene as quencher in water:acetonitrile mixtures either in the presence or absence of base. The concentration of KP ranged from 0.6 mM to 2.0 mM.

The base concentration used was always at least ten fold higher than that of KP to assure a complete dissociation of the acid. Sodium hydroxide and tetramethylammonium hydroxide (TMAOH) were indistinctly used in protic solvents, whereas only tetramethylammonium hydroxide was used in acetonitrile:water mixtures of low water content due to its higher solubility in acetonitrile.

The samples were deaerated by N_2 bubbling to eliminate oxygen from the solutions. The aqueous solutions were bubbled with N_2O. The quenching rate constants were obtained with static samples. A fresh solution was employed to obtain each decay rate; four shots were delivered to the sample and the solution was shaken between shots to avoid any interference due to the accumulation of photoproducts.

For the studies involving species **1**, **2**, **3**, **4**, and **2a** to **3c** the solutions were prepared in order to have ground state absorption values of *ca.* 0.3 at 308 nm. Solutions were equilibrated with N_2O in all the experiments.

Other details have been described in Section 2.5 of this thesis.

4.5.3 Product Studies

Photolysis of 0.4 mM KP in basic water:acetonitrile mixture (H_2O 2.78 M, molar fraction X_{water} 0.13) was done with the 308 nm laser as the excitation source. The samples received 200 shots and were then extracted with dichloromethane. The solvent was removed under vacuum, and the resulting mixture was analyzed with a Fisons GC/MS 8060/8000 Series equipped with a J&W DB5 30 m x 0.32 mm column.

HPLC studies of the irradiated solutions were carried out on a Varian instrument using a reverse phase 4.6 x 250 mm analytical Zorbax SB-C18 column, the mobile phase used was 15:85 water:methanol, the flow rate employed was 1 ml/min. The detection used a Varian 9065 Polychrom diode array detector

Quantum Yield Determination. Steady-state photolysis studies were carried out in a photoreactor, with only one 254 nm 8 W mercury lamp, and for different periods from 0 to 120 s. Ketoprofen in phosphate buffer was employed as a standard (the quantum yield of photodecarboxylation is 0.75 at pH 7.4[2]). The solutions were 1 mM in the substrate, and 80 mM in TMAOH, to ensure that all the photons would be absorbed under these conditions, and that ketoprofen would be in its anionic form. To quantitate the starting material, as well as the photoproducts produced, a calibration curve was made in the HPLC with different KP standard solutions, registering the signal at 254 nm. This calibration curve was equally employed for KP and ethylbenzophenone, which has the same chromophore structure as KP.

4.6 References

(1) Alomar, A., Ketoprofen Photodermatitis, *Contact Dermatitis*, **1985**, *12*, 112-113.

(2) Constanzo, L. L.; De Guidi, G.; Condorelli, G.; Cambria, A.; Fama, M., Molecular Mechanism of Drug Photosensitization-II. Photohemolysis Sensitized by Ketoprofen, *Photochem. Photobiol.*, **1989**, *50*, 359-365.

(3) Chignell, C. F.; Sik, R. H., The Effect of Static Magnetic Fields on the Photohemolysis of Human Erythrocytes by Ketoprofen, *Photochem. Photobiol.*, **1998**, *67*, 591-595.

(4) Chignell, C. F.; Sik, R. H., Magnetic Field Effects on the Photohemolysis of Human Erythrocites by Ketoprofen and Protoporphyrin IX, *Photochem. Photobiol.*, **1995**, *62*, 205-207.

(5) Boscá, F.; Miranda, M. A.; Carganico, G.; Mauleón, D., Photochemical and Photobiological Properties of Ketoprofen Associated with the Benzophenone Chromophore, *Photochem. Photobiol.*, **1994**, *60*, 96-101.

(6) Maguery, M. C.; Chouini-Lalanne, N.; Ader, J. C.; Paillous, N., Comparison of the DNA Damage Photoinduced by Fenofibrate and Ketoprofen, Two Phototoxic Drugs of Parent Structure, *Photochem. Photobiol.*, **1998**, *68*, 679-684.

(7) Lhiaubet, V.; Paillous, N.; Chouini-Lalanne, N., Comparison of DNA Damage Photoinduced by Ketoprofen, Fenofibric Acid and Benzophenone via Electron and Energy Transfer., *Photochem. Photobiol.*, **2001**,

(8) Boscá, F.; Miranda, M. A.; Carganico, G.; Mauleón, D., Evaluation of Ketoprofen (R,S and R/S) Phototoxicity by a Battery of *In Vitro* Assays, *J. Photochem. Photobiol. B: Bioi.*, **1995**, *31*, 133-138.

(9) Rudy, A. C.; Liu, Y.; Brater, C. D.; Hall, S. D., Stereoselective Pharmacokinetics and Inversion of (R)-Ketoprofen in Healthy Volunteers, *J. Clin. Pharmacol.*, **1998**, *38*, 3S-10S.

(10) de la Peña, D.; Martí, C.; Nonell, S.; Martínez, L. A.; Miranda, M. A., Time-resolved Near Infrared Studies on Singlet Oxygen Production by the Photosensitizing 2-Arylpropionic Acids, *Photochem. Photobiol.*, **1997**, *65*, 828-832.

(11) Martínez, L. J.; Scaiano, J. C., Transient Intermediates in the Laser Flash Photolysis of Ketoprofen in Aqueous Solutions: Unusual Photochemistry for the Benzophenone Chromophore, *J. Am. Chem. Soc.*, **1997**, *119*, 11066-11070.

(12) Monti, S.; Sortino, S.; De Guidi, G.; Marconi, G., Photochemistry of 2-(3-Benzoylmethyl)propionic Acid (Ketoprofen). 1. A Picosecond and Nanosecond Time Resolved Study in Aqueous Solution, *J. Chem. Soc., Faraday Trans.*, **1997**, *93*, 2269-2275.

(13) Monti, S.; Sortino, S.; De Guidi, G.; Marconi, G., Supramolecular Photochemistry of 2-(3-Benzoylphenyl)propionic Acid (Ketoprofen). A Study in the Beta-cyclodextrin Cavity, *New. J. Chem.*, **1998**, *22*, 599-604.

(14) Scaiano, J. C.; Abuin, E. B.; Stewart, L. C., Photochemistry of Benzophenone in Micelles. Formation and Decay of Radical Pairs, *J. Am. Chem. Soc.*, **1982**, *104*, 5673-7679.

(15) Carmichael, I.; Hug, G. L. Spectroscopy and Intramolecular Photophysics of Triplet States; In *Handbook of Organic Photochemistry*; J. C. Scaiano, Ed.; CRC Press: Boca Raton, Florida, 1989; Vol. I; 369-403.

(16) Carmichael, I.; Hug, G. L., Triplet-Triplet Absorption Spectra of Organic Molecules in Condensed Phases, *J. Phys. Chem. Ref. Data*, **1986**, *15*, 1-250.

(17) Lamola, A. A.; Hammond, G. S., Mechanisms of Photochemical Reactions in Solution. XXXIII. Intersystem Crossing Efficiencies., *J. Chem. Phys.*, **1965**, *43*, 2129-2135.

(18) Beckett, A.; Porter, G., Primary Photochemical Processes in Aromatic Molecules. Part 10. Photochemistry of Substituted Benzophenones, *Trans. Faraday Soc.*, **1963**, *59*, 2051-2057.

(19) Godfrey, T. S.; Hilpern, J. W.; Porter, G., Triplet-Triplet Absorption Spectra of Benzophenone and its Derivatives, *Chem. Phys. Lett.*, **1967**, *1*, 490-492.

(20) Minch, M. J.; Giaccio, M.; Wolff, R., Effect of Cationic Micelles on the Acidity of Carbon Acids and Phenols. Electronic and ^{1}H Nuclear Magnetic Resonance Spectral Studies of Nitro Carbanions in Micelles, *J. Am. Chem. Soc.*, **1975**, *97*, 3766-3772.

(21) McClelland, R. A.; Steenken, S., Pronounced Solvent Effects on the Absorption Spectra of the Photochemically Produced 2,4-Dinitrobenzyl Carbanion, *Can. J. Chem.*, **1987**, *65*, 353-356.

(22) Turro, N. J., *Modern Molecular Photochemistry*; University Science Books: Sausalito, 1991.

(23) Craig, B. B.; Weiss, R. G.; Atherton, S. J., Picosecond and Nanosecond Laser Photolyses of p-Nitrophenylacetate in Aqueous Media. A Photoadiabatic Decarboxylation Process?, *J. Phys. Chem.*, **1987**, *91*, 5906-5912.

(24) Sortino, S.; Scaiano, J. C., Laser Flash Photolysis of Tolmetin: A Photoadiabatic Decarboxylation with a Triplet Carbanion as the Key Intermediate in the Photodecomposition, *Photochem. Photobiol.*, **1999**, *69*, 167-172.

(25) Cosa, G.; Boscá, F.; Miranda, M. A.; Scaiano, J. C., A Laser Flash Photolysis Study of Fenofibric Acid in Aqueous Buffered Media. Unexpected Triplet State Inversion in a 4-Methoxybenzophenone Derived Compound, *Photochem. Photobiol.*, **2002**, *75*,

(26) Encinas, S.; Miranda, M. A.; Marconi, G.; Monti, S., Transient Species in the Photochemistry of Tiaprofenic Acid and its Decarboxylated Photoproduct, *Photochem. Photobiol.*, **1998**, *68*, 633-639.

(27) Krogh, E.; Wan, P., Photodecarboxylation of Diarylacetic Acids in Aqueous Solution: Enhanced Photogenetation of Cyclically Conjugated Eight π Electron Carbanions, *J. Am. Chem. Soc.*, **1992**, *114*, 705-712.

(28) Budac, D.; Wan, P., Photodecarboxylation: Mechanism and Synthetic Utility, *J. Photochem. Photobiol. A: Chem.*, **1992**, *67*, 135-166.

(29) Xu, M.; Wan, P., Efficient Photodecarboxylation of Aroyl-substituted Phenylacetic Acids in Aqueous Solution: a General Photochemical Reaction, *Chem. Commun.*, **2000**, 2147-2148.

(30) Wan, P.; Muralidharan, S., Structure and Mechanism in the Photo-retro-aldol Type reactions of Nitrobenzyl Derivatives. Photochemical Heterolytic Cleavage of C-C Bonds, *J. Am. Chem. Soc.*, **1988**, *110*, 4336-4345.

(31) Borsarelli, C. D.; Braslavsky, S. E.; Sortino, S.; Marconi, G.; Monti, S., Photodecarboxylation of Ketoprofen in Aqueous Solution. A Time-resolved Laser-induced Optoacustic Study, *Photochem. Photobiol.*, **2000**, *72*, 163-171.

(32) March, J., *Advanced Organic Chemistry;* Fourth Edition ed.; John Wiley & Sons, Inc.: New York, 1992.

(33) Smith, M. B., *Organic Synthesis*; McGraw-Hill International Editions: New York, 1994.

(34) Bockrath, B., Dorfman L. M., Submicrosecond Formation and Observation of Reactive Carbanions, *J. Am. Chem. Soc.*, **1974**, *96*, 5708-5715.

(35) Bockrath, B.; Dorfman, L. M., Protonation Rate Constants and Optical Absorption Spectra of Benzyl Carbanion Pairs in Tetrahydrofuran Solution, *J. Am. Chem. Soc.*, **1975**, *97*, 3307-3310.

(36) Arnó, M.; González, M. A.; Marín, M. L.; Zaragozá, R., First Diastereoselective Synthesis of (-)-Methyl Thyrsiflorin A, (-)-Methyl Thyrsiflorin B Acetate, and (-)-Thyrsiflorin C, *J. Org. Chem.*, **2000**, *65*, 840-846.

(37) Olah, G. A.; Narang, S. C.; Gupta, B. G. B.; Malhotra, R., Synthetic Methods and Reactions. 62. Transformations with Chlorotrimethylsilane/Sodium Iodide, a Convenient in Situ Iodotrimethylsilane Reagent, *J. Org. Chem.*, **1979**, *44*, 1247-1251.

(38) Abad, A.; Arnó, M.; Cuñat, A. C.; Marín, M. L.; Zaragozá, R., Spongian Pentacyclic Diterpenes. Stereoselective Synthesis of (-)-Dendrillol-1, *J. Org. Chem.*, **1992**, *57*, 6861-6869.

(39) These molecules were synthesized and characterized by Dr. L. Llauger.

5. Photochemistry of Diketones: Observation of a Triplet State-oxygen Adduct

5.1 Introduction

The interaction of excited states and molecular oxygen is a topic of current research motivated by the desire of better understanding the production of singlet oxygen ($^1\Delta_g$ O_2) and other reactive oxygen species. In particular the advent of photodynamic therapy, a methodology employed in cancer and epidermal disease treatment, and which relies in the production of toxins following the encounter of a photosensitizer and molecular oxygen,[1-4] has sparked interest in these types of photoprocesses in the field of photobiology.

In the case of carbonyl compounds, most of the photochemical and photophysical studies have been performed with aromatic and aliphatic ketones,[5-7] and little information is available concerning the interaction of molecular oxygen and α-diketones.

Early reports account on the photooxidation of benzil in the presence of oxygen,[8] and on the sensitized photoepoxidation of olefins in the presence of benzil or diacetyl and oxygen.[9] Bartlett *et al.* proposed that this epoxidation was not mediated by singlet oxygen, but rather by a biradical intermediate where an excited α-diketone-oxygen adduct would attack the olefin,[9] confirming the photosensitized oxygen transfer mechanism suggested by Schenck.[10,11]

Later reports (see also Scheme 5-1) based on the 1:2 stoichiometry of α-diketone (**1**) consumed to epoxide (**7**) formed, have established that the sensitizer-oxygen adduct (**3**) is only a precursor of the epoxidating agent, and does not play an active role in the olefin (**6**) epoxidation. The active species was thus determined to be an acylperoxyl radical (**5**),[12-15] formed following cleavage of the biradical (**3**). An acyl radical (**4**) also results from this cleavage, which upon oxygen trapping produces a second epoxidating agent.[12]

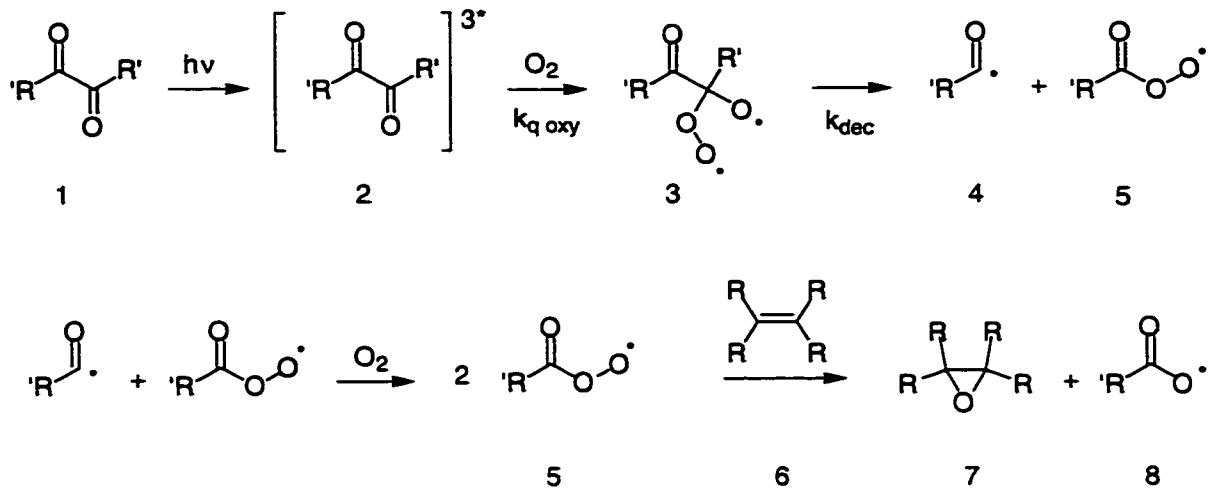

Scheme 5-1: Photooxidation of diketones in the presence of O_2 and olefins.[12,16]

There exist numerous proofs on the validity of the mechanism proposed in Scheme 5-1; we can thus mention the reduced lifetime of singlet oxygen sensitized by diketones following high laser pulse excitation. This is due to the quenching of singlet oxygen by the acylperoxyl radicals produced after the biradical cleavage.[17] The enhanced photodecomposition of α-diketones under O_2 *vs.* N_2 atmosphere, and their reduced reactivity in the presence of *trans*-stilbene provides another proof.[12] The observed epoxidation stoichiometry is another confirmation of the proposed mechanism.[15,16] There has not been however a report on the direct observation of the "Bartlett-Schenck" biradical intermediate (species **3** in Scheme 5-1).

With the aim of better understanding the photochemistry of diketones in the presence of O_2, laser flash photolysis (LFP) studies with 2,2'-thenil (TL) were done. The choice of this diketone is not casual; it is related to 2-(then-2-oyl)thiophene (TOT) (see Scheme 5-2), a substrate that was employed as a model in order to determine the micellar behavior of the non-steroidal anti-inflammatory drugs (NSAID) suprofen and tiaprofenic acid, also shown in Scheme 5-2.[18]

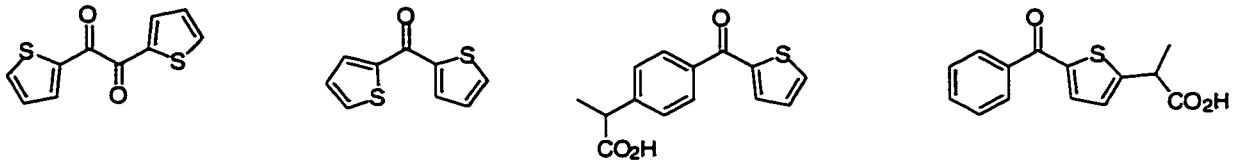

Scheme 5-2: Structure of 2,2'-thenil, 2-(then-2-oyl)thiophene, suprofen and tiaprofenic acid.

In the following sections we describe the results obtained following irradiation of TL. Spectroscopical data, together with Arrhenius parameters, product and reactivity studies are presented.

The interpretation of these results leads us to propose that the Bartlett-Schenck intermediate can be seen following the interaction of TL triplet state with oxygen, in the form of a transient absorption band centered at 340 nm. The results are discussed in terms of this hypothesis. The experimental evidence confirms this assignment, and further allows us to rule out other possible intermediates as the potential chromophore absorbing at 340 nm.

5.2 Results

5.2.1 Characterization of 2,2'-Thenil

The ground state absorption spectrum of TL obtained in acetonitrile is shown in Figure 5-1-A. The triplet energy for TL was determined at 77 K from the maximum of the lowest energy band of the phosphorescence spectra (*i.e.*, the 0-0 band) both in 4:1 methanol:ethanol and methylcyclohexane. TL fluorescence lifetime was measured following excitation by a 355 nm picosecond laser pulse. These data is presented in Table 5-1.

Table 5-1: Photophysical parameters of TL.

Measurement Type	Value
absorption maximum	[a] 307 nm; [b] 307 and 430 nm;
triplet energy in 4:1 methanol:ethanol	233 kJ/mol
triplet energy in methylcyclohexane	228 kJ/mol
fluorescence lifetime	≤ 80 ps

[a] In acetonitrile. [b] In cyclohexane; the band in the visible is not observable in higher polarity solvents.

Following irradiation of TL under a N_2 atmosphere a transient absorption spectrum is observed with maxima at 730 and 430 nm, and a shoulder at 530 nm, as shown in Figure 5-1-B. A negative band is also observed, with a minimum at 310 nm, which is due to ground state depletion, as evidenced from TL absorption in acetonitrile (Figure 5-1-A). At 350 nm the molar absorptivity is the same for the ground and excited states.

A detailed analysis of the transient spectrum at long time scales (*ca.* 330 μs after the laser pulse), once the triplet has decayed, reveals the presence of a band extending from 450 nm and up to 350 nm, where the bleaching profile becomes dominant (data not shown).

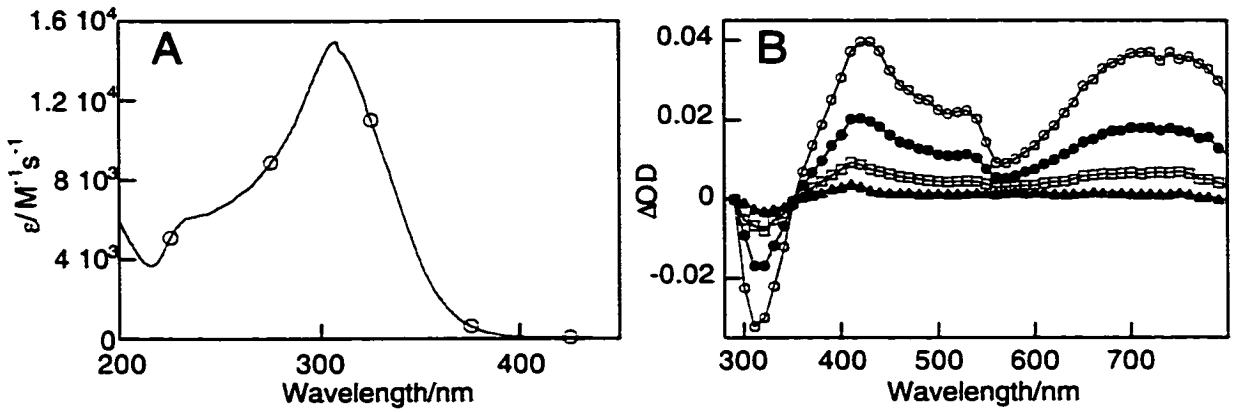

Figure 5-1: (A) Molar absorptivity of TL in acetonitrile (a few points are shown to assist in the visualization). (B) Transient absorption spectra obtained following irradiation of TL 1.21 x 10^{-4} M in acetonitrile, under N_2 atmosphere. The time windows were obtained: (○) 0.8 μs; (●) 5.4 μs; (□) 15.7 μs; (▲) 32.8 μs after the 355 laser pulse.

The reactivity of the observed transient has been established in the presence of triplet quenchers, *i.e.*, O_2, 1,3-cyclohexadiene (triplet energy 219 kJ/mol[19]), and *trans*-stilbene (triplet energy 208 kJ/mol[19]). These values are shown in Table 5-2.

Table 5-2: Reactivity of 2,2'-thenil with various substrates in acetonitrile.

Quencher	$k_q/M^{-1}s^{-1}$
[a] O_2	1.8 x 10^9
[b] *t*-stilbene	1.0 x 10^{10}
[b] 1,3-cyclohexadiene	1.0 x 10^{10}
[a] trolox	8.2 x 10^9
[a] 1,4-cyclohexadiene	4.6 x 10^8
[a] 1-methylnaphthalene	5.7 x 10^7
[a] naphthalene	not observed
[a] *N,N,N',N'*-tetramethyl-*p*-phenylendiamine	1.0 x 10^{10}

All the values obtained in acetonitrile; TL concentration in the range of 9 to 30 x 10-5 M, laser 355 nm. [a] Monitored at 720 nm, [b] monitored at 650 nm,

The quenching rate constants by trolox and by 1,4-cyclohexadiene, both good hydrogen donors, have also been measured. We also determined the reactivity towards napthalene (triplet energy 253 kJ/mol[19]), and 1-methylnaphthalene. From these data we conclude that the transient observed following laser excitation is the TL triplet state (vide infra).

5.2.2 Spectroscopy Under Oxygen

The same transient observed following excitation of TL in acetonitrile under nitrogen atmosphere is also monitored following LFP experiments in solutions equilibrated with oxygen, as can be seen in Figure 5-2-A.

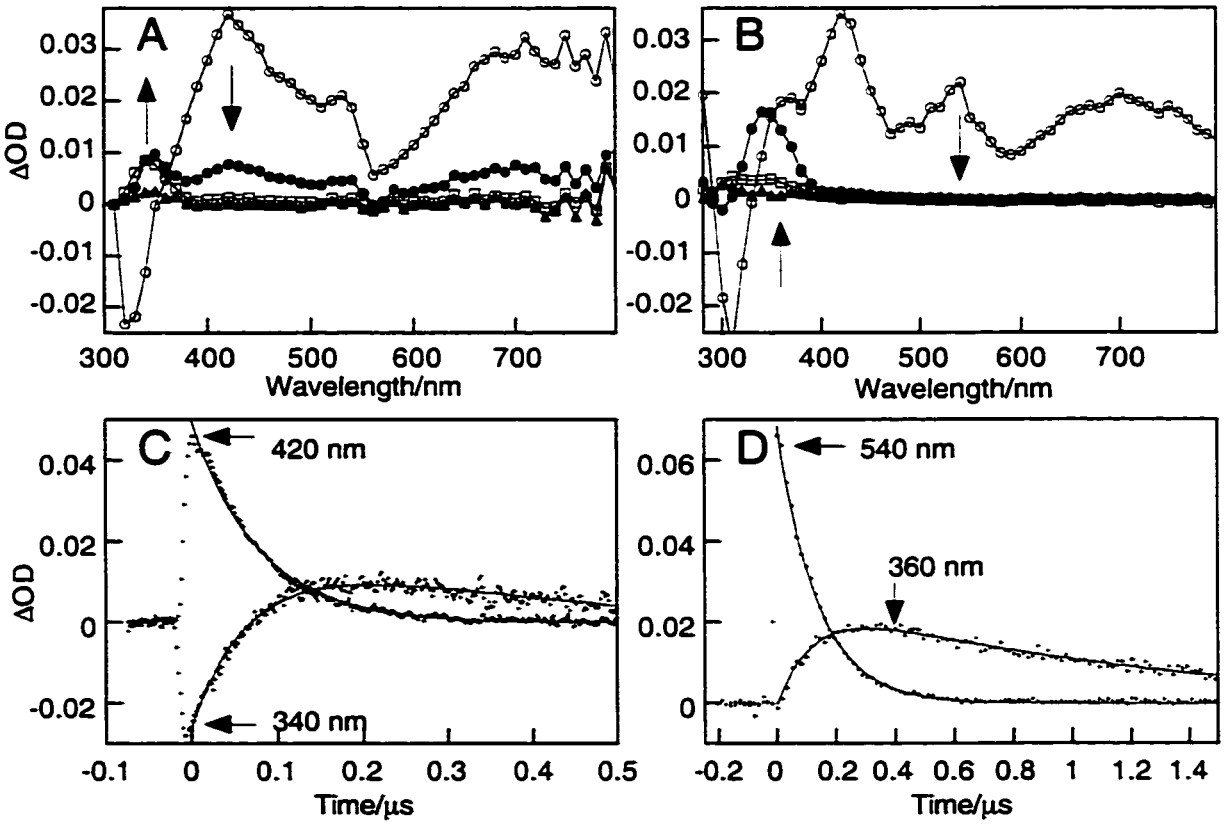

Figure 5-2: (A) Transient absorption spectra obtained following 355 nm excitation of TL 1.21 x 10^{-4} M in acetonitrile, under O_2 atmosphere. The time windows were obtained: (○) 0.028 μs; (●) 0.140 μs; (□) 0.275 μs; (▲) 0.591 μs after the laser pulse. (B) Transient absorption spectra obtained following 308 nm excitation of TL 1.6 x 10^{-5}

M in toluene, under O_2 atmosphere. The time windows were obtained: (○) 0.12 μs; (●) 0.68 μs; (□) 2.68 μs; (▲) 8.68 μs after the laser pulse. (C) Transient absorption time evolution registered at 340 nm and 420 nm; same conditions as in A. (D) Transient absorption time evolution registered at 360 nm and 540 nm; same conditions as in B.

Figure 5-2-B shows the spectra obtained after excitation of TL in toluene, under oxygen atmosphere. The spectra is qualitatively the same as that obtained for TL in acetonitrile, although it shows more structural resolution, as evidenced by the existence of three well defined bands at 420, 540 and 700 nm. We assign it to the triplet-triplet (T-T) absorption of TL.

In Figure 5-2-A we observe that a new band, with maximum at *ca.* 340 nm appears concomitant with the decay of the triplet state in acetonitrile. This band is also evident in the spectrum obtained with toluene as solvent. Figure 5-2-C shows the time profile for the transient absorption at 340 and 420 nm in acetonitrile. The fitting of these traces (solid line) shows that the growth rate constant at 340 nm (1.5×10^7 s^{-1}) has the same value as the observed rate constant for the triplet decay monitored at 420 nm (*ca.* 1.3×10^7 s^{-1}). In the former case, we also note that the growth results in a positive signal, *i.e.*, a new transient. Once again a similar situation is encountered in the case of the experiments performed with toluene as solvent. In this case we have monitored the time dependence for the growth at 360 nm (rate constant of 8.2×10^6 s^{-1}), and that for the decay at 540 nm (rate constant of 7.5×10^6 s^{-1}); the traces are shown in Figure 5-2-D. The new transient decays with a rate constant value of 3.3×10^6 s^{-1} and 1.0×10^6 s^{-1} in acetonitrile and toluene, respectively.

In order to determine if the new transient results from the interaction of TL triplet state and molecular oxygen, or rather, it is formed simultaneously with it after laser excitation, in a parallel reaction, we have measured the dependence of its growth rate constant with oxygen concentration. In Figure 5-3-A and 5-3-B we present the transient absorption time evolution, monitored at 340 nm following excitation of TL under oxygen and air equilibrated acetonitrile solutions, respectively. In the first case we obtain rate constant

values of 16.7 x 10^6 s^{-1} and 3.4 x 10^6 s^{-1} for the growth and decay. In the air equilibrated sample, the growth rate constant (3.2 x 10^6 s^{-1}) is *ca.* 5 fold smaller than that under oxygen; the decay rate constant (3.3 x 10^6 s^{-1}) is however the same under both conditions.

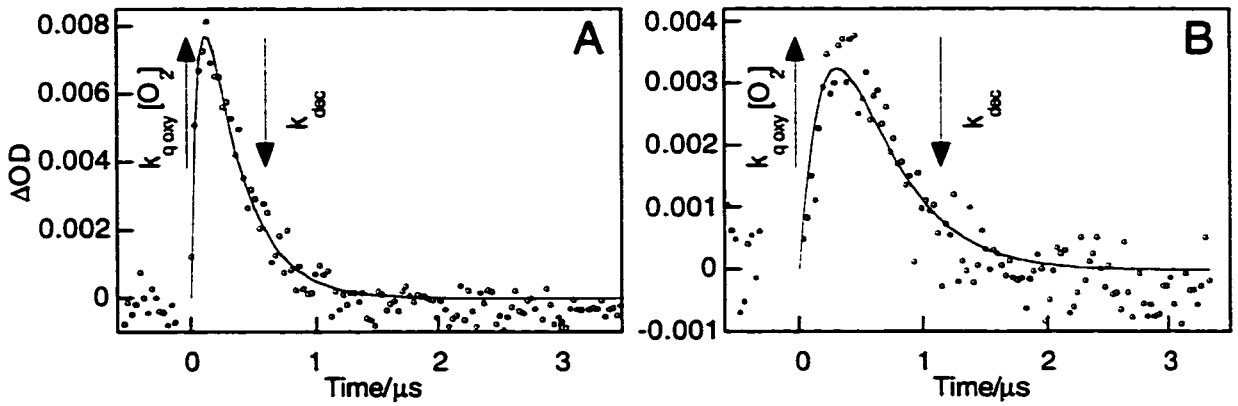

Figure 5-3: Transient absorption time dependence monitored at 340 nm, following 355 nm laser irradiation of TL 9.9 x 10^{-5} M in acetonitrile, (A) under O_2 atmosphere, and (B) in an air equilibrated solution.

The results confirm that the rate constant of formation for the new transient is the same as that measured for the triplet decay, independently of the system. Further, the fitting of the traces shown in Figures 5-3-A, and 5-3-B enables us to assess that, within the experimental error, the newly formed transient decay rate constant is independent of the oxygen concentration. This experimental evidence can be explained by assuming that the transient we observe is the same as that whose existence was proposed by Bartlett and Schenck, *i.e.*, species **3** in Scheme 5-1.[9-11] For the sake of clarity, we will, from now on refer to it as the Bartlett-Schenck intermediate.

In order to gain knowledge on the dynamics of the Bartlett-Schenck intermediate, we performed temperature dependence studies to determine the Arrhenius parameters that characterize its decay. The results were obtained both in toluene and acetonitrile, at temperatures ranging from 240 to 320 K. Figure 5-4 shows these results.

From the linear fit of the experimental values we obtain that the activation energies for the decay of the Bartlett-Schenck intermediate are 28.2 and 34.3 kJ/mol in acetonitrile and toluene respectively. The preexponential values obtained are 3.24 x 10^{11} s^{-1} for the former solvent and 1.45 x 10^{12} s^{-1} in toluene. The difference existing between these two values is within the experimental error of the ordinate.

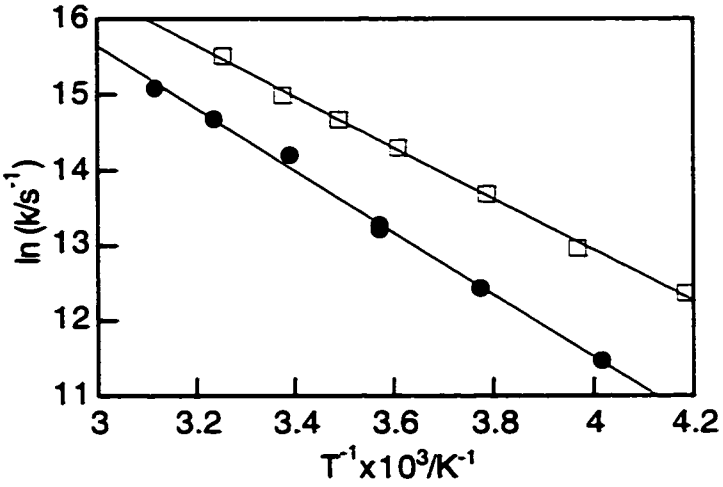

Figure 5-4: Arrhenius plot for the decay decay of the Bartlett-Schenck intermediate, determined (□) at 360 nm, following irradiation of 2.48 x 10^{-4} M TL in acetonitrile, under O_2 atmosphere, laser 355 nm; and (●) at 360 nm, following irradiation of 2.15 x 10^{-5} M TL in toluene, under O_2 atmosphere, laser 308 nm.

5.2.3 Product Studies

It has been established that diacetyl undergoes Norrish type I (*i.e.*, homolytic α-cleavage of the excited carbonyl compound[20]) photoreactions under inert atmosphere;[21] yet, its photodegradation is considerably higher under oxygen, due to photooxidation.[12] The same applies to benzil, where the quantum yield of degradation under N_2 is *ca.* 6 fold smaller than that in O_2.[8,12]

Irradiation studies were performed where TL was exposed for different periods of time to light, both under N_2, and under O_2 atmosphere. In both cases the initial photoconversion seems to take place at roughly the same speed, as can be seen from Figure

5-5. Upon increased exposure times, however, the change observed under nitrogen is more dramatic; yet, at this point the phenomena observed might be due to photoproduct irradiation.

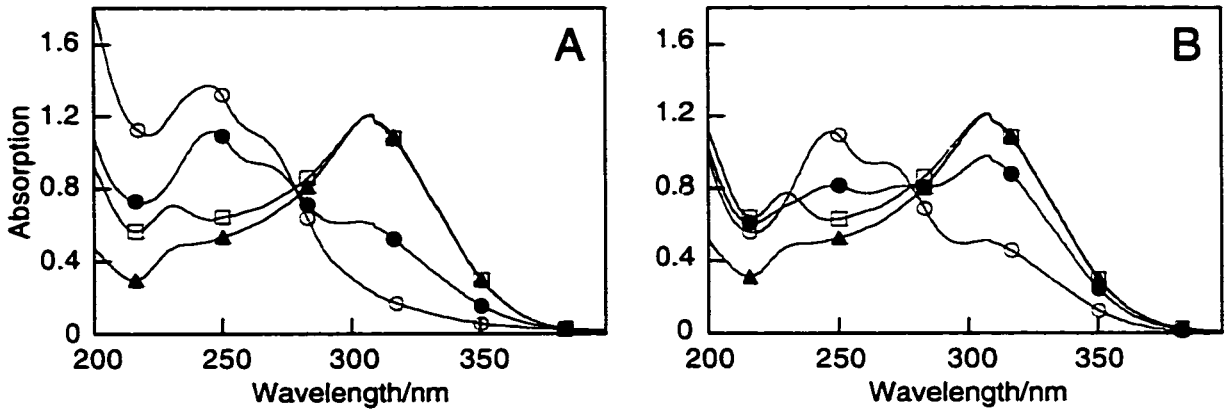

Figure 5-5: Change in ground state absorption following irradiation with 350 nm Hg lamps, of a solution of TL 8 x 10^{-5} M in acetonitrile (A) under nitrogen, and (B) under oxygen. A few points are shown to assist in the visualization. (▲) Before irradiation; (□) after 8 min of light exposure; (●) after 78 min of light exposure; (○) following 258 min of light exposure.

Analytical studies performed with an HPLC showed that 2-thiophenecarboxaldehyde was formed under nitrogen; under oxygen the species formed was and 2-thiophenecarboxylic acid.

5.2.4 Spectroscopy and Kinetics of Acyl and Acyl-Peroxyl Radical

We want to rule out any other pathway that might account for a signal with similar characteristics to that of the Bartlett-Schenck intermediate. One such possibility would be given by the generation of acyl radicals, that upon trapping by oxygen would give rise to an acylperoxyl radical. We have therefore measured the spectroscopy and the decay kinetics for both the acyl radical and the acylperoxyl radical in acetonitrile. Two mechanisms have been employed for the generation of the acyl radical, as shown in Scheme 5-3. One consists on the hydrogen abstraction of 2-thiophenecarboxaldehyde by *tert*-butoxyl (*t*-butoxyl) radicals generated upon photolysis of di-*tert*-butyl peroxide (di-*t*-butyl peroxide). The other relies on

the well established Norrish type I photofragmentation of α-hydroxy ketones (Reaction 3 in Scheme 5-3).[22,23] In our case we have employed 2,2'-thenoin as a source of acyl radicals.

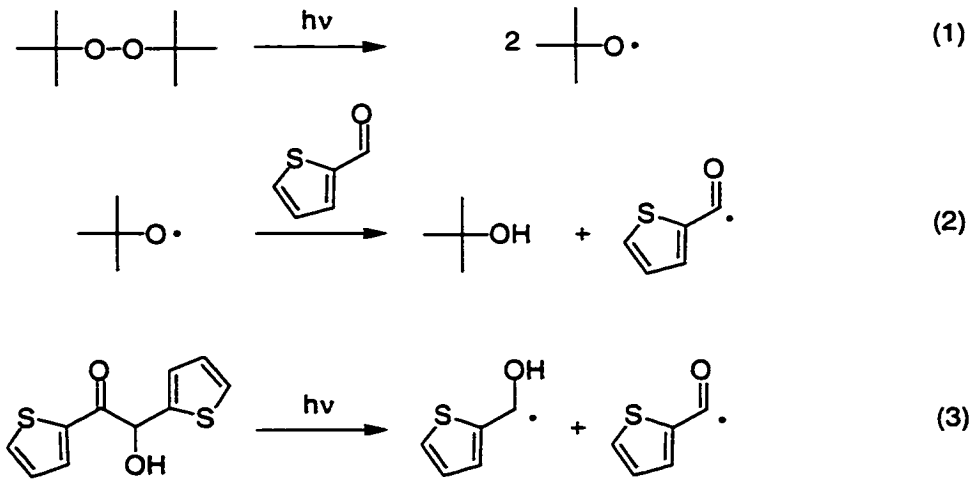

Scheme 5-3: Different mechanisms for the generation of acyl radicals.

The results obtained with di-*t*-butyl peroxyde are shown in Figures 5-6-A and 5-6-B. High concentrations of aldehyde are necessary to efficiently quench the *t*-butoxyl radical, as determined from the rate constant of quenching measured (1.5×10^7 $M^{-1}s^{-1}$). The latter value is in agreement with values reported in the literature for the reaction of benzaldehyde and *t*-butoxyl radical.[24] We should also note that although 2-thiophenecarboxaldehyde absorbs part of the excitation laser, its triplet state (observed in the first time window) is quenched by di-*t*-butyl peroxide to produce more *t*-butoxyl radicals.[25]

The results obtained following 2,2'-thenoin irradiation are shown in Figures 5-6-C and 5-6-D. Plots A and C show the acyl radical transient absorption spectra, whereas plot B and D (which are the result of experiments performed under oxygen) show the acylperoxyl radical spectra. Both acyl and acyl-peroxyl radicals absorb in a similar region as that of the Bartlett-Schenck intermediate. Important to note is that over the whole course of the time range explored (4 μs and 200 μs for acylperoxyl and acyl radicals respectively), the radicals remain as stable products. These two species can not account for a transient that disappears *ca.* 300

ns after being formed, as is the case of the intermediate we postulate is the Bartlett-Schenck intermediate.

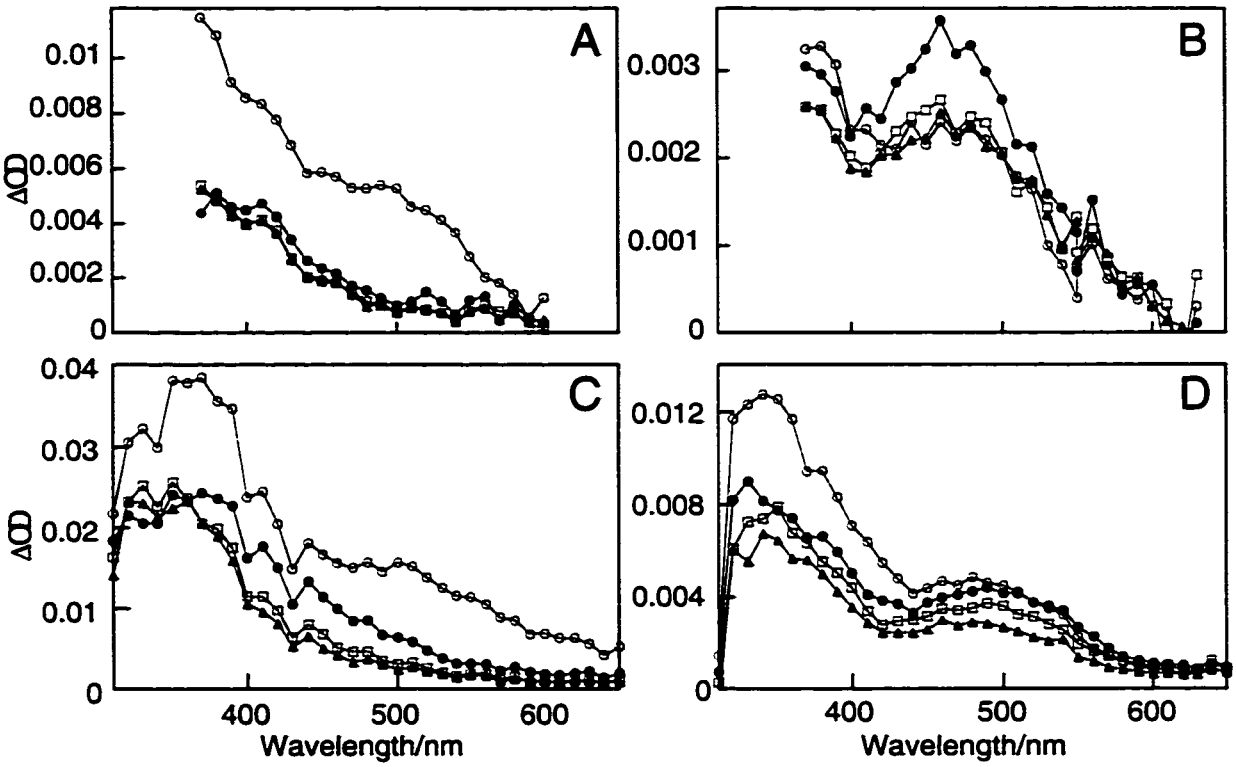

Figure 5-6: (A) and (B) Transient absorption spectra obtained following 337 nm excitation of di-*tert*-butyl peroxide in a 4:6 v:v di-*tert*-butyl peroxide:acetonitrile solution containing 2-thiophenecarboxaldehyde 0.56 M. The time windows were obtained: (○) 0.13 μs; (●) 0.85 μs; (□) 2.56 μs; and (▲) 3.39 μs after the laser pulse. (A) was obtained under N_2 equilibrated solutions; (B) was obtained with O_2 equilibrated solutions. (C) and (D) show the transient absorption spectra obtained following 308 nm excitation of 2,2'-thenoin 4.02 x 10^{-5} M in acetonitrile. In the case of (C), the solution was under N_2 atmosphere; the time windows were obtained: (○) 3.2 μs; (●) 22.4 μs; (□) 96.8 μs; and (▲) 172.0 μs after the laser pulse. In the case of (D), the solution was under O_2 atmosphere; the time windows were obtained: (○) 0.32 μs; (●) 2.48 μs; (□) 9.52 μs; and (▲) 17.10 μs after the laser pulse.

5.2.5 Reactivity of 2,2'-Thenil and 2-(Then-2-oyl)thiophene

It is interesting to measure which role the conjugated acyl group plays, and what is the influence of the aromatic rings, in the case of the interaction of α-diketones with oxygen. Previous results from other groups show that TOT has a π,π* triplet state in acetonitrile,[26,27] we can therefore anticipate that the 2-thienyl ring exhibits a completely different interaction with the acyl group in the excited triplet state of TL, compared to the interaction of the phenyl groups with the acyl group in benzophenone and benzil, which are known to be n,π* in nature in both cases. In this sense TL can provide a new insight on the effect the aromatic moiety has on the photooxidation of α-diketones.

In order to understand the influence that both the 2-thienyl ring and the second carbonyl group have in determining the reactivity of the diketone, hydrogen abstraction reactions have been chosen as a probe. The hydrogen donor employed is 1,4-cyclohexadiene. In Figure 5-7 the dependence of the decay rate constant for TL and TOT triplet states with different 1,4-cyclohexadiene concentrations are presented. Figure 5-8 shows the spectra of TL ketyl radical obtained after photoreduction of the diketone in the presence of 1,4-cyclohexadiene.

A value of *ca.* 7.4 x 10^7 $M^{-1}s^{-1}$ was determined for the quenching rate constant of TOT.[18] This is 6 times smaller than that obtained for TL (*i.e.*, 4.6 x 10^8 $M^{-1}s^{-1}$), the latter is even larger than that determined for benzophenone triplet state in the presence of 1,4-cyclohexadiene in acetonitrile, *i.e.*, 2.9 x 10^8 $M^{-1}s^{-1}$.[28] This different reactivity towards hydrogen abstraction is an indication that TL triplet excited state is n,π* in nature, like benzophenone, and contrary to TOT which is π,π*.

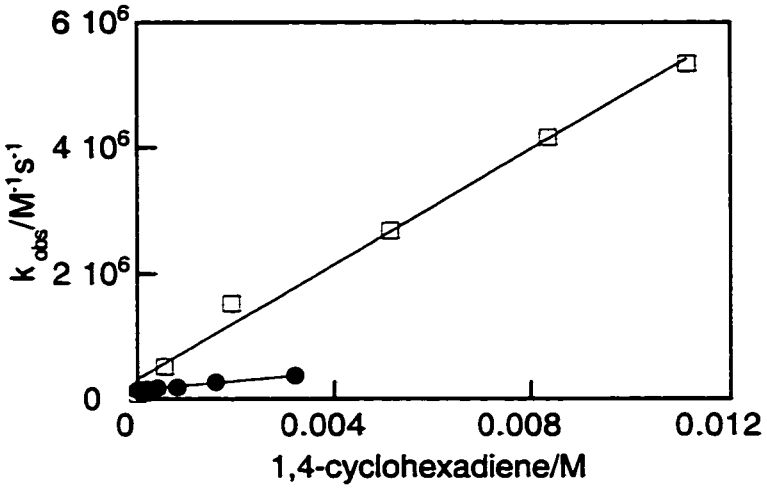

Figure 5-7: (□) Dependence of the observed decay rate constant (monitored at 720 nm) with different 1,4-cyclohexadiene concentrations following 355 nm excitation of 9.5 x 10^{-5} M TL in acetonitrile, under N_2 atmosphere. (●) Also shown is the dependence of the decay rate constant of TOT triplet, monitored at 600 nm, with different 1,4-cyclohexadiene concentrations. A solution 1 x 10^{-4} M of TOT in acetonitrile, under N_2 atmosphere was employed. Laser 308 nm.

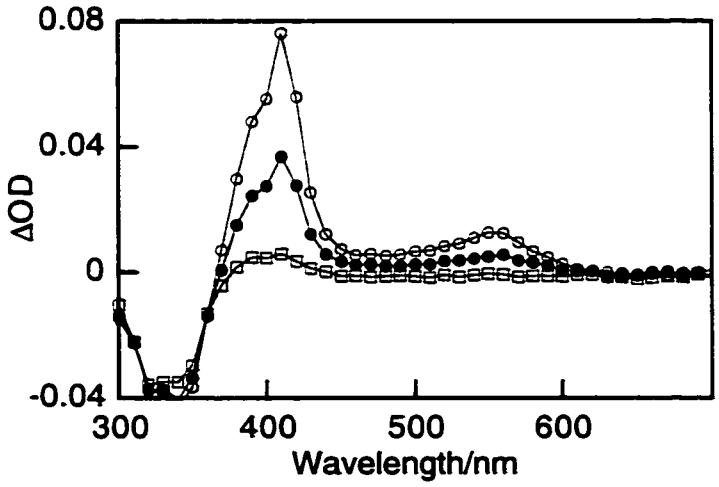

Figure 5-8: Transient absorption spectra obtained following irradiation of TL 8.0 x 10^{-5} M in acetonitrile, under N_2 atmosphere, in the presence of 1,4-cyclohexadiene 0.05 M. Under these conditions the triplet undergoes hydrogen abstraction and only the ketyl radical is detectable. The time windows were obtained: (○) 20 μs; (●) 72 μs; (□) 304 μs; (▲) 872 μs after the 355 laser pulse.

5.2.6 Benzil and Diacetyl

As part of this work, attempts were also made to observe the Bartlett–Schenck intermediate following excitation of benzil and diacetyl (see Figure 5-9), where its existence has been previously inferred from product studies.[9,12,16,17]

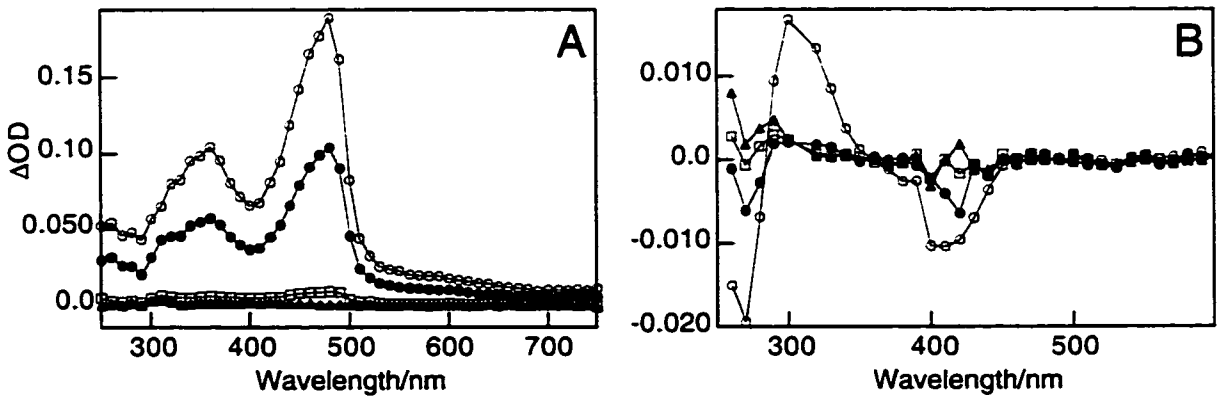

Figure 5-9: (A) Transient absorbption spectra obtained following irradiation of 5.7 x 10^{-4} M benzil in acetonitrile, under O_2 atmosphere, laser 308 nm. The time windows observed were recorded (○) 0.032 μs; (●) 0.136 μs; (□) 0.576 μs; and (▲) 1.730 μs after the laser pulse. (B) Transient absorption spectra obtained following irradiation of 0.17 M diacetyl in acetonitrile, under O_2 atmosphere, laser 308 nm. The time windows were recorded (○) 0.032 μs; (●) 0.128 μs; (□) 0.376 μs; and (▲) 1.660 μs after the laser pulse.

Transient absorption spectra were thus acquired for both species in acetonitrile under oxygen. In either case there is no spectroscopic evidence for a transient whose characteristics resemble that of the Schenck-Bartlett intermediate observed following TL excitation. Thus Figure 5-9-A shows the complete disappearance of the triplet-triplet absorption of benzil after *ca.* 1.7 μs; no new transient is detected in this region. Similarly, in Figure 5-9-B the triplet state of diacetyl with maximum at *ca.* 310 nm is observed decaying. No new transient is formed concomitant with its dissappearance. The negative signal observed at 420 nm is attributed to diacetyl fluorescence.

5.3 Discussion

5.3.1 Direct Observation of the Bartlett-Schenck Intermediate

Slightly more than thirty years have passed ever since Saltiel *et al.* first reported on the photooxidation of benzil.[8] This account was followed by the work of Bartlett *et al.*, who provided an efficient method for olefin epoxidations sensitized by α-diketones.[9] Preparative epoxidations have been made with this methodology ever since, yet the mechanism of reaction remained in the darkness. In the early 80's a series of papers by Sawaki *et al.* demonstrated that the sensitized epoxidation occurred through a series of steps which are illustrated in Scheme 5-1.[12-14,16,29] We center our attention in structure **3**, *i.e.*, the α-diketone-oxygen adduct. There exist no records of its direct observation. Our LFP results provide evidence that this species, the Bartlett-Schenck intermediate, is formed following excitation of TL.

The LFP experiments performed under nitrogen atmosphere allow the characterization of the TL triplet state. Our results leave no doubts on the nature of the main transient being TL triplet state, given its diffusion controlled quenching by *trans*-stilbene and 1,3-cyclohexadiene, which have lower triplet energies than that of TL (see Table 5-1). Further, attempts to quench the signal with naphthalene, whose triplet energy is higher than that of TL, results in no observable modification in the decay rate of TL triplet state. In the case of 1-methylnaphthalene the observed quenching is due to hydrogen abstraction and not energy transfer, judging from the observation of the ketyl radical spectra of TL (similar to that shown in Figure 5-8) in the presence of the former.

The short lifetime of TL triplet state under oxygen further confirms this assignment. In this case, the quenching of the triplet by oxygen is not purely a photophysical event, the appearance of the new band centered at 340 nm (Figure 5-2) concomitant with the decay of the triplet speaks of a photochemical process resulting in a new transient. The rate of appearance of the new transient matches that for the decay of the triplet state of TL for

different oxygen concentrations (*i.e.*, in air or oxygen equilibrated solutions). The rate constant of decay for this newly formed transient (3.3×10^6 s^{-1} in acetonitrile, and 1.0×10^6 s^{-1} in toluene) is independent on the amount of oxygen in the media, as illustrated in Figure 5-3 for experiments in acetonitrile. This is consistent with a species whose precursor is oxygen itself, and is in line with the hypothesis that the Bartlett-Schenck intermediate is observed.

There exists a report in the literature where the acyl-peroxyl radicals formed after photooxidation of diacetyl (see Scheme 5-1) can be monitored by time-resolved absorption spectroscopy. The experiment relies in the formation of an ion-pair complex following quenching of the acyl-peroxyl radicals by *N,N,N',N'*-tetramethyl-*p*-phenylenediamine (TMPD) in aerated benzene.[21] This ion-pair complex has an absorption band centered at 600 nm, where the growth rate constant for the complex formation can be monitored. The dependence of this rate constant with TMPD concentration levels off at a value of *ca.* 6×10^5 s^{-1}. These results are in agreement with our own data, if we consider that the plateau value for the growth rate constant of the ion-pair complex is the value for the formation rate constant of the acyl-peroxyl radical. In other words, the latter can not be quenched by TMPD faster than it is formed. With this argument we then observe that the rate of formation of the acyl-peroxyl radical resulting from the photooxidation of diacetyl in benzene has a similar value (*i.e.*, 0.6×10^6 s^{-1}) to the decay rate constant of the Bartlett-Schenck intermediate from TL (*i.e.*, 1.0×10^6 s^{-1} in toluene). This close proximity in the values is reassuring in that we are monitoring the decay of the Bartlett-Schenck intermediate into an acyl and an acyl-peroxyl radical in our system. Unfortunately, experiments performed in our lab following excitation of TL in the presence of TMPD did not allow us to monitor this previously described transient.

5.3.2 Evaluating the Possibility of a Norrish Type I Process

The previously discussed results strongly support the Bartlett-Schenck intermediate existence. However, an assumption we could not disregard is that following α-cleavage of the

diketone, we monitor the growth of either an acyl, or an acyl-peroxyl radical produced from the reaction of the former and oxygen.

Given the high reactivity of the acyl radical towards oxygen,[30] we can rule out the first possibility on the basis that the disappearance of the signal assigned to the Bartlett-Schenck intermediate does not depend on the oxygen concentration. The Arrhenius preexponential values (see Figure 5-4) for the decay of the Bartlett-Schenck intermediate further support this conclusion. The measured values (*ca.* 9×10^{12} s^{-1} from the average of toluene and acetonitrile measurements) indicate that we are monitoring a unimolecular rearrangement, like the cleavage of the α-diketone-oxygen adduct into products, according to Scheme 5-1. These high preexponential values are not characteristic of bimolecular reactions like radical trapping by oxygen.

The second possibility, *i.e.*, that the observed growth is due to the acyl-peroxyl radical formation, which further decays with a rate constant of 3.3×10^6 s^{-1}, can not be so easily disregarded. The former process is reportedly very fast, *i.e.*, it has a rate constant of 1.8×10^9 $M^{-1}s^{-1}$.[30] This is the same value we have measured for the quenching rate constant of TL triplet state by oxygen. It is then arguable a sequence of reactions where we monitor the growth of an acyl-peroxyl radical with the same rate as that for the decay of TL triplet state, given the immediate quenching of acyl radical by oxygen. To discard the acyl-peroxyl radical as the source of the observed growing band, experiments were recorded with di-*t*-butyl peroxide and 2-thiophenecarboxaldehyde, as well as with 2,2'-thenoin, both under N_2 and O_2 atmosphere. The latter are a convenient source of both the acyl radical and the acyl-peroxyl radical in experiments performed in nitrogen and oxygen atmosphere, respectively.

The results in Figure 5-6 show that although the absorptions due to either type of radicals are similar to that we assign to the Bartlett-Schenck intermediate, the evolution with time for the former two is completely different to that of the latter intermediate. Whereas the Bartlett-Schenck intermediate lifetime is *ca.* 300 ns, the radicals are stable species in a 4 μs period or longer.

From the observed product studies we can propose Scheme 5-4 as the operative one under the conditions employed; *i.e.*, TL excitation under oxygen atmosphere. The formation of radicals would mostly be due to the cleavage of the Bartlett-Schenck intermediate under these conditions.

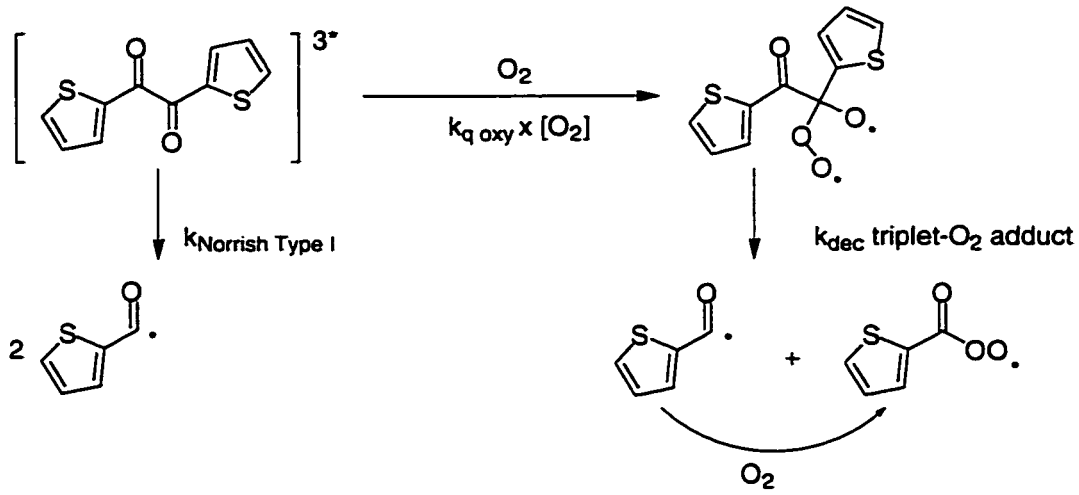

Scheme 5-4: Norrish Type I *vs.* Bartlett-Schenck intermediate formation.

5.3.3 Results with Benzil and Diacetyl

The argument employed in justifying the formation of the α-diketone-oxygen adduct relies on the biradical characteristic of the ketone triplet state. Ketones whose triplet state are n,π* in nature behave as alkoxyl radicals in reactions involving hydrogen abstraction.[20] This characteristic of ketones should also make them reactive towards molecular oxygen addition to the carbon center of the biradical structure. Such scheme was proposed to be operational for regular ketones,[31] although experimental evidence has latter on ruled out this hypothesis.[7]

In the particular case of α-diketones, sensitized olefin oxidation studies at different temperatures and in different solvents have established that the biradical hypothesis is a viable one.[16] Olefin epoxides are derived from the Bartlett-Schenck intermediate, hydroperoxides are the result of singlet oxygen mediated oxidation of the olefins (*ene*

reaction[32]). Sawaki *et al.*[16] found that there is no change on the ratio of epoxide to hydroperoxide products with changes in either solvent or temperature in the sensitized oxidation of olefins by diacetyl or benzil. This result implies that there is no solvent effect in the addition of oxygen to the triplet α-diketone; which is in line with the addition of a neutral species, *i.e.*, oxygen, to a biradical.[16]

The only factor affecting the formation of the Bartlett-Schenck intermediate is then given by the relative resonance stability of the α-diketone triplet state compared to that of its oxygen addition product, according to Sawaki *et al.*[16]

The triplet energy difference between benzil and diacetyl (higher in the latter, see also Table 5-3) would then account for the higher reactivity that diacetyl manifests towards oxygen adduct formation, compared to benzil. Thus, whereas the quantum yield for Bartlett-Schenck intermediate formation (as determined from epoxide yield) in the case of diacetyl is *ca.* 0.23, that for benzil is very low, *i.e.*, 0.022.[16]

The low value for the quantum yield of formation of the Bartlett-Schenck intermediate in the case of benzil would account for the lack of observation of this transient in LFP experiments, as illustrated in the case of Figure 5-9. The only intermediates that can be observed at such low yields are those characterized by very high molar absorptivities, and even then, the signals are extremely weak, *i.e.*, in the range of 0.005. In the case of diacetyl, the lack of signals can not be explained on this basis, given the high quantum yield of formation of the intermediate. The determining factor in this case is the low molar absorptivity of the transient, which probably reflects the absence of aromatic chromophores.

An analysis of TL triplet state energy (see Tables 5-1 and 5-3) would indicate that it is more reactive than benzil towards oxygen addition. Further, the resulting Bartlett-Schenck intermediate is more conjugated than that formed following addition of oxygen by triplet diacetyl making the former readily observable by our LFP system.

5.3.4 Support of a Biradical Structure

A closer analysis of the triplet energies for TL and TOT, and a comparison to those of diacetyl and acetone, and benzil and benzophenone (see table 5-3); as well as an examination of the reactivity towards hydrogen abstraction for TL and TOT, allow us to better understand why we observe the Bartlett-Schenck intermediate after TL irradiation.

Table 5-3: Triplet energies of ketones and diketones.

ketone	R = CH_3	R = phenyl	R = 2-thienyl
R-CO-R	[a] 330 kJ/mol	[a] 287 kJ/mol	[b] 263, [c] 261 kJ/mol
R-CO-CO-R	[a] 235 kJ/mol	[a] 215 kJ/mol	[b] 228, [c] 233 kJ/mol

[a] From reference[19]. [b] In methylcyclohexane, [c] in methanol:ethanol 4:1.

Diacetyl forms the oxygen adduct quantitatively, benzil only with very low yields. In the latter, we expect a delocalization of the electron at the carbon center of the biradical structure along the benzil ring, delocalization that is not operational in diacetyl. This factor reduces the triplet energy for benzil as compared to diacetyl, but also accounts for its lower reactivity towards oxygen. In the case of the thienyl substituted ketones, we first note that the 2-thienyl ring stabilizes the TOT triplet state more than phenyl stabilizes that of benzophenone relative to their ground states, the extreme case being acetone, which lacks any aromatic substituent. An electron donating effect is also observed with 2-thienyl, which determines that the lower triplet state of TOT is π,π^* in nature.[27] This is supported by a lower hydrogen abstraction rate constant by TOT compared to benzophenone, whose lowest triplet state is n,π^* in nature. Interestingly, TL is not only less stabilized with respect to the ground state by the 2-thienyl substituent compared to the stabilization of benzil by phenyl; but its triplet energy value is also very close to that of diacetyl, evidencing little effect on the presence of the 2-thienyl ring. This inefficient stabilization of the triplet diketone by the 2-thienyl ring is also paralleled by its lack of influence on the nature of the lowest triplet state

of TL, which is n,π^*, as evidenced by its rate constant for hydrogen abstraction. TL triplet state seems therefore to be isoelectronic with diacetyl.

Regarding the nature of the decay of the Bartlett-Schenck intermediate, its slower decay in toluene as compared to acetonitrile (with lifetimes of 1.0 and 0.3 μs, respectively) is due to a higher activation energy for decay in the former solvent, as compared to acetonitrile. An important correlation to make is that the difference in activation energies, *ca.* 6.1 kJ/mol larger in a low polarity solvent, is almost the same, but with opposite sign, as the difference in the lowest triplet state energy for the diketone in these solvents (5 kJ/mol larger in high polarity solvents). In order to cleave into an acyl and an acyl-peroxyl radical, it thus seem that the Bartlett-Schenck intermediate first has to reach a transition state which structure and energy are not influenced by the polarity of the media.

5.4 Conclusions

This work was initially triggered by our interest in learning more about the interaction of molecular oxygen and triplet excited states, in particular, diketones. This interest relies on a general concern in the photobiological field of better understanding the phenomena occurring in the encounter of oxygen and an excited state.

Based on our knowledge on the photochemical behavior of 2-then-oyl-aromatic systems, 2,2'-thenil was chosen as the substrate of study.

The studies performed with the LFP technique have rendered, for the first time, a readily detectable triplet α-diketone-oxygen adduct, *i.e.*, the Bartlett-Schenck intermediate. The possibility of monitoring this new transient has enabled us to establish some of its dynamic parameters, like its decay activation energy and preexponential factor. Further, from these values, and experimental observations, we anticipate that its reactivity will be able to be studied under conditions of fast generation and slow deactivation, like those encountered at lower temperatures. The quenching rate constant of the α-diketone triplet state by oxygen (with an energy of activation equal to that for diffusion) is not affected by low temperatures. The decay rate constant of the Bartlett-Schenck intermediate on the other hand is considerable lower in these conditions, given its high decay activation energy. Thus, low temperatures render a clear window for experiments in the microsecond time regime, where the formation and decay lifetimes are well resolved in time.

The observations we have made are in line with those of Sawaki *et al.*, who anticipated that the reactivity of an α-diketone is given by its triplet state stability.[16] The triplet state of 2,2'-thenil being isoenergetic with diacetyl, results in a higher yield of Bartlett-Schenck intermediate that can be readily observed, due to the higher comjugation, with absorption time-resolved techniques, contrary to the case of benzil.

5.5 Materials and Methods

Materials. 2,2'-Thenil (di-2-thienylethanedione), 2,2'-thenoin and 2-(then-2-oyl)thiophene were purchased from Maybridge Chemical Co. Ltd. (Trevillett, Tintagel, Cornwall, England). These samples were sublimed under reduced pressure before use.

Diacetyl (2,3-butanedione), 1,3-cyclohexadiene and 1,4-cyclohexadiene were distilled before use, benzil was recristalized in methanol, di-*tert*-butyl peroxide was treated on alumina column before use, *N*,*N*,*N*',*N*'-tetramethyl-*p*-phenylenediamine was sublimed under reduced pressure before use, 2-thiophenecarboxaldehyde, 2-thiophenecarboxylic acid, *trans*-stilbene, trolox, naphthalene and 1-methylnaphthalene were used as received, these materials and ethanol, were purchased from Sigma-Aldrich Canada (Oakville, ON, Canada). All solvents were HPLC-grade and purchased from OmniSolv (Gibsstown, NJ, USA), and were used without further purification.

5.5.1 Steady-state and Time-resolved Studies

Nanosecond Laser Flash Photolysis. 2,2'-Thenil (TL) concentration was 0.08 to 2 mM for irradiation at 355 nm. When the excitation was carried out at 308 nm the sample concentration was 0.01 mM. These values ensured an absorption of 0.2-0.5 in the laser cell at the excitation wavelength.

Other details have been described in Section 2.5 of this thesis.

Steady-state Measurements. Phosphorescence spectroscopy was performed using a Perkin Elmer LST 50 luminescence spectrometer. The spectra were recorded at 77 K in different glasses. Absorption spectra were recorded using a Varian CARY 1E spectrophotometer.

5.5.2 Product Studies

HPLC studies of the irradiated solutions were carried out on a Varian instrument using a reverse phase 4.6 x 250 mm analytical Zorbax SB-C18 column, the mobile phase used was 15:85 water:methanol, the flow rate employed was 1 ml/min. The detection used a

Varian 9065 Polychrom diode array detector. The absorption spectra and retention times of the products were compared to those of the commercially available materials 2-thiophenecarboxaldehyde and 2-thiophenecarboxylic acid.

Samples were also analyzed on a 3 x 250 mm analytical Zorbax SB-C8 column inserted in a Waters Integrity System consisting of a Waters 996 photodiode array detector, a thermobeam mass detector and a Waters 2690 separation module. Samples were eluted on a solvent gradient of acetonitrile:water 60:40 up to pure acetonitrile, emplying a flow rate of 0.3 ml/min

5.6 References

(1) Hsi, R. A.; Rosenthal, D. I.; Glatstein, E., Photodynamic Therapy in the Treatment of Cancer, *Drugs*, **1999**, *57*, 725-734.

(2) Takemura, T.; Ohta, N.; Nakajima, S.; Sakata, I., Critical Importance of the Triplet Lifetime of Photosensitizer in Photodynamic Therapy of Tumor, *Photochem. Photobiol.*, **1989**, *50*, 339-344.

(3) Ochsner, M., Photophysical and Photobiological Processes in the Photodynamic Therapy of Tumors, *J. Photochem. Photobiol. B: Biol.*, **1997**, *39*, 1-18.

(4) Dahl, T. A., Direct Exposure of Mammalian Cells to Pure Exogenous Singlet Oxygen ($^1\Delta_g O_2$), *Photochem. Photobiol.*, **1993**, *57*, 248-254.

(5) Schweitzer, C.; Mehrdad, Z.; Noll, A.; Grabner, E.-W.; Schmidt, R., Oxygen Quenching of $n\pi^*$ Triplet Phenyl Ketones: Local Excitation and Local Deactivation, *Helv. Chim. Acta*, **2001**, *84*, 2493-2507.

(6) Nau, W. M.; Scaiano, J. C., Oxygen Quenching of Excited Aliphatic Ketones and Diketones, *J. Phys. Chem.*, **1996**, *100*, 11360-11367.

(7) Bendig, J.; Schmidt, R.; Brauer, H.-D., Sensitization of O_2 ($^1\Delta_g$) by *N*-Methylacridone. Solvent and O_2-Concentration Dependence and $^{16}O/^{18}O$ Isotope Exchange Experiments, *Chem. Phys. Lett.*, **1993**, *202*, 535-541.

(8) Saltiel, J.; Curtis, H. C., Photooxidation of Benzil, *Mol. Photochem.*, **1969**, *1*, 239-243.

(9) Shimizu, N.; Bartlett, P. D., Photooxidation of Olefins Sensitized by α-Diketones and by Benzophenone. A Practical Epoxidation Method with Biacetyl, *J. Am. Chem. Soc.*, **1976**, *98*, 4193-4200.

(10) Gollnick, K., Type II Photoooxigenation Reactions in Solution, *Adv. Photochem.*, **1968**, *6*, 1-122.

(11) Gollnick, K.; Schenck, G. O., Mechanism and Stereoselectivity of Photosensitized Oxygen Transfer Reactions, *Pure Appl. Chem.*, **1964**, *9*, 507-525.

(12) Sawaki, Y.; Foote, C. S., Mechanism of Photoepoxidation of Olefins with α-Diketones and Oxygen, *J. Org. Chem.*, **1983**, *48*, 4934-4940.

(13) Sawaki, Y.; Ogata, Y., Reactivities of Acylperoxy Radicals in the Photoreaction of α-Diketones and Oxygen, *J. Org. Chem.*, **1984**, *49*, 3344-3349.

(14) Sawaki, Y.; Ogata, Y., Photoepoxidation of Olefins with Benzoins and Oxygen. Epoxidation with Acylperoxy Radical, *J. Am. Chem. Soc.*, **1981**, *103*, 2049-2053.

(15) Bartlett, P. D.; Roof, A. A. M.; Shimizu, N., The Efficiency of Benzil-sensitized photoepoxidation: A Correction, *J. Am. Chem. Soc.*, **1982**, *104*, 3130-3131.

(16) Sawaki, Y., Mechanistic Study on the Photo-oxidation of α-Diketones with Oxygen, *Tetrahedron*, **1985**, *41*, 2199-2205.

(17) Darmanyan, A. P.; Foote, C. S.; Jardon, P., Interaction of Singlet Oxygen with Peroxy and Acylperoxy Radicals, *J. Phys. Chem.*, **1995**, *99*, 11854-11859.

(18) Martínez, L. J.; Cosa, G.; Scaiano, J. C., Photochemistry of 2-(Then-2-oyl)thiophene in the Presence of Hydrogen Donors: Reactivity and Magnetic Field Effects, Unpublished results.

(19) Carmichael, I.; Hug, G. L. Spectroscopy and Intramolecular Photophysics of Triplet States; In *Handbook of Organic Photochemistry*; J. C. Scaiano, Ed.; CRC Press: Boca Raton, Florida, 1989; Vol. I; 369-403.

(20) Turro, N. J., *Modern Molecular Photochemistry*; University Science Books: Sausalito, 1991.

(21) Hoshino, M.; Kagata, M.; Seki, H.; Seto, H., Studies of Acetylperoxy Radicals Produced by Photolysis of Biacetyl in Aerated Benzene Solutions. Ion-Pair Formation with Tetramethyl-*p*-phenylenediamine, *J. Am. Chem. Soc.*, **1996**, *118*, 2160-2165.

(22) Phan, X. T., Photochemical α-Cleavage of 2,2-Dimethoxy-2-Phenylacetophenone and 1-Hydroxycyclohexyl Phenyl Ketone Photoinitiators. Effect of Molecular Oxygen on Free Radical Reaction in Solution, *J. Rad. Curing.*, **1986**, *13*, 11-17.

(23) Fouassier, J. P.; Lougnot, D. J.; Bassi, G. L.; Nicora, C., Reactivity and Excited State Processes in a Polymeric Photoinitiator, *Polym. Commun.*, **1989**, *30*, 245-248.

(24) Chatgilialoglu, C.; Lunazzi, L.; Macciantelli, D.; Placucci, G., Absolute Rate Constants for Hydrogen Abstraction from Aldehydes and Conformational Studies of the Corresponding Aromatic Acyl Radicals, *J. Am. Chem. Soc.*, **1984**, *106*, 5252-5256.

(25) Scaiano, J. C.; Wubbels, G. G., Photosensitized Dissociation of Di-*tert*-butyl Peroxide. Energy Transfer to a Repulsive Excited State, *J. Am. Chem. Soc.*, **1981**, *103*, 640-645.

(26) Ortica, F.; Romani, A.; Favaro, G., Light-induced Hydrogen Abstraction from Isobutanol by Thienyl Phenyl, Dithienyl, and Thienyl Pyridyl Ketones, *J. Phys. Chem. A*, **1999**, *99*, 1335-1341.

(27) Becker, R. S.; Favaro, G.; Poggi, G.; Romani, A., Photophysical Properties of Some Thienyl Ketones: An Experimental and Theoretical Study, *J. Phys. Chem.*, **1995**, *99*, 1410-1417.

(28) Encinas, M. V.; Scaiano, J. C., Reaction of Benzophenone Triplets with Allylic Hydrogens. A Laser Flash Photolysis Study, *J. Am. Chem. Soc.*, **1981**, *103*, 6393-6397.

(29) Sawaki, Y., Mechanism of Photooxidation and Photoepoxidation with Cyclic α-Diketones, *Bull. Chem. Soc. Jpn.*, **1983**, *56*, 3464-3470.

(30) Brown, C. E.; Neville, A. G.; Rayner, D. M.; Ingold, K. U.; Lusztyk, J., Kinetic and Spectroscopic Studies on Acyl Radicals by Time-resolved Infrared Spectroscopy, *Austr. J. Chem.*, **1995**, *48*, 363-379.

(31) Gorman, A. A.; Rodgers, M. A. J., The Quenching of Aromatic Ketone Triplets by Oxygen: Competing Singlet Oxygen and Biradical Formation?, *J. Am. Chem. Soc.*, **1986**, *108*, 5074-5078.

(32) Gilbert, A.; Baggott, J., *Essentials of Molecular Photochemistry*; Blackwell Scientific Publications: Oxford, 1991.

6. Radical Chemistry of a Melanin Precursor: Adrenaline

6.1 Introduction

Adrenaline, together with noradrenaline and dopamine, belongs to the general class of compounds known as catecholamines. Their basic structure is that of *o*-dihydroxybenzene containing an amine substituent. These molecules act both as neurotransmitters in the brain, and as hormones in the blood system.[1] They are produced in the organism by the enzyme tyrosine hydroxylase, which transforms tyrosine into dopa, a first intermediate in their synthesis (see Scheme 6-1).[2]

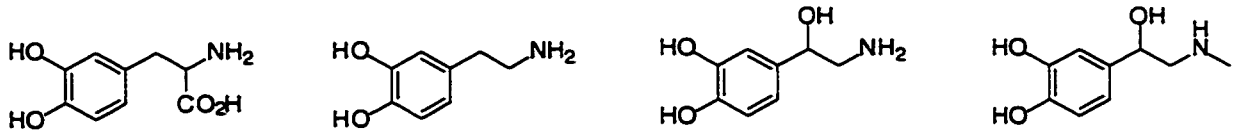

Scheme 6-1: Structure of Catecholamines.

Following oxidation, these catecholamines ultimately form melanin pigments (see also Figure 1-6), which are known for their protection against solar radiation.[3,4] The protective effect is due not only to a screening effect of the solar radiation, but also the antioxidant effect of melanin plays an important role as a scavenger of radicals arising from photosensitized processes.[3,5-7] A recent study thus proposes a synergistic photoprotective mechanism for melanin.[5]

Catecholamines share a common oxidation pathway.[8-13] It is initiated by the oxidation of the dihydroxybenzylamine to the amine semiquinone radical; the latter disproportionates to form aminoquinone, which upon cyclisation forms leucoaminochrome. Leucoaminochrome further oxidizes to form leucoaminochrome semiquinone radical, which upon subsequent disproportionation generates aminochrome. The latter rearranges to aminoleutine. In Scheme 6-2 we exemplify this series of reactions with adrenaline. In the case of adrenaline semiquinone radical, the structure shown has been determined in acetate buffer pH 5 in the presence of Zn^{+}, by ESR techniques following photooxidation.[13]

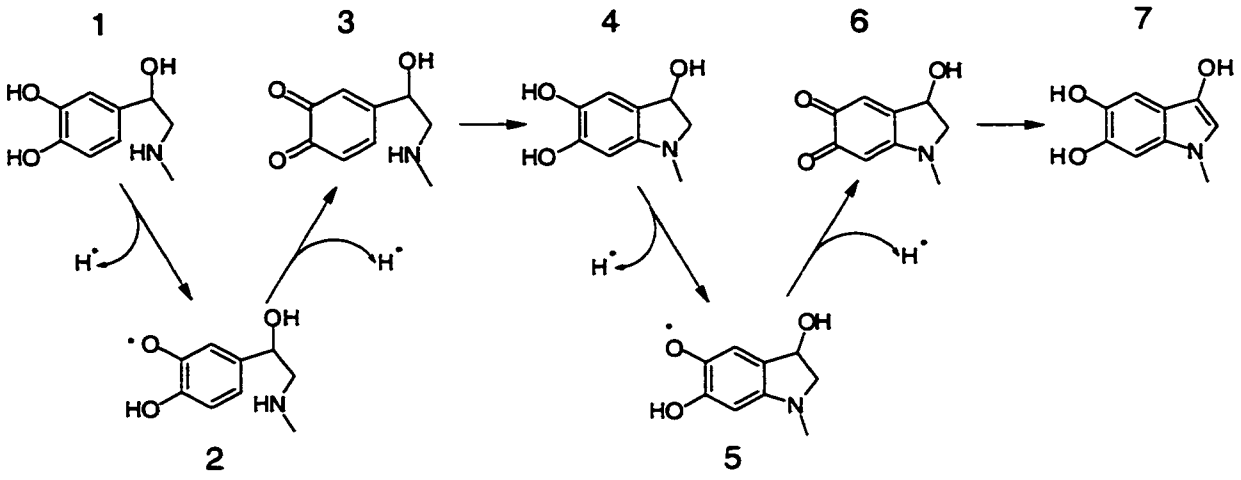

Scheme 6-2: Oxidation of adrenaline. (1) adrenaline, (2) adrenaline semiquinone radical, (3) adrenoquinone, (4) leucoadrenochrome, (5) leucoadrenochrome semiquinone radical, (6) adrenochrome, (7) adrenoleutine.

The conversion of the aminodihydroxybenzene to aminoquinone is mediated by the action of oxidative enzymes;[8,9,12,14-17] the subsequent steps in the oxidation are proposed to be independent of enzyme activity.[10] The kinetics of formation of the different transients involved in the oxidation of dopa to dopachrome, as well as their spectroscopy, have been described following pulse radiolysis studies.[10,11] A recent report also discusses the oxidation of dopamineleutine, the dihydroxyindole, into its semiquinone radical; this work also compares the antioxidant activity of melanin, dopaleutine and dopamineleutine, in terms of their reactivity towards radical-like species.[5]

Interestingly, no such reactivity has been analyzed for the catecholamines, and although enzymes initiate their oxidation (*vide supra*), we can not rule out the possibility of radical attack on these species. This is particularly important in the case of dopamine, where the immediate products following its oxidation, *i.e.*, dopamine semiquinone radical and dopamine quinone, are precursors of the potent neurotoxin 6-hydroxydopamine, involved in oxidative stress neuronal degeneration.[18] An understanding of their reactivity is also

important to assess their antioxidant effect, in view of reports accounting for their radical scavenging properties.[19]

In this work we analyze the reactivity of adrenaline towards radical-like substrates such as *tert*-butoxyl (*t*-butoxyl) radicals and triplet benzophenone, in order to predict the feasibility of radical mediated degeneration of catecholamines.

The choice of *tert*-butoxyl radicals and triplet benzophenone as the oxidating agents of adrenaline is not casual. Previous results existing in the literature, where the former are quenched by well known radical scavengers,[5,20-22] will allow us to establish a comparison among these different species and adrenaline.

6.2 Results

6.2.1 Reaction with *tert*-Butoxyl Radicals

The low solubility of adrenaline in di-*tert*-butyl peroxide:acetonitrile mixtures, as well as in pure acetonitrile, required the addition of acetic acid (2.2 % v:v; *ca.* 0.4 M) to help dissolve this substrate in the experiments hereon described.

The irradiation of di-*tert*-butyl peroxide (di-*t*-butyl peroxide), with a short wavelength (*i.e.*, shorter than 355 nm) nanosecond laser pulse produces *t*-butoxyl radicals within the duration of the pulse. Upon their formation these radicals will decay by first order processes involving either elimination of acetone and production of methyl radical (β cleavage), or reaction with the solvent; this is shown in the second step in Scheme 6-3. Alternatively, in the presence of a hydrogen donor, the radicals will be reduced to the corresponding alcohol, concomitant with the oxidation of the donor (see Step 3 in Scheme 6-3).

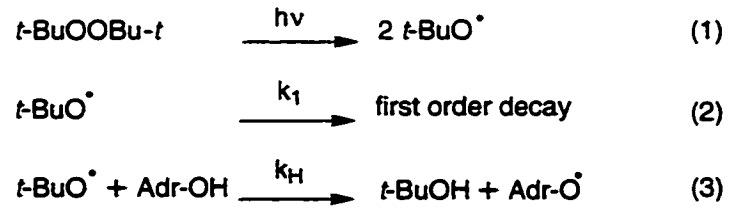

Scheme 6-3: Steps involved in *t*-butoxyl radical formation and consumption.

Following the formation of *t*-butoxyl radicals after excitation with a 337 nm laser, and in the presence of adrenaline as a hydrogen donor, we can readily monitor with our laser flash photolysis (LFP) system the appearance of a transient with an absorption band at 380 nm, increasing in value at shorter wavelengths (see Figure 6-1). This transient also presents a band in the visible which extends in the near IR, *i.e.*, from 500 nm and over 700 nm. The spectrum could be monitored up to 320 nm; at shorter wavelengths the ground state absorbance of di-*t*-butyl peroxide precluded the acquisition of a signal with our LFP system. We assign the observed spectrum to the semiquinone radical resulting from the oxidation of

adrenaline (species **2** in Scheme 6-2). It matches those spectra obtained following pulse radiolysis studies of dopa in aqueous solution containing NaN_3 at pH 6,[11] and of 3,5-di-*tert*-butyl-1,2-benzoquinone under N_2O atmosphere at pH 3.[23]

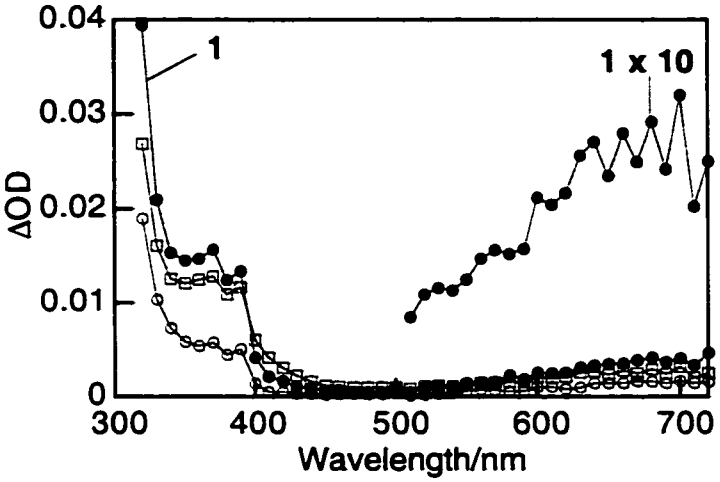

Figure 6-1: Transient absorption spectra of 2.9 x 10^{-3} M adrenaline under N_2 atmosphere, in 38:60:2 di-*tert*-butyl peroxide:acetonitrile:acetic acid. Laser wavelength 337 nm. Time windows: (○) 0.56 μs; (●) 4.72 μs; and (□) 17.00 μs after the laser pulse.

We monitored the dependence of the growth rate constant for the semiquinone radical with adrenaline concentration at 370 nm; the data is presented in Figure 6-2.

Based on Equation 6-1 and Scheme 6-3, it is possible to establish a quenching rate constant for the reaction of *t*-butoxyl radicals with adrenaline (k_H) of 1.5 x 10^8 $M^{-1}s^{-1}$. From the value of the intercept at the origin, we obtain a rate constant for the first order decay of *t*-butoxyl radical (k_1) of 2.6 x 10^5 s^{-1}. From the latter value we can rule out the possibility of the reaction of adrenaline with methyl radicals arising following β cleavage of *t*-butoxyl radicals, given that the latter are quenched before this cleavage can occur. Thus our measured reactivity is characteristic for the reaction of *t*-butoxyl radicals with adrenaline.

Equation 6-1: $$k_{exp} = k_1 + k_H \times [Adr - OH]$$

Previous results from this group show a high reactivity of α-hydrogens in alkylamines towards *t*-butoxyl radicals. This is the result of the stability of α-aminoalkyl radicals, which is also reflected in the transition state of the reaction of hydrogen abstraction leading to this type of radicals.[24]

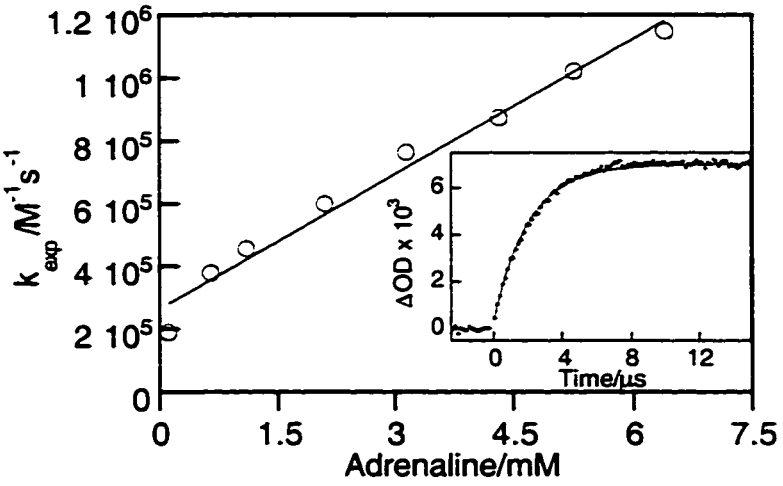

Figure 6-2: Observed growth rate constant for the formation of the adrenaline semiquinone radical measured at 370 nm, in the presence of different amounts of adrenaline, in 38:60:2 di-*tert*-butyl peroxide:acetonitrile:acetic acid. The inset shows the time dependence of the absorption at 370 nm for an adrenaline concentration of 1.09 x 10^{-3} M. Laser wavelength 337 nm, N_2 bubbled.

It is therefore important to establish which role, if any, the amino group or the benzylic hydrogen plays in the oxidation of the catecholamines. In this sense, it is worth mentioning that both, bond dissociation energies involving the formation of phenoxy radicals from phenols as well as α-aminoalkyl radicals from α-aminoalkanes are very similar in value, *i.e.*, 368 kJ/mol.[25,26]. This bond dissociation energy is the same characterizing a benzylic hydrogen.[27]

The methodology we employ in our experiments provides kinetic, not mechanistic information.[28] Although we only observe the semiquinone radical spectra, we can not rule out on this sole basis the possibility of hydrogen abstraction at the α-amino position, which could result in a transparent radical in our system, and an overestimation of the reactivity of

the phenol moiety.[24] In order to establish if such a process is viable in our system, we performed kinetic measurements with 1-hydroxy-1-phenyl-2-methylaminoethane (halostachine) in the presence of a constant concentration of benzhydrol, employed as a signal carrier (see Scheme 6-4). The situation is similar to that described in Scheme 2-3. Halostachine is a good model compound since the structural differences with adrenaline are 3 atoms away for the amine nitrogen. Even at concentrations as high as 42 mM on halostachine, the observed growth rate (monitored at 330 nm) was the same as that obtained with no halostachine, *ca.* 3.3 x 10^5 $M^{-1}s^{-1}$. At the same concentration of adrenaline, the observed rate would be *ca.* 6.3 x 10^6. Thus 5% is the highest estimate for the possibility of hydrogen abstraction at centers other than the phenylhydroxy moiety (step 3 in Scheme 6-4).

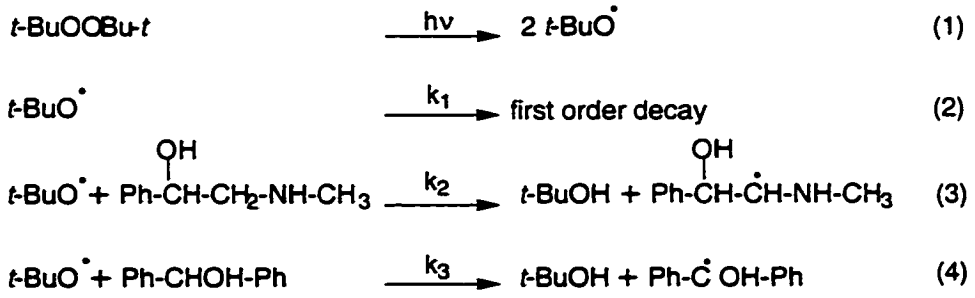

Scheme 6-4: Reaction mechanism for the deactivation of *t*-butoxyl radicals in the presence of halostachine and benzhydrol, as a signal carrier.

As part of our experiments we also monitored the fate of the semiquinone radical over time. Figures 6-3-A and 6-3-B show the transient absorption spectra, and the evolution of the absorbance with time (monitored at 370 nm and 400 nm), respectively. In the latter case the experimental traces are best fitted by a second order function.

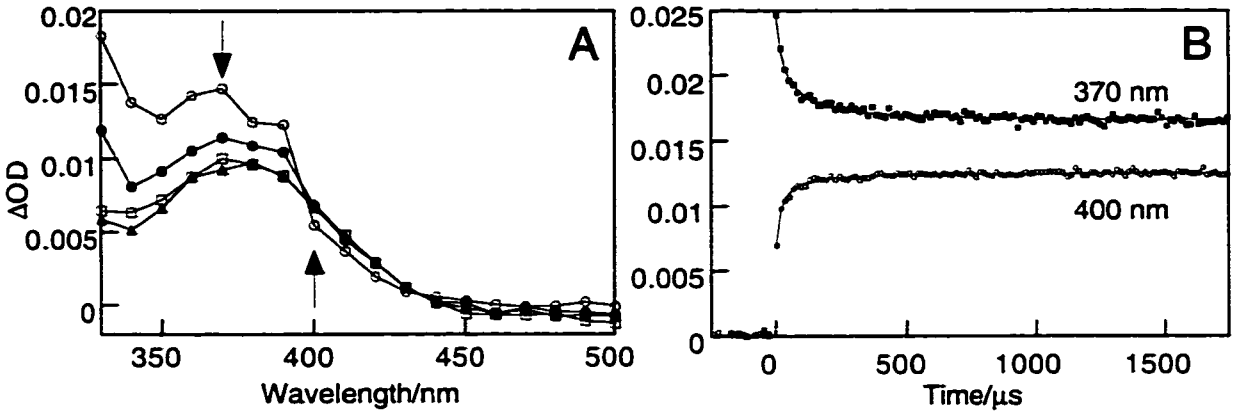

Figure 6-3: (A) Transient absorption spectra of 3.0 x 10^{-3} M adrenaline under N_2 atmosphere, in 38:60:2 di-*tert*butyl peroxide:acetonitrile:acetic acid. Laser wavelength 337 nm. Time windows: (○) 23 μs; (●) 113 μs; (□) 449 μs; and (▲) 812 μs after the laser pulse. (B) Time evolution for the absorption at 370 and 400 nm, obtained with a laser pulse energy of 2.66 mJ/pulse.

The transient spectra obtained 812 μs after the laser pulse matches that reported for aminoquinones formed as a result of the oxidation of their respective catecholamines.[10,11] These aminoquinones are formed following disproportionation of two semiquinone radicals,[9-12,16] as exemplified in Scheme 6-5 for adrenaline.

A disproportionation is supported in our case by the observed temporal evolution of the semiquinone radical absorbance, fitted with a second order rate expression, and also by the quadratic power dependence for the transient absorption measured at 400 nm, 1700 μs after the laser pulse (data not shown).

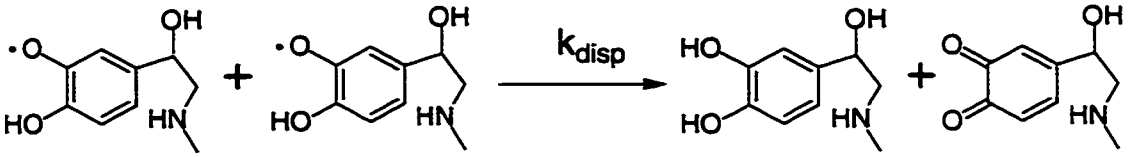

Scheme 6-5: Disproportionation of adrenaline semiquinone radical.

In order to determine the disproportionation rate constant k_{disp}, it is necessary to know the molar absorptivity for the semiquinone radical. This results from the mathematical

relationship existing between the experimentally observed disproportionation rate constant (k_{obs}), determined by changes in transient absorbance, and the real rate constant k_{disp}, which accounts for changes in the concentration of the semiquinone radical (see Equation 6-2).

Equation 6-2: $$k_{obs} = \frac{k_{disp}}{\varepsilon_{SQ} \times l}$$

where (l) is the optical path length of the cell.

6.2.2 Reaction with Benzophenone

Following excitation, benzophenone undergoes efficient intersystem crossing to the lowest excited triplet state, which is n,π^* in nature.[29] This state is very reactive towards hydrogen abstraction, and in the case of phenols, rate constants of benzophenone quenching in the range of 8 x 10^7 to 5 x 10^9 $M^{-1}s^{-1}$ have been obtained in acetonitrile and benzene.[30] However, not only hydrogen abstraction, but also electron transfer,[31] energy transfer or other type of physical deactivation may be operational in the case of triplet benzophenone, as is shown in Scheme 6-6.[20,30]

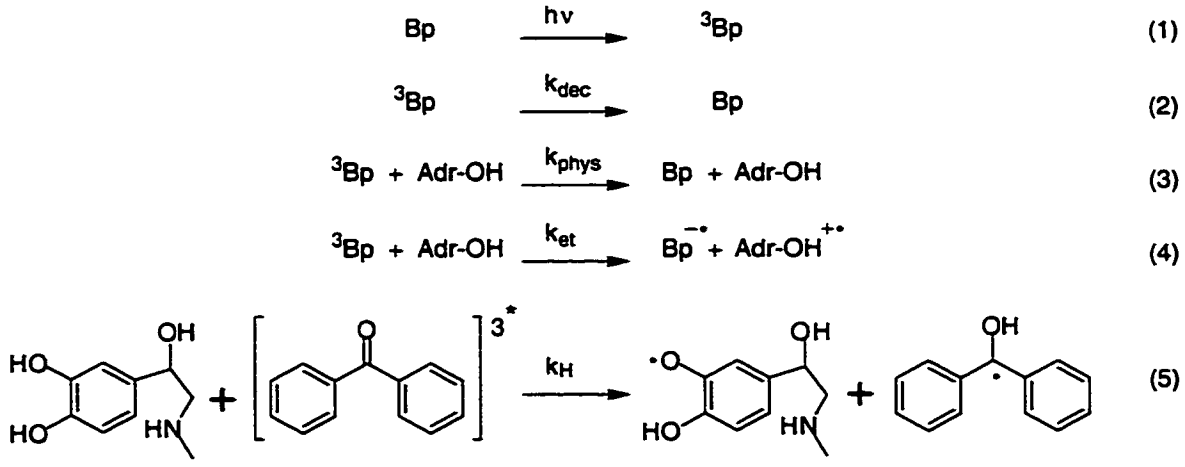

Scheme 6-6: Deactivation mechanism for triplet benzophenone in the presence of adrenaline (Adr-OH).

We measured the decay rate constant of triplet benzophenone in the presence of different concentrations of adrenaline, and obtained a value for the quenching rate constant of 1.3 x 10^9 $M^{-1}s^{-1}$. In order to establish to which extent the observed quenching is due to hydrogen abstraction (Step 5), and how important are the other possible mechanisms proposed in Scheme 6-6 (Steps 2 to 4), we evaluated the ratio of absorbances from the triplet state (ΔOD_T), and from the ketyl radical (ΔOD_K). The former obtained immediately after the laser pulse, and the latter measured after the decay of the triplet state is complete (see Equation 6-3).

Equation 6-3:
$$\frac{k_H}{k_{obs}} = \frac{\Delta OD_K}{\Delta OD_T} \times \frac{\varepsilon_T}{\varepsilon_K}$$

where k_H is the rate constant for hydrogen abstraction, k_{obs} is the measured quenching rate constant (*i.e.*, k_{obs} is equal to the addition of k_{dec}, k_{phys}, k_{et}, and k_H), and ε_T and ε_K are the molar absorptivities for the triplet state and the ketyl radical respectively.

These measurements are commonly performed at 545 nm,[20] or 530 nm[32] where the molar absorptivities for both transients are well established. Given that the absorption of adrenaline semiquinone radical has a band extending from *ca.* 500 nm and to the red, (Figure 6-1), we used the ratio of absorbances measured at 500 nm. We then compared the value obtained following 95% quenching by adrenaline, to that obtained following 95% quenching by 1,4-cyclohexadiene, under the same conditions. The latter is a good hydrogen donor, and the allylic radical obtained following its oxidation is transparent over the whole visible range.[33] The decay traces obtained in the presence of both quenchers are shown in Figure 6-4-A.

We obtained values for the ratio of ketyl radical to triplet state transient absorption at 500 nm of 0.45 and of 0.43 when employing adrenaline and 1,4 cyclohexadiene as hydrogen donors, respectively. This values are within a 5% error difference, that for adrenaline being larger than that for the alkene, where hydrogen abstraction is the only operational mode of

quenching. We can thus assume that all the deactivation by adrenaline is due to hydrogen abstraction by benzophenone triplet state.

A comparison of the transient absorption spectra obtained following triplet benzophenone quenching by 1,4-cyclohexadiene to that obtained following quenching by adrenaline evidences the presence of the semiquinone radical of adrenaline, as can be observed following the subtraction of both spectra in Figure 6-4-B. We can now determine the molar absorptivity for the semiquinone radical at 370 nm, by employing the known value for the ketyl radical at 550 nm, *i.e.*, 3300 ± 700 $M^{-1}cm^{-1}$.[34]

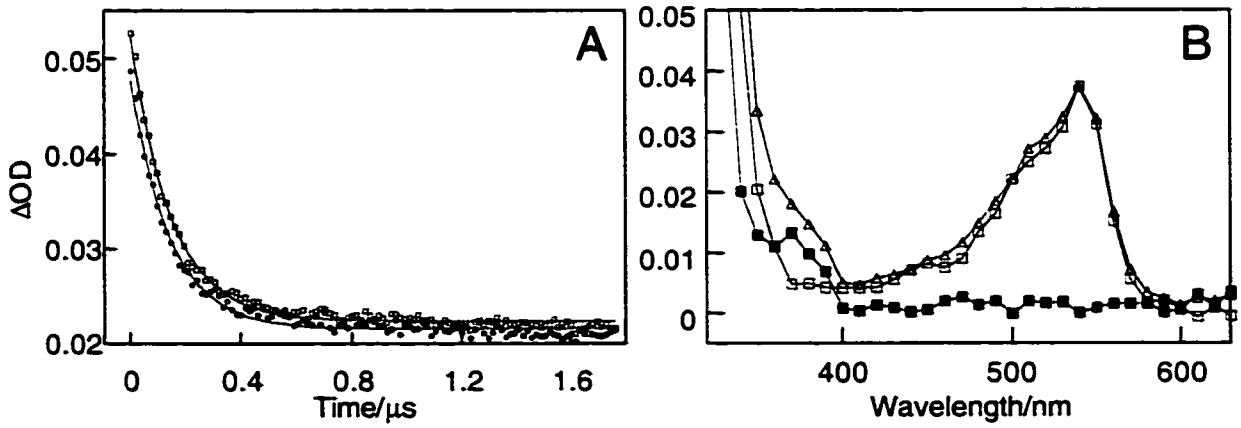

Figure 6-4: (A) Time evolution for the transient absorption at 500 nm following excitation of benzophenone in the presence of (●) adrenaline 5.9 x 10^{-3} M, and (□) 1,4-cyclohexadiene 2.05 x 10^{-2} M. (B) Transient absorption spectra obtained 0.9 μs after the laser pulse, in the presence of (△) adrenaline 5.9 x 10^{-3} M, and (□) 1,4-cyclohexadiene 2.05 x 10^{-2} M. Also shown is the difference between both traces, which were normalized at 500 nm (■). Experiments were performed under N_2 atmosphere, in 98:2 acetonitrile:acetic acid v:v. The Laser wavelength employed was 355 nm.

Judging from Figure 6-4-B and Figure 6-1, we can consider negligible the absorbance at 550 nm due to the adrenaline semiquinone radical. The contribution of the ketyl radical absorbance at 370 nm can on the other hand be subtracted by the spectra of pure ketyl radical obtained with 1,4-cyclohexadiene, in a similar manner as done in Figure 6-4. Employing

Equation 6-4 we can now calculate the molar absorptivity at 370 nm for the adrenaline semiquinone radical ($\varepsilon_{SQ\,370}$).

Equation 6-4:
$$\varepsilon_{SQ_{370}} = \frac{\Delta OD_{SQ_{370}}}{\Delta OD_{K_{550}}} \times \varepsilon_{K_{550}}$$

where $\varepsilon_{K\,550}$ is the molar absorptivity of the ketyl radical at 550 nm, and $\Delta OD_{K\,550}$ and $\Delta OD_{SQ\,370}$ are the absorbances due to the ketyl radical and the semiquinone radical at 550 and 370 nm, respectively. A value of 1400 ± 300 $M^{-1}cm^{-1}$ is obtained in this manner for the molar absorptivity of the semiquinone radical at 370 nm. This value is within experimental error, the same as that previously determined for catechol in benzene at 383 nm, *ca.* 1500 ±300 $M^{-1}cm^{-1}$.[35]

With the molar absorptivity value at 370 nm, and that for the observed second order rate constant obtained for the semiquinone radical disproportionation, we calculate the disproportionation rate constant for the semiquinone radical according to Equation 6-2. The value we obtain is 35 ± 0.8 x 10^8 $M^{-1}s^{-1}$. The value reported in the literature for dopa in buffer pH 7.7 is 0.98 x 10^8 $M^{-1}s^{-1}$.[10]

6.3 Discussion

The antioxidant effect of phenols has received considerable attention; and there exist numerous reports on the radical scavenging properties of these substrates.[20,25,36-40] However, to our knowledge, the reactivity of catecholamines has not been analyzed with radical-like species. We therefore have employed *t*-butoxyl radicals and the triplet state of benzophenone as a source of oxidazing agents, to establish the activity of adrenaline as a radical scavenger.

In Table 6-1 we present the values for the rate constant of hydrogen abstraction from adrenaline obtained in this work, and we compare them with those obtained for other biologically relevant substrates of similar structure. Also shown in Table 6-1 are the rate constants for phenol and *p*-methoxyphenol, as model structures.

Table 6-1: Hydrogen abstraction rate constants from different radical scavengers by benzophenone and *t*-butoxyl radical.

Substrate	Rate constant for hydrogen abstraction, $k_H \times 10^{-8}$ $M^{-1}s^{-1}$							
	benzophenone triplet state				*t*-butoxyl radical			
	benzene	Ref.	**acetonitrile**	Ref.	**benzene**	Ref.	**acetonitrile**	Ref.
phenol	**13**	30	**0.8**	30	**3.3**	35	[a] **0.22**	35
p-methoxyphenol	**45**	30	**39**	30	**16**	35	[a] **1.1**	35
adrenaline	-	-	**13**	*c*	-	-	**1.5**	*c*
dopaleutine	**69**	5	**84**	5	-	-	**8.1**	5
melatonin	-	-	**76**	21	-	-	**0.34**	21
vitamin E	**51**	20	**60**	22	**38**	20	[b] **6.6**	20

[a] In methanol; [b] in wet acetonitrile; [c] this work. The error is given by the last significant figure.

6.3.1 Reaction with *tert*-Butoxyl Radicals

To perform our experiments it was necessary to add acetic acid (2.2% v:v; *ca.* 0.4 M) in acetonitrile to increase adrenaline solubility. The latter is insoluble in benzene, and therefore we could not determine the kinetics of hydrogen abstraction in this solvent.

Under our experimental conditions we did not observe hydrogen abstraction on position α to the amino group. This is understandable on the basis that the lone pair of electrons in the nitrogen atom is protonated. The resonance stabilization of the α-amino radical by this lone pair of electrons will not be operational under this condition,[24] neither is the stabilization of the transition state leading to this radical.

We can rule out the possibility of reaction of methyl radicals with adrenaline under our experimental conditions. They are formed following the disproportionation of *t*-butoxyl radicals, and based on our results this process occurs with a rate constant of 2.6×10^5 s^{-1}, in agreement to that previously determined for this reaction in the same solvent.[41] At the range of adrenaline concentrations employed all *t*-butoxyl radicals are consumed before they disproportionate.

Quantitative predictions have been formulated for kinetic solvent effects (KSE) that permit the extrapolation of the data for hydrogen atom abstraction by a radical (for example *t*-butoxyl) from a phenol in a given solvent, based on the known value in a different media.[37,42,43] These predictions are based on three assumptions; each substrate hydrogen bonds to only one solvent molecule; the equilibrium rate constant for this bonding is independent of the surrounding media; and finally, due to steric reasons, the hydrogen atom of the donor can not be directly abstracted by the acceptor, rather the acceptor has first to replace the solvent molecule in the complex formed by the hydrogen donor-solvent molecule.[37]

The three assumptions explain the difference observed in the reactivity of phenol and *p*-methoxyphenol with *t*-butoxyl radical in methanol *vs.* benzene. Qualitatively, we would expect a similar increase in the radical scavenging activity of adrenaline in going from

acetonitrile (where hydrogen bonding is strong) to benzene. However, given its relevance in biological systems, we are interested in the reactivity of adrenaline in protic solvents, such as alcohols or water. Based on the previous assumptions, we can expect a considerable decrease in the radical scavenging ability in the latter systems for adrenaline due to the stronger hydrogen bonding present in these systems. Results obtained with 2,2,5,7,8,-pentamethyl-6-hydroxychroman, related to vitamin E, show a 30 fold decrease in the hydrogen atom abstraction rate constant by 1,1,-diphenyl-2-picrylhydrazil (DPPH) radical in going from hexane to n-propanol.[40] Employing 3,5-di-*tert*-butylcatechol (an *o*-dihydroxybenzene like adrenaline) as a hydrogen donor, the decrease in rate constant is *ca.* 250 fold for the same change in solvents.[40] The same relative changes in hydrogen abstraction rate constants are expected if *t*-butoxyl radicals (rather than DPPH) are employed, according to the kinetic solvent effect theory of Ingold *et al.*[37]

Extrapolating these results to adrenaline, we would also expect a considerable reduction in its radical scavenging power in n-propanol.

6.3.2 Reaction with Benzophenone

The observed increase in the rate constant for hydrogen abstraction in acetonitrile when employing benzophenone as compared to *t*-butoxyl radical has been previously described with other phenols.[20,35] Thus we observe in Table 6-1 that an order of magnitude difference in reactivity in acetonitrile also applies to vitamin E, phenol and *p*-methoxyphenol. Futher, in the case of melatonin, an indole derivative of similar structure to aminoleutines, although lacking the dihydroxy functionality of the latter, the reactivity with benzophenone is *ca.* 200 fold larger than that with *t*-butoxyl radical. This is explained by the stabilization, due to polar effects, of the transition state leading to the photoreduction of benzophenone, which counteracts the stronger hydrogen bonding of the radical scavengers with acetonitrile.[20,35] These polar effects are not operational in the case of hydrogen abstraction by *t*-butoxyl radical and other radicals.[37]

Our results show that the mechanism of quenching of the benzophenone triplet state is due solely to hydrogen abstraction. At the conditions employed the nitrogen atom in the catecholamine is protonated (*vide supra*), and therefore electron transfer from this species to benzophenone will not occur, however we can not rule out this possibility in water at pH 7.4. As in the case of the reaction with *t*-butoxyl radicals, no reaction to form α-aminoradicals takes place in our media. This is also explained by protonation of the nitrogen atom at the amine functional group.

We have been able to determine the molar absorptivity of adrenaline semiquinone radical at 370 nm following its reaction with benzophenone triplet state, and from this value we have calculated the second order rate constant for disproportionation. Our value is *ca.* 35 fold larger than that established in water. At the present time we can not determine if this difference is only due to solvent effects, or the inherent errors with which the values have been obtained also play a role.

6.3.3 Other Intermediates in Catecholamine Oxidation

The time resolution of our setup does not allow us to follow over time the subsequent steps in adrenaline oxidation, involving the conversion of adrenoquinone into adrenochrome. However we consider it worth to analyze the other intermediates formed in the oxidation of adrenaline and other catecholamines.[8-13] In this sense, both leucoadrenochrome and aminoleutin pose very interesting structures in terms of radical scavenging potential.

Electron donating groups substituted ortho or para to the reactive hydroxyl group wherefrom hydrogen is abstracted stabilize the radical formed, and also the transition state leading to its formation. This explains the higher reactivity of adrenaline and *p*-methoxyphenol in comparison to that of phenol. In the case of vitamin E, a 6 member heterocyclic ring reduces the dihedral angle existing between the lone pair of the *p*-oxygen atom in the heterocyclic ring, and the hydroxyl group. This results in its enhanced antioxidant activity. A similar structure can be observed both in the case of aminoleutine and leucoadrenochrome (see Scheme 6-2), and based on the known activity of vitamin E, and on

calculations of bond dissociation energies,[36] we can predict that these species will be more reactive as hydrogen donors towards radicals than their catecholamine precursors.

The reactivity of dopaleutine (an aminoleutine, see Scheme 6-2) as a hydrogen donor has been reported with quenching experiments done with benzophenone and fluorazophore-P, one value has also been reported for the reaction with *t*-butoxyl radicals.[5] From the results obtained with benzophenone we observe that aminoleutine is about as reactive as vitamin E in acetonitrile, and *ca.* 6.5 times more reactive than adrenaline (Table 6-1). Care should be taken in analyzing the reactivity of these molecules with benzophenone, given that they are affected by charge transfer effects.[21]

An analysis based on the reactivity of these molecules with *t*-butoxyl radicals presents a much clearer picture; thus from the values measured for dopaleutine we establish that its reactivity is as high as that of vitamin E, and *ca.* 5 times higher than that of the catecholamine. Further, the reactivity relies on the hydroxyl moiety of dopaleutine, given the low reactivity of melatonin, an analog of dopaleutine that lacks the hydroxy groups. The rate constant for reaction of the former with *t*-butoxyl radicals is *ca.* 24 fold lower than that of dopaleutine.

6.4 Conclusions

We report for the first time absolute rate constants for the reaction of a catecholamine with an organic radical species (*i.e.*, *t*-butoxyl radical) in the absence of metals.

Adrenaline is a modest radical scavenger, however we predict that the reactivity of the products of its oxidation exhibit an enhanced reactivity towards free radicals. This is in view of the good overlap existing between the lone pair of electrons in the nitrogen atom of the newly formed heterocyclic ring, and the hydroxy group in the benzene moiety. This overlap (and the heterocycle) is nonexistent in adrenaline and the other catecholamines, previous to their oxidation. In the presence of high radical concentration, we therefore believe that the oxidation of adrenaline into melanin will proceed towards complete polymerization following the steps shown in Scheme 6-2, where each new species will have enhanced antioxidant power compared to its immediate precursor. This enhanced reactivity would ensure the complete elimination of undesired intermediates in adrenaline oxidation, following radical mediated lesions.

6.5 Materials and Methods

Materials. Adrenaline ((±) 4-[1-hydroxy-2-methylamino)ethyl]-1,2-benzenediol), benzhydrol, di-*tert*-butyl peroxide (treated in alumina column before use) and 1,4-cyclohexadiene (distilled before use) were purchased from Sigma-Aldrich Canada (Oakville, ON, Canada). Halostachine ((±)1-hydroxy-1-phenyl-2-methylaminoethane) was purchased from Lancaster (Windham, NH, USA). Benzophenone from BDH Chemicals Ltd. (Poole, England) was recrystallized in ethanol before use. Acetonitrile was HPLC-grade and purchased from OmniSolv (Gibsstown, NJ, USA), and was used without further purification. Acetic acid, glacial, was purchased from Anachemia (Montreal, QC, Canada).

Nanosecond Laser Flash Photolysis. A minimum of 8 shots at each wavelength were acquired to record the spectra. For the power dependence studies 40 to 60 shots were accumulated for each measurement, to improve the signal to noise ratio due to the low intensity of the signals. The rate constant for hydrogen abstraction by di-*t*-butyl peroxide was determined from the growth monitored at 370 nm. Up to 30 shots were accumulated. In the case of studies performed with benzophenone, the 355 nm laser was employed. In this case no more than 4 shots were accumulated to obtain each kinetic trace.

Fresh solutions were prepared every day before experiments. The solvent employed in all cases was prepared by mixing 60 parts in volume of acetonitrile with 2.25 parts in volume of acetic acid glacial, and bringing to 100 parts with di-*t*-butyl peroxide (approximately 38 parts in volume). These values ensured an absorbance by di-*t*-butyl peroxide of 0.3-0.5 in the laser cell at the excitation wavelength. Sample stability was checked under nitrogen atmosphere. There was no observed change after 3 h, as determined by steady-state absorption spectroscopy.

Other details of the laser system have been described in Section 2.5 of this thesis.

6.6 References

(1) Voet, D.; Voet, J. G., *Biochemistry*; John Wiley & Sons, Inc.: New York, 1990.

(2) Rhoades, R.; Pflanzer, R., *Human Physiology;* Second Edition ed.; Saunders College Publishing: Orlando, 1992, 268-269.

(3) Schmitz, S.; Thomas, P. D.; Allen, T. M.; Poznansky, M. J.; Jimbow, K., Dual Role of Melanins and Melanin Precursors as Photoprotective and Phototoxic Agents: Inhibition of Ultraviolet Radiation-induced Lipid Peroxidation, *Photochem. Photobiol.*, **1995**, *61*, 650-655.

(4) Kollias, N.; Sayre, R. M.; Zeise, L.; Chedekel, M. R., Photoprotection by Melanin, *J. Photochem. Photobiol. B: Biol.*, **1991**, *9*, 135-160.

(5) Zhang, X.; Erb, C.; Flammer, J.; Nau, W. M., Absolute Rate Constants for the Quenching of Reactive Excited States by Melanin and Related 5,6-Dihydroxyindole Metabolites: Implications for Their Antioxidant Activity, *Photochem. Photobiol.*, **2000**, *71*, 524-533.

(6) Reszka, K. J.; Matuszak, Z.; Chignell, C. F., Lactoperoxidase-catalyzed Oxidation of Melanin by Reactive Nitrogen Species Derived from Nitrite (NO_2^-): an EPR Study, *Free Rad. Biol. Med.*, **1998**, *25*, 208-216.

(7) Stepién, K.; Porebska-Budny, M.; Hollek, A. M.; Wilczok, T., The Inhibiting Effect of Catecholamine-melanins on UV-induced Lecithin Peroxidation, *J. Photochem. Photobiol. B: Biol.*, **1992**, *15*, 223-231.

(8) Adak, S.; Bandyopadhyay, U.; Bandyopadhyay, D.; R., B., Mechanism of Horseradish Peroxidase Catalyzed Epinephrine Oxidation: Obligatory Role of Endogenous O_2^- and H_2O_2, *Biochemistry*, **1998**, *37*, 16922-16933.

(9) Ferrari, R. P.; Laurenti, E.; Ghibaudi, E. M.; Casella, L., Tyrosinase-catecholic Substrates *in Vitro* Model: Kinetic Studies on the *o*-Quinone / *o*-Semiquinone Radical Formation, *J. Inorg. Biochem.*, **1997**, *68*, 61-69.

(10) Chedekel, M. R.; Land, E. J.; Thompson, A.; Truscott, T. G., Early Steps in the Free Radical Polymerisation of 3,4-Dihydroxyphenylalanine (Dopa) into Melanin, *J. Chem. Soc., Chem. Commun.*, **1984**, 1170-1172.

(11) Lambert, C.; Truscott, T. G.; Land, E. J.; Riley, P. A., Role of Azide Concentration in Pulse Radiolysis Studies of Oxidation: 3,4-Dihydroxyphenylalanine, *J. Chem. Soc. Faraday Trans.*, **1991**, *87*, 2939-2942.

(12) Marques, F.; Duarte, R. O.; Moura, J. J. G.; Bicho, M. P., Conversion of Adrenaline to Indolic Derivatives by the Human Erythrocyte Plasma Membrane, *Biol. Signals*, **1996**, *5*, 275-282.

(13) Kalyanaraman, B.; Felix, C. C.; Sealy, R. C., Electron Spin Resonance-spin Stabilization of Semiquinones Produced During Oxidation of Epinephrine and Its Analogues, *J. Biol. Chem.*, **1984**, *259*, 354-358.

(14) Rosei, M. A.; Blarzino, C.; Foppoli, C.; Mosca, L.; Coccia, R., Lipooxygenase-catalyzed Oxidation of Catecholamines, *Biochem. Biophys. Res. Commun.*, **1994**, *200*, 344-350.

(15) Odajima, T.; Onishi, M., Formation of Adrenochrome from Epinephrine by Myeloperoxidase Via a Free Radical: Its Biological Significance, *Jpn. J. Oral Biol.*, **1997**, *39*, 297-303.

(16) Giulivi, C.; Cadenas, E., Oxidation of Adrenaline by Ferrylmyoglobin, *Free Rad. Biol. Med.*, **1998**, *25*, 175-183.

(17) Jewett, S. L.; Eddy, L. J.; Hochstein, P., Is the Autoxidation of Catecholamines Involved in Ischemia-reperfusion Injury?, *Free Rad. Biol. Med.*, **1989**, *6*, 185-188.

(18) Palumbo, A.; Napolitano, A.; Barone, P.; D'Ischia, M., Nitrite- and Peroxide-Dependent Oxidation Pathways of Dopamine: 6-Nitrodopamine and 6-Hydroxydopamine Formation as Potential Contributory Mechanisms of Oxidative Stress- and Nitric Oxide-Induced Neurotoxicity in Neuronal Degeneration, *Chem. Res. Toxicol.*, **1999**, *12*, 1213-1222.

(19) Graham, D. G.; Tiffany, S. M.; Bell, J. W. R.; Gutknecht, W. F., Auto-oxidation *versus* covalent binding of quinones as the Mechanism of Toxicity of Dopamine, 6-Hydroxy Dopamine, and Related Compounds Toward C1300 Neuroblastoma Cells *in Vitro*, *Mol. Pharmacol.*, **1978**, *14*, 644-653.

(20) Evans, C.; Scaiano, J. C.; Ingold, K. U., Absolute Kinetics of Hydrogen Abstraction from α-tocopherol by Several Reactive Species Including an Alkyl Radical, *J. Am. Chem. Soc.*, **1992**, *114*, 4589-4593.

(21) Scaiano, J. C., Exploratory Laser Flash Photolysis Study of Free Radical Reactions and Magnetic Field Effects in Melatonin Chemistry, *J. Pineal Res.*, **1995**, *19*, 189-195.

(22) Encinas, M. V.; Lissi, E. A.; Olea, A. F., Quenching of Benzophenone by Vitamins A and C and by Sulfur Containing Aminoacids and Peptides, *Photochem. Photobiol.*, **1985**, *42*, 347-352.

(23) Jovanovic, S. V.; Kónya, K.; Scaiano, J. C., Redox Reactions of 3,5-Di-*tert*-butyl-1,2-Benzoquinone. Implications for Reversal of Paper Yellowing, *Can. J. Chem.*, **1995**, *73*, 1803-1810.

(24) Griller, D.; Howard, J. A.; Marriott, P. R.; Scaiano, J. C., Absolute Rate Constants for the Reactions of *tert*-Butoxyl, *tert*-Butylperoxyl, and Benzophenone Triplet with Amines: The Importance of a Stereoelectronic Effect, *J. Am. Chem. Soc.*, **1981**, *103*, 619-623.

(25) Wright, J. S.; Johnson, E. R.; DiLabio, G. A., Predicting the Activity of Phenolic Antioxidants: Theoretical Method, Analysis of Substituents Effects, and Applications to Major Families of Antioxidants, *J. Am. Chem. Soc.*, **2001**, *123*, 1173-1183.

(26) Burkey, T. J.; Castelhano, A. L.; Griller, D.; Lossing, F. P., Heats of Formation and Ionization Potentials of Some α-Aminoalkyl Radicals, *J. Am. Chem. Soc.*, **1983**, *105*, 4701-4703.

(27) Griller, D.; Kanabus-Kaminska, J. M. Homolytic Bond Dissociation Energies for Some Simple Organic Molecules; In *Handbook of Organic Photochemistry*; J. C. Scaiano, Ed.; CRC Press: Boca Raton, Florida, 1989; Vol. II; 359-362.

(28) Scaiano, J. C. Laser Photolysis in Polymer Chemistry; In *Degradation and Stabilization of Polymers*; H. H. G. Jellinek and H. Kachi, Eds.; Elsevier: Amsterdam, 1989; Vol. 2; 1-39.

(29) Turro, N. J., *Modern Molecular Photochemistry*; University Science Books: Sausalito, 1991.

(30) Das, P. K.; Encinas, M. V.; Scaiano, J. C., Laser Flash Photolysis Study of the Reactions of Carbonyl Triplets with Phenols and Photochemistry of *p*-Hydroxypropiophenone, *J. Am. Chem. Soc.*, **1981**, *103*, 4154-4162.

(31) Bhattacharyya, K.; Das, P. K., Nanosecond Transient Processes in the Triethylamine Quenching of Benzophenone Triplets in Aqueous Alkaline Media. Substituent Effect, Ketyl Radical Deprotonation, and Secondary Photoreduction Kinetics, *J. Phys. Chem.*, **1986**, *90*, 3987-3993.

(32) Muldoon, M. J.; McLean, A. J.; Gordon, C. M.; Dunkin, I. R., Hydrogen Abstraction from Ionic Liquids by Benzophenone Triplet Excited States, *Chem. Commun.*, **2001**, 2364-2365.

(33) Encinas, M. V.; Scaiano, J. C., Reaction of Benzophenone Triplets with Allylic Hydrogens. A Laser Flash Photolysis Study, *J. Am. Chem. Soc.*, **1981**, *103*, 6393-6397.

(34) Johnston, L. J.; Lougnot, D. J.; Wintgens, V.; Scaiano, J. C., Photochemistry of Diphenylketyl Radicals: Spectroscopy, Kinetics, and Mechanisms, *J. Am. Chem. Soc.*, **1988**, *110*, 518-524.

(35) Das, P. K.; Encinas, M. V.; Steenken, S.; Scaiano, J. C., Reaction of *tert*-Butoxy Radicals with Phenols. Comparison with the Reactions of Carbonyl Triplets, *J. Am. Chem. Soc.*, **1981**, *103*, 4162-4166.

(36) Pratt, D. A.; DiLabio, G. A.; Brigati, G.; Pedulli, G. F.; Valgimigli, L., 5-Pyrimidinols: Novel Chain-breaking Antioxidants More Effective than Phenols, *J. Am. Chem. Soc.*, **2001**, *123*, 4625-4626.

(37) Snelgrove, D. W.; Lusztyk, J.; Banks, J. T.; Mulder, P.; Ingold, K. U., Kinetic Solvent Effects on Hydrogen-atom Abstractions: Reliable, Quantitative Predictions Via a Single Empirical Equation, *J. Am. Chem. Soc.*, **2001**, *123*, 469-477.

(38) Bowry, V. W.; Ingold, K. U., The Unexpected Role of Vitamin E (α-Tocopherol) in the Peroxidation of Human Low-density Lipoprotein, *Acc. Chem. Res.*, **1999**, *32*, 27-34.

(39) de Heer, M. I.; Korth, H. G.; Mulder, P., Poly Methoxy Phenols in Solution: O-H Bond Dissociation Enthalpies, Structures, and Hydrogen Bonding, *J. Org. Chem.*, **1999**, *64*, 6969-6975.

(40) Barclay, L. R. C.; Edwards, C. E.; Vinqvist, M. R., Media Effects on Antioxidant Activities of Phenols and Catechols, *J. Am. Chem. Soc.*, **1999**, *121*, 6226-6231.

(41) Small, R. D., Jr.; Scaiano, J. C., Differentiation of Excited State and Biradical Processes. Photochemistry of Phenyl Alkyl Ketones in the Presence of Oxygen, *J. Am. Chem. Soc.*, **1978**, *100*, 4512.

(42) Valgimigli, L.; Banks, J. T.; Lusztyk, J.; Ingold, K. U., Solvent Effects on the Antioxidant Activity of Vitamin E, *J. Org. Chem.*, **1999**, *64*, 3381-3383.

(43) Valgimigli, L.; Banks, J. T.; Ingold, K. U.; Lusztyk, J., Kinetic Solvent Effects on Hydroxylic Hydrogen Atom Abstractions Are Independent of the Nature of the Abstracting Radical. Two Extreme Tests Using Vitamin E and Phenol, *J. Am. Chem. Soc.*, **1995**, *117*, 9966-9971.

7. Photophysical Properties of DNA-dyes

7.1 Introduction

Different analytical techniques have been developed to assess DNA-damage.[1-9] They rely on the formation of cleavage events in the damaged inter-nucleosomal DNA; by the action of endonucleases,[10] or following treatment with mild alkali. These treatments result in the partial unwinding of double stranded-DNA (dsDNA) to give small fragments of single stranded-DNA (ssDNA).[11] The experimental magnitude being measured is either the unwinding speed, or a parameter related to the amount of ssDNA; in the latter case it is worth mentioning the widely used Comet Assay Analysis as an example.

The alkaline comet assay is an analytical method for detection of DNA-damage.[1,11-17] This approach is based on the size-selective migration of DNA structures in an electric field. This results in the formation of a nuclear DNA migration pattern with the morphology of a 'comet'. Small fragments or relaxed loops of DNA migrate into the tail of the comet, while undamaged DNA remains in the comet head. Following nucleic acid staining, the length and the proportion of fluorescence observed in the comet tail is used as a surrogate for DNA-damage.[1] The advantage of the comet assay is that it measures DNA-damage in individual cells. Thus, it is also called single cell electrophoresis. However, a major drawback of the assay is operator bias/subjectivity, which may affect both data acquisition and analysis.

The topics presented in this and the following chapter result from a discussion with researchers at Health Canada, as to establish a simple yet sensitive method to determine DNA-damage. As a result of our discussions we directed our efforts towards an objective analytical method, based on photophysical parameters intrinsic to a dye and its environment, such as quantum yield, spectral shifts or lifetimes. In that sense in the present chapter nine different DNA-dyes were assessed for their photophysical parameters, to determine if they could be used to detect single- *vs.* double-stranded DNA ratio; this value being an expression of DNA-damage. The dyes studied are PicoGreen and three other unsymmetric cyanine dyes (YOYO-1 iodide, SYBR Green I, and SYBR Gold); the phenanthridinium dyes (Ethidium

Bromide and Propidium Iodide); and the benzimide or indole derived dyes (Hoechst 33342, Hoechst 33258, and DAPI).

We report absorption and fluorescence spectral shifts, fluorescence quantum yields and lifetimes for each of these dyes, both when free in solution or complexed with ssDNA or dsDNA. The goal is to establish the potential of these dyes to measure ssDNA to dsDNA ratios. While photophysical and complexation information is currently available for some of these dyes in the presence of dsDNA, this information has been obtained under a variety of experimental conditions (*i.e.*, ionic strength, dye:DNA ratio, pH, etc),[18-38] which influence the photophysical behavior of the dye-DNA complexes, making comparisons difficult.[21]

Little information is available on the photophysics for dye-ssDNA complexes. We present our results obtained for ssDNA and dsDNA, in aqueous buffered solutions at pH 7.4 under identical conditions and dye:DNA ratios. We compare the photophysical behavior for each dye in the different binding states, as well as among the dyes at a given binding state, and discuss the observed differences. With this information we determine which photophysical properties and DNA-stain dyes are most suitable for DNA-damage screening.

We also present results obtained at different pH with the bisbenzimide dyes, that explain their mechanism of nonradiative deactivation from the singlet excited state. This study provides valuable spectroscopic information on these useful biological stains under a consistent set of experimental conditions, and more insight into the mechanism of deactivation for the excited singlet state of these dyes.

Some of the measurements presented here were obtained by K.-S. Focsaneanu while working as part of the Undergraduate Research Scholarship Program at the University of Ottawa. Her help is greatly appreciated.

7.2 Results

7.2.1 Steady-state Absorption and Fluorescence Spectra

The structure of the dyes under study is shown in Figure 7-1. Figure 7-2 shows the normalized absorption and corrected fluorescence spectra. The absorption maxima of dye-dsDNA complexes are in agreement with those previously reported.[38]

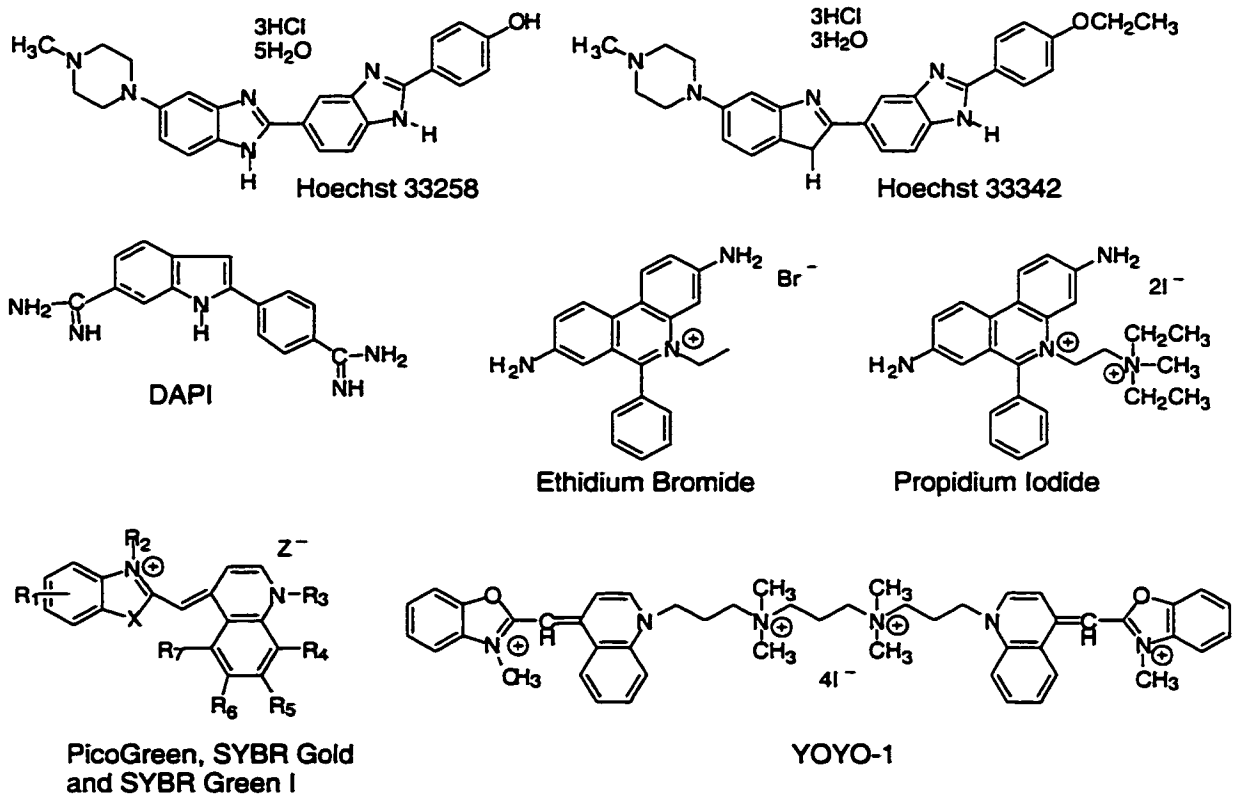

Figure 7-1: Structure of the dyes under study. In the case of PicoGreen and SYBR Gold, X is either S or O. Many different substituents can be found on the conjugated rings (R^i). The counterion Z^- is chloride, iodide, perchlorate, and or various sulfonates.[20,30]

There is a marked red shift in the absorption maxima upon complexation to DNA, independently of whether the DNA is unwound or not (see Table 7-1). This shift is due to a decrease in polarity in the dye's environment when going from free dye to dye complexed to

DNA. The shift is the largest for the phenanthridinium dyes (40 nm on average); it is in the 12 to 14 nm range for the benzimide/indole dyes; and with the exception of YOYO-1 (*vide infra*), the other three cyanine dyes present the smallest shift upon binding to DNA. In all the dyes except YOYO-1, the shape of the absorption band does not change upon complexation to either ssDNA or dsDNA. In the case of YOYO-1, the observed change has been attributed to formation of an intramolecular dimer between the two "YO" components when the dye is free in solution; upon intercalation this dimer disappears.[19,22] Following binding to DNA, the YOYO–1 absorption band resembles that of the other cyanine dyes. A close examination of the absorption bands for dye-ssDNA and dye-dsDNA complexes shows that they match exactly, with the exception of YOYO-1, PicoGreen and SYBR Green I. In these three dyes, this band is broader for dye-ssDNA than for dye-dsDNA complexes, and even broader for the free dye (see Figure 7-2-F, 7-2-H and 7-2-I). A similar effect is also observable in their emission spectra.

The fluorescence measurements for the dyes in aqueous buffer solution showed very weak emission; in particular, peak assignments for the cyanine dyes are difficult due to the poor signal-to-noise obtained (see Figure 7-2). Within the error, all the fluorescence spectra for the free dyes match the shape of the spectra of the DNA bound dyes, with exception of YOYO-1. In the latter case this might be due to the excitation of the intramolecular dimer rather than the monomer (*vide supra*).

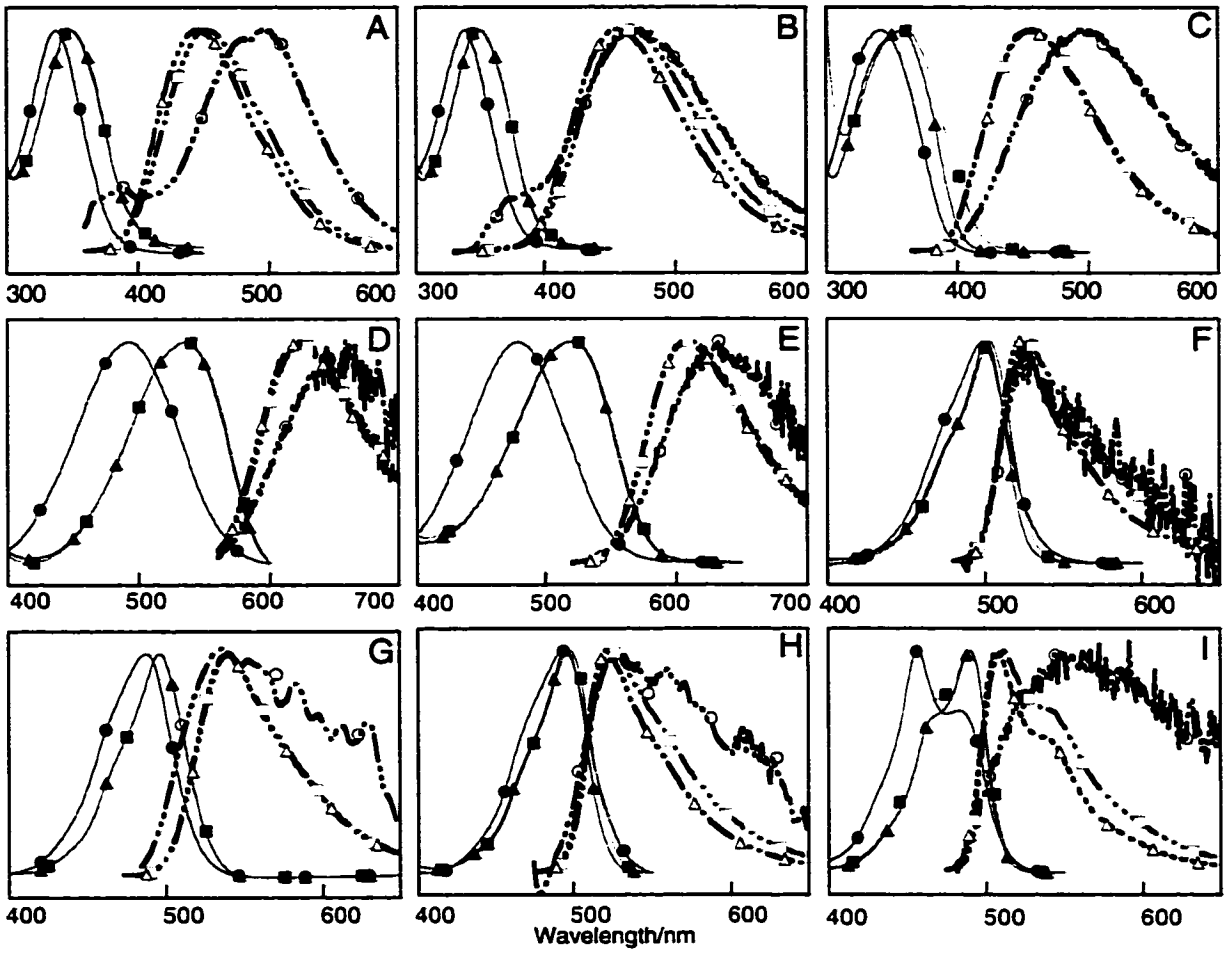

Figure 7-2: Normalized absorption spectra for dyes in (●) 0.01 M Tris buffer, (■) with ssDNA and (▲) with dsDNA. Normalized corrected fluorescence spectra for dyes in (○) 0.01 M Tris buffer, (□) with ssDNA and (△) with dsDNA. (A) Hoechst 33258, (B) Hoechst 33342, (C) DAPI, (D) PIH, (E) EtBr, (F) PicoGreen, (G) SYBR Gold (the fluorescence of the free dye has been smoothed), (H) SYBR Green I (the fluorescence of the free dye has been smoothed), (I) YOYO-1. The concentrations employed are those stated in Table 7-1. A few points are shown to assist in the visualization.

The fluorescence maxima present a blue shift in going from free dye to dye-DNA complexes. These shifts are similar or even more pronounced for dye bound to dsDNA than for ssDNA (see Table 7-1). The cyanine dyes show the smallest shift upon complexation to DNA.

Table 7-1: Steady-state absorption and fluorescence maximum determined for the dyes under study when free in solution or complexed to ssDNA or dsDNA.

Dye	[Dye]/μM	[DNA]/μM	Free dye	Dye-ssDNA	Dye-dsDNA
			Abs. – Em./nm	Abs. – Em./nm	Abs. – Em./nm
[a] H33258	2	20	337 - 508	349 - 466	349 - 458
[a] H33342	2	20	336 - 471	350 - 466	350 - 456
[a] DAPI	2	20	341 - 496	358 - 456	356 - 455
PIH	10	100	493 - 652	536 - 624	536 - 624
EtBr	5	50	479 - 632	520 - 610	520 - 608
PicoGreen	1.0	10	498 - 528	503 - 525	501 - 522
SYBR Gold	3.0	30	487 - 546	496 - 540	496 - 540
SYBR Green I	2.8	30	494 - 530	498 - 525	496 - 522
YOYO-1	1.0	10	457 - 549	490 - 510	490 - 507

[a] The measurements for the free dye were taken with a concentration 10 fold higher than that employed in solutions with DNA (*i.e.*, [Dye] is 20 μM). The spectral resolution is ≥ 1 nm.

7.2.2 Fluorescence Quantum Yields and Lifetime Measurements

Table 7-2 shows the fluorescence quantum yields (Φ_F) for the dyes when free or complexed to double stranded and single stranded DNA. From these data we note that the increase in fluorescence quantum yield upon dsDNA complexation is ~400-1000 fold for the cyanine dyes. The fluorescence enhancement for the benzimide/indole and phenanthridinium dyes does not exceed 30-fold. Table 7-2 also shows the fluorescence quantum yield ratio between dye-ssDNA and dye-dsDNA. This value ranges between 0.5 and 0.65 for all the benzimide/indole dyes and cyanine dyes with the exception of SYBR Gold, for which the value is larger than 0.8. Ethidium bromide and PIH show the largest ratio, *i.e.*, close to 1.

Table 7-2: Quantum yields of fluorescence determined for the dyes under study when free in solution or complexed to ssDNA or dsDNA. Also shown are the dye-ssDNA and dye-dsDNA fluorescence ratios, as well as the free dye to dye-dsDNA ratios.

Dye	Fluorescence quantum yield (Φ_F)			ssDNA:dsDNA	Free dye:dsDNA
	Free dye	Dye-dsDNA	Dye-ssDNA		
[a] H33258	0.015	0.42	0.20	0.48	~ 1:30
[a] H33342	0.034	0.38	0.22	0.57	~ 1:10
[a] DAPI	0.019	0.34	0.19	0.55	~ 1:20
[b] PIH	0.008	0.13	0.12	0.93	~ 1:20
[b] EtBr	0.039	0.35	0.35	1.00	~ 1:10
[c] PicoGreen	0.0006	0.64	0.30	0.47	< 1:1000
[c] SYBR Gold	0.0006	0.66	0.55	0.84	< 1:1000
[c] SYBR Green I	0.0004	0.69	0.39	0.57	< 1:1500
[c] YOYO-1	0.001	0.38	0.25	0.66	~ 1:400

The concentrations employed are the same as those stated in Table 7-1. The standards used for fluorescence quantum yields were *a*) quinine bisulfate,[39] *b*) rhodamine 101,[40,41] and *c*) fluorescein.[42]

The decay profiles for the different dyes, when bound to ssDNA and dsDNA are shown in Figure 7-3. This figure also shows the decay profiles for the free dyes in the buffer solutions, with the exception of the cyanine dyes, for which the lifetimes were within the instrument response time, *i.e.*; 80 ps or shorter. Table 7-3 presents the decay rate constants and their weight obtained from the best fittings to the decay traces. When a monoexponential fit did not adjust well, biexponential fittings were used. The results show that ethidium bromide and PIH have monoexponential decays when complexed to dsDNA or ssDNA or when free in aqueous buffer solution.

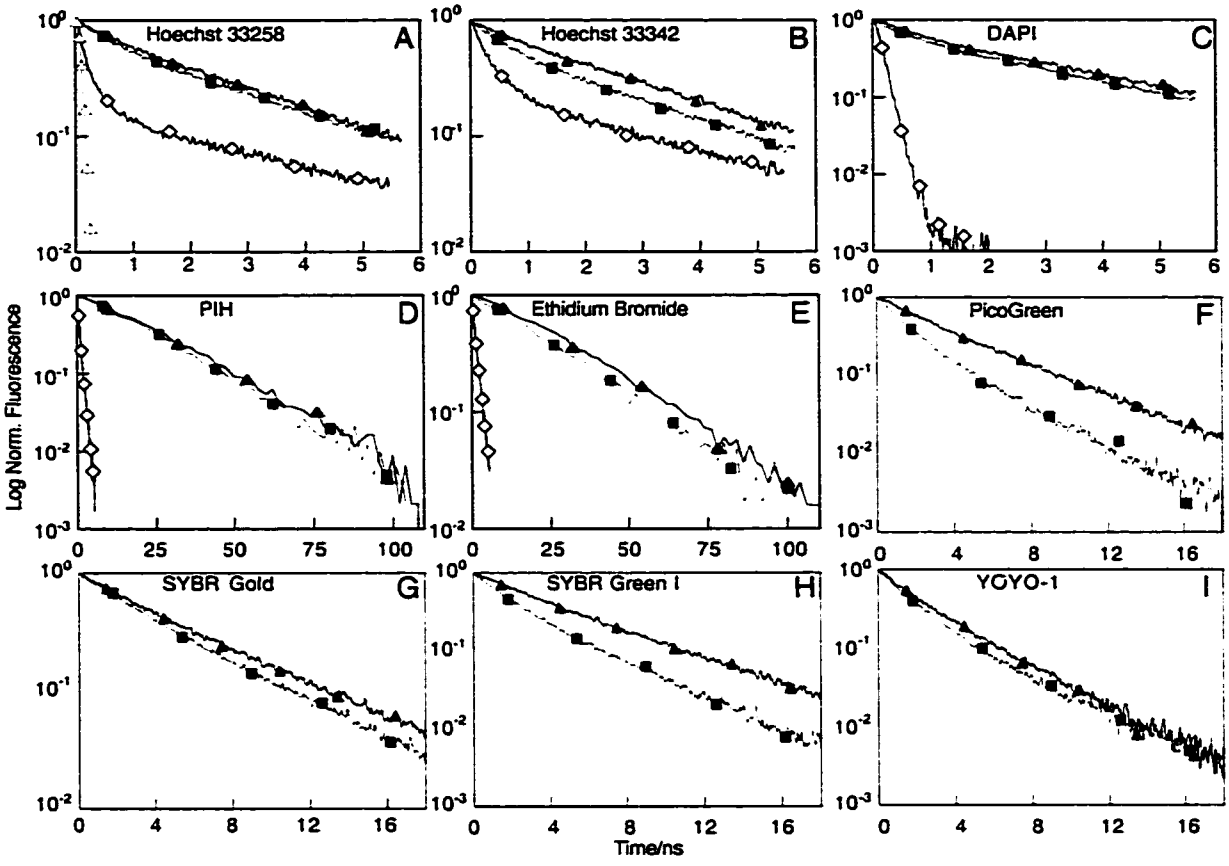

Figure 7-3: Normalized fluorescence decay profiles for the dyes in 0.01 M Tris buffer (a few points are shown to assist in the visualization), (■) with ssDNA and (▲) with dsDNA. (A) Hoechst 33258, (B) Hoechst 33342, (C) DAPI, (D) PIH, (E) EtBr, (F) PicoGreen,[43] (G) SYBR Gold, (H) SYBR Green I, (I) YOYO-1. In Figure 7-3-A the picosecond laser profile is observed (△). Figures 7-3-A, -B, -C, -D and -E also show the decay traces for the free dye in Tris buffer (◇).

The cyanine dyes can be adequately fit by monoexponential decays when complexed to dsDNA (with the exception of YOYO-1), but when bound to ssDNA, their decay is best treated as a biexponential. For the benzimide/indole dyes, an analysis of the lifetimes of the bisbenzimidazole dyes measured at different pH values (see Table 7-4 and Figure 7-4-A and 7-4-B), and a comparison to those values obtained with DNA, shows that in all cases the decays are biexponential.

Table 7-3: Decay rate constants and average lifetimes determined for the dyes under study at buffer pH 7.4 and when complexed to ss or dsDNA.

Dye	[a][Dye]/μM	[a][DNA]/μM	k_1/ns^{-1}	A_1	k_2/ns^{-1}	A_2	τ_{dec}/ns	[b] τ_{rad}/ns
H33258	20	ds 200	0.265	0.42	0.711	0.57	1.94	4.62
	20	ss 200	0.342	0.64	1.544	0.39	1.22	6.10
	135	none	0.30	0.18	5.63	0.89	0.20	13.33
H33342	40	ds 400	0.305	0.63	0.764	0.34	2.21	5.82
	40	ss 400	0.366	0.60	1.843	0.40	1.05	4.77
	500	none	0.325	0.27	3.724	0.75	0.35	18.4
DAPI	25	ds 250	0.278	0.63	0.716	0.39	2.20	6.39
	25	ss 250	0.287	0.53	0.775	0.49	1.88	9.95
	200	none	6.33	1.1	-	-	0.16	8.42
PIH	160	ds 1000	0.044	1.06	-	-	21.4	177
	160	ss 1000	0.048	1.05	-	-	19.8	175
	500	none	1.17	1.0	-	-	0.855	106
EtBr	30	ds 300	0.033	1.07	-	-	28.3	79.9
	30	ss 300	0.039	1.02	-	-	25.1	70.7
	660	none	0.655	0.98	-	-	1.56	40.0
PicoGreen	11	ds 70	0.235	0.97	-	-	4.26	6.85
	11	ss 70	0.862	0.51	0.325	0.49	1.67	5.58
SYBR Gold	30	ds 300	0.183	0.97	-	-	5.64	8.58
	30	ss 300	0.277	0.77	0.115	0.227	4.16	7.53
SYBR Green I	30	ds 300	0.215	0.97	-	-	4.78	6.94
	30	ss 300	0.649	0.50	0.244	0.48	2.26	5.78
YOYO-1	10	ds 100	0.293	0.55	0.620	0.44	2.30	6.06
	10	ss 100	0.770	0.64	0.284	0.39	1.67	6.57

[a] Concentrations used for the experiments. [b] Radiative lifetime values calculated according to Equation 7-1.

In the case of Hoechst 33342, one component, the longer lived one, is constant in all cases, and the only change is its relative weight. Further, the results are similar to those of Hoechst 33258, with the exception of the measurements taken on buffers at pH 7.4 and 12. In the case of DAPI, the indole derived dye, its decay is biexponential in all the conditions studied (see Figure 7-4-C). The weight of the slower component however is negligible either at pH 7.4 or 4 and it could be due to background noise. At pH 1 both components are relevant. The decay measured at pH 12 presents different values and weights for the rate constants in comparison to the results obtained at other pH values.

Table 7-3 also shows the lifetimes (τ_{dec}) for the different dyes, calculated from the average of the two rate constants weighted by their pre-exponential factor in the case of biexponential decays. When bound to ssDNA or dsDNA all the dyes show lifetimes in the range of 1 to 5 ns, with the exception of ethidium bromide and PIH whose lifetimes are in the range of 20 to 30 ns.

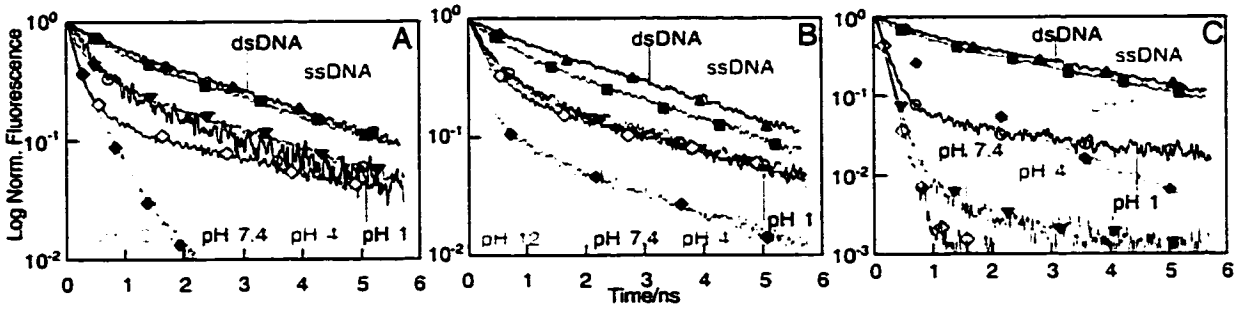

Figure 7-4: Normalized fluorescence decay profiles for saturated solutions of the free dyes at different pH values (a few points are shown to assist in the visualization). (A) Hoechst 33258, (B) Hoechst 33342, (C) DAPI. Also shown for comparison are the decay traces for the dyes complexed (■) with ssDNA and (▲) with dsDNA.

To test the accuracy of our fluorescence quantum yield and lifetime measurements we calculated, based on Equation 7-1, the radiative lifetimes (τ_{rad}), see Table 7-3, for dye-ssDNA and dye-dsDNA complexes, as well as for free dye in solution.

Equation 7-1: $$\tau_{rad} = \frac{\tau_{dec}}{\Phi_F}$$

The similarity of the values obtained for both dye-ssDNA and dye-dsDNA complexes gives us confidence in our measurements, since the radiative lifetimes would not be expected to change much for complexation in different forms of DNA. Some discrepancy is observed in the radiative lifetime calculated for the free Hoechst dyes. This is probably due to saturation effects in the streak camera, which results in an underestimated weight for the faster component, and therefore and overestimated average lifetime (τ_{dec}).

Table 7-4: Decay rate constants and average lifetimes determined at different pH values for saturated solutions of the benzimide/indole dyes.

Media	Dye	k_1/ns^{-1}	A_1	k_2/ns^{-1}	A_2	τ_{dec}/ns
Buffer pH 1.0	H33258	0.34	0.28	2.28	0.77	0.54
	H33348	0.36	0.32	3.04	0.73	0.43
	DAPI	0.21	0.06	5.12	1.02	0.19
Buffer pH 4.0	H33258	0.38	0.39	3.77	0.65	0.38
	H33348	0.37	0.33	3.55	0.71	0.38
	DAPI	5.78	-	-	-	0.17
Buffer pH 7.4	H33258	0.30	0.18	5.63	0.89	0.20
	H33348	0.32	0.27	3.72	0.75	0.35
	DAPI	6.33	-	-	-	0.16
Buffer pH 12.0	H33258	1.49	0.27	5.14	0.82	0.22
	H33348	0.46	0.13	6.78	0.96	0.15
	DAPI	0.85	0.34	3.19	0.72	0.39

7.2.3 Time-resolved Fluorescence Spectra

Time-resolved fluorescence spectra were obtained for all dye-DNA complexes except for the phenanthridinium ones (see Figure 7-5). In all cases the spectra maximum are red-shifted relative to those obtained under steady-state conditions (compare Table 7-1 to Table 7-5). This is due to self-absorption present under the experimental conditions used in time-resolved experiments, where ground state absorptions around 0.5 are necessary at the laser excitation wavelength. The red shifts are more clearly observed with the cyanine dyes, which have a small Stokes shift (see Figure 7-2 and Table 7-1).

Two time windows are shown for each dye; they are averages taken from 0 to 1.2 ns and from 1.8 ns to 18 ns. There is a clear difference between the benzimide/indole dyes and the cyanine dyes. The emission from the former shifts to the red with time. This effect is more prominent for Hoechst 33258 (see Figure 7-5-A and 7-5-B) and is less evident in DAPI (Figure 7-5-E and 7-5-F). Also, the red shift is more pronounced in dye-ssDNA complexes (*i.e.*, 5 to 10 nm depending on the dye) as compared to dye-dsDNA complexes (lower than 3 nm) for all these dyes (see Table 7-5).

Cyanine dyes, on the contrary, did not show any change in fluorescence spectra with time when complexed either with ssDNA or dsDNA. The only exception is SYBR Gold, whose emission spectrum is slightly red shifted over time, both in ssDNA and dsDNA complexes. An analysis of the dye-ssDNA and dye-dsDNA spectra for the cyanine dyes reveals the same band-broadening already observed in steady-state emission experiments in going from dye-dsDNA to dye-ssDNA complexes.

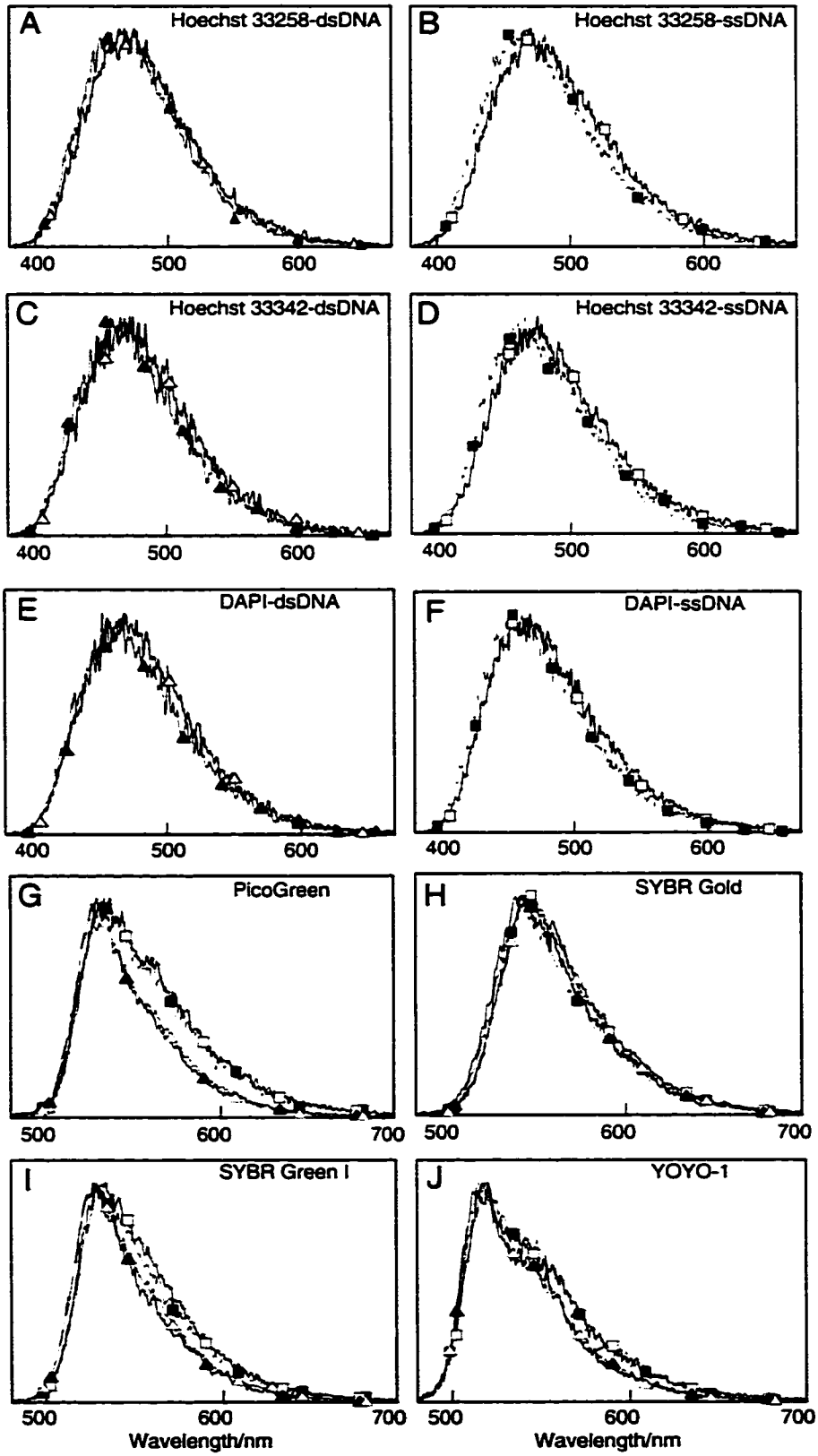
A
Hoechst 33258-dsDNA
B
Hoechst 33258-ssDNA
C
Hoechst 33342-dsDNA
D
Hoechst 33342-ssDNA
E
DAPI-dsDNA
F
DAPI-ssDNA
G
PicoGreen
H
SYBR Gold
I
SYBR Green I
J
YOYO-1
400
500
600
700
Wavelength/nm

Figure 7-5: Normalized time-gated fluorescence spectra for: (A) Hoechst 33258-dsDNA, (B) Hoechst 33258-ssDNA, (C) Hoechst 33342-dsDNA, (D) Hoechst 33342-ssDNA, (E) DAPI-dsDNA, (F) DAPI-ssDNA. (▲) Corresponds to 0-1.2 ns time windows; (△) corresponds to 1.8-18 ns respectively. (G) PicoGreen, (H) SYBR Gold, (I) SYBR Green I, (J) YOYO-1. A few points are shown to assist in the visualization. (▲) dye-dsDNA, 0-1.2 ns, (△) dye-dsDNA, 1.8-18 ns, (■) dye-ssDNA, 0-1.2 ns, (□) dye-ssDNA, 1.8-18 ns. The solution conentrations are those stated in Table 7-3.

Table 7-5: Time evolution of fluorescence maximum, determined for the dyes under study when complexed to ssDNA or dsDNA. Peaks are red-shifted in comparison to those of Table 7-1 due to self-absorption present under the high absorbance (*i.e.*, ~ 0.5 at the excitation wavelength) employed for the acquisition. The dye concentrations are those specified in Table 7-3.

Dye	Time window/ns	Dye-ssDNA Em./nm	Dye-dsDNA Em./nm
H33258	0-1.2	467	466
	1.8-18.0	473	470
H33342	0-1.2	464	467
	1.8-18.0	475	470
DAPI	0-1.2	460	466
	1.8-18.0	465	466
PicoGreen	0-1.2	535	529
	1.8-18.0	535	529
SYBR Gold	0-1.2	542	541
	1.8-18.0	546	545
SYBR Green I	0-1.2	531	528
	1.8-18.0	531	528
YOYO-I	0-1.2	518	516
	1.8-18.0	518	516

7.2.4 Circular Dichroism

We have measured the circular dichroism (CD) signals for PicoGreen in the presence of dsDNA and ssDNA, as well as in aqueous buffer solution. Previous studies reported with Ethidium Bromide,[44] DAPI,[45] and cyanine dyes[22,34,46] have proven useful in determining the binding mode for these dyes both at low and high dye:DNA ratios. However no such measurements have been reported with PicoGreen.

PicoGreen in aqueous buffer does not show a CD signal; in contrast, when complexed with DNA, induced circular dichroism (ICD) is evident. In Figure 7-6 we show the results of ICD measurements performed on PicoGreen, at low dye:DNA ratio (*i.e.*, 1:10) and high dye:DNA ratio (1:1) both for dye-dsDNA (Figure 7-6-A) and dye-ssDNA complexes (Figure 7-6-B). The CD spectrum for dye:dsDNA 1:10 shows a negative band which coincides with the absorption of PicoGreen. The same sign and shape are obtained for the CD of dye:ssDNA in a 1:10 ratio, though the intensity is about 2/3 that of dye:dsDNA.

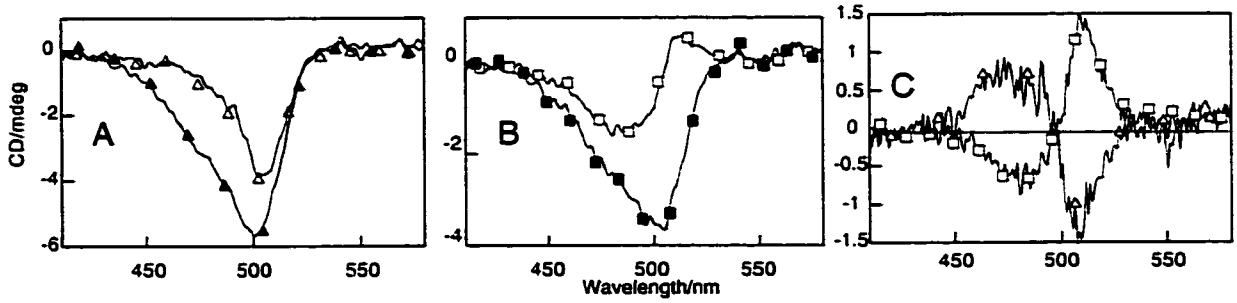

Figure 7-6: Circular Dichroism spectra performed on PicoGreen-DNA complexes (a few points are shown to assist in the visualization). (A) PicoGreen-dsDNA complexes; (▲) 0.020 mM PicoGreen, 0.200 mM dsDNA (1:10), (◊) 0.020 mM PicoGreen, 0.020 mM dsDNA (1:1), (B) PicoGreen-ssDNA complexes; (◊) 0.020 mM PicoGreen, 0.200 mM ssDNA (1:10), (◊) 0.020 mM PicoGreen, 0.020 mM ssDNA (1:1). In (C) the CD exciton spectra obtained according to Equation 7-2 are shown for (◊) dye-dsDNA (1:1), and (◊) dye-ssDNA (1:1) complexes.

Results obtained under high dye:DNA ratios (*i.e.*, 1:1) showed a much different spectrum both for dye-dsDNA and dye-ssDNA. In the former, the negative peak is slightly red shifted and the band is much narrower than that at low dye:DNA ratios (see Figure 7-6-A). For ssDNA the resulting CD spectrum at high dye:DNA ratio showed a -/+ pattern with increasing wavelengths, changing sign at 506 nm. Suspecting that this spectrum is due both to monomer and exciton (*i.e.*, dimers of PicoGreen in a chiral environment) signals, we subtracted from the spectra obtained at high dye:DNA ratios (1:1) that obtained at low ratios (1:10) for dye-ssDNA complexes, according to Equation 7-2.[45,47] We also performed this equation with the signals of dye-dsDNA complexes.

Equation 7-2: $$\theta_{dimer} = \theta_{obs} - \frac{\theta_{monomer}}{\kappa}$$

where κ is a constant, dependent on the monomer contribution ($\theta_{monomer}$) to the observed CD signal (θ_{obs}). In this way, we removed the monomer contribution from the total CD signal, which is a result of both monomer and dimer PicoGreen (θ_{dimer}) molecules in a chiral environment. In order to obtain the characteristic conservative spectrum of an exciton (*i.e.*, a spectrum where the integrated rotational strength will be zero),[47] κ takes a value of 2.0 in the case of the dye-dsDNA complexes, and 3.2 for the dye-ssDNA ones (see also table 7-6). The resulting conservative spectra are shown in Figure 7-6-C. Whereas the dye-ssDNA complex shows a -/+ pattern with increasing wavelengths, that of dye-dsDNA has the opposite shape, *i.e.*, +/-. They cross the zero line, and each other, at 497 nm, the absorptium maximum of PicoGreen.

7.2.5 High Dye Loading, Time-resolved and Steady-state Studies.

We tested the effects stoichiometric combinations of dye to DNA base pairs (*i.e.*, ~1:1 dye:DNA base pair) would exert on the lifetimes measured. To that effect we analyzed both Hoechst 33258 and PicoGreen in a 1:2 and 1:1 dye:DNA ratio, respectively. Under high dye loading, multiple binding is known to occur both with cyanine dyes,[22] and also with

Hoechst 33258.[28,31] Figure 7-7-A shows the decay traces for Hoechst 33258 when complexed to dsDNA and ssDNA in a 1:2 ratio, and also for a 1:10 ratio. Whereas in the latter case the decays are biexponential (see Table 7-3), those observed with the 1:2 dye:DNA complexes can only be adjusted with triexponential curves. The decays are also considerably faster compared to those observed at low dye:DNA ratio (1:10). The slowest component in both cases (*i.e.*, ssDNA and dsDNA) is the same, within experimental error, and equal to that observed with the free dye and the dye when complexed in a 1:10 ratio with DNA, either in its double or single stranded form. The weight of this component on the other hand, is small, *i.e.*, less than 15%. The two main rate components are *ca.* 1 ns^{-1} and 5 ns^{-1} both for complexes with dsDNA and ssDNA.

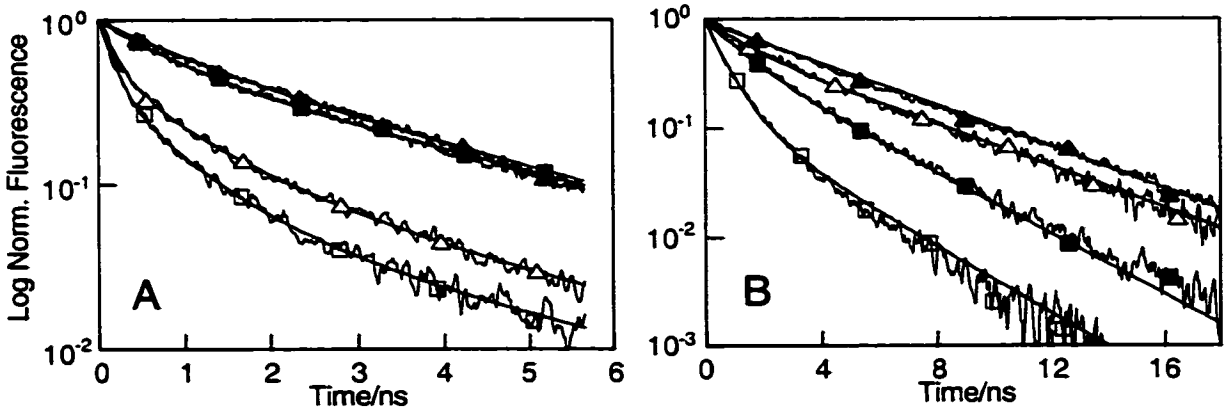

Figure 7-7: High dye loadings. (A) Normalized decay for Hoechst 33258-ssDNA and -dsDNA complexes at different dye:DNA ratios. (▲) 0.02 mM Hoechst 33258, 0.20 mM dsDNA (1:10), (△) 0.02 mM Hoechst 33258, 0.040 mM dsDNA (1:2), (■) 0.02 mM Hoechst 33258, 0.20 mM ssDNA (1:10), (□) 0.02 mM Hoechst 33258, 0.040 mM ssDNA (1:2). (B) Normalized decay for PicoGreen-ssDNA and -dsDNA complexes at different dye:DNA ratios. (▲) 0.010 mM PicoGreen, 0.10 mM dsDNA (1:10), (△) 0.010 mM PicoGreen, 0.010 mM dsDNA (1:1), (■) 0.010 mM PicoGreen, 0.10 mM ssDNA (1:10), (□) 0.010 mM PicoGreen, 0.010 mM ssDNA (1:1). A few points are shown to assist in the visualization.

Figure 7-7-B presents the results obtained with PicoGreen-DNA complexes in a 1:1 and 1:10 dye:DNA ratio. The decay for a given complex is faster in the 1:1 ratio than for a

1:10 ratio, both for dye-ssDNA or dye-dsDNA complexes. One more decay constant to that obtained under 1:10 dye:DNA ratio has to be added to fit the curves obtained in 1:1 ratios. Thus dye-dsDNA complexes present biexponential decay in the latter situation, and the decay of dye-ssDNA is triexponential (see Table 7-6). The additional decay pathway can be considered as resulting from energy transfer processes among closely located dye molecules in the DNA framework. It has been postulated that "unspecifically" located dye molecules act as energy acceptors of excited dyes intercalated in DNA.[28,31] Considering that not all of the intercalated dye molecules would be quenched, and that the non-quenched dye will still exhibit its intrinsic monoexponential or biexponential decay in the case of PicoGreen-dsDNA and -ssDNA complexes, respectively, we fitted the decay for PicoGreen-DNA complexes according to Equations 7-3 and 7-4 for dye-dsDNA and -ssDNA complexes, respectively.

Equation 7-3
$$I = a \times e^{-k \times t} + (1 - a) \times e^{-0.22 \times t}$$

Equation 7-4
$$I = a \times e^{-k \times t} + \left[\frac{(1 - a)}{2} \times \left(e^{-0.86 \times t} + e^{-0.32 \times t} \right) \right]$$

where a represents the weight of the fluorescence component arising from DNA-intercalated dye molecules subject to the intermolecular quenching process, and k is the value for the energy transfer rate constant. The results of the fitting are shown on Figure 7-7, and Table 7-6 presents the values of a and k obtained for PicoGreen-DNA complexes.

Table 7-6: Fraction of dye remaining as monomers in the CD spectra (1/κ); fraction of dye decaying without energy transfer interactions (1-*a*); and decay rate constants for the quenching by energy transfer processes in PicoGreen-DNA complexes (*k*).

dye	$1/\kappa$	$1-a$	k/ns^{-1}
PicoGreen-dsDNA	0.50	0.63	0.81
PicoGreen-ssDNA	0.31	0.27	1.60

All measurements determined at high dye:DNA ratios. Results based on Equations 7-2, 7-3, and 7-4.

7.3 Discussion

7.3.1 Absorption and Fluorescence Spectra.

The nine DNA-dyes examined display a variety of fluorescence deactivation modes, as previously reported.[23,26,33,35,48-51] Upon non-covalent binding of these dyes to DNA, the radiationless deactivation modes can be frequently attenuated, resulting in fluorescence enhancement. Absorbance or fluorescence shifts and changes in fluorescence lifetimes can also be detected upon complexation of the dyes to DNA. It is the magnitude of these changes (particularly the increase in the fluorescence quantum yield) that enables their use as DNA probes. However, it is unknown whether these properties have sufficient sensitivity to distinguish between ssDNA and dsDNA. The purpose of this work was to determine whether the photophysical properties of any of these dyes would allow this distinction, for possible use in a new analytical method to quantitate DNA-damage.

The results demonstrate that although there is a bathochromic shift in the dye absorption spectra upon complexation to DNA, there is no significant shift between dye-ssDNA and dye-dsDNA complexes. The same is true of fluorescence which is blue shifted regardless of whether the dye is complexed to ssDNA or dsDNA. These solvatochromic shifts in absorption and fluorescence are frequently the result of different degrees of solvation following changes in the dipole moment of the chromophore upon photoexcitation or decay to the ground state. The magnitude of these shifts is dependent not only on the size of the change in dipole moment but also on the surrounding media characteristics, which will vary with the location of the dye in the DNA structure. As an example, fully intercalated dyes are more protected from a polar environment than groove-bound dyes.

YOYO-1 and other unsymmetric cyanine dyes are known to intercalate,[19,22,25] and our CD results show that PicoGreen is also an intercalator (*vide infra*). The small solvatochromic shift caused by DNA intercalation reveals a negligible change in their dipole moments. On the other hand, the phenantridinium dyes, also well known as DNA

intercalators, show substantial changes in their spectroscopic characteristics and therefore in their dipole moments when bound to DNA. The benzimide/indole dyes show a smaller solvathochromic effect than the phenantridinium ones following complexation with DNA. The former family of dyes binds to the groove of DNA and consequently they remain more exposed to water.[31,48] Their change in dipole moment could be as large as that of the phenantridinium dyes, however given the smaller change in the surrounding media upon complexation, the solvatochromic shift is not so pronunced.

Another feature of the cyanine dyes when free in solution is the broadening of their absorption and fluorescence spectra compared to those of the complexed dye. This broadening is also evident in going from dsDNA to ssDNA, and is the only spectral characteristic distinguishing either form of DNA. It is not possible however, to determine their relative amounts based on this parameter. The broadening is due to emission of several equilibrated excited state rotational conformers, rather than to solvent relaxation around excited free dye or dye-ssDNA complexes (where the dye is less protected from water than when complexed to dsDNA). Upon binding to ssDNA, some of these conformations are lost, and the effect is even more pronounced upon binding to dsDNA, thus resulting in narrower spectra. A similar effect has been reported for another series of cyanine dyes upon intramolecular bridging.[33]

7.3.2 Time-resolved Measurements.

An inspection of the fluorescence quantum yield values obtained in the current study for the DNA-dyes when bound to both forms of DNA (see Table 7-2), shows that three of the dyes studied (SYBR Gold and the two phenantridinium dyes) are not suited for differentiating ssDNA from dsDNA based on fluorescence lifetimes. The fluorescence intensity ratios of optically matched solutions of these dye-ssDNA and dye-dsDNA complexes are too similiar, indicating poor discrimination; *i.e.*, based on Equation 7-1, we expect similar τ_{dec} for both types of dye-DNA complexes.

To further check the potential of the dyes as probes for measuring DNA-damage, we determined the fluorescence lifetimes for the nine DNA-dyes (see Table 7-3) when complexed to ssDNA and dsDNA. No discrimination was found for the phenantridinium dyes, as anticipated from the results of Φ_F. The radiationless deactivation mechanism for these dyes is related to protonation of the solvent by the excited dye.[35,50] This deactivation mode is suppressed in the presence of DNA and the result is an extension of the fluorescence lifetime, similar to the long lifetimes found for these dyes in low polarity solvents and micellar solutions. These dyes are not sensitive enough in their photodeactivation mechanism to differentiate between the two forms of DNA, and therefore an analysis based on lifetimes would not be successful. This is particularly surprising considering that ethidium bromide has been previously used to determine DNA-damage based on selective emission from dsDNA. However, these studies were carried out under high dye:DNA base pair ratios, *i.e.*, 2:1.[6] Under these conditions energy transfer among neighboring dye molecules in the DNA backbone results in fluorescence self-quenching, as has been recently demonstrated with ethidium bromide,[35] and Hoechst 33258;[28,31] and as is shown with PicoGreen in the present study (*vide infra*). This quenching is more sensitive for dye-ssDNA than dye-dsDNA (*vide infra*) leading to selective emission from dye-dsDNA complexes.

The benzimidazole/indole dyes form groove binding complexes with DNA. These dyes, like the phenantridinium, are also very sensitive to pH changes, presenting various protonation centers. There are different explanations for the mechanism of fluorescence deactivation of the bisbenzimide dyes. The resemblance of the decay values for Hoechst 33258 and its phenoxyethyl derivative (Hoechst 33342) at pH values below 7 rules out the suggestion that non-radiative deactivation of the excited state dye consists of an intramolecular proton transfer from the phenol to the closest benzimidazole nitrogen. This transfer would result in the keto form of the dye (see Scheme 7-1).[49] A similar keto form could occur at higher pH values, when the phenol is deprotonated in its ground state. This would explain why at pH 12 both dyes (Hoechst 33342 and Hoechst 33258) decay with

different kinetics. At pH 7.4 the faster component of the decay for Hoechst 33258 does resemble that of pH 12, indicating that the phenol is partially dissociated. Kalninsh *et al.* have also shown that one benzimidazole substituted with both the phenol and piperazine units does not present a low fluorescence in neutral aqueous solutions, as occurs with the bisbenzimidazole dyes. It seems therefore that at pH values below 7 the key factor is related to two benzimidazole units, one with the piperazine as a substituent, the other one with the phenol (or its alkylated form).[49]

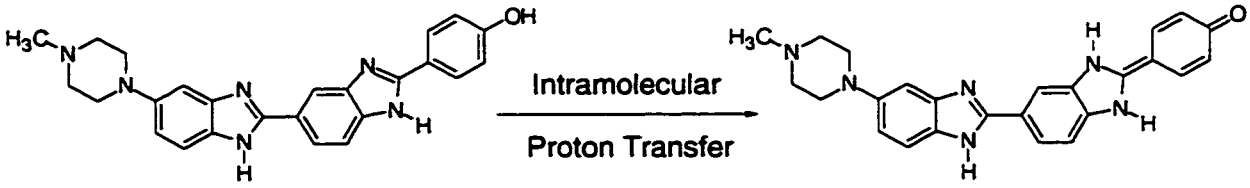

Scheme 7-1: Intramolecular proton transfer in Hoechst 33342, as proposed by Kalninsh *et al.*[49]

At low pH values the piperazine unit is protonated, with both nitrogen atoms being involved in the hydrogen bonding, the one attached to the benzimidazole ring contributing to a lesser extent, since it has a lower pKa. It is reasonable to assume that, upon excitation, there is certain degree of charge transfer from the protonated piperazine-bisbenzimide sub-unit to the phenol-bisbenzimide one, resulting in a stronger, planar bond among the two benzimidazole units. Previous calculations show that this charge transfer does occur, and the interconnecting bond between the two benzimidazole units becomes planar and stronger in the excited state.[49] NMR studies done on Hoechst 33258 show that the dye binds to the minor groove of the DNA, resulting in a planar conformation involving the phenol and the two benzimidazole units.[48]

It seems reasonable therefore to assume that the longer lived component arises from the conformer presenting both benzimidazole units in a planar conformation. This is the predominant conformation in dsDNA due to a tight binding in the DNA groove, and its contribution decreases in ssDNA where the binding allows more flexibility. In aqueous solutions with pH lower than 7, the planar conformer, formed following charge transfer, is

less predominant than in DNA, and most of the dye decays *via* rotation along the benzimide axis. This is the decay pathway accounting for the faster component. At pH 12 the piperazine unit is mostly non-protonated, therefore the charge transfer state is not accessible, and most of the excited dye decays nonradiatively *via* intramolecular rotation. These results are also in agreement with the spectral shifts observed. At low pH values the fluorescence spectra are red-shifted as compared to pH 12 (data not shown), suggesting a higher dipole moment in the former (resulting from the charge transfer state).

The previous results show sensitivity to the binding media for the Hoechst dyes. Thus ssDNA presents a higher contribution from the faster component in comparison to dsDNA. However, for a method to detect DNA-damage based on lifetimes of excited dye-DNA complexes, it is desirable that the complex exhibits simple decay kinetics. This is not the case for the Hoechst dyes.

Our results with DAPI confirm those previously presented regarding its deactivation mechanism.[18,51] Thus, the long component is attributed to the unprotonated form of the dye, whereas the short one is attributed to a protonated form which further decays following H^+ transfer to the solvent. The lifetime obtained at pH 12 is not monoexponential as has been previously described, rather we observe two decay constants. These rate constants do not differ considerably from each other, as can be observed from Figure 7-4 and Table 7-4; and qualitatively, the results agree with those already published.[18,51]

The use of DAPI to determine DNA-damage is impractical for the same reasons given for the Hoechst dyes; requiring cumbersome algorithms to determine the relative amount of both forms of DNA.

From the results obtained with the cyanine dyes, we observe that YOYO-1 presents biexponential decays both, with ssDNA and with dsDNA. This is the only cyanine dye presenting biexponential decays when complexed with dsDNA, the other three analyzed in this work exhibit monoexponential decays. YOYO-1 is a bichromophore presenting two units of the cyanine dye YO connected by an aliphatic chain. Previous studies have shown

that whereas YO has a biexponential decay when complexed to CT DNA, YOYO-1 decay is better fitted with a triexponential curve.[23] The additional decay pathway in dsDNA observed for YOYO-1, is most probably due to the existence of more than one kind of dye-DNA complex, where the first subunit affects the intercalation of the second YO subunit, (*i.e.*, cooperative binding). YOYO-1 presenting biexponential decays in dsDNA, is somewhat inconvenient for DNA-damage assessment based on lifetime analysis. On the contrary PicoGreen is well suited for the analysis of DNA-damage since its decay is monoexponential in the presence of dsDNA and the lifetime for dsDNA is much longer than that for ssDNA.[43] Similar results were obtained for SYBR Green I. Further, lifetimes are slightly longer for the latter, which reduces the demand for very fast time resolution during the data acquisition step.

An analysis of the time-resolved fluorescence spectra reveals that the benzimide/indole dyes show a time-dependent spectral shift. These spectral shifts are due to solvent relaxation around the newly formed dipole. No fluorescence shift is observed with the cyanine dyes when the spectra are monitored over time. This is in agreement with no change in their dipole moment following the absorption of light, as established from steady-state absorption measurements. These results indicate that the broadening observed in steady-state spectra, for dye-ssDNA when compared to dye-dsDNA, is present immediately after excitation, and is not due to solvent relaxation. It is consistent with emission from different rotamers of the cyanine dyes formed immediately (*i.e.*, within the laser pulse) after excitation (*vide supra*). As it has been previously reported, the lifetime of the dye when free in solution is governed by rotation to any of its other conformers. This process requires less than 5 ps, as calculated from the quantum yield of the free dye and the obtained radiative lifetimes (see Equation 7-1).[23,43,52]

We note that while the phenanthridinium dyes and the cyanine dye SYBR Gold possess unfavorable photophysical properties for use in discrimination of ssDNA *vs.* dsDNA, it is these properties which make these DNA-dyes ideal for use in some other

applications, such as the alkaline comet assay. When staining DNA in the comet assay, it is important that both ssDNA and dsDNA demonstrate similar fluorescence quantum yields and decay rates. Indeed, the ratio of dye-ssDNA to dye-dsDNA fluorescence quantum yields are 1.00, 0.93, and 0.84 respectively for ethidium bromide, propidium iodide and SYBR Gold compared to 0.57 for another popular DNA-dye, SYBR Green I. The ratio of ssDNA to dsDNA fluorescence decay lifetime for these dyes are 0.89, 0.93 and 0.74. DNA-dyes which display high quantum yields for dsDNA and faster fluorescence decay of ssDNA (*e.g.* SYBR Green I), result in decreased sensitivity of detection in the tail region of DNA comets. Indeed due to rapid photobleaching in the tail region of comets stained with SYBR Green I, a larger reduction in Tail Moment occurs in SYBR Green I stained comets compared to PIH stained comets under constant illumination.[53] Since SYBR Gold background signal is *ca.* 500-fold smaller than that of the phenanthridinium dyes in the absence of DNA (see Table 7-2), it is the DNA-dye of choice for use with the alkaline comet assay.

7.3.3 Circular Dichroism and Dye:DNA Ratio Studies.

The negative signals we obtained from the ICD measurements with PicoGreen show that the dye is intercalated, and that intercalation occurs with the long axis of the chromophore parallel to the DNA base-pair pocket long axis (see Scheme 7-2).[22,54,55] Further, based on previous results obtained with other dyes of the family, the benzoylthiazole part of the chromophore can be assumed to be sandwiched between to adjacent purines along a strand.[46] The same is true for the dye-ssDNA complex; however, the smaller ICD signal obtained with the latter *i.e.*, 2/3 of that with dye-dsDNA, is related to a looser configuration of the dye in the less restricting ssDNA environment. In fact the ICD signal is described by Equation 7-5:[55]

Equation 7-5 $$R = f \times |\mu|^2 \times \left[1 - 2 \times (\cos^2 \gamma)\right]$$

where R is proportional to the magnitude of the CD signal (see also Scheme 7-2).

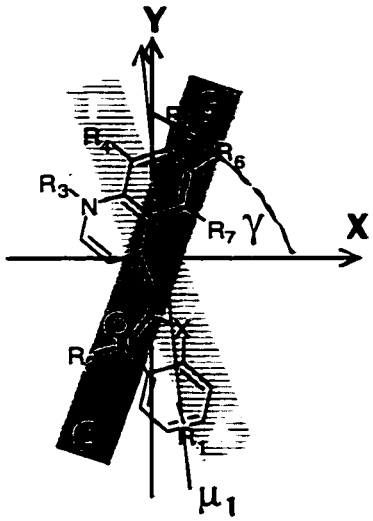

Scheme 7-2: Definitions of axes and angles in DNA-dye systems, using A-T and G-C base pairs to show the intercalation pocket. Also shown is the orientation PicoGreen takes within the pocket.[54]

The looser the dye-DNA complex, the bigger the range of γ values the dye molecules will take when complexed to DNA, and therefore the smaller the signal measured. An alternative explanation involving non-quantitative complexation of the dye (requiring 30% free dye) appears unlikely, but cannot be completely ruled out.

The CD spectra obtained at high dye:DNA ratios are a clear evidence for dye-dye interaction both in dsDNA and ssDNA backbones. The characteristic conservative spectra (a spectrum where the total integrated area equals zero[47]) obtained after analysis of the data according to Equation 7-2, are due to a dimer formed with identical chromophores.[47] Similar spectra have been observed with DAPI,[45] and the cyanine dyes YO, YOYO-1,[22] and TO-PRO,[34] under conditions of high dye:DNA ratios. The different shape of the exciton for ssDNA and dsDNA, *i.e.*, -/+ and +/- pattern with increasing wavelength, respectively (see Figure 7-6-C), is indicative of the different nature of the dimers formed in each type of DNA.

Another result obtained from the analysis of Equation 7-2 and the parameter κ (see Table 7-6), is the amount of PicoGreen molecules involved in forming the dimers in each type of DNA. The constant κ is inversely proportional to the amount of monomer present on the

DNA backbone; thus, the smaller value of κ obtained with dsDNA reflects that more dye is bound independently from other PicoGreen molecules. The κ value we have obtained is also in agreement with time-resolved results under high dye-loading conditions (*vide infra*).

Once the nature of the binding between PicoGreen and ssDNA is established, it still remains to be explained why, if we have only one kind of complex, it presents a biexponential rate law. The same explanation will presumably apply to SYBR Green I and SYBR Gold, which are similar to PicoGreen in their photobehavior. The fact that the trace is biexponential may reflect two different phenomena. We are either dealing with two types of binding of the dye, or there exists some DNA that renatured before data acquisition took place. The dye:DNA ratio employed was low enough as to have only intercalation in the case of dsDNA; however, ssDNA, that may have a lower binding constant,[3,8,56,57] might show other forms of dye interaction. Another possibility which we cannot rule out is that a purine-purine site along the strand will present a different decay than a purine-pyrimidine, which will also be different to a pyrimidine-pyrimidine one. In relation to the possibility that some DNA may have renatured, we tested our method of DNA denaturation by comparing the DNA absorbance at 260 nm, immediately after the denaturation process, for a treated sample and an untreated one. We thus determined that within the experimental error, all the sample had been denatured.[58] In principle, some DNA could renature before data acquisition, however this short delay was kept to only 15 min. We cannot rule out either of the two possibilities described, and, conceivably, we may be dealing with a system presenting both some traces of renatured DNA, and some non-intercalated bound dye. This uncertainty does not influence our ability to discriminate between ssDNA and dsDNA.

To further assess time-resolved studies of cyanine dye-DNA complexes as a means to determine DNA-damage, we studied the effect high dye:DNA ratio plays in the decay of the complexes. This is important to establish a range of dye:DNA ratios where an analytical technique could be applied. The results presented in Figure 7-7-B show that upon increasing the ratio of PicoGreen to DNA, both dye-ssDNA and dye-dsDNA complexes exhibit a

marked decrease in their average lifetime. This is more evident for ssDNA complexes. This is due to energy transfer quenching of an excited PicoGreen molecule from closely located dye molecules. This mechanism has already been shown operative with Hoechst 33258 and ethidium bromide when complexed to dsDNA.[28,35]

The analysis of the new decay profiles according to equations 7-3 and 7-4 enables us to determine which fraction of molecules decay in the normal way, *i.e.*; are not quenched by neighboring dye molecules. These results are shown in Table 7-6, along with the values of the fraction of dye molecules that do not have a close neighbour, as obtained from CD measurements (this number is given by the fraction of dye molecules that do not give rise to a conservative spectrum). Both results show a good correlation.

The decrease in lifetimes observed at high dye:DNA ratios, more pronounced for PicoGreen complexes with ssDNA than with dsDNA, explains the high sensitivity accomplished in other recently developed methods of DNA-damage determination based on steady-state fluorescence measurements of unwound DNA. In these methods, dye:DNA ratios of 2:1,[3] and 1:2.5,[8] were employed.

Similar results to those of PicoGreen were obtained with Hoechst 33258, although the sensitivity accomplished is not as good (see Figure 7-7-A). It is clear from these traces that an extra decay parameter has to be employed to fit the decays, as compared to low dye:DNA ratio situations. The results obtained with Hoechst 33258 would account for its sensitivity when employed in the "Fluorometric Analysis of DNA Unwinding" (FADU) technique.[9] The energy transfer processes as determined with PicoGreen and Hoechst have a bigger effect on the emission from dye-ssDNA complexes than they do on that from dye-dsDNA ones. Although we have not measured ethidium bromide under such conditions of high dye:DNA ratios, previous studies with dsDNA show a biexponential decay for this complex upon increasing the dye content. Therefore, this mechanism is also operative with dsDNA.[35] Considering that ethidium bromide has been employed in the FADU techniques in a 2:1 dye:DNA ratio with considerable success,[6] it is to be expected that energy transfer or self-

quenching present under high dye loading are more sensitive for the ssDNA than the dsDNA complexes with this dye.

7.4 Conclusions

Different photophysical parameters of dye-DNA complexes have been evaluated in this work; little difference in spectral position and amplitude was found when comparing ssDNA and dsDNA bound dyes. Lifetime values of dye-ssDNA and dye-dsDNA complexes have proven to be the most reliable technique to determine ssDNA and dsDNA ratios.

Many different dyes were studied, exhibiting either intercalation or groove binding to DNA under low dye:DNA ratios. Only intercalating dyes exhibit decay kinetics simple enough to attempt a lifetime-based analytical procedure.

The cyanine dyes PicoGreen and SYBR Green I proved to be the most suitable DNA-dyes for the analysis. These dyes are specific for DNA staining due to their high sensitivity to environmental restrictions to mobility. The same quality makes them excellent probes for DNA-damage assessment. While the phenanthridinium dyes and SYBR Gold are not useful for discrimination between ss- and dsDNA, they possess the ideal photophysical properties for use in other applications for determination of DNA-damage, such as the comet assay. From our CD signals we have established that PicoGreen effectively intercalates into both ssDNA and dsDNA. The effects of high dye concentrations indicate that the dimers observed in CD spectra are responsible for the energy transfer or self-quenching decay observed in fluorescence time-resolved studies. The formation of dimers is higher in ssDNA than dsDNA, and therefore dye-ssDNA complexes are more prone to undergo energy transfer deactivation than complexes formed with dsDNA. This explains the success of DNA-damage assessment techniques such as FADU and others.[3,6,8,9]

A method may thus be developed that uses the time evolution of the photophysical properties of DNA-dyes to monitor DNA-damage, in which subjectivity in the data analysis is eliminated. This topic is discussed in great detail in the following chapter.

7.5 Materials and Methods

Materials. PicoGreen dsDNA quantitation reagent, YOYO-1 iodide, SYBR Green I , and SYBR Gold nucleic acid gel stain were all obtained from Molecular Probes (Eugene, OR, USA). Propidium Iodide Hydrate (PIH), Hoechst 33342 (bisbenzimide trihydrochloride) and 4'-6-diamidino-2-phenylindole (DAPI), were from Sigma-Aldrich Canada (Oakville, ON, Canada). Hoechst 33258 (bisbenzimide) and 2,7-diamino-10-ethyl-9-phenylphenanthridinium bromide (Ethidium Bromide) came from Calbiochem (San Diego, CA, USA).

For quantum yield measurements, the following standards were used: quinine bisulfate (Φ_F 0.546 in 1 *N* H_2SO_4[39]) from Acros Organics (Morris Plains, NJ, USA), rhodamine 101 (Φ_F 1.00 in ethanol 99.99%[40,41]) from Fluka (Oakville, ON, Canada), and fluorescein (Φ_F 0.92 in 0.1 M NaOH[42]) from Molecular Probes (Eugene, OR, USA). The Tris buffer solutions were prepared in distilled and deionized water with Trizma pre-set crystals (reagent grade, pH 7.4), Na_2EDTA from Sigma-Aldrich Canada (Oakville, ON, Canada), and NaCl (optical grade) from Alfa Aesar (Ward Hill, MA, USA). Calf Thymus DNA (Type I) (CT DNA) and Salmon Testes DNA (Type III) (ST DNA) were obtained from Sigma-Aldrich. All solvents were HPLC-grade and purchased from OmniSolv (Gibsstown, NJ, USA), and were used without further purification.

Solution Preparation. A stock buffer solution of pH 7.4 was prepared containing Tris 0.01 M, EDTA 0.001 M, and NaCl 0.10 M. Stock solutions of various concentrations of dsDNA were prepared in the buffer, ranging from 200 μM to 2 mM in DNA. The unit used to define DNA concentration or dye:DNA ratios along this paper is a base pair of nucleotides, unless otherwise stated. The DNA solutions were sonicated for 30 s (in order to reduce the DNA chain length), shaken for 1 h, and stored at -4 ^{0}C. The 260:280 nm absorption ratio for DNA solutions gave a value of 1.9, indicating excellent sample purity.[58] The dyes, as received from the suppliers, were kept at -20 ^{0}C. Every day, freshly prepared

solutions using the stocks were made, with the dye:DNA base pair concentration ratio equal to 1:10, unless otherwise specified. The DNA concentration per nucleotide was determined by absorption spectroscopy using the extinction coefficient of 6600 $M^{-1}cm^{-1}$ at 260 nm for calf thymus DNA.[58] PicoGreen concentration was estimated by using the reported molar extinction coefficient of 70,000 $M^{-1}cm^{-1}$.[27] SYBR Green I and SYBR Gold concentrations were estimated assuming a molar extinction coefficient of at least 50,000 $M^{-1}cm^{-1}$, as reported for all cyanine dyes.[38] While not in use, all solutions were kept wrapped in aluminum foil and submerged in an ice bath to avoid decomposition of the dye. For the ssDNA, all conditions were the same, except that the samples (before addition of the dye) were heated in a boiling water bath for 30 min in order to denature the DNA. Complete denaturation was confirmed by comparing the absorption ratio at 260 nm for the heated (ssDNA) and non-heated (dsDNA) samples. A value of 1.32 was obtained, in good agreement with the literature value.[58] The solutions were subsequently cooled (in order to avoid renaturation) by diluting the sample 1/8 parts with cold buffer. The dye was added once the solution was cold, to avoid its degradation. Both dsDNA and ssDNA solutions were left to equilibrate with the dye for a maximum of 5 min before measurement.

To determine fluorescence quantum yields, the buffer solutions containing free dye, dye and dsDNA, as well as dye and ssDNA, were optically matched at the excitation wavelength. The absorbance was always kept below 0.05 to avoid self-absorption of the fluorescence. Given the low Stokes shift in the cyanine dyes (*vide infra*), these were always excited in the blue region of their absorption band. Under these conditions, the fluorescence spectra were recorded. The fluorescence spectra of quinine bisulfate, fluorescein, or rhodamine 101, with an absorption at the excitation wavelength matching that of the dye at that same wavelength, were also measured with the same instrumental parameters used with the dye solutions. Quinine bisulfate was used as standard for the bisbenzimide dyes; for PIH and ethidium bromide the standard used was rhodamine 101; and fluorescein was used for the cyanine dyes. Following correction by instrument efficiency, and subtraction of the solvent

signal for the dye emission, all spectra were integrated and the ratio of the areas for the dye solutions and the standard determined.

Excitation spectra were run for all samples in order to check for dye purity; in all cases the spectrum matched that of the corresponding absorption (data not shown) indicating that fluorescence was originating from the DNA-stain dye under study.

Lifetime measurements were taken under similar conditions as those of steady-state fluorescence; however, solutions had to be more concentrated in order to supply a ground state absorption higher than 0.5 at the excitation wavelength, necessary for obtaining good signal-to-noise ratio in the picosecond and nanosecond laser-systems.

Circular Dichroism (CD) spectra were taken on solutions of PicoGreen 0.020 mM and different amounts of both dsDNA and ssDNA. The buffer solution spectrum was taken and used as a blank to which the CD signals were subtracted.

Instrumentation. The picosecond laser system was briefly discussed in Section 2.5 of this thesis.

Due to the relatively low laser power employed and the small number of shots required to obtain the signals, deterioration of the sample was negligible (as checked by changes in ground state absorption spectra), and all the experiments were carried out in static 7 x 7 mm fused silica cuvettes. In the case of ethidium bromide and propidium iodide-DNA complexes (lifetimes longer than 15 ns) the samples were excited with the third harmonic of a Surelite Nd:YAG laser of 6 ns duration. See Section 2.5 for further details regarding the laser system.

Steady-state fluorescence spectroscopy was carried out using a Photon Technology International version 1.2 X luminescence spectrometer. Fused silica cuvettes (Luzchem Research, Morin Heights, QU, Canada) with a 10 mm optical path were employed in all these experiments. Absorption spectra were recorded using a Varian CARY 1E spectrophotometer.

Circular Dichroism experiments were performed on an AVIV 202 spectrometer provided with a 450 watt Xenon arc lamp. Linear polarization was achieved by means of a MgF_2 polarizer. The RMS noise of the instrument is 0.06 mdeg at 500 nm.

7.6 References

(1) Ostling, O.; Johanson, K. J., Microelectrophoretic Studies of Radiation-induced DNA Damages in Individual Mammalian Cells, *Biochem. Biophys. Res. Commun.*, **1984**, *123*, 291-298.

(2) Rösl, F., A Simple and Rapid Method for Detection of Apopthosis in Human Cells, *Nucleic Acids Res.*, **1992**, *20*, 5243.

(3) Rogers, K. R.; Apostol, A.; Madsen, S. J.; Spencer, C. W., Detection of Low Dose Radiation Induced DNA Damage Using Temperature Differential Fluorescence Assay, *Anal. Chem.*, **1999**, *71*, 4423-4426.

(4) Compton, M. M.; Cidlowski, J. A., Rapid in Vivo Effects of Glucocorticoids on the Integrity of Rat Lymphocyte Genomic Deoxiribonucleic Acid., *Endocrinology*, **1986**, *118*, 38-45.

(5) Faccineti, A.; Tessarollo, L.; Mazzocchi, M.; Kingston, R.; Collavo, D.; Biasi, G., An Improved Method for the Detection of DNA Fragmentation, *J. Immunol. Methods*, **1991**, *136*, 125-131.

(6) Birnboim, H. C.; Jevcak, J. J., Fluorimetric Method for Rapid Detection of DNA Strand Breaks in Human White Blood Cells Produced by Low Doses of Radiation, *Cancer Res.*, **1981**, *41*, 1889-1892.

(7) Kohn, K. W., Principles and Practice of DNA Filter Elution, *Pharmacol. Ther.*, **1991**, *49*, 55-77.

(8) Elmendorff-Dreikorn, K.; Chauvin, C.; Slor, H.; Kutzner, J.; Batel, R.; Muller, W. E.; Schroder, H. C., Assessment of DNA Damage and Repair in Human Peripheral Blood Mononuclear Cells Using a Novel DNA Unwinding Technique, *Cell. Mol. Biol.*, **1999**, *45*, 211-218.

(9) Baumstark-Khan, C.; Hentschel, U.; Nikandrova, Y.; Krug, J.; Horneck, G., Fluorometric Analysis of DNA Unwinding (FADU) as a Method for Detecting Repair-induced DNA Strand Breaks in UV-irradiated Mammalian Cells, *Photochem. Photobiol.*, **2000**, *72*, 477-484.

(10) Wyllie, A. H., Glucocorticoid Induced Thymocyte Apoptosis is Associated with Endogenous Endonuclease Activation, *Nature*, **1980**, *284*, 555-556.

(11) Horváthová, E.; Slamenová, D.; Hlinciková, L.; Mandal, K. T.; Gábelová, A.; Collins, A. R., The Nature and Origin of DNA Single-strand Breaks Determined with the Comet Assay, *Mutat. Res.*, **1998**, *409*, 163-171.

(12) Olive, P. L., DNA Damage and Repair in Individual Cells: Applications of the Comet Assay in Radiobiology, *Int. J. Radiat. Biol.*, **1999**, *75*, 395-405.

(13) Böcker, W.; Rolf, W.; Bauch, T.; Müller, W.-U.; Streffer, C., Automated Comet Assay Analysis, *Cytometry*, **1999**, *35*, 134-144.

(14) Collins, A. R.; Dobson, V. L.; Dusinská, M.; Kennedy, G.; Stetina, R., The Comet Assay: What Can it Really Tell Us?, *Mutat. Res.*, **1997**, *375*, 183-193.

(15) Pouget, J.-P.; Douki, T.; Richard, M.-J.; Cadet, J., DNA Damage Induced in Cells by γ Radiation as Measured by HPLC/GC-MS and HPLC-EC and Comet Assay, *Chem. Res. Toxicol.*, **2000**, *13*, 541-547.

(16) McNamee, J. P.; McLean, J. R. N.; Ferrarotto, C. L.; Bellier, P. V., Comet Assay: Rapid Processing of Multiple Samples, *Mutat. Res.*, **2000**, *466*, 63-69.

(17) Rojas, E.; Lopez, M. C.; Valverde, M., Single Cell Gel Electrophoresis Assay: Methodology and Applications, *J. Chromatogr., B:*, **1999**, *722*, 225-254.

(18) Barcellona, M. L.; Cardiel, G.; Gratton, E., Time-resolved Fluorescence of DAPI in Solution and Bound to Polydeoxynucleotides, *Biochem. Biophys. Res. Commun.*, **1990**, *170*, 270-280.

(19) Carlsson, C.; Larsson, A.; Jonsson, M.; Albinsson, B.; Nordén, B., Optical and Photophysical Properties of the Oxazole Yellow DNA Probes YO and YOYO, *J. Phys. Chem.*, **1994**, *98*, 10313-10321.

(20) Haugland, R. P.; Yue, S. T.; Millard, P. J.; Roth, B. L. "Cyclic Substituted Unsymmetrical Cyanine Dyes", United States Patent Office, US5436134, 1995.

(21) Kumar, C. V.; Turner, R. S.; Asuncion, E. H., Groove Binding of a Styrylcyanine Dye to the DNA Double Helix: the Salt Effect, *J. Photochem. Photobiol. A: Chem.*, **1993**, *74*, 231-238.

(22) Larsson, A.; Carlsson, C.; Jonsson, M.; Albinsson, B., Characterization of the Binding of the Fluorescent Dyes YO and YOYO to DNA by Polarized Light Spectroscopy, *J. Am. Chem. Soc.*, **1994**, *116*, 8459-8465.

(23) Netzel, T. L.; Nafisi, K.; Zhao, M.; Lenhard, J. R.; Johnson, I., Base-content Dependence of Emission Enhancements, Quantum Yields, and Lifetimes for Cyanine Dyes Bound to Double-strand DNA: Photophysical Properties of Monomeric and Bichromophoric DNA Stains, *J. Phys. Chem.*, **1995**, *99*, 17936-17947.

(24) Rye, H. S.; Quesada, M. A.; Peck, K.; Mathies, R. A.; Glazer, A. N., High-Sensitivity Two-Color Detection of Double-Stranded DNA with a Confocal Fluorescence Gel Scanner Using Ethidium Homodimer and Thiazole Orange, *Nucleic Acids Res.*, **1990**, *19*, 327-333.

(25) Rye, H. S.; Yue, S.; Wemmer, D. E.; Quesada, M. A.; Haugland, R. P.; Mathies, R. A.; Glazer, A. N., Stable Fluorescent Complexes of Double-Stranded DNA with Bis-intercalating Cyanine Dyes: Properties and Applications, *Nucleic Acids Res.*, **1992**, *20*, 2803-2812.

(26) Sauerwein, B.; Murphy, S.; Schuster, G. B., Dynamics of Solute Motion: Photoisomerization Shows Linear Dependence on Solvent Mass, *J. Am. Chem. Soc.*, **1992**, *114*, 7920-7922.

(27) Singer, V. L.; Jones, L. J.; Yue, S. T.; Haugland, R. P., Characterization of PicoGreen Reagent and Development of a Fluorescence-based Solution Assay for Double-stranded DNA Quantitation, *Anal. Biochem.*, **1997**, *249*, 228-238.

(28) Stokke, T.; Steen, H. B., Multiple Binding Modes for Hoechst 33258 to DNA, *J. Hystochem. Cytochem.*, **1985**, *33*, 333-338.

(29) Tuma, R. S.; Beaudet, M. P.; Jin, X.; Jones, L. J.; Cheung, C.-Y.; Yue, S.; Singer, V. L., Characterization of SYBR Gold Nucleic Acid Gel Stain: A Dye Optimized for Use with 300-nm Ultraviolet Transilluminators, *Anal. Biochem.*, **1999**, *268*, 278-288.

(30) Yue, S. T.; Singer, V. L.; Roth, B. L.; Mozer, T. J.; Millard, P. J.; Jones, L. J.; Xiaokui, J.; Haugland, R. P. "Substituted Unsymmetrical Cyanine Dyes with Selected Permeability", World Intelectual Property Organization, WO96/13552, 1996.

(31) Loontiens, F. G.; Regenfuss, P.; Zechel, A.; Dumortier, L.; Clegg, R. M., Binding Characteristics of Hoechst 33258 with Calf Thymus DNA, Poly[d(A-T)], and d(CCGGAATTCCGG): Multiple Stoichiometries and Determination of Tight Binding with a Wide Spectrum of Site Affinities., *Biochemistry*, **1990**, *29*, 9029-9039.

(32) Spielmann, H. P.; Wemmer, D. E.; Jacobsen, J. P., Solution Structure of DNA Complex with the Fluorescent Bis-intercalator TOTO Determined by NMR Spectroscopy, *Biochemistry*, **1995**, *34*, 8542-8553.

(33) Sczepan, M.; Rettig, W.; Bricks, Y.; Slominski, Y. L.; Tolmachev, A. I., Unsymmetric Cyanines: Chemical Rigidization and Photophysical Properties., *J. Photochem. Photobiol. A: Chem.*, **1999**, *124*, 75-84.

(34) Petty, J. T.; Bordelon, J. A.; Robertson, M. E., Thermodynamic Association of Cyanine Dyes with DNA, *J. Phys. Chem. B*, **2000**, *104*, 7221-7227.

(35) Byrne, C. D.; de Mello, A. J., Photophysics of Ethidium Bromide Complexed to CT DNA: A Maximum Entropy Study, *Biophys. Chem.*, **1998**, *70*, 173-184.

(36) Wilson, W. D.; Krishnamoorthy, C. R.; Wang, Y.-H.; Smith, J. C., Mechanism of Intercalation: Ion Effects on the Equilibrium and Kinetic Constants for the Interaction of Propidium and Ethidium with DNA, *Biopolymers*, **1985**, *24*, 1941-1961.

(37) Morgan, A. R.; Lee, J. S.; Pulleyblank, D. E.; Murray, N. L.; Evans, D. H., Ethidium Fluorescence Assays. Part I. Physicochemical Studies, *Nucleic Acids Res.*, **1979**, *7*, 547-570.

(38) Haugland, R. P., *Handbook of Fluorescent Probes and Research Chemicals:* 6 ed.; Molecular Probes, Inc.: Eugene, OR, 1996, 161-174.

(39) Melhuish, W. H., Quantum Efficiencies of Fluorescence of Organic Substances: Effect of Solvent and Concentration of the Fluorescent Solute, *J. Phys. Chem.*, **1961**, *65*, 229-235.

(40) Karstens, T.; Kobs, K., Rhodamine B and Rhodamine 101 as Reference Substances for Fluorescence Quantum Yield Measurements, *J. Phys. Chem.*, **1980**, *84*, 1871-1872.

(41) Eaton, D. F. Luminescence Spectroscopy; In *Handbook of Organic Photochemistry*; J. C. Scaiano, Ed.; CRC Press, Inc: Boca Raton, 1989; Vol. 2; 231-238.

(42) Weber, G.; Teale, F. W. J., Determination of the Absolute Quantum Yield of Fluorescent Solutions, *Trans. Faraday Soc.*, **1957**, *53*, 646-655.

(43) Cosa, G.; Focsaneanu, K.-S.; McLean, J. R. N.; Scaiano, J. C., Direct Determination of Single to Double Stranded DNA Ratio in Solution Applying Time-resolved Fluorescence Measurements of Dye-DNA Complexes, *Chem. Commun.*, **2000**, 689-690.

(44) Krugh, T. R.; Wittlin, F. N.; Cramer, S. P., Ethidium Bromide-Dinucleotide Complexes. Evidence for Intercalation and Sequence Preferences in Binding to Double-Stranded Nucleic Acids, *Biopolymers*, **1975**, *14*, 197-210.

(45) Kubista, M.; Akerman, B.; Nordén, B., Characterization of Interaction Between DNA and 4',6-Diamidino-2-phenylindole by Optical Spectroscopy, *Biochemistry*, **1987**, *26*, 4545-4553.

(46) Bunkenborg, J.; Gadjev, N. I.; Deligeorgiev, T.; Jacobsen, J. P., Concerted Intercalation and Minor Groove recognition of DNA by a Homodimeric Thiazole Orange Dye, *Bioconjugate Chem.*, **2000**, *11*, 861-867.

(47) Cantor, C. R.; Schimmel, P. R., *Part II: Techniques for the Study of Biological Structure and Function*; W. H. Freeman and Company: San Francisco, 1980; Vol. 2.

(48) Fede, A.; Labhardt, A.; Bannwarth, W.; Leupin, W., Dynamics and Binding Mode of Hoechst 33258 to d(GTGGAATTCCAC)$_2$ in the 1:1 Solution Complex as Determined by Two-dimensional ^{1}H NMR, *Biochemistry*, **1991**, *30*, 11377-11388.

(49) Kalninsh, K. K.; Pestov, D. V.; Roshchina, Y. K., Absorption and Fluorescence Spectra of the Probe Hoechst 33528, *J. Photochem. Photobiol. A: Chem.*, **1994**, *83*, 39-47.

(50) Sailer, B. L.; Nastasi, A. J.; Valdez, J. G.; Steinkamp, J. A.; Crissman, H. A., Differential Effects of Deuterium Oxide on the Fuorescence Lifetimes and Intensities of Dyes with Different Modes of Binding to DNA., *J. Histochem. Cytochem.*, **1997**, *45*, 165-175.

(51) Szabo, A. G.; Krajcarski, D. T.; Cavatorta, P.; Masotti, L.; Barcellona, M. L., Excited State pKa Behaviour of DAPI. A Rationalization of the Fluorescence Enhancement of DAPI in DAPI-Nucleic Acid Complexes., *Photochem. Photobiol.*, **1986**, *44*, 143-150.

(52) Gilbert, A.; Baggott, J., *Essentials of Molecular Photochemistry*; Blackwell Scientific Publications: Oxford, 1991.

(53) Ward, T. H.; Marples, B., SYBR Green I and the Improved Sensitivity of the Single-cell Electrophoresis Assay, *Int. J. Radiat. Biol.*, **2000**, *76*, 61-65.

(54) Nordén, B.; Tjerneld, F., Structure of Methylene Blue-DNA Complexes Studied by Linear and Circular Dichroism, *Biopolymers*, **1982**, *21*, 1713-1734.

(55) Lyng, R.; Härd, T.; Nordén, B., Induced CD of DNA Intercalators: Electric Dipole Allowed Transitions, *Biopolymers*, **1987**, *26*, 1327-1345.

(56) Arndt-Jovin, D. J.; Jovin, T. M., *Methods in Cell Biology*; Academic Press, Inc.: New York, 1989; Vol. 30, 417-448.

(57) Kapuscinski, J.; Darzynkiewickz, Z.; Melamed, M. R., Luminescence of the Solid Complexes of Acridine Orange with RNA, *Cytometry*, **1982**, *2*, 201-211.

(58) Gallagher, S. R. Quantitation of DNA and RNA with Absorption and Fluorescence Spectroscopy; In *Current Protocols in Molecular Biology*; F. M. Ausubel, R. Brent, R. E. Kingston, D. D. Moore, J. G. Seidman, J. A. Smith and K. Struhl, Eds.; Greene Pub. Associates and Wiley-Interscience: New York, 1994; Vol. 3; A.3D.1-A.3D.8.

8. Novel DNA-damage Detection Technique Applying Time-resolved Fluorescence Measurements

8.1 Introduction

Damage to DNA in its biological environment has been associated with alterations in DNA sequence, aberrant gene expression, increased mutation rates, cell transformation and the development of cancer. DNA-damage can arise as a result of inherent DNA chemical instability, as a by-product of endogenous cellular processes such as oxidative metabolism,[1] or by exposure to exogenous genotoxic agents.[2] The disruption of the structural or functional integrity of DNA is therefore an important first step in establishing the carcinogenic potential of a chemical or physical agent.

Chemical damage to DNA will frequently render a weakened polymer structure at the site of the attack; upon appropriate treatment these damaged sites will result in strand scissions,[3,4] eventually causing unwinding of DNA (see also Scheme 1-6).[5] Many analytical techniques currently employed in quantifying DNA-damage rely on the production of single stranded DNA (ssDNA) from double stranded DNA (dsDNA) following an unwinding protocol. For example, the comet assay,[6-9] the fluorometric analysis of DNA unwinding,[10,11] the alkaline filter elution,[12], or temperature unwinding techniques.[13] In all these techniques the damage the DNA has suffered is "translated" into a measurable property, the amount of ssDNA produced.

The work described in the previous chapter indicates that one way to measure the amount of ssDNA and dsDNA present in solution is given by the fluorescence lifetime of dye-DNA complexes. We found that PicoGreen is the best dye (out of nine commercial DNA-stain dyes explored) suited for this purpose.[14] PicoGreen belongs to a family of recently patented[15,16] fluorescent stains derived from unsymmetric cyanine dyes which exhibit high increase (*ca.* 1000 fold) in their fluorescence quantum yields upon binding to double-stranded DNA (dsDNA) as compared to free in solution, making them very sensitive probes for DNA detection. These dyes are free to rotate about their central methine bridge while in solution, but this non-radiative deactivation pathway is closed when the dye

intercalates in between the DNA base-pairs, (see Figure 8-1). This explains their high sensitivity as dsDNA sensors.[17,18]

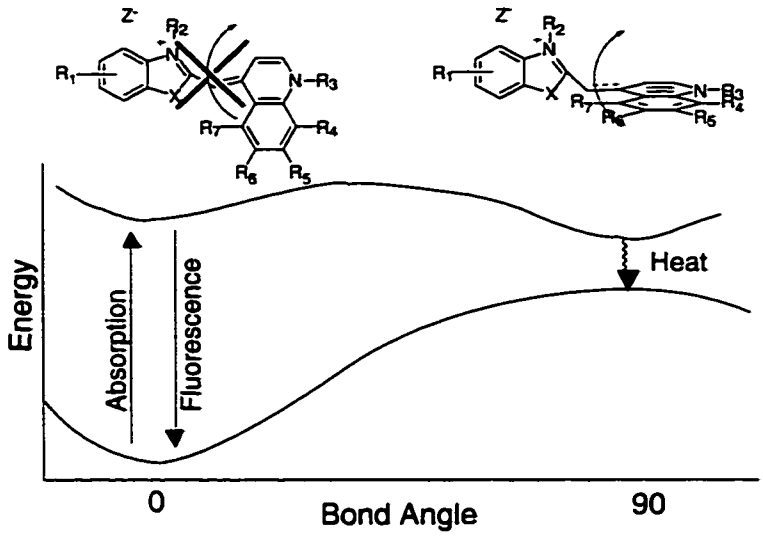

Figure 8-1: Diagram representing the ground-state and singlet-excited state of PicoGreen. Following excitation of the *trans* form to the excited *trans*-singlet state, twisting along the methine bridge converts the molecule into the excited perpendicular singlet state wherefrom it decays nonradiatively, following internal conversion, to the perpendicular ground state.[19,20] Upon intercalation in DNA, this internal rotation is restricted, and the excitation energy is mostly dissipated following emission.

Fluorescence is the main tool employed in the quantification of ssDNA in many other techniques developed to assess DNA-damage. Some of these techniques make use of PicoGreen as the fluorophore; yet, in all these cases steady-state measurements rather than time-resolved ones have been employed.[13,21] The fluorescence lifetime is an intensive property, *i.e.*, it is not dependent on the amount of fluorophore, and it is unique to a dye in a given environment. Lifetime measurements thus render reliable results without the need for blanks. The latter is not true for steady-state fluorescence experiments, where it is necessary to compare the intensities arising from stained damaged DNA to those rendered by stained control samples.

In what follows we describe a new technique, based on fluorescence lifetimes, to assess DNA-damage produced in white blood cells. We first discuss the fluorescence lifetime of PicoGreen-DNA complexes in solution, in various ratios of ssDNA to dsDNA, to establish a calibration curve that enables an assessment of the ratio of the two forms of DNA in an unknown sample based on lifetime preexponential values. The effect the viscosity of support materials has on dye-DNA fluorescence lifetimes is also addressed. We also report the fluorescence parameters we have obtained for the support materials employed in the unwinding protocol. These results will influence the manipulation of the substrate to be measured. As part of this chapter we also introduce preliminary results where we evaluate the sensitivity of our technique, following different unwinding protocols, on damaged calf thymus DNA (CT DNA). Finally, with the previous information, we discuss our results obtained with the DNA isolated from gamma (γ) radiated sheep white blood cells.

This work has been done with the collaborations of Dr. J. R. N. MacLean at Health Canada, and A. L. Vinette, in our group. Greater details regarding the manipulation of the samples obtained from sheep blood can be found in the M.Sc. Thesis of A. L. Vinette. The interdisciplinary nature of this project requires a diversity of areas of expertise. My contribution leans towards the spectroscopic and kinetic studies, while blood processing, unwinding protocols and the comparison of the advantages of this new technique relative to the comet assay are dominated by contributions from A. L. Vinette.

8.2 Results

8.2.1 Dye-dsDNA and Dye-ssDNA Mixtures in Solution

In the present work we have exploited the possibility that in a complex with single-stranded DNA (ssDNA) a less rotationally restricted dye should be present, as compared to that with dsDNA (shown pictorially in Figure 8-2). This difference can be reflected in the fluorescence lifetimes of dye-DNA complexes. To that effect, we have studied the complexes formed with PicoGreen, a representative of the family of cyanine dyes which exhibits the greatest sensitivity for selective detection of dsDNA in solution.[13,15,16,22].

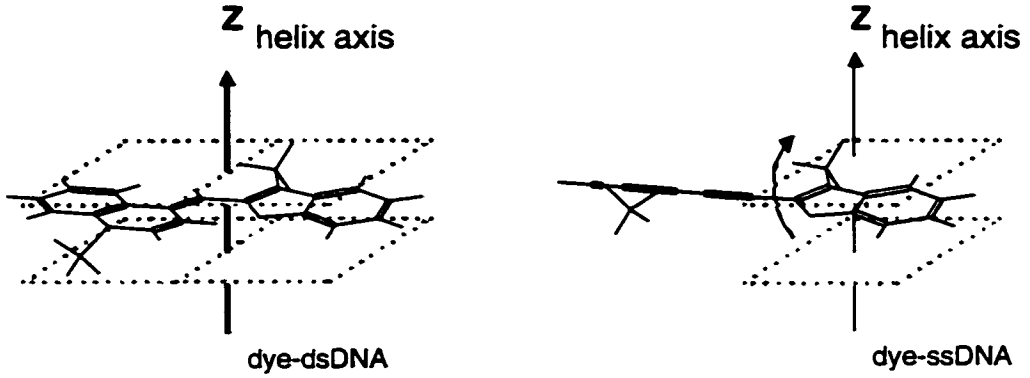

Figure 8-2: Schematic representation of dye-dsDNA and dye-ssDNA complexes; z is the direction of the helix axis. The planes represent the DNA bases.

The results obtained following 355 nm irradiation of a sample with a $\leq$ 50 ps laser pulse (presented in the previous chapter) show a virtually pure monoexponential decay with a lifetime of 4.5 ns for dye-dsDNA (for both CT or ST type DNA).[23] The decay obtained for the complex formed with ssDNA is biexponential, with lifetimes of 1.16 ns (51%) and 3.09 ns (49%), where the weight of each exponential is given in brackets (Figure 8-3).

In view of the noticeable difference in fluorescence lifetimes between dye-ssDNA complex and dye-dsDNA complex, we attempted and succeeded in developing an analytical technique that would enable us to monitor in solution the ssDNA:dsDNA ratio with a simple method devoid of any operator subjectivity. To that effect, we determined the fluorescence

lifetimes in different mixtures containing known amounts of ssDNA, dsDNA (we employed both CT DNA and ST DNA) and PG; the traces are observed in Figure 8-3.

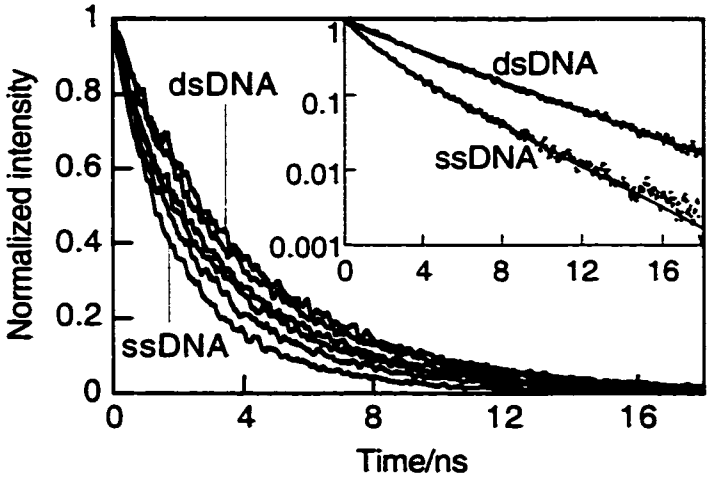

Figure 8-3: Normalized fluorescence decay profiles measured on static 2 ml quartz cells in air equilibrated solutions of DNA in TRIS buffer pH 7.4 following 355 nm laser excitation; ST DNA base-pair concentration 150 μM, PG 11 μM, for 100% dsDNA; 80% dsDNA; 60% dsDNA; 40% dsDNA; 20% dsDNA; and dsDNA alone. Insert: semilog plot and fit for dsDNA (single exponential) and ssDNA (double exponential).

Assuming that dye-ssDNA and dye-dsDNA complexes behave independently of each other, we expect a triexponential decay in this system (Equation 8-1); *i.e.*, dye-dsDNA decays with its characteristic rate constant, and ssDNA complexes exhibit their biexponential decay.[23]

Equation 8-1: $$I = a_{ds}e^{-k_{ds}t} + a_2e^{-k_2t} + a_3e^{-k_3t}$$

where a_{ds} is the preexponential factor for dsDNA, and k_{ds} is the reciprocal of its lifetime, while a_2, a_3, k_2 and k_3 are the corresponding parameters for ssDNA, and t is the time.

Though complicated in appearance, we know the three decay rate constants for this system (that of dsDNA, and each of the two for ssDNA); on the other hand, the addition of the preexponential factors for the decays has to be equal to one for the normalized profile.

At this point a 6 variable function initially needed to fit this decay (three pre-exponential values, and three decay rate constants), is now reduced to one with two parameters, *i.e.*, two pre-exponential values. Further, since the relative values for the two pre-exponential values for the ssDNA decay are known, and coincidentally they are about equal, *i.e.*,

$$a_{ds} + a_2 + a_3 = 1$$
$$a_2 \equiv a_3$$

Combined these factors lead to a one parameter fit according to Equation 8-2:

Equation 8-2: $$I = a_{ds}e^{-0.22t} + \frac{(1 - a_{ds})}{2}\left(e^{-0.86t} + e^{-0.32t}\right)$$

The fitting of the decay traces obtained at different ssDNA:dsDNA ratios, employing Equation 8-2, is observed in Figure 8-4-A. When we plot the recovered pre-exponential value (a_{ds}) corresponding to the dsDNA rate constant *vs.* the fraction of dsDNA in the sample (see Figure 8-4-B) for CT DNA and for ST DNA, a straight line is obtained with a slope of 0.80 and an intercept of 0.048. The theoretical line should go through the origin and have a slope of 1.0. The difference is not surprising, analysis according to Equation 8-2 of computer simulated data shows that only perfect data (*i.e.*, noise-free) leads to perfect recovery of the pre-exponential factors, particularly for the pure forms, dsDNA and ssDNA; addition of random noise always leads to apparent small weights for other DNA components. Effectively, the percentage of dsDNA present in a sample can be calculated according to Equation 8-3, although we note that different instruments may lead to slightly different deviations from the ideal equation; in this sense a recalibration may be desirable.[23]

Equation 8-3: $$\%\ \text{dsDNA} = 100\left(\frac{a_{ds} - 0.048}{0.80}\right)$$

It is worthwhile noting that for the simulated decay traces, the rate constants used for ssDNA (0.32 and 0.86 x 10^9 s^{-1}) and dsDNA (0.22 x 10^9 s^{-1}) were those determined in the

absence of the other form of DNA, and are the same for CT or ST DNA, and are not adjustable parameters.

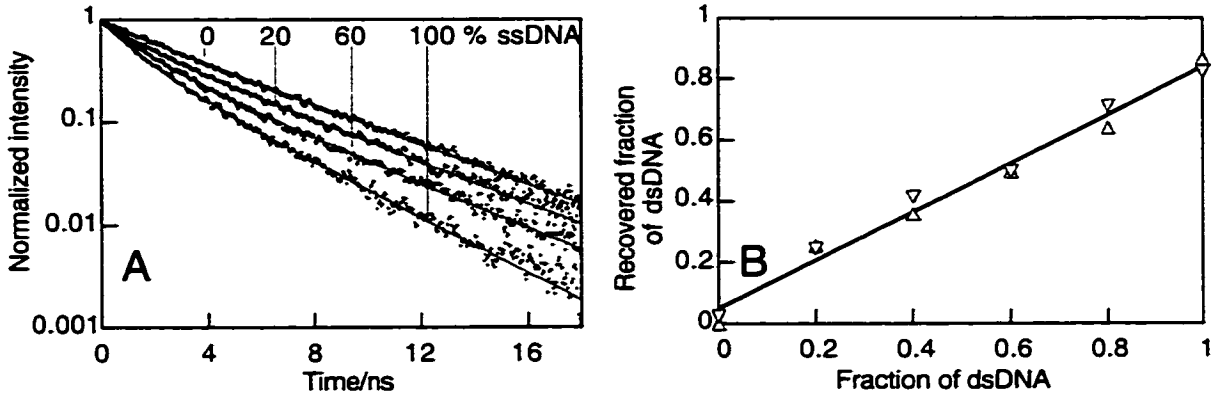

Figure 8-4: (A) Normalized fluorescence decay profiles measured on static 2 ml quartz cells in air equilibrated solutions of DNA in TRIS buffer pH 7.4 following 355 nm laser excitation; ST DNA base-pair concentration 150 μM, PG 11 μM, for various percentages of dsDNA, showing the fit of the data to the one-parameter function of Equation 8-2. (B) Linear plot of the recovered dsDNA fraction as a function of the actual fraction in the sample for (△) CT DNA and for (▽) ST DNA.

8.2.2 Spectroscopy of Support Materials

The existing protocols employed in the manipulation of cells, with the aim of isolating the DNA from other cellular components, require the use of support materials. Many reports describe the treatment of cells embedded in agarose with lysis buffers, to remove the cellular membrane, proteins and RNA, leaving intact the DNA backbone.[5-9,21,24] On similar support materials, the DNA isolated in the previous step is subjected to unwinding, to "translate" the damage to which the cell has been subjected. In our research towards the development of a new DNA-damage assessment technique based on dye-DNA fluorescence lifetimes, these are necessary steps, common to other techniques; yet, it is important to establish what effect the agarose might have on PicoGreen-DNA complex fluorescence lifetimes. It is also necessary to establish to which extent background signals, arising from

fluorescence of the solid matrix employed in supporting the agarose gels, or the gels themselves, may interfere with the kinetic traces for dye-DNA complexes.

Reports on the solvent viscosity dependence of the lifetime for cyanine-stilbene dyes are a concern in establishing a DNA-damage technique where the DNA substrate is to be analyzed fixed in a viscous support material (*i.e.*, agarose).[17,25,26] We measured the lifetime of dye-ssDNA and dye-dsDNA embedded in high strength analytical grade agarose gel (0.75% w:w in phosphate buffer solution (PBS) pH 7.4). The results are shown in Figure 8-5 for both forms of dye-DNA complexes; also shown for comparison are the decay traces for PicoGreen when complexed to both forms of DNA in phosphate buffer solutions. Note that in both cases, the fluorescence decay traces obtained with PicoGreen-DNA embedded in agarose gel matches those obtained with the dye-DNA complexes in phosphate buffer saline solutions.

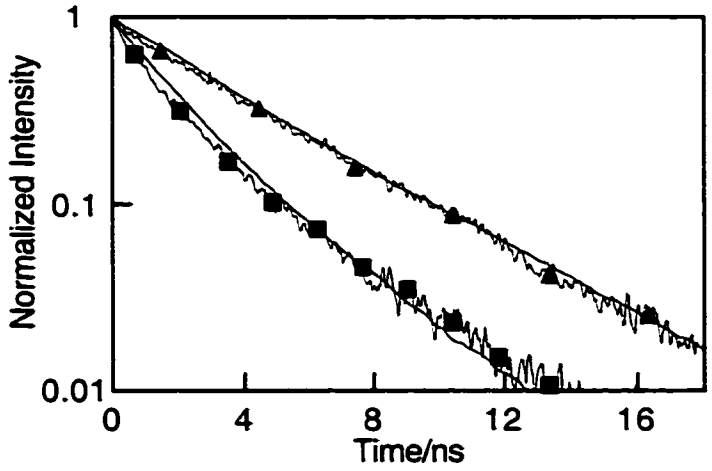

Figure 8-5: Fluorescence decay of PicoGreen (5 μM) complexed to (■) ssDNA (50 μM in base pairs), and (▲) dsDNA (50 μM in base pairs), in agarose gel 0.75% w:w in PBS. Overlaid are the smoothed traces corresponding to PicoGreen-ssDNA and PicoGreen-dsDNA complex in PBS, respectively, extracted from Figure 8-4. A few points are shown to assist in the visualization.

The way cells are handled involves casting a mixture of agarose and cell suspensions on a solid matrix, commercially known as Gelbond®. The DNA material embedded in the gel

remains on this support unless physically removed. To establish this material compatibility with our measurements, we checked its absorbance as well as steady-state and time-resolved fluorescence characteristics. The results are presented in Figure 8-6.

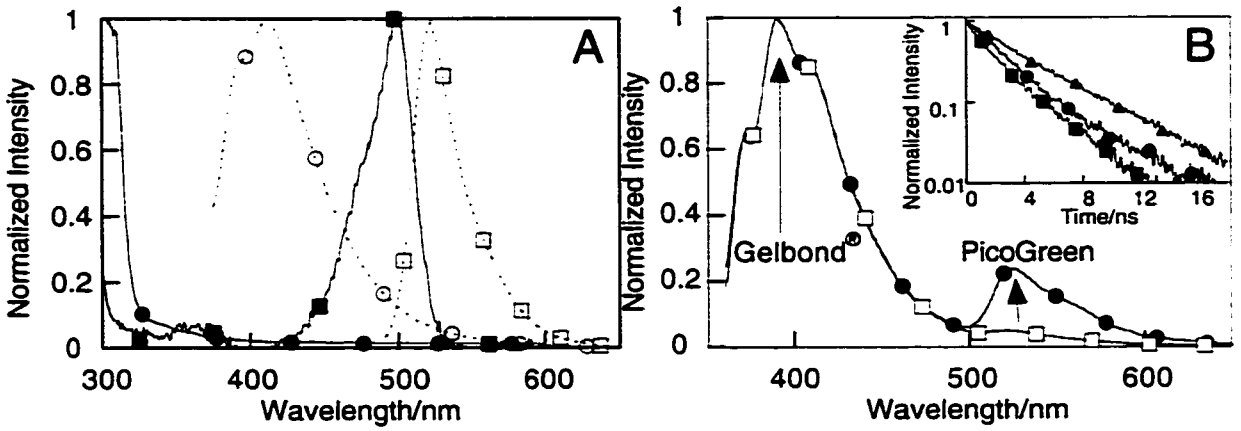

Figure 8-6: (A) Normalized (●) absorption and (○) fluorescence spectra of Gelbond®; the latter was measured with a 350 nm excitation wavelength. Also shown are the normalized (■) absorption and (□) fluorescence spectra of PicoGreen in phosphate buffer, pH 7.4. (B) Fluorescence spectra of PicoGreen-dsDNA complexes supported on agarose-Gelbond®; PicoGreen 5 μM, dsDNA 50 μM in base pairs. (□) Supported in a 200 μl agarose, 1 x 1 cm² surface gel. (●) Supported in a 500 μl agarose, 1 x 1 cm² surface gel. The inset in Figure 8-6-B shows (●) the fluorescence decay of Gelbond®; also shown for comparison are the decay traces of (■) PicoGreen-ssDNA and (▲) PicoGreen-dsDNA complexes, from Figure 8-4. The points shown are intended to assist in the visualization.

Gelbond® absorption extends over the visible part of the spectrum, as can be observed from Figure 8-6-A. In particular, at 355 nm, the wavelength employed in our studies, the absorbance band is clearly observed. Figure 8-6-B shows the relative intensity of fluorescence from Gelbond® casted with two films of DNA-agarose of different thickness. Note the relative intensities due to DNA stained with PicoGreen, and due to Gelbond® fluorescence. In particular, the dye-DNA complex emission is negligible for the thinner film. The inset of Figure 8-6-B also shows that the time evolution of Gelbond® fluorescence would interfere with the signal from PicoGreen-DNA complexes. Thus, this support material can

not be used in the latter stages of a DNA-damage assessment technique, *i.e.*, when time-resolved fluorescence measurements are necessary.

8.2.3 Effects of Gamma Radiation and Unwinding Time on DNA

In order to analyze DNA-damage, proper conditions in terms of cell lysis and DNA unwinding must first be established. While it is important to find conditions for unwinding the damaged DNA, at the same time it is desirable that little or no unwinding occurs in an undamaged sample.

We have employed hydroxyl radicals ($HO^{\bullet}$) as a source of DNA-damage, generated following gamma radiation (γ radiation). The energy deposited in water by this radiation produces its ionization, as shown in Step 1 in Scheme 8-1. In a collision between the ionized water molecule with a second water molecule the hydroxyl radical is produced (Step 2 in Scheme 8-1). The resulting high energy electron loses energy and becomes hydrated (Step 3 in Scheme 8-1), and ultimately reduces a proton to a hydrogen atom.[27] The effects of γ radiation on aqueous solutions containing DNA is well established.[27,28] Following a dose of 1 Gy (equivalent to 1 J of energy deposited in a kg of substance) 1000 single strand breaks and 40 double strand breaks are produced per cell.[27,28]

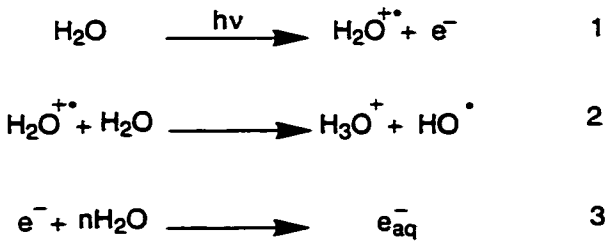

Scheme 8-1: Formation of $HO^{\bullet}$ following gamma radiation of aqueous solutions.[27]

Having established a method for reliable DNA-damage production we then searched for appropriate conditions of DNA unwinding employing commercially available sources of the biopolymer. The results presented in Figure 8-7 show the relative amount of ssDNA produced following the unwinding of CT DNA for different time-periods, and under different

conditions in terms of pH, as determined from the decay traces analyzed according to Equations 8-2 and 8-3 (data not shown). We observe that under low pH conditions such as [HO^-] 0.005 M and 0.01 M, no unwinding, and therefore no ssDNA is produced, within the experimental error. The amount of single stranded DNA becomes noticeable only after unwinding for 45 min at an [HO^-] concentration of 0.05 M; no detectable ssDNA amount is registered up to the previous unwinding time. A two-fold increase in [HO^-] concentration dramatically changes our results, and at [HO^-] 0.1 M, complete unwinding of DNA is observed after 15 min.

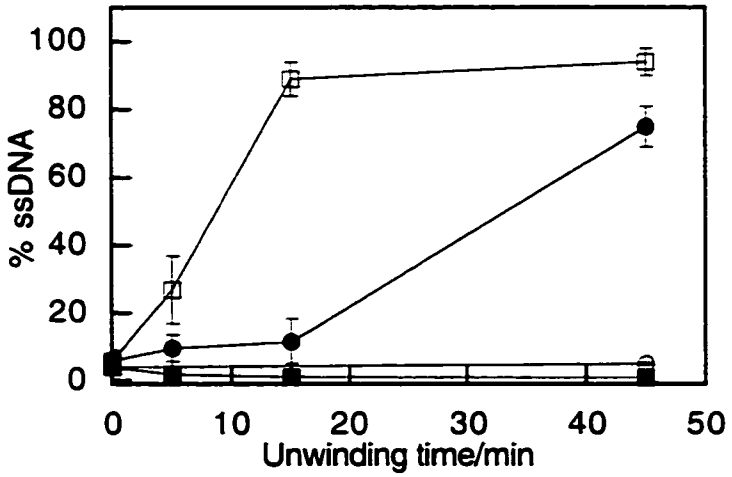

Figure 8-7: Amount of ssDNA produced following different unwinding times employing unwinding buffers of (□) 0.1 M, (●) 0.05 M, (■) 0.01 M, (○) 0.005 M. The samples consisted of a 100 μl agarose gel containing CT DNA 90 μM in base pairs (*i.e.*, 9 nmoles of CT DNA base pairs per gel). After unwinding and neutralization, 150 μl of PicoGreen 5.8 μM were added (*i.e.*, 0.87 nmoles of PicoGreen per gel).

We also monitored fluorescence decay lifetimes for PicoGreen-CT DNA complexes, following different γ radiation doses. The idea is to establish DNA-damage detection limits for a given unwinding condition. We thus subjected CT DNA to 5 and 10 Gy of γ radiation and later unwound it with [HO^-] 0.06 M, and compared it with a blank obtained with non irradiated DNA unwound under the same conditions. The results are shown in Figure 8-8.

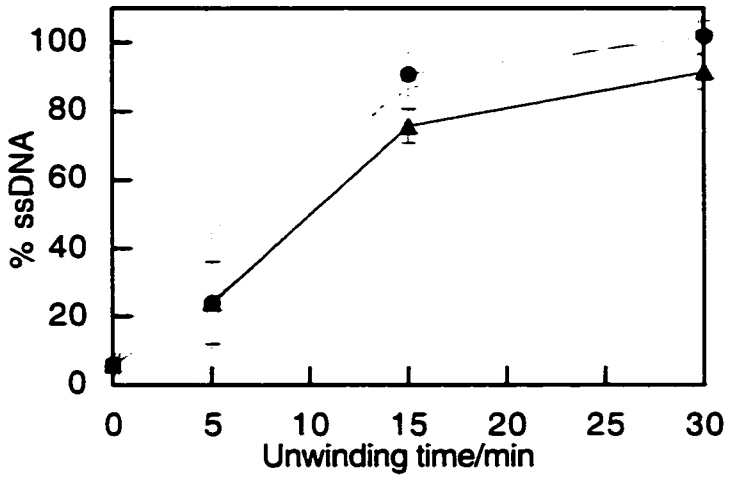

Figure 8-8: Amount of ssDNA produced from CT DNA samples following different unwinding times employing an unwinding buffer 0.06 M in HO^-. DNA gels received (▲) 0, (●) 5, and (□) 10 Gy γ radiation. The samples consisted of a 100 μl agarose gel containing CT DNA 90 μM (*i.e.*, 9 nmoles of CT DNA base pairs per gel). After unwinding and neutralization, 150 μl of PicoGreen 5.8 μM were added (*i.e.*, 0.87 nmoles of PicoGreen per gel).

8.2.4 DNA-damage Assessment in White Blood Cells

The results obtained with CT DNA (*vide supra*) allow us to establish a range of unwinding conditions to employ on the DNA isolated from white blood cells. Different samples were thus prepared for the analysis of the DNA-damage. White blood cells extracted from sheep blood were irradiated for different time periods, to deliver different doses of γ radiation ranging from 0 to 100 Gy. These samples were then subject to three different unwinding conditions. Unwinding with an $[HO^-]$ concentration of 0.01 M for 20 min, and unwinding with $[HO^-]$ 0.05 M for 5 and 10 min. The decay traces obtained for the PicoGreen-DNA complexes, and the amount of ssDNA quantified in each case according to Equations 8-2 and 8-3, are presented in Figure 8-9 for the different conditions employed.

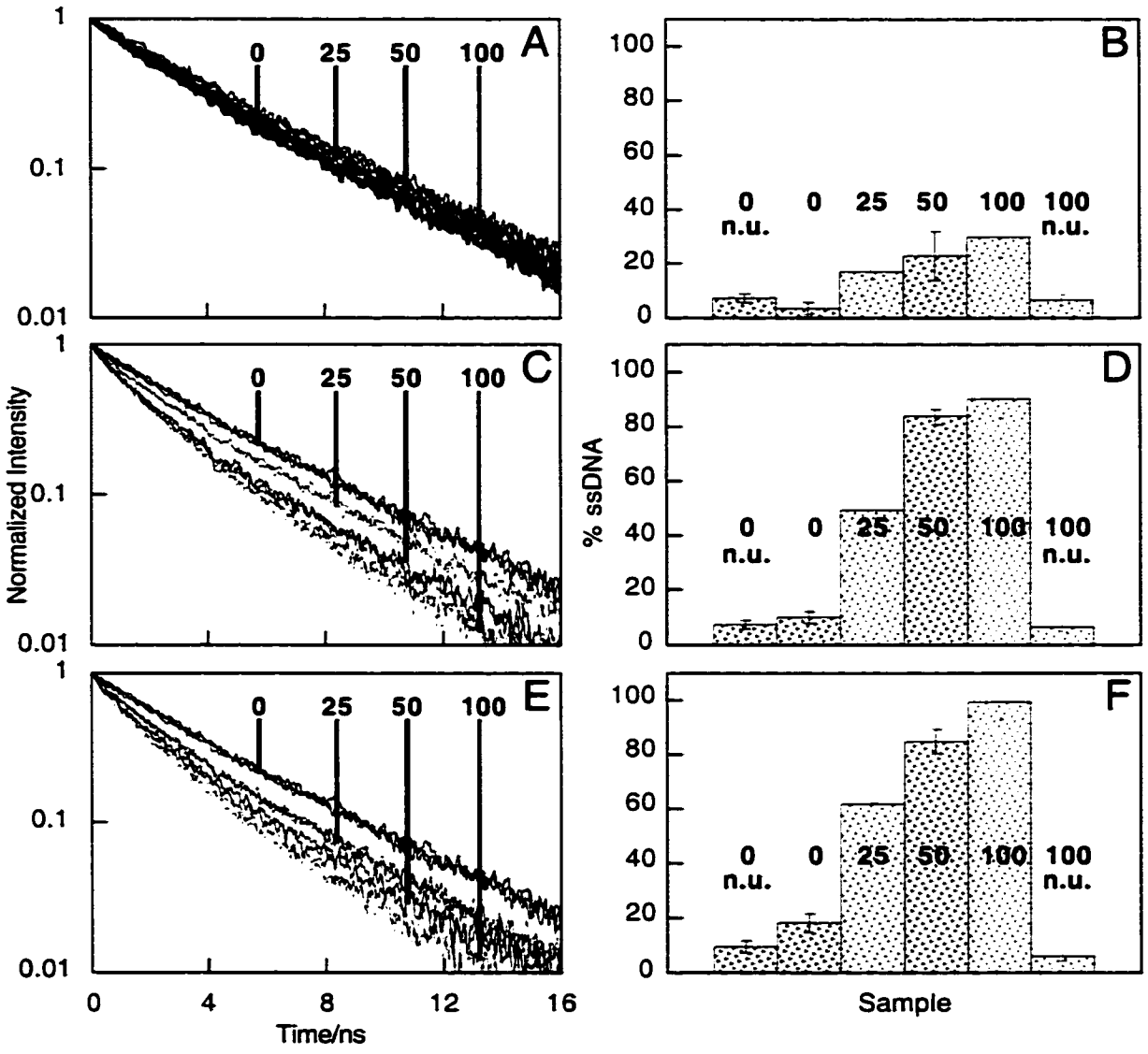

Figure 8-9: (A), (C), and (E), Fluorescence decay traces obtained for PicoGreen-DNA complexes from DNA samples extracted from sheep white blood cells. Figures (B), (D), and (F) show the amounts of ssDNA produced following the unwinding, calculated from Equations 8-2 and 8-3 and the respective decay traces. The samples were subject to different doses of γ radiation and unwinding conditions. (A) and (B) [HO⁻] 0.01 M, 20 min; (C) and (D) [HO⁻] 0.05 M, 5 min; (E) and (F) [HO⁻] 0.05 M, 10 min. The samples consisted of a 150 μl agarose gel containing 1 x 10^6 white blood cells (*i.e.*, each gel had 6 μg of DNA, approximately 9.5 nmoles of base pairs. After unwinding and neutralization, 150 μl of PicoGreen 5.8 μM were added (*i.e.*, 0.87 nmoles of PicoGreen per gel).

Table 8-1 also presents the values of ssDNA as extracted from Equations 2 and 3. The trend observed in Figures 8-9-A and 8-9-B is the expected one, however the results are within experimental error. Upon an increase in the [HO^-] concentration (0.05 M) of the unwinding buffer we observe an increased sensitivity, particularly for low damage conditions. We managed to measure the damage produced for a dose as low as 5 Gy within these conditions (see Figure 8-10 and Table 8-1).

Table 8-1: Amount of ssDNA measured in white blood cells following different conditions of γ radiation and unwinding times.

Unwinding conditions		% ssDNA following γ radiation					
[HO^-]/M	Time/min	0 Gy	5 Gy	10 Gy	25 Gy	50 Gy	100 Gy
0	0	7.4	-	-	-	-	6.7
0.01	20	3	-	-	17	23	30
0.05	5	10	-	-	49	84	90
0.05	10	18	[a] 32	[a] 44	62	85	100

The data was extracted according to Equations 8-2 and 8-3, from the results presented in Figures 8-9 and 8-10. Each value is the mean of three independent measurements. [a] These values are the mean of six independent measurements.

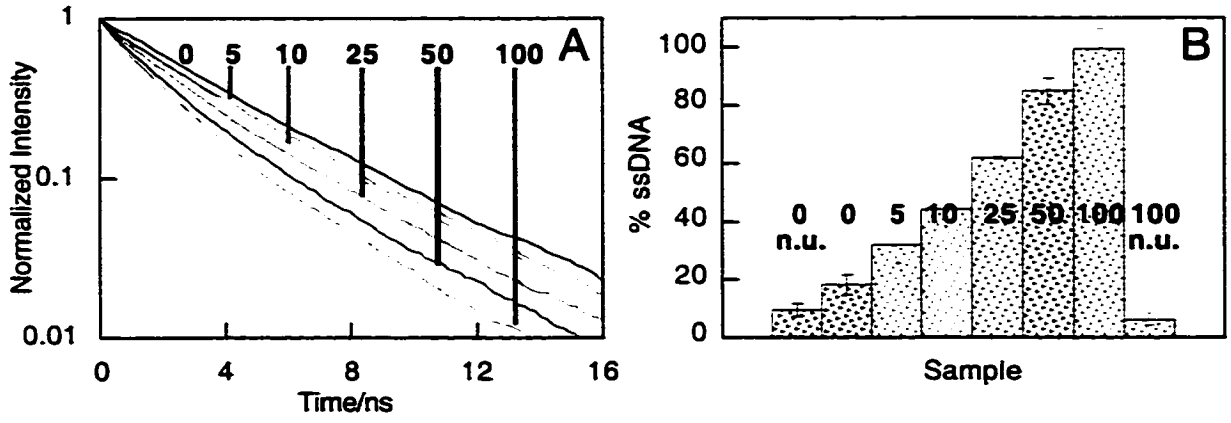

Figure 8-10: (A) Fluorescence decay traces obtained for PicoGreen-DNA complexes from DNA samples extracted from sheep white blood cells; only one trace (smoothed) is

presented for each DNA-damage. The samples were subject to different doses of γ radiation and unwound for 10 min with [HO⁻] 0.05 M. (B) amounts of ssDNA produced following the unwinding, calculated from Equations 8-2 and 8-3. The samples consisted of a 150 μl agarose gel containing 1 x 10^6 white blood cells (*i.e.*, each gel had 6 μg of DNA, approximately 9.5 nmoles of base pairs. After unwinding and neutralization, 150 μl of PicoGreen 5.8 μM were added (*i.e.*, 0.87 nmoles of PicoGreen per gel).

8.3 Discussion

The results presented in Chapter 7 of this thesis showed the possibility of employing fluorescence lifetimes of PicoGreen-DNA complexes to determine ssDNA to dsDNA ratios.[14,23] In this work we pursue the objective of establishing a technique for the measurement of DNA-damage with that approach. It is therefore necessary to establish the conditions and potential of the method. In this sense we have explored the minimum amount of analyte necessary for a measurement, as well as the minimum damage detectable in terms of strand breaks (SB), to establish a field of applicability of the technique. These issues are discussed in the following sections, in relationship to our results with CT and ST DNA, and DNA isolated from white blood cells (*vide supra*).

As the source of DNA-damage we have chosen different doses of γ radiation. This damage is mostly due to the production of hydroxyl radicals by the latter.[3,4,29,30] A recent publication reports on the quantification of single strand breaks (SSB) and double strand breaks (DSB) produced on the DNA, as well as on the number of base modifications resulting in alkaline labile sites (ALS) following administration of a given dose of this type of radiation.[31]

8.3.1 Sensitivity to DNA-damage

The sensitivity to DNA-damage will be given by two factors; one of them is the minimum measurable difference in ssDNA to dsDNA ratio, which is intrinsic to the instrument response and the photophysics of the dye-DNA system. The other magnitude is dependent on the biggest differentiation in the ratio of the two forms of DNA produced, for a given dose of γ radiation. This will be a function of the protocol employed in the unwinding of the DNA isolated from the cells.

The results obtained with CT and ST DNA and shown in Figure 8-4 demonstrate that PicoGreen-DNA fluorescence lifetimes easily report differences of *ca.* 20% in the relative amount of ssDNA to dsDNA.[23] Further, the results are independent of the DNA source,

i.e., salmon testes *vs.* calf thymus. This represents the first step towards the development of an analytical method, and involves the parametrization of the decay equations, as well as establishing a relationship between preexponential factors and the relative amount of dsDNA present in a given mixture of ssDNA to dsDNA. Once we have obtained the necessary parameters with simple systems (those derived from Equations 8-2 and 8-3), we can now analyze more complex situations, *i.e.*, DNA embedded in agarose support, and latter on DNA isolated from white blood cells.

We searched our best unwinding conditions employing commercially available forms of the biopolymer, and we established from the results presented in Figure 8-7, that by employing [HO^-] concentrations of 0.05 M we would attain the necessary sensitivity. In fact, a five fold decrease in the HO^- concentration results in no unwinding whereas a two fold increase from [HO^-] 0.05 M results in complete unwinding after 15 min for an undamaged sample. We also established that the optimum unwinding time would be between 10 to 15 min, for a DNA-damage produced with 5 Gy of γ radiation (Figure 8-8).

We tested our conditions with DNA isolated from irradiated and non-irradiated sheep blood cells. The analysis of the data presented in Figures 8-9 and 8-10 and Table 8-1 shows that the best conditions to analyze DNA-damage produced by up to 100 Gy is given by 10 min of unwinding at [HO^-] 0.05 M. In fact, following a reduction by half on the unwinding time (Figure 8-9-C and 8-9-D) we observe that up to 100 Gy damage the unwinding is not complete. In this case we are not in the best conditions since the full scale of the technique (given by a value of 100% ssDNA) is far from being reached. This situation is even more drastically evidenced when the unwinding concentration of HO^- is reduced by a factor of five. Figures 9-A and 9-B are a clear evidence that although the trend observed in the amount of ssDNA produced following unwinding, is in line with the damage exerted on the white blood cells, the result is far from ideal in terms of differentiation by the amount of ssDNA. The observed trend with milder conditions of the unwinding buffer indicates that the latter can be employed successfully where it is necessary to analyze stronger damage. This can be

observed following a close inspection of Figure 8-11, compiling the data of Figures 8-9 and 8-10. We can also infer from this plot that whenever it is necessary to asses lower amounts of DNA-damage, stronger unwinding conditions should be employed.

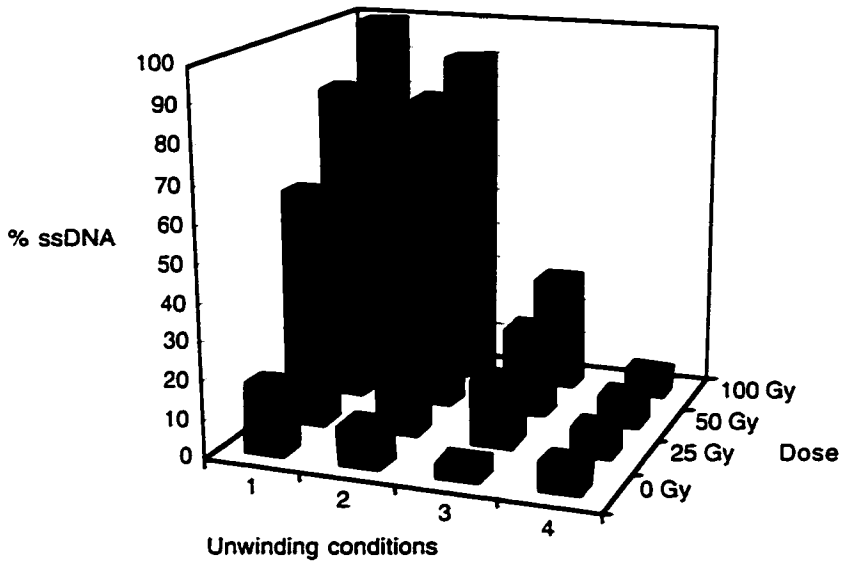

Figure 8-11: Percent of ssDNA produced following different doses of γ radiation (0, 25, 50 and 100 Gy, as shown on the plot) and unwinding with: (1) [HO⁻] 0.05 M, 10 min, (2) [HO⁻] 0.05 M, 5 min, (3) [HO⁻] 0.01 M, 20 min (4) No unwinding. The samples consisted of a 150 μl agarose gel containing 1 x 10^6 white blood cells (*i.e.*, each gel had 6 μg of DNA, approximately 9.5 nmoles of base pairs). After unwinding and neutralization, 150 μl of PicoGreen 5.8 μM were added (*i.e.*, 0.87 nmoles of PicoGreen per gel).

8.3.2 Relevance of the Magnitudes Measured

An important question to answer is which range of DNA-damage values are those we can successfully measure. Our present results are capable of reporting damages as low as those introduced by 5 Gy of γ radiation. Under these conditions up to 5000 single strand breaks, and 200 double strand breaks are introduced per cell.[27,28] This dose of γ radiation is very high, although reports exist following the Chernobyl accident, that people receiving doses as high as 10 Gy have survived for more than 14 years.[32] We believe that at the

present time, our technique can be employed as a fast diagnostic of exposure to high doses of nuclear radiation.

Radiotherapy treatments usually involve doses as high as 2 Gy.[21] Those ones can become detectable by our technique, upon selecting stronger unwinding conditions that result in complete DNA unwinding (*i.e.*, 100% ssDNA) following 5 Gy radiation. We believe that under these conditions we can accurately assess DNA-damage following γ radiation with doses spanning from 0 to 5 Gy.

DNA-damage studies performed *in vitro*, to establish the phototoxic properties of pharmaceutical products, are quantified in terms of single strand breaks produced. Phototoxic drugs reportedly produce *ca.* 1 strand break every 6000 base pairs.[33,34] With our method, we can detect even lower values after appropriate unwinding of the DNA (see Table 8-2).

Food preservation is another discipline involved in γ irradiation of biological substrates. Values in the order of 1000 Gy or higher are usually employed in food preservation.[35-37] While our present conditions of work are not capable of differentiating a 100 Gy from a 1000 Gy radiation exposure, upon an adjustment of the unwinding conditions (lower basicity of the solution employed), our method would be able to assess rapidly if food has been treated or not.

The previous values and the corresponding disciplines are summarized in Table 8-2.

Table 8-2: Calculated yield of strand breaks, per million base pairs, produced by γ radiation, UV light irradiation, and intrinsic causes in living mammals.

Discipline	strand breaks (SB)	Source of damage
Radiotherapy treatments[21]	0.371	2 Gy γ ray dose
Chernobyl survivors[32]	1.85	10 Gy γ ray dose
Food irradiation[35-37]	185	1000 Gy γ ray dose
Drug phototoxicity studies[33,34]	[a] 80 - 300	UV light
Spontaneous DNA-damage[38]	1.43	metabolism, per hour

SB values are calculated assuming 1000 single strand breaks and 40 double strand breaks per cell (containing 6 x 10^{-6} μg DNA, equivalent to 5.61 x 10^{9} base pairs of DNA) per Gy of γ radiation. [a] Values are calculated from those previously reported *i.e.*, 0.5 to 2 strand breaks for supercoiled ΦX174 DNA (5386 base pairs).[33,34]

8.3.3 Analyte Quantities

A different aspect involves the minimum analyte amount we can reliably detect with our technique. Previous results (those presented in the previous chapter[23]) show that high dye:DNA ratios (*i.e.*, dye:DNA > 1:10) are not operational, given the possibility of intermolecular interactions between two dye molecules under these conditions, which affect the kinetic laws employed in the fitting. The chromophore amount thus fixes that of DNA (*i.e.*, DNA base-pair molarity has to be *ca.* ten fold higher than the dye concentration). The minimum amount of dye (and therefore that of DNA) to be employed in our measurements is, on the other hand, predetermined by the sensitivity of our detector and the efficiency of the signal pickup of our optical setup.

The volume of sample explored by the laser, in each shot, is given by a cylinder of *ca.* 0.4 cm length and 0.4 cm in diameter, *i.e.*, we excite a volume of *ca.* 0.05 ml. Given that we can readily measure PicoGreen at concentrations of 10 μM when complexed with 100 μM base pairs of DNA, it means that 0.5 nmoles of dye, and correspondingly, 5 nmoles of DNA

base pairs can be easily detected with our system. The latter value is equivalent to *ca.* 3 μg of DNA.

Experiments performed with DNA embedded in gels were done in such a way as to produce 0.1 ml gels containing 6 μg of DNA each (*i.e.*, DNA from 1 x 10^6 cells). These gels were then plugged into NMR tubes, where the sample was excited and a signal was measured. See Figure 8-12.

The wavelength limitations of the picosecond Nd/YAG laser employed allowed us to excite only at 355 nm. At this wavelength the absorbance of PicoGreen is quite low, its molar extintion coefficient being 12.3 times lower than that at the absorbance maximum at 497 nm. The possibility of exciting at 497 nm wavelength would thus reduce the necessary amount of PicoGreen, and therefore that of DNA material, by a factor of *ca.* 10. An improvement on the signal pickup would also result in a considerable decrease in the minimal amount of cells needed to assess DNA-damage. At the present only 6% of the emission is picked up by a collimating lenses of 3.6 cm aperture located 7.85 cm away from the sample. The use of an ellipsoidal mirror surrounding the sample would allow us to capture and measure almost 100% of the emitted photons, enabling us to reduce the amount of cells by a factor of 16.

Upon inclusion of these modifications we would then be able to reduce the amount of cells by a factor of *ca.* 160, and measure the DNA extracted from approximately 6 x 10^3 cells.

8.3.4 Reproducibility

All the results in Table 8-1 are the mean of three independent measurements; those obtained following 5 and 10 Gy doses of γ radiation (and also shown in Table 8-1) are the mean of six independent measurements. The standard deviation is *ca.* 5 in% of ssDNA and we therefore conclude that the results are reliable as far as differences, in ratios of ssDNA to dsDNA, are equal to or higher than 10 in% of ssDNA.

It is important to mention that two main problems were found during the development of the technique. The first difficulty we encountered was the high emission

from Gelbond®, the support material, as observed in Figure 8-6. In fact, the emission intensity from this material is as strong as that of PicoGreen-dsDNA complexes as used in our experimental conditions. Further, the lifetime of Gelbond® is in the range of those for PicoGreen-ssDNA and PicoGreen-dsDNA. This prompted a first change in our methodology and we casted the gels in well plates of *ca.* 200 µl capacity, where they were processed and extracted for the measurements. The later was done by taking a portion of the gel with the tip of a NMR tube, and employing the later as a sample holder. A second difficulty resulting in lack of reproducibility was attributed to poor lysis and unwinding conditions in these well plates, this is the result of employing very small volumes of the necessary buffer solutions. Ultimately we found that the best results are those obtained when the cells are lysed, and the isolated DNA unwound, while embedded in the agarose gel, supported on Gelbond®. After neutralization of the gels, these are peeled off from Gelbond® and stained with PicoGreen. Figure 8-12 summarizes the steps of the protocol we followed in our experiments.

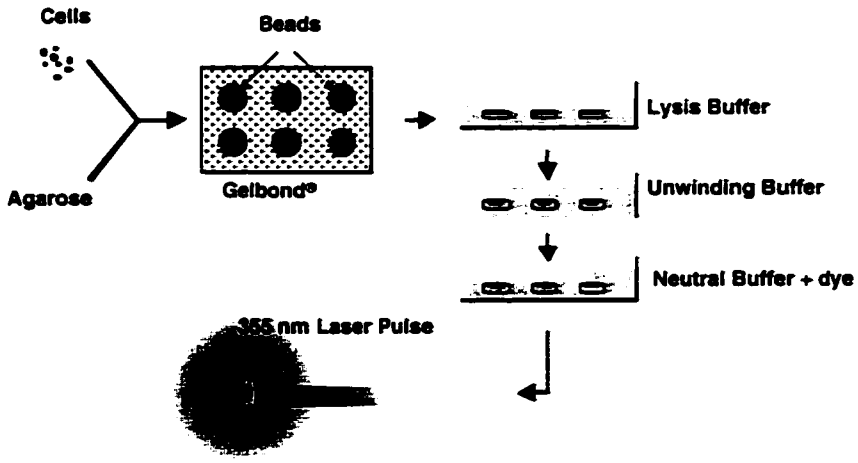

Figure 8-12: Protocol employed in the isolation of DNA from white blood cells, and its subsequent staining and excitation.

8.4 Conclusions

We have introduced a new technique for DNA-damage assessment based on time-resolved measurements of dye-DNA complexes. This technique is devoid of many of the problems encountered with other methods. There is no need for operator judgement on the nature of the sample, an issue encountered in the comet assay. In contrast with the currently employed steady-state fluorescence techniques,[11,13,21] there is no need for blanks, given that the lifetime is a sole measure of the ratio of ssDNA to dsDNA; further, it is independent on the amount of sample employed, as far as a ratio of 1:10 (or smaller) in dye to DNA base pairs is maintained in all measurements.[14]

At the present stage of development this method is capable of monitoring as low as 5 Gy of γ radiation, and up to 100 Gy. We further believe that upon appropriate conditioning, higher sensitivity can be achieved, and the technique might therefore find applications as a fast diagnostic tool, relevant in problems of human exposure to low radiation doses.

Although the technique lacks the ability to monitor damage on a single cell basis, as the comet assay,[6-9,39] its strength relies in that one measurement results in the monitoring of a statistically relevant population of sample. Yet, very little sample is necessary if modifications are made to our current setup; we estimate that 6×10^3 cells can be reliably measured at a time.

Finally, we note that while our work involved a sophisticated picosecond fluorescence system, similar measurements could be developed around less expensive light sources, such as short pulse diodes.

8.5 Materials and Methods

Materials. Sheep blood was obtained from the Animal Diseases Research Institute at Agriculture Canada (Ottawa, ON, Canada). PicoGreen dsDNA quantitation reagent (PG) was obtained from Molecular Probes (Eugene, OR, USA) and kept at –20 °C until use. Hank's Balanced Salt Solution without phenol red, 0.1 μm filtered (HBSS) was from Gibco BRL Life Technologies (Grand Island, NY, USA). Calf thymus DNA (Type I), salmon testes DNA (Type III), Trizma pre-set crystals (reagent grade, pH 7.4), phosphate buffered sodium heparin at 500 units/ml, fluorescein, fluorescein diacetate, ethidium bromide sodium hydroxide (NaOH) and *N*-lauroyl sarcosine sodium salt (SLS) were obtained from Sigma Chemical Company (St.-Louis, MO, USA). Agarose high strength, analytical grade, ultra pure DNA grade (low-melting point (LMP) agarose) was obtained from Bio-Rad Laboratories (Hercules, CA, USA). Dimethyl sulfoxide (DMSO), trishydroxymethylaminomethane (Tris base) and sodium tetra ethylene diamine tetraacetate (EDTA), sodium phosphate monobasic and sodium phosphate dibasic were obtained from Fischer Scientific (Fairlawn, NJ, USA). Iso-octylphenoxypolyethoxy-ethanol (Triton x-100), sodium chloride (NaCl), potassium hydroxide (KOH) and hydrochloric acid (HCl) were from BDH (Toronto, ON, Canada). The TAE buffer, 10x pH 8.4 was from Roche Diagnostics (Manheim, Germany). Wright-Geimsa Stain was obtained from EM Science (Gibbstown, NJ, USA). All solvents and chemicals were used without further purification.

Solution Preparation. All solutions were prepared with 18 MΩ water (Milli-Q plus PF unit, Millipore Corp., Bedford, MA, USA). Distilled deionized water (ddH_2O) for red blood cell lysis was sterilized by passing it through a 0.2 μm filter (Acrodisc, low protein binding, Gelman Sciences (Ann Arbour, MI, USA)). The saline rescue solution, also sterilized in the same way as the water for red blood lysis, consisted of 1.8% NaCl and ddH_2O. Fluorescein diacetate was prepared at 5 mg/ml in acetone. The ethidium bromide solution was prepared at 200 μg/ml in HBSS. The working viability stain was prepared by

adding 50 μl of the ethidium bromide solution and 7.5 μl of the fluorescein diacetate solution to 1.2 ml of HBSS. The PBS solution consisted of 58 mM Na_2HPO_4, 17 mM NaH_2PO_4 and 68 mM NaCl in ddH_2O to achieve a pH of 7.4. The agarose solution was prepared in PBS pH 7.4 to 0.75% consistency (w:v). The lysis A buffer consisted of 2.5 M NaCl, 100 mM EDTA, 10 mM Tris base, 1% SLS, adjusted to pH 10, 1% Triton x-100 and 10% DMSO was added to the lysing solution immediately before use, to assist in the removal of cellular proteins. The Tris buffer consisted of 10 mM Trizma pre-set crystals, 1 mM Na_2EDTA and 100 mM NaCl in ddH_2O to achieve a pH of 7.4. Various concentrations of the unwinding buffer were prepared with distilled deionized H_2O, ranging from 0.1 M to 0.5 M KOH. The neutralizing solutions were prepared at 0.1 and 1 M HCl in ddH_2O. The Geimsa stain was prepared by adding 5 ml of the Geimsa solution to 100 ml ddH_2O. The PicoGreen staining solution was prepared by adding 196 μl of PicoGreen to 10 ml of Tris buffer solution (1:50 dilution of the stock solution supplied by Molecular Probes to obtain a 5.9 μM solution) and the solution was stored at 4 °C and protected from light.

DNA Experiments in Buffer Solutions. CT DNA and ST DNA suspensions were prepared in a Tris buffer solution (10 mM) pH 7. The ssDNA was obtained after boiling a dsDNA solution for 30 min followed by immediate immersion on an ice bath. Complete denaturation was confirmed by comparing the absorption ratio at 260 nm for the heated (ssDNA) and non-heated (dsDNA) samples. A value of 1.32 was obtained, in good agreement with the literature value.[40] DNA samples were 70 to 150 μM; PicoGreen concentration was 11 μM in all cases.

Isolation of White Blood Cells from Sheep Whole Blood.[41] All plastic ware used during the isolation process was made of polypropylene, and high binding plastics, such as polystyrene, were avoided as they bind cells to the centrifuge tube walls. A volume of 100 ml of sheep whole blood was collected in a culture flask containing 10 ml of phosphate buffered sodium heparin. The sheep whole blood was dispensed into centrifuge tubes (15 ml of whole blood x 8 centrifuge tubes) and kept on ice for 30 min. Red blood cells were lysed

with 15 ml of ice cold sterile water for no longer than 30 s, then 15 ml of ice cold sterile saline solution was added to stop the red blood cell lysis and restore the cellular osmotic pressure. The mixtures were centrifuged for 1 h at 1500 rpm. The supernatants were decanted and the red blood lysis was repeated (5 ml of sterile water and 5 ml of sterile saline solution) to remove the remaining red blood cells. The white blood cells were collected by centrifugation for 15 min at 1500 rpm. The supernatants were decanted and the white blood cell pellets were resuspended in 2.5 ml HBSS and pooled.

Cell Viability and Concentration Determination.[41] To determine the cell concentration and viability, an aliquot of the cell suspension (50 µl) was taken and mixed with viability stain (50 µl) then dispensed onto a hemacytometer and examined by fluorescence microscopy (Olympus BX-60, 20x UPlanAPO objective with U-MNB (blue band) filter cube). Under these conditions, non-viable cells appeared red while viable cells fluoresced green due to the conversion of fluorescein diacetate to fluorescein by membrane esterases in metabolically competent (viable) cells. This method allowed for the concentration determination of the cells per ml.

To determine whether the cells had been harmed during isolation manipulations, a Geimsa stain test was performed. A drop of the cell suspension was dispensed onto a 75 mm x 25 mm microscope slide and allowed to dry. The slide was then submerged into the Geimsa staining solution for 5-10 min, removed and allowed to dry. Once dried, the slide was submerged into a methanol solution for 5-10 min, removed and allowed to dry. The dried slide was observed under a contrast microscope (Nikon LABOPHOT (Nikon Canada Inc. (Mississauga, ON, Canada), 60x PlanApo objective).

Irradiation.[41] The white blood cell suspension was centrifuged for 30 min at 1500 rpm. The supernatant was discarded and the pellet was resuspended in HBSS to obtain a cell concentration of 60 million cells/ml. The white blood cell suspension was divided and dispensed into glass vials (as many vials as there are gamma doses), and put on ice. For 1-5 Gy gamma doses, irradiations were carried out using the Gammacell® 40 reactor (Atomic

Energy of Canada Ltd., Radiochemical Company) ^{137}Cesium source with a dose of 0.955 Gy/min For 10, 50 and 100 Gy gamma doses, irradiations were carried out using the Gammacell® 220 reactor (Atomic Energy of Canada Ltd., Radiochemical Company) ^{60}Cobalt source with a dose of 38.462 Gy/min All irradiations were performed with the glass vials, containing the cell suspension, on ice.

In the case of CT DNA irradiations, the samples were appropriatey diluted to have a DNA concentration equivalent to that present in 60 million cells/ml, and the solutions were treated in the same way as the white blood cell suspensions.

Casting. Gelbond® strips (agarose gel support medium from BioWhittaker Molecular Applications (Rockland, ME, USA)) were cut in 6 cm x 10 cm dimension. For each dose of gamma radiation, a volume of 50 µl of white blood cell suspension was mixed with 125 µl of 0.75% agarose. An aliquot of 150 µl of the cell suspension (containing at least 1 million cells) was dispensed as a bead onto a strip of Gelbond® (6 beads per strip i.e. 3 radiation doses in duplicate).

Lysing and Unwinding. Once the Gelbond®-supported agarose gels (referred to as gels from here on forward) had solidified, they were submerged into a 100 mm petri dish containing 50 ml of ice cold Lysis A buffer and kept at 4 °C overnight. After at least 14 h [42], the lysing solution was removed and the gels were rinsed with ice cold HBSS. The gels were then submerged into a 100 mm petri dish containing 50 ml of ice cold unwinding buffer and kept at 4 °C for 0 to 45 min (depending on the experiment). Once the unwinding time had lapsed, the gels were rinsed with ice cold HBSS and 50 ml of fresh ice cold HBSS was dispensed onto the gels and they were kept at 4 °C until staining.

Staining. The pH 7.4 buffer was removed, and the gels were stained with 150 µl of a solution of PicoGreen 5.88 µM (*ca.* 9 x 10^{-10} moles of PicoGreen were added to each gel). The gels were left overnight at 4 ^{0}C, and the excess liquid was removed the following day.

Instrumentation. The picosecond laser and streak camera employed in the data acquisition have been described in Section 2.5 of this thesis.

8.6 References

(1) Loeb, L., Endogenous Carcinogenesis: Molecular Oncology into the Twenty-first Century-Presidential Address, *Cancer Res.*, **1989**, *49*, 5489-5496.

(2) Mullaart, E.; Lohman, P. H. M.; Berends, F.; Vijg, J., DNA Damage Metabolism and Aging, *Mutat. Res.*, **1990**, *237*, 189-210.

(3) Burrows, C. J.; Muller, J. G., Oxidative Nucleobase Modifications Leading to Strand Scission, *Chem. Rev.*, **1998**, *98*, 1109-1151.

(4) Pogozelski, W. K.; Tullius, T. D., Oxidative Strand Scission of Nucleic Acids: Routes Initiated by Hydrogen Abstraction from the Sugar Moiety, *Chem. Rev.*, **1998**, *98*, 1089-1107.

(5) Frenkel, K.; Klein, C. B., Methods Used for Analyses of "Environmentally" Damaged Nucleic Acids, *J. Chromatogr.*, **1993**, *618*, 289-314.

(6) Olive, P. L., DNA Damage and Repair in Individual Cells: Applications of the Comet Assay in Radiobiology, *Int. J. Radiat. Biol.*, **1999**, *75*, 395-405.

(7) Horváthová, E.; Slamenová, D.; Hlincíková, L.; Mandal, K. T.; Gábelová, A.; Collins, A. R., The Nature and Origin of DNA Single-strand Breaks Determined with the Comet Assay, *Mutat. Res.*, **1998**, *409*, 163-171.

(8) Rojas, E.; Lopez, M. C.; Valverde, M., Single Cell Gel Electrophoresis Assay: Methodology and Applications, *J. Chromatogr., B:*, **1999**, *722*, 225-254.

(9) Collins, A. R.; Dobson, V. L.; Dusinská, M.; Kennedy, G.; Stetina, R., The Comet Assay: What Can it Really Tell Us?, *Mutat. Res.*, **1997**, *375*, 183-193.

(10) Birnboim, H. C.; Jevcak, J. J., Fluorimetric Method for Rapid Detection of DNA Strand Breaks in Human White Blood Cells Produced by Low Doses of Radiation, *Cancer Res.*, **1981**, *41*, 1889-1892.

(11) Baumstark-Khan, C.; Hentschel, U.; Nikandrova, Y.; Krug, J.; Horneck, G., Fluorometric Analysis of DNA Unwinding (FADU) as a Method for Detecting Repair-induced DNA Strand Breaks in UV-irradiated Mammalian Cells, *Photochem. Photobiol.*, **2000**, *72*, 477-484.

(12) Kohn, K. W., Principles and Practice of DNA Filter Elution, *Pharmacol. Ther.*, **1991**, *49*, 55-77.

(13) Rogers, K. R.; Apostol, A.; Madsen, S. J.; Spencer, C. W., Detection of Low Dose Radiation Induced DNA Damage Using Temperature Differential Fluorescence Assay, *Anal. Chem.*, **1999**, *71*, 4423-4426.

(14) Cosa, G.; Focsaneanu, K.-S.; McLean, J. R. N.; McNamee, J. P.; Scaiano, J. C., Photophysical Properties of Fluorescent DNA-dyes Bound to Single- and Double-stranded DNA in Aqueous Buffered Solution., *Photochem. Photobiol.*, **2001**, *73*, 585-599.

(15) Haugland, R. P.; Yue, S. T.; Millard, P. J.; Roth, B. L. "Cyclic Substituted Unsymmetrical Cyanine Dyes", United States Patent Office, US5436134, 1995.

(16) Yue, S. T.; Singer, V. L.; Roth, B. L.; Mozer, T. J.; Millard, P. J.; Jones, L. J.; Xiaokui, J.; Haugland, R. P. "Substituted Unsymmetrical Cyanine Dyes with Selected Permeability", World Intelectual Property Organization, WO96/13552, 1996.

(17) Netzel, T. L.; Nafisi, K.; Zhao, M.; Lenhard, J. R.; Johnson, I., Base-content Dependence of Emission Enhancements, Quantum Yields, and Lifetimes for Cyanine Dyes Bound to Double-strand DNA: Photophysical Properties of Monomeric and Bichromophoric DNA Stains, *J. Phys. Chem.*, **1995**, *99*, 17936-17947.

(18) Carlsson, C.; Larsson, A.; Jonsson, M.; Albinsson, B.; Nordén, B., Optical and Photophysical Properties of the Oxazole Yellow DNA Probes YO and YOYO, *J. Phys. Chem.*, **1994**, *98*, 10313-10321.

(19) Saltiel, J., The Role of Phantom States in the *cis-trans* Isomerization of Stylbene, *J. Am. Chem. Soc.*, **1967**, *89*, 1036-1037.

(20) Gilbert, A.; Baggott, J., *Essentials of Molecular Photochemistry*; Blackwell Scientific Publications: Oxford, 1991.

(21) Elmendorff-Dreikorn, K.; Chauvin, C.; Slor, H.; Kutzner, J.; Batel, R.; Muller, W. E.; Schroder, H. C., Assessment of DNA Damage and Repair in Human Peripheral Blood Mononuclear Cells Using a Novel DNA Unwinding Technique, *Cell. Mol. Biol.*, **1999**, *45*, 211-218.

(22) Singer, V. L.; Jones, L. J.; Yue, S. T.; Haugland, R. P., Characterization of PicoGreen Reagent and Development of a Fluorescence-based Solution Assay for Double-stranded DNA Quantitation. *Anal. Biochem.*, **1997**, *249*, 228-238.

(23) Cosa, G.; Focsaneanu, K.-S.; McLean, J. R. N.; Scaiano, J. C., Direct Determination of Single to Double Stranded DNA Ratio in Solution Applying Time-resolved Fluorescence Measurements of Dye-DNA Complexes, *Chem. Commun.*, **2000**, 689-690.

(24) Reinhardt-Poulin, P.; McLean, J. R.; Deslauriers, Y.; Gorman, W.; Cabat, S.; Rouabhia, M., The Use of Silver-stained "Comets" to Visualize DNA Damage and Repair in Normal and *Xeroderma pigmentosum* Fibroblasts After Exposure to Simulated Solar Radiation, *Photochem. Photobiol.*, **2000**, *71*, 422-425.

(25) Sauerwein, B.; Murphy, S.; Schuster, G. B., Dynamics of Solute Motion: Photoisomerization Shows Linear Dependence on Solvent Mass, *J. Am. Chem. Soc.*, **1992**, *114*, 7920-7922.

(26) Sczepan, M.; Rettig, W.; Bricks, Y.; Slominski, Y. L.; Tolmachev, A. I., Unsymmetric Cyanines: Chemical Rigidization and Photophysical Properties., *J. Photochem. Photobiol. A: Chem.*, **1999**, *124*, 75-84.

(27) Ward, J. F. DNA Damage Produced by Ionizing Radiation in Mammalian Cells: Identities, Mechanisms of Formation, and Reparability; In *Progress in Nucleic Acid Research and Molecular Biology*; Academic Press, Inc.: New York, 1988; Vol. 35; 95-125.

(28) Goodhead, D. T., Initial Events in the Cellular Effects of Ionizing Radiations: Clustered Damage in DNA, *Int. J. Radiat. Biol.*, **1994**, *65*, 7-17.

(29) Dizdaroglu, M.; von Sonntag, C.; Schulte-Frohlinde, D., Strand Breaks and Sugar Release by γ-Irradiation of DNA in Aqueous Solution, *J. Am. Chem. Soc.*, **1975**, *97*, 2277-2278.

(30) Doddridge, Z. A.; Cullis, P. M.; Jones, G. D. D.; Malone, M. E., 7,8-Dihydro-8-oxo-2'-deoxyguanosine Residues in DNA Are Radiation Damage "Hot" Spots in the Direct γ Radiation Damage Pathway, *J. Am. Chem. Soc.*, **1998**, *120*, 10998-10999.

(31) Pouget, J.-P.; Douki, T.; Richard, M.-J.; Cadet, J., DNA Damage Induced in Cells by γ Radiation as Measured by HPLC/GC-MS and HPLC-EC and Comet Assay, *Chem. Res. Toxicol.*, **2000**, *13*, 541-547.

(32) Gottlöber, P.; Steinert, M.; Weiss, M.; Bebeshko, V.; Belyi, D.; Nadejina, N.; Stefani, F. H.; Wagemaker, G.; Fliedner, T. M.; Peter, R. U., The Outcome of Local radiation Injuries: 14 Years of Follow-up after the Chernobyl Accident., *Radiat. Res.*, **2001**, *155*, 409-416.

(33) Artuso, T.; Bernadou, J.; Meunier, B.; Piette, J.; Paillous, N., Mechanism of DNA Cleavage Mediated by Photoexcited Non-steroidal Antiinflammatory Drugs, *Photochem. Photobiol.*, **1991**, *54*, 205-213.

(34) Chouini-Lalanne, N.; Defais, M.; Paillous, N., Non-steroidal Antiinflammatory Drug-photosensitized Formation of Pyrimidine Dimer in DNA, *Biochem. Pharmacol.*, **1998**, *55*, 441-446.

(35) Beaulieu, M.; Béliveau, M.; D'Aprano, G.; Lacroix, M., Dose Rate Effect of γ Irradiation of Phenolic Compounds, Polyphenol Oxidase, and Browning Mushrooms (*Agaricus Bisporus*), *J. Agric. Food. Chem.*, **1999**, *47*, 2537-2543.

(36) Zareena, A. V.; Variyar, P. S.; Gholap, A. S.; Bongirwar, D. R., Chemical Investigation of Gamma-irradiated Saffron (*Crocus Sativus L.*), *J. Agric. Food. Chem.*, **2001**, *49*, 687-691.

(37) Fan, X.; Gates, R. A., Degradation of Monoterpenes in Orange Juice by Gamma Radiation, *J. Agric. Food. Chem.*, **2001**, *49*, 2422-2426.

(38) Billen, D., Spontaneous DNA Damage and Its Significance for the "Negligible Dose" Controversy in Radiation Protection, *Radiat. Res.*, **1990**, *124*, 242-245.

(39) Böcker, W.; Rolf, W.; Bauch, T.; Müller, W.-U.; Streffer, C., Automated Comet Assay Analysis, *Cytometry*, **1999**, *35*, 134-144.

(40) Gallagher, S. R. Quantitation of DNA and RNA with Absorption and Fluorescence Spectroscopy; In *Current Protocols in Molecular Biology*; F. M. Ausubel, R. Brent, R. E. Kingston, D. D. Moore, J. G. Seidman, J. A. Smith and K. Struhl, Eds.; Greene Pub. Associates and Wiley-Interscience: New York, 1994; Vol. 3; A.3D.1-A.3D.8.

(41) These experiments were performed by Ms. A. L. Vinette.

(42) Banáth, J. P.; Kim, A.; Olive, P. L., Overnight Lysis Improves the Efficiency of Detection of DNA Damage in the Alkaline Comet Assay, *Radiat. Res.*, **2001**, *55*, 564-571.

9. Final Comments and Future Directions

9.1 Final Comments

The work presented in this thesis has been intended to gain insight into different aspects of the photosensitization problematic. Studies on the photochemical and photophysical behavior of different pharmaceutical products have been performed with the aim of better understanding their photostability; this in turn will assist in predicting and preventing the appearance of adverse phototoxic and photoallergic reactions. The role protecting substrates might play, and the involvement of their potential intermediates has also been evaluated as part of this work. A considerable amount of effort has also been dedicated to the development of new strategies for assessing photosensitized damage of the genetic material in living cells.

The studies of ketoprofen and fenofibric acid, two pharmaceutical products closely related to the benzophenone chromophore, have rendered new understanding of basic photophysical and photochemical behavior. In the case of ketoprofen, the results predict an efficient singlet state mediated decarboxylation, occurring within picoseconds, and followed up by protonation of the resulting carbanion in ca., 210 ns. This fast deactivation almost certainly rules out the involvement of the excited state or any of the subsequent intermediates in adverse photosensitization effects. A similar situation arises for fenofibric acid, which rapidly, i.e., within 625 ns, decays to starting material or photoproducts. Given these fast decays characterizing the longer lived transients of both ketoprofen and fenofibric acid, oxygen involvement in their deactivation in the living tissues is predicted not to play a major role. Results from solvent dependence studies further anticipate that in the low polarity media characterizing lipid bilayers their deactivation will even be faster than that typical of the aqueous environment in the cytosol region of cells.

The phototoxicity reported for these molecules can therefore be only explained by the production of photoproducts which lack a fast deactivation mechanism, and are therefore prone to undergo type I reactions with cellular components, or type II reactions with the oxygen in the cell. The low yield of photodegradation for fenofibric acid in comparison to

that of ketoprofen, and the different triplet state configurations expected for the photoproducts of the former and the latter (at least 50 times more reactive in the latter case for type I photoprocesses) would account for the smaller amount of phototoxic and photoallergic effects reported for fenofibric acid vs. ketoprofen.

This work also reports photophysical parameters of dye-DNA complexes, values that are employed in the development of a new DNA damage assessment technique where the intensive property given by fluorescence lifetimes is proven to be a good probe for strand breaks of the genetic material. These results are not only important from their applicable point of view, but provide a basic understanding of the photophysical parameters of these dyes. A good knowledge of the latter can be employed in assisting in the device of new fluorescent probes which would show marked sensitivity to DNA, yet would require little instrumental capabilities

The analysis of the radical scavenging potential of melanin precursors, and the study of a new reactive oxygen species characteristic of α-diketones, also constitute an important part of the present work. The former results predict that upon a radical mediated lesion, the oxidation of catecholamines will proceed towards the final formation of melanin, precluding the formation of undesirable intermediates, which will be rapidly consumed. In what involves the study of the new reactive oxygen species, at the present time there is no reason to believe in its direct implication in photosensitization reactions in living organisms. It is important however, to consider that such a mechanism might be a viable one with α-ketoacids, such as pyruvic acid.

9.2 Future Directions

The knowledge gained in the systems presented here has exposed new alternatives where to direct future research efforts.

An enumeration of these alternatives is given in the following sections.

9.2.1 Photophysical and Photochemical Properties of Pharmaceutical Products

Development of pharmaceutical products is an active area of research, and new drugs are being commercialized on a regular basis, with the potential for side effects upon light exposure. It is consequently foreseeable that mechanistic studies of drug photodegradation will be an area of ongoing interest. The methodologies presented in the Time-resolved Laser Techniques section (Chapter 2) of this thesis might therefore constitute a guideline for this type of studies.

1. Measurement of the lifetimes for singlet decay and triplet generation (readily attainable with time-resolved femtosecond spectroscopy), as well as fluorescence quantum yields for 3-ethylbenzophenone (the parent structure of ketoprofen), in different polarity solvents are desirable. These results would assist in determining if the efficient decarboxylation of ketoprofen in polar solvents is the result of a slow intersystem crossing from the lowest singlet excited state.
2. Determination of equilibrium constants for DNA complexation with ketoprofen and 3-ethylbenzophenone, as well as with fenofibric acid and photoproducts **1** and **2**, and comparison of these values, to determine the role coulombic repulsion between DNA and the drugs have in this interaction. This would assist in assessing if reported DNA damage is due to the interaction of the drugs with DNA (which are expected to have a low binding constant with the latter), or rather it is due to the interaction of the photoproducts and DNA (in this case, the lack of coulombic repulsion would result in a higher binding constant).

3. Time-resolved studies with ketoprofen anion included within a zeolite framework, a project currently under way with the assistance of M. N. Chrétien, has given promising results, where the deactivation of the carbanion is extremely prolonged in the anhydrous zeolite environment. These results are further supported by deuterium incorporation in ethylbenzophenone, following irradiation of ketoprofen included within a zeolite, under D_2O atmosphere. These results will further be explored in the near future, to establish the possibility of performing intermolecular alkylation reactions within the zeolite framework.
4. Time-resolved and product studies of different halo-alkyl substituted ketoprofen molecules in a given zeolite framework should result in the formation of high yields of intramolecular alkylation of the photogenerated ketoprofen carbanion. A comparison of decay lifetimes for an haloalkyl ketoprofen carbanion in zeolites with different physical constrains would reveal the role steric hindrance due to the zeolite framework plays in the intramolecular alkylation. Different spectators could also be coincluded. These would provide the basis for the understanding of the photochemistry of carbanions within the solid framework of zeolites, where ketoprofen and its derivatives would be excellent probes due to their fast and effective decarboxylation into carbanions.
5. Experiments performed with halo-alkyl substituted ketoprofen derivatives in polar aprotic solvents, a project currently under way with the assistance of Dr. L Llauger, both in the absence and presence of water will report on intramolecular reactions and protonation rate constants, respectively, for the corresponding carbanions.

9.2.2 Reactivity of the Bartlett-Schenck Intermediate

1. It is desirable to perform studies where nucleophilic quenchers and electron donors, of established low reaction activation energies, are employed as quenchers of the Bartlett-Schenck intermediate. The requirement of low activation energies

would allow performing the experiments at low temperatures, where time evolution occurs in different time decades for the formation and decay of the intermediate. These studies would be aimed at understanding the reactivity of this species.

9.2.3 Catecholamines as Antioxidants

1. Rate constants for the quenching of radical species by dopa, dopamine and neuroadrenaline in the same systems as that determined for adrenaline are necessary. Different radicals of biological relevance should be addressed in these studies.

9.2.4 DNA-stain Dyes and DNA Damage Assessment

1. Time-resolved lifetimes of PicoGreen with different homopolymers like poly-dG, poly-dA or poly-dT and poly-dC would report on the sensitivity of the chromophore to purinic and pyrimidinic pockets within ssDNA. This would assist in understanding the photophysical behavior of the dye in the presence of single stranded DNA obtained from natural sources.
2. It is desirable the development of a new dye whose radiative lifetime is at least 3 fold larger than that of PicoGreen, the dye we have employed in our measurements. Such a dye would allow lifetime studies to be performed with commercially available low cost oscilloscopes. Both quinoline and benzothiazole moieties are characterized by short radiative lifetimes in solution. The preparation of a methine bridged dye constituted by two chromophore units each characterized by long radiative lifetimes (i.e., 15 ns) would result in a new fluorescent stain where the sensitivity to environment rigidity would still be given by the methine bridge as in the case of PicoGreen. The radiative lifetime would however be presumably larger.

3. Alternatively to a DNA damage assessment technique based on dye-DNA fluorescence lifetimes, it is foreseeable a methodology based on steady-state fluorescence spectroscopy of a mixture of two dyes and DNA. Three requisites are necessary for a given combination of dyes to work: (i) One of the dyes should be equally sensitive to ssDNA and dsDNA, as is the case of ethidium bromide in our studies; (ii) the second dye should have a different quantum yield of fluorescence for both forms of the biopolymer, PicoGreen would be perfectly suited; and (iii) they should have no emission overlap. Appropriate combinations of these two dyes, based on their molar absorptivities and fluorescence quantum yields, would result in a mixture that upon complexation to DNA would emit two resolved fluorescence bands. One band would act as an internal standard reporting the total amount of DNA. The second band would be sensitive to how much DNA is in either form. A ratio of the intensity of both bands would readily give the desired result, upon previous calibration.
4. A time-resolved fluorescence microscope may be devised to be employed in the Comet Assay, where the head and tail parameters characterizing this technique will be objectively determined based on the characteristic fluorescence lifetimes of PicoGreen-dsDNA (present in the comet head) and PicoGreen-ssDNA (present in the comet tail).
5. At the present stage of development the DNA damage assessment technique could be readily used in the determination of food irradiation with γ ray, upon convenient calibration for the high doses employed in these methodologies of food preservation.

9.3 Claims to Original Research

1. The elucidation of the photodegradation mechanism of fenofibric acid in aqueous solution is reported. It involves decarboxylation from the triplet state with a quantum yield of 0.06. These decarboxylation takes place from the n,π^* triplet state configuration of fenofibric acid. The low reactivity towards decarboxylation by fenofibric acid and towards hydrogen abstraction by its derivatives is assigned to a solvent mediated triplet state inversion (n,π^* to π,π^* in going from acetonitrile to water). Similar results are found for 4-methoxybenzophenone.
2. The reactivity of ketoprofen acid is determined for both prototropic forms in different solvents. The results evidence that photodecarboxylation of ketoprofen is a singlet state mediated photoprocess arising from the anionic form of the acid. This result constitutes the first account of singlet state photochemistry for a benzophenone-related compound. Benzylic carbanion reactivity has been determined within the anhydrous zeolite framework following diffuse reflectance studies of ketoprofen carboxylate (joint work with M. N. Chrétien). In a similar manner the reactivity of benzylic carbanions has been determined in aqueous solutions pH 12 following time-resolved LFP measurements of haloalkyl derivatives of ketoprofen.
3. The photochemical and photophysical behavior of 2,2'-thenil, an α-diketone, has been established. The results lead to the first ever observation of an oxygen-triplet state adduct as the one suggested by Bartlett, Saltiel and Schenck. Solvent dependence studies indicate a higher activation energy of decay for this intermediate in toluene, as compared to acetonitrile.
4. Absolute rate constants for the reaction of adrenaline with *tert*-butoxyl radicals and benzophenone are reported; no such values have been previously recorded.

5. Photophysical parameters of dye-DNA complexes are reported with single stranded DNA, and the values are compared to those obtained with double stranded DNA; whereas there exists accounts on the latter values, no such parameters have been previously established with single stranded DNA.
6. Fluorescence lifetimes of PicoGreen-DNA complexes can be used to report ssDNA to dsDNA ratios with ca., ± 5% accuracy. Upon calibration, these lifetime measurements provide a highly reliable analytical technique to determine DNA damage by estimation of ssDNA to dsDNA ratios of properly hydrolyzed DNA samples (joint work with A. L. Vinette).

9.4 Publications

9.4.1 Resulting from Research Presented in this Thesis

1. Cosa, G.; Martínez, L. J.; Scaiano, J. C., Influence of Solvent Polarity and Base Concentration on the Photochemistry of Ketoprofen: Independent Singlet and Triplet Pathways, *PCCP*, **1999**, 1, 3533-3537.
2. Cosa, G.; Focsaneanu, K.-S.; McLean, J. R. N.; Scaiano, J. C., Direct Determination of Single to Double Stranded DNA Ratio in Solution Applying Time-resolved Fluorescence Measurements of Dye-DNA Complexes, *Chem. Commun.*, **2000**, 689-690.
3. Cosa, G.; Focsaneanu, K.-S.; McLean, J. R. N.; McNamee, J. P.; Scaiano, J. C., Photophysical Properties of Fluorescent DNA-dyes Bound to Single- and Double-stranded DNA in Aqueous Buffered Solution., *Photochem. Photobiol.*, **2001**, 73, 585-599.
4. Cosa, G.; Purohit, S.; Boscá, F.; Miranda, M. A.; Scaiano, J. C., A Laser Flash Photolysis Study of Fenofibric Acid in Aqueous Buffered Media. Unexpected Triplet State Inversion in a 4-Methoxybenzophenone Derived Compound, *Photochem. Photobiol.*, **2002**, 75, 193-200.
5. Cosa, G.; Scaiano, J. C. Laser Techniques in the Study of Drug Photochemistry; In Phototoxicity of Drugs: Mechanistic Bases and Risk Prediction; J. V. Castell and M. A. Miranda, Eds.; Royal Society of Chemistry, Submitted.
6. Boscá, F.; Cosa, G.; Miranda, M. A.; Scaiano, J. C., Inversion of 4-Methoxybenzophenone Triplet in Aqueous Solutions, In preparation.

9.4.2 Other Publications

1. Sortino, S.; Cosa, G.; Scaiano, J. C., pH Effects on the Efficiency of the Deactivation Pathways of Naphazoline: A Combined Steady State and Time Resolved Study, *New J. Chem.*, **2000**, 24, 159-163.
2. Corrent, S.; Cosa, G.; Scaiano, J. C.; Galletero, M. S.; Alvaro, M.; García, H., Intrazeolite Photochemistry. 26. Photophysical Properties of Nanosized TiO_2 Clusters Included in Zeolites Y, β, and Mordenite., *Chem. Mater.*, **2001**, 13, 715-722.
3. Cosa, G.; Chrétien, M. N.; Galletero, M. S.; Fornés, V.; García, H.; Scaiano, J. C., Photocatalytic Activity of a Multi-component System Assembled within Zeolites. Case of 2,4,6-Triphenylpyrylium or Ruthenium Trisbipyridyl Photosensitizers and Titanium Dioxide Relays within Zeolite Y, *J. Phys. Chem. B*, **2002**, 106, 2460-2467.
4. Cosa, G.; Galletero, M. S.; Fernández, L.; Márquez, F.; García, H.; Scaiano, J. C., Tuning the Photocatalytic Activity of Titanium Dioxide by Encapsulation Inside Zeolites. Exemplified: Case of Thianthrene Photooxygenation and Horseradish Peroxidase Photodeactivation, In preparation.